VOLUME 78 JANUARY 17, 1974 NUMBER 2

JPCHAx

THE JOURNAL OF PHYSICAL CHEMISTRY

PUBLISHED BIWEEKLY BY THE AMERICAN CHEMICAL SOCIETY

THE JOURNAL OF

PHYSICAL CHEMISTRY

BRYCE CRAWFORD, Jr., *Editor*
WILMER G. MILLER, *Associate Editor*
ROBERT W. CARR, Jr., FREDERIC A. VAN-CATLEDGE, *Assistant Editors*

EDITORIAL BOARD: A. O. ALLEN (1970–1974), C. A. ANGELL (1973–1977), V. A. BLOOMFIELD (1974–1978), J. R. BOLTON (1971–1975), L. M. DORFMAN (1974–1978), M. FIXMAN (1970–1974), H. S. FRANK (1970–1974), R. R. HENTZ (1972–1976), W. J. KAUZMANN (1974–1978), R. L. KAY (1972–1976), D. W. McCLURE (1974–1978), R. M. NOYES (1973–1977), J. A. POPLE (1971–1975), B. S. RABINOVITCH (1971–1975), H. REISS (1970–1974), S. A. RICE (1969–1975), F. S. ROWLAND (1973–1977), R. L. SCOTT (1973–1977), A. SILBERBERG (1971–1975), J. B. STOTHERS (1974–1978), W. A. ZISMAN (1972–1976)

AMERICAN CHEMICAL SOCIETY, *1155 Sixteenth St., N.W., Washington, D. C. 20036*

Books and Journals Division

JOHN K CRUM *Director*
RUTH REYNARD *Assistant to the Director*

CHARLES R. BERTSCH *Head, Editorial Processing Department*
D. H. MICHAEL BOWEN *Head, Journals Department*
BACIL GUILEY *Head, Graphics and Production Department*
SELDON W. TERRANT *Head, Research and Development Department*

©Copyright, 1974, by the American Chemical Society. Published biweekly by the American Chemical Society at 20th and Northampton Sts., Easton, Pa. 18042. Second-class postage paid at Washington, D. C., and at additional mailing offices.

All manuscripts should be sent to *The Journal of Physical Chemistry*, Department of Chemistry, University of Minnesota, Minneapolis, Minn. 55455.

Additions and Corrections are published once yearly in the final issue. See Volume 77, Number 26 for the proper form.

Extensive or unusual alterations in an article after it has been set in type are made at the author's expense, and it is understood that by requesting such alterations the author agrees to defray the cost thereof.

The American Chemical Society and the Editor of *The Journal of Physical Chemistry* assume no responsibility for the statements and opinions advanced by contributors.

Correspondence regarding accepted copy, proofs, and reprints should be directed to Editorial Processing Department, American Chemical Society, 20th and Northampton Sts., Easton, Pa. 18042. Head: CHARLES R. BERTSCH. Assistant Editor: EDWARD A. BORGER. Editorial Assistant: JOSEPH E. YURVATI.

Advertising Office: Centcom, Ltd., 142 East Avenue, Norwalk, Conn. 06851.

Business and Subscription Information

Send all new and renewal subscriptions *with payment* to: Office of the Controller, 1155 16th Street, N.W., Washington, D. C. 20036. Subscriptions should be renewed promptly to avoid a break in your series. All correspondence and telephone calls regarding changes of address, claims for missing issues, subscription service, the status of records, and accounts should be directed to Manager, Membership and Subscription Services, American Chemical Society, P.O. Box 3337, Columbus, Ohio 43210. Telephone (614) 421-7230.

On changes of address, include both old and new addresses with ZIP code numbers, accompanied by mailing label from a recent issue. Allow four weeks for change to become effective.

Claims for missing numbers will not be allowed (1) if loss was due to failure of notice of change in address to be received before the date specified, (2) if received more than sixty days from date of issue plus time normally required for postal delivery of journal and claim, or (3) if the reason for the claim is "issue missing from files."

Subscription rates (1974): members of the American Chemical Society, $20.00 for 1 year; to nonmembers, $60.00 for 1 year. Those interested in becoming members should write to the Admissions Department, American Chemical Society, 1155 Sixteenth St., N.W., Washington, D. C. 20036. Postage to Canada and countries in the Pan-American Union, $5.00; all other countries, $6.00. Air freight rates available on request. Single copies for current year: $3.00. Rates for back issues from Volume 56 to date are available from the Special Issues Sales Department, 1155 Sixteenth St., N.W., Washington, D. C. 20036.

Subscriptions to this and the other ACS periodical publications are available on microfilm. Supplementary material not printed in this journal is now available in microfiche form on a current subscription basis. For information on microfilm or microfiche subscriptions, write Special Issues Sales Department at the address above.

Notice to Authors last printed in the issue of December 6, 1973

THE JOURNAL OF

PHYSICAL CHEMISTRY

Volume 78, Number 2 January 17, 1974

JPCHAx 78(2) 93-202 (1974)
ISSN 0022-3654

ห้องสมุด กรมวิทยาศาสตร์ 1A
15 มี.ค. 2517

COMMUNICATIONS TO THE EDITOR

■ Supplementary material for this paper is available separately, in photocopy or microfiche form. Ordering information is given in the paper.

* In papers with more than one author, the asterisk indicates the name of the author to whom inquiries about the paper should be addressed.

AUTHOR INDEX

THE JOURNAL OF
PHYSICAL CHEMISTRY

Registered in U. S. Patent Office © Copyright, 1974 by the American Chemical Society

VOLUME 78, NUMBER 2 JANUARY 17, 1974

Low-Temperature Chemical Ionization Mass Spectrometry of Methane–Hydrogen Mixtures

Robert C. Pierce and Richard F. Porter*

Department of Chemistry, Cornell University, Ithaca, New York 14850 *(Received July 2, 1973)*

Publication costs assisted by the National Science Foundation

Low-temperature chemical ionization studies of dilute mixtures of CH_4(g) in D_2(g) have revealed new aspects of the mechanism for the proton transfer reaction $CH_4D^+ + CH_4 \rightarrow CH_3D + + CH_5^+$. The second-order rate constant measured under zero repeller field conditions and low source pressures of CH_4 is temperature independent from 83 to 155°K, indicating zero activation energy for the process. The rate constant decreases with increasing temperature between 155 and 300°K. For T (source) = 83°K, k_2 (second order) = (3.7 ± 1.0) × 10^{-9} cc/molecule sec, which is approximately two orders of magnitude higher than values reported for temperatures near 300°K. Enhancement of the rate of the proton transfer reaction at low temperatures is examined in terms of the effects of repeller fields and thermal energies of the reactants. The kinetics of the process at increased CH_4 densities is interpreted by a mechanism involving a limiting steady-state behavior with respect to CH_4D^+ ions. A detailed kinetic analysis of the proton transfer reaction involves consideration of the activated intermediate $[C_2H_8D^+]^*$.

Introduction

Thermoneutral proton transfer reactions of the type

$$ND_3H^+ + ND_3 \longrightarrow ND_2H + ND_4^+ \quad (1)$$

have long been of interest to investigators of ion–molecule reactions. Most of these bimolecular processes are fast in the ion–molecule sense ($k \approx 1 \times 10^{-9}$ cc/molecule sec).[1] Aquilanti and Volpi[2] observed the process

$$CH_4D^+ + CH_4 \longrightarrow CH_3D + CH_5^+ \quad (2)$$

in a high-pressure mass spectrometer study of D_2–CH_4 mixtures at 300°K. Lawrence and Firestone have investigated reaction 2 as the chain-propagating step, in radiation-induced exchange experiments of isotopic methanes at 298 and 195°K in the pressure range 0.85–0.95 atm.[3] The observed initial rates of CH_3D formation are equivalent at both temperatures and are consistent with a bimolecular rate constant, $k \approx 1 \times 10^{-12}$ cc/molecule sec in this regime. With a tandem in-line arrangement of two mass spectrometers Abramson and Futrell have determined the rate constant for the reaction

$$CD_5^+ + CH_4 \longrightarrow CH_4D^+ + CD_4 \quad (3)$$

of 3.3 × 10^{-11} cc/molecule sec at 300°K.[4] Chong and Franklin have found that high-pressure ion–molecule reactions of CH_4–CD_4 mixtures at ~400°K produce CD_4H^+ and CH_4D^+ in high concentrations.[5] Their ultimate analysis shows that reactions of the type 2 and 3 proceed at rate constants qualitatively in agreement with Futrell's value and that virtually all the methanium ions are formed through reactions of isotopic methane ions with methane.

The observation in our laboratory that reaction 2 proceeds more rapidly at low source temperatures than at room temperature stimulated the investigation which follows.

Experimental Section

The low-temperature chemical ionization source used in the present investigation has previously been described.[6] The mass analyzer is constructed from an Extranuclear 270-9 quadrupole spectrometer and a 24-stage Mg–Al particle multiplier. Details of its construction have also been considered previously.[6] The only noteworthy modification is the addition of a second 4-in. diffusion pump mounted to provide differential pumping for the ion source region.

Materials. Methane-d_4 (minimum isotopic purity of 99 atom % D) was obtained from Merck Sharp and Dohme.

All other gases were Matheson reagent grade. The gas purities were checked by running neat high-pressure spectra ($P_s \geq 0.20$ mm) of the reagents both at low and high temperatures and comparing the observed ion intensities with published spectra.

Procedure. The pressure (P_s) range of investigation was between 0.02 and 0.35 mm and the temperature range between 83 and 310°K. Premixed samples of CH_4:D_2 were employed in the dilution range 1:24 to 1:2600. Chemical ionization spectra of CH_4:H_2, CD_4:D_2, and CD_4:H_2 mixtures with molar compositions of 1:24 and 1:230 were also investigated. Spectra of CH_4:D_2 mixtures with compositions 1:99 and 1:49 were recorded at 84°K under source field strengths varying from 0 to 25 V/cm.

Results

The exothermic proton transfer reaction of H_3^+ to CH_4($\Delta H = -25$ kcal/mol) yields CH_5^+ and CH_3^+ (decomposition product of $[CH_5^+]^*$) as previously observed.[2] By increasing the source pressure from 0.05 to 0.20 mm the relative intensity of CH_3^+ is reduced considerably due to the enhanced collisional stabilization of $[CH_5^+]^*$. The secondary ions $C_2H_5^+$ and $C_2H_3^+$ appear in the more concentrated mixtures in low relative intensity as a result of secondary reactions involving ions formed by direct electron impact ionization of CH_4. As the ion source is cooled at constant pressure the CH_3^+ ion decreases in intensity relative to CH_5^+. At temperatures below 140°K ($P_s = 0.22$ mm) the $C_2H_9^+$ ion produced by the condensation reaction of CH_5^+ with CH_4 appears in low relative intensity.[7] The $C_2H_9^+$ intensity increases with decreasing source temperature to 80°K, the lowest temperature attainable experimentally. For a gas mixture of H_2:CH_4 = 24:1 at $P_s = 0.22$ mm the ratio $\Sigma I(CH_5^+)/\Sigma I_i$ was found to be constant within the limits 0.51 ± 0.05 in the temperature range 83–200°K.

In studies of CH_4:D_2 mixtures the formation of CH_5^+ at 290°K by reaction 2 is observed. The $I(CH_5^+)/I(CH_4D^+)$ ratio is relatively insensitive to temperature from 310 to 250°K. However at about 250°K the intensity of CH_5^+ increases as that of CH_4D^+ decreases until the source reaches 140°K; at lower source temperatures the $I(CH_5^+)/I(CH_4D^+)$ ratio approaches a limiting value of about 1.8. This behavior and that observed for a CD_4–H_2 mixture is indicated in Figure 1. Apparent multiple proton transfer processes are not observed within the limits of our sensitivity.

Experimental ion intensity measurements for the CH_4–D_2 system over a wide range of composition are indicated in Figure 2. In Figure 3 are shown data illustrating the effect of composition as gas mixtures become more concentrated in CH_4. It is significant to note that for all compositions of D_2:CH_4 greater than 100:1 at least 99% of the total ionization is accounted for by the major ions D_3^+, CH_5^+, and CH_4D^+ and smaller contribution from D_5^+ (ions formed by electron impact of CH_4 under these conditions are negligible).

The effect of pressure on the ion intensity ratio $I(CH_5^+)/I(CH_4D^+)$, observed for a gas mixture with composition CH_4:D_2 = 1:196 is shown in Figure 4. Under these conditions the relative hydrocarbon intensities are sufficiently large for high precision measurements. It should be noted that in the pressure dependence data (Figure 4) at any source pressure above 0.15 mm the ratio $\Sigma[I(CH_4D^+) + I(CH_5^+)]/\Theta I_i$ is constant within experimental observation. The effect of temperature on the relative intensities of

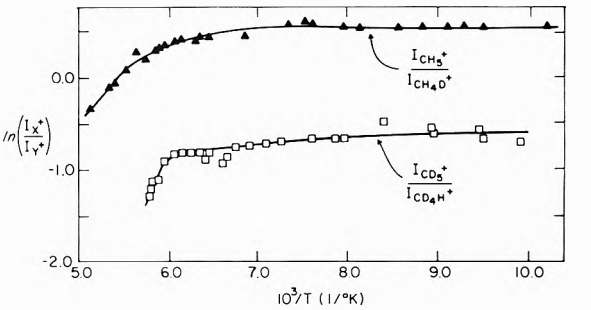

Figure 1. Semilog plots of $I(CH_5^-)/I(CH_4D^+)$ and $I(CD_5^+)/I(CD_4H^+)$ *vs.* $10^3/T$: sample compositions, CH_4:D_2 = 1:24 (P_s = 0.22 mm) and CD_4:H_2 = 1:250 (P_s = 0.16 mm), respectively; field strength (E) = 10.0 V/cm.

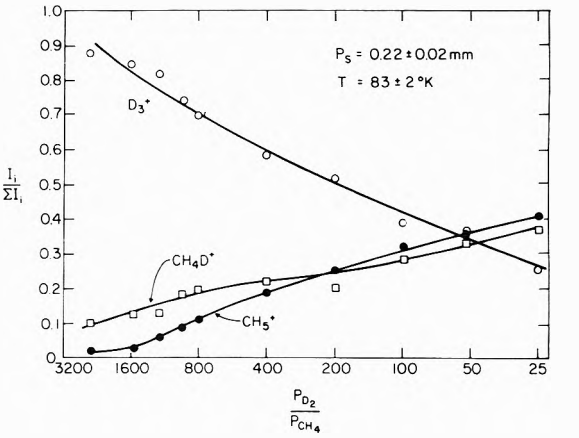

Figure 2. Relative intensities of major ions in CI spectra of CH_4–D_2 mixtures as a function of sample composition (E = 10.0 V/cm).

methanium ions observed with CH_4–D_2 and CD_4–H_2 mixtures is shown in Figures 1 and 5, respectively.

Discussion

The absence of $C_2H_3^+$ or $C_2H_5^+$ in the chemical ionization spectra of dilute mixtures of CH_4 in D_2 indicates that processes due to ions arising from electron impact of methane, *i.e.*

$$CH_4^+ + CH_4 \longrightarrow CH_3 + CH_5^+ \qquad (4)$$

are of minor importance. As indicated in Table I processes involving CH_3^+ by primary ionization do lead to production of $C_2H_5^+$ ions in low relative abundance. However, under these conditions the intensity of CH_5^+ due to reaction 4 is but a minor fraction of the total CH_5^+ intensity. In these systems the higher proportions of the mixed isotopic species ($C_2H_4D^+$, etc.) arise predominantly from the processes

$$CH_3^+ + D_2 \rightarrow \begin{matrix} CH_2D^+ & HD \\ + & \\ CHD_2^+ & H_2 \end{matrix} \qquad (5)$$

$k = 1.7 \times 10^{-10}$ cc/molecule sec

$$CH_2^+ + D_2 \rightarrow \begin{matrix} CHD^+ & HD \\ + & \\ CD_2^+ & H_2 \end{matrix} \qquad (6)$$

$k = 3.1 \times 10^{-10}$ cc/molecule sec

and subsequent reaction of the product ions with CH_4.[8]

Reactions of the type

TABLE I: Mass Spectra of Isotopic Methane–Hydrogen Mixtures

m/e	Ion	$I_i/\Sigma I_i$	m/e	Ion	$I_i/\Sigma I_i$
$CH_4:H_2$ = 1:24		P_S = 0.22 mm, T = 83°K	$CD_4:D_2$ = 1:24		P_S = 0.22 mm, T = 83°K
3	H_3^+	0.3360	6	D_3^+	0.2150
15	CH_3^+	0.0046	18	CD_3^+	0.0442
16	CH_4^+	0.0026	20	CD_4^+	0.0342
17	CH_5^+	0.5100	21	CD_4H^+	0.0526
29	$C_2H_5^{+a}$	0.0987	22	CD_5^+	0.4270
33	$C_2H_9^+$	0.0407	30	$C_2D_3^{+a}$	0.0493
			34	$C_2D_5^+$	0.0920
			41	$C_2D_8H^+$	0.0177
			42	$C_2H_9^+$	0.0664
$CH_4:D_2$ = 1:24		P_S = 0.23 mm, T = 83°K	$CD_4:H_2$ = 1:24		P_S = 0.22 mm, T = 83°K
6	D_3^+	0.2400	3	H_3^+	0.3120
16	CH_4^+	0.0409	20	CD_4^+	0.0372
17	CH_5^+	0.4000	21	CD_4H^+	0.3140
18	CH_4D^+	0.2530	22	CD_5^+	0.2140
			29	$C_2D_3H^{+a}$	0.0021
29	$C_2H_5^+$	0.0131	30	$C_2D_3^+$	0.0215
30	$C_2H_4D^{+a}$	0.0108	31	$C_2D_3H^+$	0.0081
31	$C_2H_3D_2^+$	0.0149	32	$C_2D_3H_2^+$	0.0216
32	$C_2H_2D_3^+$	0.0090	33	$C_2D_4H^+$	0.0178
33	$C_2H_9^+$	0.0141	34	$C_2D_5^+$	0.0089
34	$C_2H_8D^+$	0.0021	41	$C_2D_8H^+$	0.0089
			42	$C_2D_9^+$	0.0238

[a] Possible minor contributions from N_2D^+ or N_2H^+ impurities.

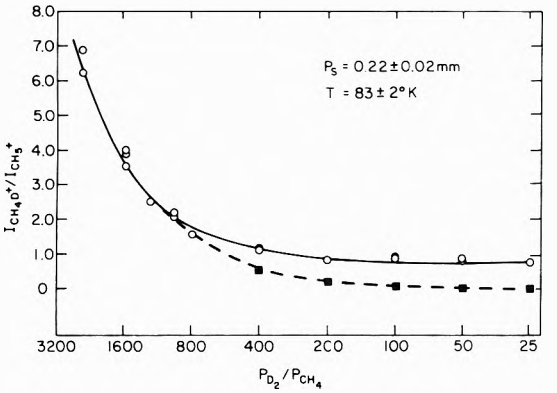

Figure 3. The ratio $I(CH_4D^+)/I(CH_5^-)$ for CH_4–D_2 mixtures as a function of sample composition (E = 10.0 V/cm): experimental points (O) and calculated values (■) (representing second-order kinetic behavior in the limiting region).

$$CH_5^+ + D_2 \longrightarrow CH_4D^+ + HD \qquad (7)$$

in principle can account for substantial ion interconversion. Numerous workers[8-10] have demonstrated that this reaction does not occur however to a noticeable degree in a high-pressure ionization source at high temperatures. We rule this out as a possible reaction for CH_5^+ consumption at 83°K since the CH_5^+ precursor, CH_4D^+, is not observed to undergo exchange with D_2 to form $CH_3D_2^+$. The occurrence of reaction 7 at 83°K is hence also considered to be unlikely.

Kinetic Analysis. For the kinetic analysis of reaction 2, we will discuss separately results for two experimental regimes. The following reaction sequence will be referred to in our kinetic analysis.

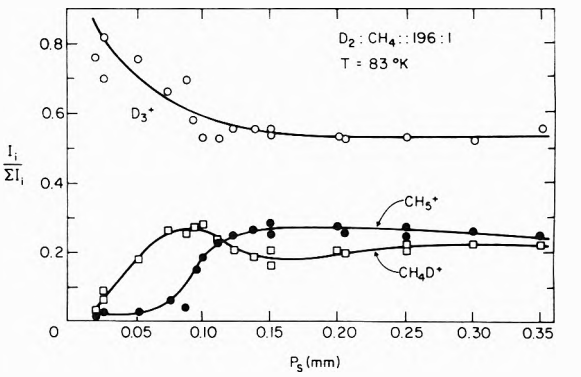

Figure 4. Relative intensities of major ions in the CI spectra of CH_4–D_2 as a function of source pressure (E = 10.0 V/cm).

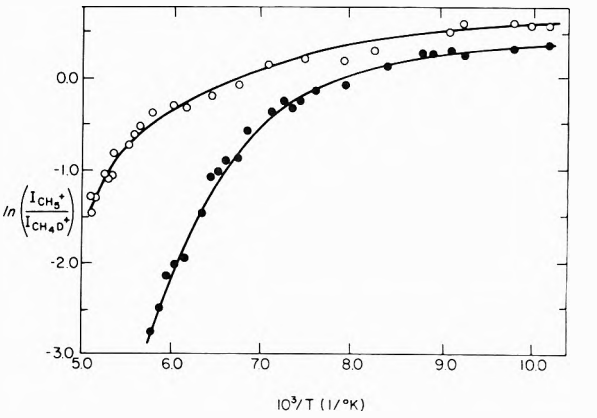

Figure 5. Semilog plots of $I(CH_5^+)/I(CH_4D^+)$ *vs.* $10^3/T$: sample compositions, CH_4:D_2 = 1:240 (P_S = 0.15 mm); E = (●) 10 V/cm and (O) 0.0 V/cm.

$$D_2^+ + D_2 \xrightarrow{k_0} D_3^+ + D \qquad (8)$$

$$D_3^+ + CH_4 \xrightarrow{k_1} D_2 + CH_4D^+ \qquad (9)$$

$$CH_4D^+ + CH_4 \xrightarrow{k_2} CH_3D + CH_5^+ \qquad (2)$$

$$CH_4D^+ + CH_4 \xrightarrow[D_2]{k_3} C_2H_8D^+ \qquad (10)$$

$$CH_5^+ + CH_4 \xrightarrow[H_2]{k_4} C_2H_9^+ \qquad (11)$$

The second-order rate constant k_0 reported at 300°K is 1.44×10^{-9} cc/molecule sec.[11] The rate constant k_1(H), obtained by Burt, *et al.*, for the reaction $H_3^+ + CH_4 \rightarrow H_2 + CH_5^+$ at 298°K is 1.6×10^{-9} cc/molecule sec.[12] An exponential decrease in $I(D_3^+)$ for very dilute mixtures of CH_4–D_2 is observed as noted in Figure 2. In that range of composition where $I(CH_5^+)$ is negligible and CH_4 is consumed by reaction 9 alone a determination of k_1(D) may be made if the mean residence time (τ_r) of the D_3^+ ions can be determined. The mean drift velocity of an ion in a region of high E/P (region of experimental measurements) has been calculated by Wannier.[13] Wannier predicts that

$$\tau_r = \frac{d}{\langle v_d \rangle} = \frac{2\pi d P(\mu\alpha)^{1/2}}{0.9048EkT} \qquad (12)$$

where d is distance from the electron beam to the ion exit hole in cm, P is the source pressure in dynes/cm², μ is the reduced mass of the ion and D_2 molecule in grams, α is the polarizability of the neutral gas in cc, E is the field strength in statvolts/cm, k is Boltzmann's constant, and T is in °K. Using d = 0.50 cm, $P = 2.92 \times 10^2$ dyn/cm², μ

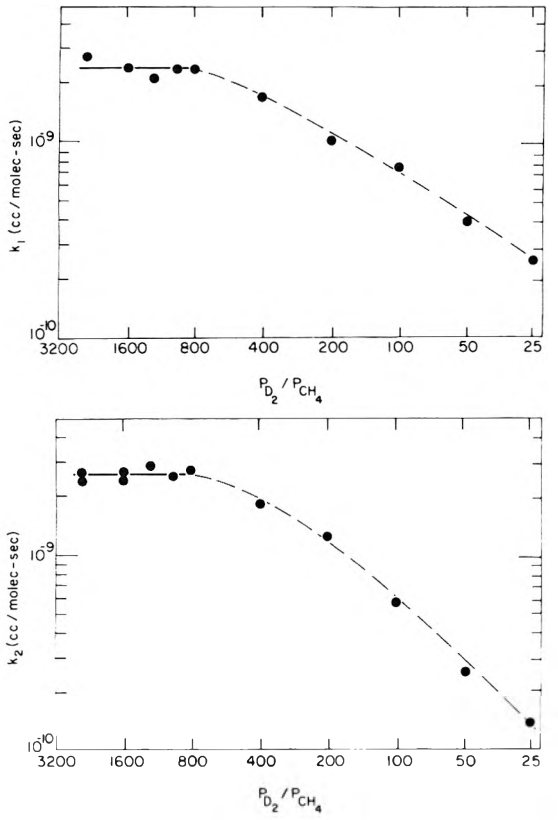

Figure 6. Values of k_1 and k_2 as a function of sample composition (true rate constants are indicated by solid lines).

$= 4.00 \times 10^{-24}$ g, $\alpha = 0.79 \times 10^{-24}$ cc, $E = 3.3 \times 10^{-2}$ statvolts/cm, and $T = 83°K$ we obtain $\tau_r(D_3^+) = (4.70 \pm 0.40) \times 10^{-6}$ sec.

Use of the pseudo-first-order relationship

$$k_1(D) = \frac{RT}{P(CH_4)}\left(\frac{1}{\tau_r(D_3^+)}\right)\left[-\ln\frac{I(D_3^+)}{I^0(D_3^+)}\right] \qquad (13)$$

allows us to evaluate $k_1(D)$ at 83°K (see Figure 6). For the range of dilute composition we find $k_1(D) = (2.4 \pm 0.2) \times 10^{-9}$ cc/molecule sec which, when corrected for isotopic factors, yields $k_1(H) = (3.3 \pm 0.2) \times 10^{-9}$ cc/molecule sec. Comparison of this result with that obtained at 298°K shows that k_1 is not strongly dependent on temperature; we expect that k_0 behaves similarly.

Proton Transfer Mechanism at Low Methane Density. In Figure 3 a plot of the ion current ratio $I(CH_4D^+)/I(CH_5^+)$ *vs.* $P(D_2)/P(CH_4)$ indicates that reaction 2 follows second-order behavior for very dilute mixtures of CH_4 in D_2. Deviation from second-order behavior is noted for mixtures of D_2:CH_4 with compositions less than 800:1 (compare experimental data with extrapolated curve in Figure 3). In the limit of low partial pressure of CH_4, reaction 2 is the rate-limiting step and evaluation of k_2 may be made through the relationship

$$k_2 = \frac{RT}{P(CH_4)}\left(\frac{1}{\tau_r(CH_4D^+)}\right)\left[-\ln\frac{I(CH_4D^+)}{I^0(CH_4D^+)}\right] \qquad (14)$$

From eq 12 we obtain for the CH_4D^+ residence time, $\tau_r = (5.50 \pm 0.40) \times 10^{-6}$ sec. This leads to a value of k_2 for reaction 2 of $(2.7 \pm 0.2) \times 10^{-9}$ cc/molecule sec. The true CH_4D^+ residence time is probably slightly shorter than that calculated from eq 12 since the average drift distance for a CH_4D^+ ion is expected to be shorter than that assumed from the source geometry. Thus the true value of

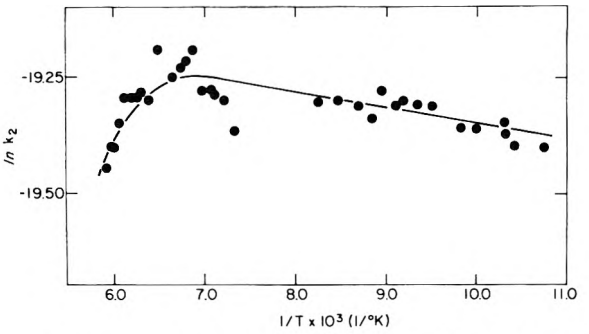

Figure 7. Arrhenius plot for k_2: CH_4:D_2 = 1:1000, E = 0.0 V/cm.

k_2 is probably slightly greater than that calculated. An alternate procedure for calculation of k_2 will be discussed subsequently.

Analysis of zero field data in the regime where reaction 2 is the rate-limiting step in the proton transfer analysis indicates that k_2 has essentially zero activation energy (from Figure 7 $\Delta E = +0.06 \pm 0.10$ kcal/mol from 83 to 155°K). Thus at higher temperatures the reduced reaction rate must reflect temperature-dependent preexponential factors in the rate constant. In the region of low temperature where the ratios of CH_5^+/CH_4D^+ approach a constant value (Figures 1 and 5) we observe k_2 attaining a collisionally limited maximum value.

Proton Transfer Mechanism at High CH_4 Densities. As the CH_4 density in the ion source is increased (Figure 3), the rate of production of CH_4D^+ through reaction 9 approaches the rate of disappearance of CH_4D^+ through reaction 2. Under these conditions we expect the intensity CH_4D^+ to reach a steady-state value with respect to source pressure above a minimum value when the ratio of CH_4 to D_2 in the gas mixture is constant (Figure 4). At high source pressures and increased ion drift distances (or longer ion residence times) a steady-state condition for CH_4D^+ should be determined by equating the rates of reactions 9 and 2. In the limit of high ion residence times this leads to the approximate expression

$$k_2/k_1 \approx I(D_3^+)/I(CH_4D^+) \qquad (15)$$

From the data in Figure 4 we obtain $k_2/k_1 \approx 2.0$ and from the data in Table I we obtain $k_2/k_1 \approx 1.0$. Although these results can not be taken to give an accurate value for k_2, they do indicate that k_2 and k_1 are nearly equal in magnitude at 83°K. We thus set $k_2 = (3.7 \pm 1.0) \times 10^{-9}$ cc/molecule sec.

Temperature Dependence Measurements. Explanation of the enhancement of reaction 2 with decreasing temperature involves a detailed kinetic analysis of the microscopic processes represented on the macroscopic scale by k_2. Reaction 2 may be viewed as the complex process

$$CH_4D^+ + CH_4 \underset{k_{-11}}{\overset{k_{11}}{\rightleftharpoons}} [C_2H_8D^+]^* \longrightarrow CH_5^+ + CH_3D \qquad (16)$$

with deactivation

$$[C_2H_8D^+]^* + M \longrightarrow C_2H_8D^+ + M \qquad (17)$$

Energetics of complex formation enter into the analysis of the complex lifetime and its decomposition mechanism. The results of experimental measurements of mean ion energies in chemical ionization sources indicate that the relative kinetic energy of reactant ion and molecule is at most four times the total internal energy under our oper-

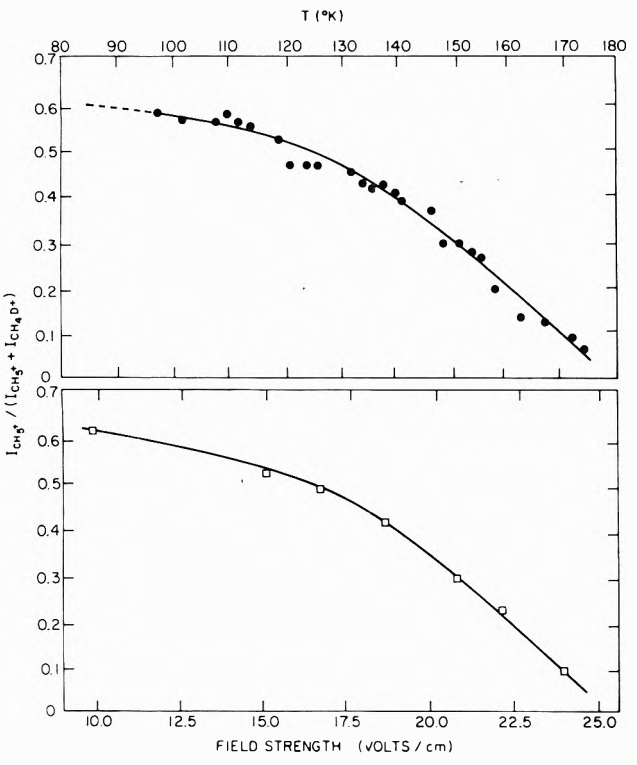

Figure 8. The ratio $I(CH_5^+)/[I(CH_5^+) + I(CH_4D^+)]$ *vs.* T and field strength at P_s = 0.15 mm: sample compositions, (●) CH_4:D_2 = 1:240 (E = 10.0 V/cm) and (□) D_2:CH_4 = 200:1 (T = 84°K), respectively.

ating conditions.[14] At 83°K the internal energy of the reactants is about 0.11 eV and hence the upper limit for their relative kinetic energy is about 0.44 eV. With this information a rough estimate of the lifetime of the intermediate $[C_2H_8D^+]^*$ may be attempted by application of RRK theory.[15] The lifetime is represented by

$$\tau = 10^{-13}[(E - E^*)/E]^{1-S} \text{ sec} \qquad (18)$$

where S is the number of "active" vibrational modes of the complex, E is the sum of the relative energy and internal energy of the reactants, and the $|\Delta H|$ for the condensation reaction, and finally E^* is the threshold energy for complex decomposition. The values of $|\Delta H|$ and E^* were taken as 0.17 eV;[7] the maximum S is 27. For relative kinetic energies less than 0.44 eV τ is calculated. As the kinetic energy of CH_4D^+ decreases toward the thermal limit τ increases to about 10^{-6} sec for a source temperature of 83°K.

In reviewing the data it is now evident that proton transfer occurs only in those processes where CH_4D^+ plus CH_4 yield a long-lived $[C_2H_8D^+]^*$. It is through this complex that the transfer occurs. In proposing the following structure for $[C_2H_8D^+]^*$ we see two possible reaction pathways. Structure 19a on statistics alone should represent 20% of all complexes and structure 19b 80% if H and D attach are equally probable. Activated decomposition of these complexes should yield for (19a) purely CH_4D^+ plus CH_4 by rupture of the three center bond and for (19b) a mixture of $CH_4D^+ + CH_4$ and $CH_5^+ + CH_3D$. Correlation of the low-temperature limiting behavior of the $I(CH_5^+)/I(CH_4D^+)$ ratio to the decomposition mechanism in-

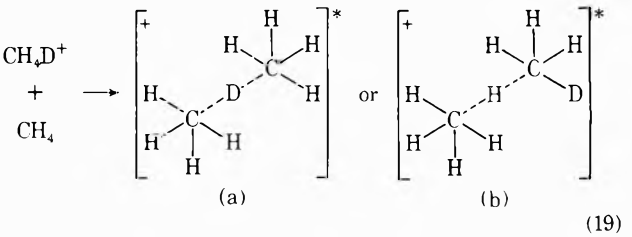

(19)

volves a detailed analysis of the kinetic factors governing CH_5^+ and CH_4D^+ production. At higher temperatures we merely see the effects of diminished complex formation and hence lower incidence of complex decomposition to yield the CH_5^+ ion. Under conditions in which complex formation approaches high efficiency (*i.e.*, low temperature and high gas densities) it is anticipated that the complex decomposition will govern the observed $I(CH_5^+)/I(CH_4D^+)$ ratio. For increasingly more dilute mixtures the extent of complex formation decreases due to the decreased CH_4D^+–CH_4 collision number.

As the data in Figure 8 show, an increase in source repeller field results in a decrease in the rate of proton transfer from CH_4D^+ to CH_4 (reaction 2). The effect is too large to be ascribed solely to lowering of the ion residence time at higher fields. As noted in Figure 8, the effect of repeller field parallels roughly that due to temperature. Since the initial kinetic energy of a reacting CH_4D^+ ion is important considering the mechanism of proton transfer, the effect of repeller field is not surprising. The dramatic curvature in the temperature dependence measurements, obtained with zero and nonzero field conditions (Figure 5), reveals the combined effects of repeller field and temperature on the rate of reaction 2. At low temperatures efficient quenching of the kinetic energy of CH_4D^+ arising from thermal and electrostatic effects is apparent.

Acknowledgment. We are grateful for support by the Army Research Office—Durham, North Carolina, and the National Science Foundation (Grant No. GH 33637) through the Materials Science Center, Cornell University.

References and Notes

(1) M. S. B. Munson and F. H. Field, *J. Amer. Chem. Soc.*, **87**, 4242 (1965).
(2) V. Aquilanti and G. G. Volpi, *J. Chem. Phys.*, **44**, 2307 (1966).
(3) R. H. Lawrence, Jr., and R. F. Firestone, *J. Amer. Chem. Soc.*, **87**, 2288 (1965).
(4) F. P. Abramson and J. H. Futrell, *J. Chem. Phys.*, **45**, 1925 (1966).
(5) Shuang-Ling Chong and J. L. Franklin, *J. Chem. Phys.*, **55**, 641 (1971).
(6) R. C. Pierce and R. F. Porter, *J. Amer. Chem. Soc.*, **95**, 3849 (1973).
(7) F. H. Field and D. P. Beggs, *J. Amer. Chem Soc.*, **93**, 1585 (1971).
(8) M. S. B. Munson, F. H. Field, and J. L. Franklin, *J. Amer. Chem. Soc.*, **85**, 3584 (1963).
(9) T. H. Pratt and R. Wolfgang, *J. Amer. Chem. Soc.*, **83**, 10 (1961).
(10) S. Wexler, *J. Amer. Chem. Soc.*, **85**, 272 (1963).
(11) B. G. Ruben and L. Friedman, *J. Chem. Phys.*, **37**, 1636 (1962).
(12) J. A. Burt, J. L. Dunn, M. J. McEwan, M. M. Sutton, A. E. Roche, and H. I. Schiff, *J. Chem. Phys.*, **52**, 6062 (1970).
(13) G. H. Wannier, *Bell Syst. Tech. J.*, **23**, 170 (1953).
(14) G. G. Meisels, C. Chang, J. A. Taylor, and G. J. Sroka, Abstracts, 20th Annual Conference on Mass Spectrometry and Allied Topics, Dallas, Tex., June 1972, p 331.
(15) H. S. Johnston, "Gas Phase Reaction Rate Theory," Ronald Press, New York, N. Y., 1966.

Photolysis of 2-Methyl-1-butene at Photon Energies below and above the Ionization Energy

Hélène Gagnon, Guy J. Collin,* and Claude Bertrand

Département des Sciences Pures, Université du Québec à Chicoutimi, Chicoutimi, Québec, Canada GFH 2B1

(Received February 2, 1973; Revised Manuscript Received October 24, 1973)

Publication costs assisted by département des Sciences Pures, UQC, Chicoutimi, Quebec, Canada

We have studied the fragmentation of the 2-methyl-1-butene molecule at 8.4 eV which essentially leads to the formation of allene, isoprene, and ethylene as well as methyl, *tert*-pentyl (addition of the hydrogen atom to the double bond), and ethyl radicals. The measured k_d/k_c (methyl/*tert*-pentyl) ratio is of the order of 1.6 ± 0.2. The isomerization of the excited molecule is a negligible process, at least between 0.05 and 200 Torr (6.6–26,000 Nm^{-2}). The above characteristics are found at 10.0 and at 11.6–11.8 eV with, in addition, the formation of 2-methyl-2-butene. The data suggest that an ionic mechanism is probably involved in the formation of this compound. At 10.0 eV the ion quantum yield is 0.20_7 ± 0.005 and at 11.6–11.8 eV it is $0.33 \pm 0.01_5$.

Introduction

Although photochemical studies of simple olefins are plentiful in the near-ultraviolet and in the vacuum ultraviolet,[1-5] the C_5 olefins have not been subjected to systematic research except in rare cases.[2b,c,6] Recently, we studied the photochemistry of normal pentene[7] and we also began a study of *cis*-2-pentene.[8] This article which deals with the photolysis of 2-methyl-1-butene at 8.4, 10.0, and 11.6–11.8 eV emphasizes mainly (1) the fragmentation reactions of the excited and superexcited molecules; (2) the fragmentation of pentyl radicals formed by the addition of a hydrogen atom to the double bond; and (3) the possible ionic reactions.

Experimental Section

Most of the experimental techniques have already been described.[5,7] The krypton lamp is equipped with a CaF_2 window which cuts out the 116.5-nm line. The argon lamp (11.6–11.8 eV) has also been described in the literature.[9] The 2-methyl-1-butene was an API product (99.90 ± 0.08%) previously degassed under high vacuum and at a low temperature. The analysis of the starting material shows only the presence of isoprene (0.024%), 1-pentene (0.020%), and 2-methyl-2-butene (0.046%). The actinometry was carried out by comparing the yields obtained to those of the products of the photochemistry of isobutene in similar conditions for the three lamps at 1.0 and 10 Torr.[4,10] The separation of 1-butene from isobutene was accomplished on a column of *n*-octane/Porasil C 120/150 mesh (Chromatographic Specialities Ltd.).

Results

The irradiation of 2-methyl-1-butene gives a linear graph for the yields of all products against time (Figures 1 and 2). Thus, providing that the percentage of transformation of the monomer remains less than 1%, one might ignore the reactions involving the products resulting from the fragmentation of the monomer. In the presence of oxygen (5%), the isobutene quantum yield increases sharply at lower pressures. Other quantum yields do not appear to be affected by the pressure, at least between 13 and 1330 Nm^{-2}. At 8.4 eV, the quantum yields of the C_5H_{10} products are negligible: $\Phi(C_5H_{10}) \leq 0.005$ (Table I). At 10.0 eV and at 11.6–11.8 eV, the quantum yields and distribution of the products are similar to those obtained at 8.4 eV, even in the presence of oxygen (Table II). Table III shows the yields of the higher boiling compounds formed when oxygen is not present. The quantum yield of 2-methyl-2-butene, formed in the presence of oxygen, is also sensitive to various additives (Table IV).

The ion current formed during the 10.0- and the 11.6–11.8-eV photolysis was recorded at several pressures between 40 and 1330 Nm^{-2} (0.3–10 Torr), and compared with the ion current obtained for isobutene: $\Phi_{10.0}(\text{ion}) = 0.207$[10] and $\Phi_{11.6\text{-}11.8}(\text{ion}) = 0.31$.[4] Results are shown at 10.0 eV (Figure 3), and similar results were found at 11.6–11.8 eV. Independent use was made of the two cells of a double cell, such as described in ref 9.

Discussion

A. Radical Reactions. The presence of oxygen in the sample has an important effect on the yields of methane, ethane, propane, etc. (Tables I–III). Mainly, if not completely, these products are formed by a radical mechanism. The ethane is formed completely by the combination of two methyl radicals since there is no formation of *n*-butane. The 2,2-dimethylbutane is formed by the combination of methyl and *tert*-pentyl radicals whereas the latter are formed by the addition of a hydrogen atom to the double bond of the monomer. Although the ratios of the rate constants of reactions 1a, 1b, and 1c are not known, reaction 1a might be considered insignificant and from what is known of the 1-butene and 2-butene systems, k_{1a}/k_1 is of the order of 0.02.[11] Reaction 1c is probably of lesser importance[12] still. Therefore, as a first approximation, one might consider that all the thermal hydrogen atoms add to the terminal methylene group of the monomer. At 8.4 eV, 3-methylpentane, which should be formed by the combination of the methyl and the $C_2H_5CH(CH_3)CH_2$ radicals, is a minor product. At 10.0 eV, its quantum yield is 0.01_3. Taking into account the yield of 2,2-dimethylbutane, this indicates (all things being equal) that at 8.4 eV the k_{1c}/k_{1b} ratio is less than or equal to 0.02; at 10.0 eV the same ratio is equal to 0.12.

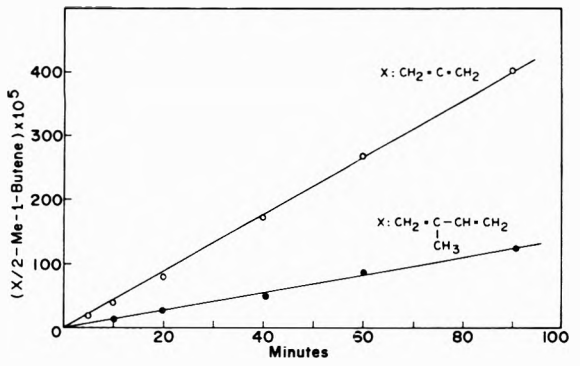

Figure 1. Relative yields of decomposition products *vs.* irradiation time: incident energy 8.4 eV; total pressure 22,160 Nm^{-2} (2-methyl-1-butene 175 Nm^{-2}; O_2 10 Nm^{-2}; balance helium).

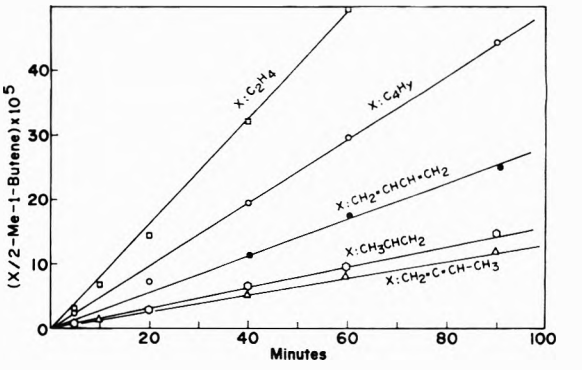

Figure 2. Relative yields of decomposition products *vs.* irradiation time. Incident energy and total pressure the same as in Figure 1: C_4H_8 = 1-C_4H_8 + *i*-C_4H_8 + 1,3-C_4H_6.

TABLE I: Photolysis of 2-Methyl-1-butene at 8.4-eV Ionization Energy

2-Methyl-1-butene[a]	230–665	1330	133	44	6.6–7.6
O_2[a]	10–33		6.6		
He[a]	76,000				
Irradiation time[b]	30–330	30	60	15	15
% transformation[c]	0.9[d]	0.75	1.6	3.0	7.5
Methane	0.03[e]	0.14	0.04	*f*	*f*
Acetylene	0.006	0.01	0.009	0.005	0.007
Ethylene	0.088	0.11	0.090	0.077	0.10
Ethane	0.006	0.55	0.044[g]	0.49	0.83
Propene	0.017	0.027	0.032	0.068	0.05
Propane	0.002	0.06	0.004	0.11	0.16
Propyne	0.06	0.07	0.083		0.09
Propadiene	0.45	0.45	0.45	0.45	0.45
1-Butene	0.003	0.02	0.015		0.04
Isobutene	0.02	0.06	0.10	0.16	0.50
1,3-Butadiene	0.032	0.02	0.02		0.02
1,2-Butadiene	0.014	0.012	0.013	0.011	0.01
Isoprene	0.15	*f*	*f*	*f*	*f*

[a] In Nm^{-2}. [b] In minutes. [c] % transformation = (C_2 + C_3 + C_4 + C_5) × 100/[2-methyl-1-butene]. [d] Six analyses between 30 and 330 min, final value. [e] Quantum yields. [f] Not measured. [g] Ethane yield decreases at higher oxygen concentration.

The increase in this ratio is in agreement with the observations already made with other systems.[5,8] At least at 10.0 eV a fraction of the hydrogen atoms do not behave like thermal atoms. The *tert*-pentyl radicals which are formed in reaction 1b have sufficient internal energy to decompose at low pressures.[13]

$$H + C_2H_5C(CH_3)=CH_2 \longrightarrow H_2 + C_5H_9 \quad (1a)$$

$$H + C_2H_5C(CH_3)=CH_2 \longrightarrow (C_2H_5C(CH_3)_2)^* \quad \Delta H = -39 \text{ kcal mol}^{-1} \quad (1b)$$

$$H + C_2H_5C(CH_3)=CH_2 \longrightarrow (C_2H_5CH(CH_3)CH_2)^* \quad (1c)$$

$$(C_2H_5C(CH_3)_2)^* \longrightarrow CH_3 + i\text{-}C_4H_8 \quad (2)$$

$$(C_2H_5C(CH_3)_2)^* + M \longrightarrow C_2H_5C(CH_3)_2 + M \quad (3)$$

However, this fragmentation is competing with stabilization by collision. The yield of isobutene depends upon the pressure (Table I). The same holds true for methyl and *tert*-pentyl radicals. At pressures over 1330 Nm^{-2} (10 Torr), the majority if not all of the *tert*-pentyl radicals are stabilized by collision.[13] Although the formation of the unsaturated radicals (vinyl, allyl, etc.) is not apparent, these might, if they are formed, react rapidly with the monomer, therefore, not giving rise to radical–radical reactions. Such being the case, the only radical–radical

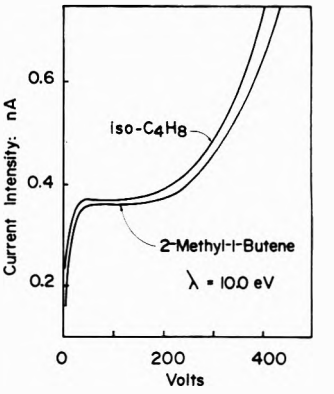

Figure 3. Saturation current *vs.* voltage obtained during the irradiation of isobutene and 2-methyl-1-butene at 123.6 nm. The incident intensity of the krypton lamp was kept constant.

type reactions to be considered are those involving the methyl, ethyl, and *tert*-pentyl radicals.

$$CH_3 + CH_3 \longrightarrow C_2H_6 \quad (4)$$

$$CH_3 + C_2H_5 \longrightarrow C_3H_8 \quad (5)$$

$$CH_3 + t\text{-}C_5H_{11} \longrightarrow CH_4 + C_5H_{10} \quad (6a)$$

$$CH_3 + t\text{-}C_5H_{11} \longrightarrow C_2H_5C(CH_3)_3 \quad (6b)$$

$$2t\text{-}C_5H_{11} \longrightarrow C_5H_{10} + i\text{-}C_5H_{12} \quad (7a)$$

$$2t\text{-}C_5H_{11} \longrightarrow \begin{matrix} & C & C & & \\ & | & | & & \\ C-C- & C & - & C- & C-C \\ & | & | & & \\ & C & C & & \end{matrix} \quad (7b)$$

The other disproportionation and combination reactions are insignificant due to either the low yield of the radicals involved or the small rate constants.[14] It has been shown that the methylbutenes, formed in reactions 6a and 7a, consist of three 2-methyl-1-butene and one 2-methyl-2-butene molecules.[15] The quantum yield Φ(reactions 6a + 6b) equals 0.20 ± 0.05 at 8.4 eV. According to the different yields measured, the calculated k_{6a}/k_{6b} ratio is 1.6 ± 0.2.[16] This value is close to that reported in the photolysis of trimethylethylene.[17] The C_6 olefins may be formed by at least two mechanisms: the first involving the methyl and the substituted butenyl radicals, the second involving the singlet methylene radical and the monomer. In vacuum ultraviolet photochemistry, methylene radicals are produced in the singlet state.[18] One may assign a limiting

Table II: Quantum Yields in the Photolysis of 2-Methyl-1-butene above Ionization Energy

2-Methyl-1-butene[a]	1330	1330	133	133	6.6	1330	1330	133	133	8.0
O_2[a]	66		10			66		10		
Incident energy	10.0	10.0	10.0	10.0	10.0	11.7	11.7	11.7	11.7	11.7
Methane	0.078	0.15	0.024	0.15	0.195	0.043	0.127	0.022	0.177	0.215
Acetylene	0.013	0.005	0.01	0.008	0.024	0.008	0.009	0.009	0.011	0.017
Ethylene	0.092	0.08	0.115	0.083	0.105	0.072	0.073	0.093	0.12	0.092
Ethane	0.009	0.45	0.028[d]	0.494	0.67	0.007	0.205	0.005	0.50	0.35
Propene	0.018	0.02	0.021	0.024	0.030	0.013	0.017	0.015	0.033	0.31
Propane	0.04	0.062	0.00	0.05	0.097	0.028	0.05	0.004	0.088	0.075
Propyne			0.06	0.06				0.02	0.025	
Propadiene	0.32	0.32	0.32	0.32	0.32	0.25	0.25	0.25	0.25	0.25
C_4H_y[b]	c	0.062	0.11	0.11	0.35	0.045	0.048	0.12	0.163	0.263
1,2-Butadiene	0.023	c	0.022	0.020	0.03	0.015	0.017	0.016	0.026	0.031
2-Methyl-2-butene	0.46	c	0.35	0.515	0.50	1.54	1.84	0.275	0.79	0.42
Isoprene	c	c	c	0.10	0.08	c	c	0.06	0.05	c

[a] In Nm^{-2}. [b] 1-Butene + isobutene + 1,3-butadiene. [c] Not measured. [d] Ethane quantum yield decreases at higher oxygen concentration.

TABLE III: Photolysis of 2-Methyl-1-butene at 8.4 and 10.0 eV[a]

2-Methyl-1-butene, Nm^{-2}	1750	1330
Incident energy, eV	8.4	10.0
Isopentane	0.07[b]	0.057
2-Methyl-2-butene	0.05	0.246
2,2-Dimethylbutane	0.16	0.107
1-Methyl-1-ethylcyclopropane	0.012	0.006
2,3-Dimethyl-1-butene	0.012	0.015
2-Methyl-1-pentene	0.03	0.03
3-Methylpentane	0.002	0.013
2-Ethyl-1-butene	0.04	0.037
3-Methyl-2-pentene (cis + trans)	0.005	0.02
3,3-Dimethylpentane[d]	0.02	d
C_{10}[c]	0.04	d

[a] All yields are 0.00 in the presence of 5% added oxygen with the exception of 2-methyl-2-butene in the krypton photolysis (see Table II). [b] Quantum yields. [c] Uncertain retention time. [d] Not measured.

TABLE IV: Irradiation of 2-Methyl-1-butene at 10.0 eV[a]

Additive (%)	Φ(2-methyl-2-butene)
	0.35
SF_6 (5,10)	0.245, 0.227
N_2O (5)	0.27
C_7H_8[b] (5,10)	0.23, 0.25
NH_3(5,10)	0.166, 0.162
$CH_3C_6H_9$[c] (5,10)	0.30, 0.20[d]

[a] 2-Methyl-1-butene pressure; 133 Nm^{-2} (1.0 Torr) in all the experiments; 5% oxygen added; irradiation time, 30 min. [b] Toluene. [c] Methylcyclopentane. [d] In this experiment the isopentane yield is lower than 0.02.

value of 0.02 to the yield of the methylene radicals, since the yield of 1-methyl-1-ethylcyclopropane is zero in the presence of oxygen.[19] The substituted butenyl radicals are formed by at least two mechanisms

$$C_2H_5C(CH_3)=CH_2 + h\nu \longrightarrow H + C_5H_9 \quad (8)$$

$$C_2H_5C(CH_3)=CH_2 + R \longrightarrow RH + C_5H_9 \quad (9)$$

where R is a radical liable to react with the monomer. Depending upon the structure of the C_5H_9 radical which reacts with the methyl radical, the reaction provides one of the olefins mentioned in Table III. It is then possible to take into account all these radical–radical reactions and compile the radical quantum yields (Table V).

B Fragmentation of the 8.4-eV Excited 2-Methyl-1-butene Molecule. The absorption of photons leads to the formation of excited molecules. These molecules may be stabilized by collision, or decompose, as in reactions 10–12.

TABLE V: Radical Yields in the Photolysis of 2-Methyl-1-butene

	Incident energy, eV	
	8.4	10.0
CH_3	1.44 ± 0.15	1.24 ± 0.15
H	0.45 ± 0.10	0.41 ± 0.10
C_2H_5	0.07 ± 0.03	0.07 ± 0.03
CH_2	0.02 ± 0.01	0.02 ± 0.02
C_5H_9	0.08 ± 0.02	0.08 ± 0.02
Total	2.06 ± 0.31	1.82 ± 0.32

$$C_2H_5C(CH_3)CH_2 + h\nu \longrightarrow (C_2H_5C(CH_3)=CH_2)^{**} \quad (10)$$

$$(C_2H_5C(CH_3)=CH_2)^{**} + M \longrightarrow C_2H_5C(CH_3)=CH_2 + M \quad (11)$$
(for other C_5H_{10} isomer)

$$(C_2H_5C(CH_3)=CH_2)^{**} \longrightarrow \text{products} \quad (12)$$

At 8.4 eV, the quantum yield of the C_5H_{10} isomeric compounds is very low: Φ(isomeric C_5H_{10}) ≤ 0.01. Then, if the excited molecule isomerizes, it will decompose before being stabilized by collision. Furthermore, the products analyzed in presence of oxygen have quantum yields independent of pressure. One may conclude that the stabilization by collision of the 8.4-eV excited molecules is not an important process. Only the decomposition reactions should then be considered. The products of this decomposition are similar to those obtained in the photolysis of 2-methyl-2-butene[17] and of 3-methyl-1-butene,[20] but their relative yields are quite different. Thus, isomerization of the excited molecule, if it occurs, is a process of minor importance, and fragmentation is very fast. The main product is allene.

$$(C_2H_5C(CH_3)=CH_2)^{**} \longrightarrow C_3H_4 + C_2H_6 \quad \Delta H = 34 \text{ kcal mol}^{-1} \quad (13a)$$

$$(C_2H_5C(CH_3)=CH_2)^{**} \longrightarrow C_3H_4 + 2CH_3 \quad \Delta H = 116 \text{ kcal mol}^{-1} \quad (13b)$$

$$(C_2H_5C(CH_3)=CH_2)^{**} \longrightarrow C_3H_4 + C_2H_5 + H \quad \Delta H = 130 \text{ kcal mol}^{-1} \quad (13c)$$

Reaction 13a should be insignificant due to the low quantum yield of molecular ethane (*i.e.*, formed in the presence of oxygen): Φ(13a)/Φ(13) ≤ 0.03. From the measured quantum yields of the radicals (Table V), the Φ(13c)/Φ(13b) ratio is lower than 0.13 at 8.4 eV. The formation of isoprene is also important.

$$(C_2H_5C(CH_3)=CH_2)^{**} \longrightarrow C_5H_8 + H_2 \quad \Delta H = 27 \text{ kcal mol}^{-1} \quad (14a)$$

$$(C_2H_5C(CH_3)=CH_2)^{**} \longrightarrow C_5H_8 + 2H \qquad \Delta H = 131 \text{ kcal mol}^{-1} \quad (14b)$$

No comment is made about the k_{14a}/k_{14b} ratio since the yield of molecular hydrogen has not been measured. However, reaction 14b is in agreement with an important formation of hydrogen atoms. Other less important reactions following the fragmentation of the excited molecule are also responsible for the formation of 1,3- and 1,2-butadienes, ethylene, etc.

$$(C_2H_5C(CH_3)=CH_2)^{**} \longrightarrow C_4H_6 + CH_4(CH_3 + H) \quad (15a)$$

$$(C_2H_5C(CH_3)=CH_2)^{**} \longrightarrow C_2H_4 + \cdots ? \quad (15b)$$

These reactions, thermodynamically possible, are however too numerous and cannot be discussed in detail here. The total yield of the measured molecular products is about 0.9. It appears again that stabilization is not an important process even at a total pressure of 200 Torr. The fragmentation of these excited molecules leads to the formation of one molecular product and two stable radicals. In the 200-nm gaseous flash photolysis, the predominant fate of the excited 2-methyl-1-butene molecule is the fission of the β(C-C) bond to give stable methyl and β-methallyl radicals.[21]

C. Ionic Reactions. The results obtained at 10.0 and 11.6–11.8 eV (Table III) show that the decomposition of the superexcited molecules gives essentially the same products. However two remarks should be made. The first deals with the decrease in the quantum yields of the products due to the formation of excited ions (ionization potential of 2-methyl-1-butene: 9.12 eV[22])

$$(C_2H_5C(CH_3)=CH_2)^{**} \rightarrow [(C_2H_5C(CH_3)=CH_2)^+]^* + e^- \quad (16)$$

The recorded ion current (Figure 3) shows that the ion quantum yields are the following: 0.207 ± 0.005 at 10.0 eV and 0.33 at 11.6–11.8 eV. In addition, in the presence of oxygen, the 2-methyl-2-butene quantum yield is altered by sulfur hexafluoride, nitrous oxide, toluene, methylcyclopentane, and ammonia in various proportions. Nitrous oxide and sulfur hexafluoride are known to be good electron scavengers. Therefore, the negative species issued from the capture by SF_6 or N_2O interferes with one (or several) precursor of 2-methyl-2-butene. Toluene, methylcyclopentane, and ammonia generally do not react with the chemical products in the gas phase, with the exception of ions. Consequently, an ion-molecule reaction between the parent ion (or any other ion issued from this parent ion) and one of the three mentioned additives interferes with the formation of 2-methyl-2-butene. Then, in presence of oxygen, 2-methyl-2-butene is formed *via* the parent ion. In fact it is difficult to accept that this product is formed by an electron during the neutralization of the parent ion in the homogeneous phase since the resulting molecule would be similar to an excited molecule in the energy range studied here. It would thus decompose to allene and other products. We must admit either a neutralization on the walls or other ionic reactions. It is worthy to note that the isomerization reactions of the $C_4H_8^+$ ions have already been observed.[23]

$$[C_2H_5C(CH_3)=CH_2^+]^* \rightleftharpoons [M^+]^* \rightleftharpoons [((CH_3)_2C=CHCH_3)^+]^* \quad (17)$$

Toluene is liable to react with the 2-methyl-1-butene ion by charge transfer and eliminate part of the formation of this product. Methylcyclopentane is liable to react by hydride (H^-) transfer since there is no formation of isopentane (Table IV). Nevertheless a kinetic chain mechanism should be called upon to take into account the high 2-methyl-2-butene quantum yield which is larger than the ion quantum yield at 10.0 eV and larger than unity even in the presence of oxygen at 11.6–11.8 eV. At these energies, the excited parent ion has sufficient energy to decompose since the appearance potential of $C_4H_7^+$ fragment ion is 10.85 eV.[24]

Acknowledgments. We wish to thank the National Research Council of Canada and l'Université du Québec à Chicoutimi for their help and support throughout this work.

References and Notes

(1) J. R. McNesby and H. Okabe, *Advan. Photochem.*, **3**, 157 (1964).
(2) (a) P. Borrell, P. Cashmore, A. Cervenka, and F. C. James, *J. Chim. Phys.*, 229 (1970); (b) P. Borrell and P. Cashmore, *Trans. Faraday Soc.*, **65**, 2412 (1969); (c) P. Borrell and A. Cervenka, *J. Chem. Soc., Faraday Trans. 1*, **68**, 345 (1972).
(3) E. Tschuikow-Roux, *J. Phys. Chem.*, **71**, 2355 (1967).
(4) J. Herman, K. Herman, and P. Ausloos, *J. Chem. Phys.*, **52**, 28 (1970).
(5) G. J. Collin and P. M. Perrin, *Can. J. Chem.*, **50**, 2823 (1972).
(6) A. B. Callear and H. K. Lee, *Trans. Faraday Soc.*, **64**, 2017 (1968).
(7) P. M. Perrin and G. J. Collin, *Can. J. Chem.*, **51**, 724 (1973).
(8) G. J. Collin and P. M. Perrin, *Can. J. Chem.*, **50**, 2391 (1972).
(9) R. Gorden, Jr., R. E. Rebbert, and P. Ausloos, *Nat. Bur. Stand., Techn. Note*, 496 (1969).
(10) A. A. Siddiqi, C. T. Chen, G. G. Meisels, and R. Gorden, Jr., *J. Chem. Phys.*, **57**, 4506 (1972).
(11) W. E. Falconer and W. A. Sunder, *Int. J. Chem. Kinet.*, **4**, 315 (1972).
(12) W. E. Falconer and W. A. Sunder, *Int. J. Chem. Kinet.*, **3**, 395 (1971).
(13) C. W. Larson, B. S. Rabinovitch, and D. C. Tardy, *J. Chem. Phys.*, **47**, 4570 (1967).
(14) J. O. Terry and J. H. Futrell, *Can. J. Chem.*, **45**, 2327 (1967).
(15) J. H. Georgakakos, B. S. Rabinovitch, and C. W. Larson, *Int. J. Chem. Kinet.*, **3**, 535 (1971).
(16) Due to the presence of small traces of air on the chromatogram the methane yield is not so precise as other yields. This ratio is calculated through the ratio k_6k_6/k_4k_7, which would be 4 if it were determined by statistical factors only.
(17) G. J. Collin and C. M. Gaucher, *Can. J. Chem.*, in press.
(18) (a) T. W. Eder and R. W. Carr, *J. Phys. Chem.*, 73, 2074 (1969); (b) A. K. Dhingra and R. D. Koob, *ibid.*, **74**, 4490 (1970).
(19) F. H. Dorer and B. S. Rabinovitch, *J. Phys. Chem.*, **69**, 1952 (1965).
(20) G. J. Collin and C. Bertrand, *J. Photochem.*, in press.
(21) F. Bayrakceken, J. H. Brophy, R. D. Fink, and J. E. Nicholas, *J. Chem. Soc., Faraday Trans. 1*, **69**, 228 (1972).
(22) J. L. Franklin, J. G. Dillard, H. M. Rosenstock, J. T. Herron, K. Draxl, and F. H. Field, *Nat. Stand. Ref. Data Ser., Nat. Bur. Stand.*, **26**, 55 (1969).
(23) S. G. Lias and P. Ausloos, *Nat. Bur. Stand. (U.S.), J. Res.*, **75A**, 591 (1971); L. W. Sieck, S. G. Lias, L. Hellner, and P. Ausloos, *ibid.*, **76A**, 115 (1972).
(24) F. P. Lossing, *Can. J. Chem.*, **50**, 3973 (1972).

Radiolysis of Liquid Hydrocarbon–Nitrous Oxide Solutions. The Precursors of Nitrogen[1]

G. R. Freeman* and T. E. M. Sambrook

Department of Chemistry, University of Alberta, Edmonton, Canada T6G 2G2 *(Received July 26, 1973)*

When nitrous oxide is added to liquid alkanes, the yield of nitrogen $g(N_2)_{HC}$ that results from energy initially absorbed in the hydrocarbon increases to a plateau value when the nitrous oxide concentration is increased. The plateau value $g(N_2)_{HC} = 5.2 \pm 0.2$ has been observed to extend over a 40-fold range of concentration in liquid ethane. The same plateau value has been observed in propane, extending over a fivefold concentration range. Similar plateaus exist in cyclohexane and methylcyclopentane, and appear also to exist in cyclopropane and neopentane. Secondary reactions involving oxygen-containing anionic intermediates do not form nitrogen in these solutions. Nitrogen results from the reaction of nitrous oxide with primary radiolytic species. The primary species appear to be mainly electrons, but a small contribution from neutral excited molecules cannot be excluded. The yield of primary species that react with nitrous oxide to form nitrogen is $g(\text{primary species})_{HC} = 5.2 \pm 0.3$ in ethane, propane, cyclopropane, neopentane, methylcyclopentane, and cyclohexane.

Introduction

The yield of nitrogen from the radiolysis of solutions of nitrous oxide in liquids is related to the yield of electrons scavenged by the nitrous oxide.[2] However, the total amount of nitrogen formed is commonly believed to be greater than the number of electrons scavenged.[3-9] This belief is based on the following observations that, taken together, seem quite convincing.

(1) For several hydrocarbon solvents, the nitrogen yields from solutions containing more than 3 mol % nitrous oxide ($G(N_2) > 5$)[3,5-7,9] is greater than the gas-phase ionization yields in the hydrocarbons (G(ionization) ≈ 4). On the other hand, the yields of alkyl radicals R generated by the reaction $e^- + RX \rightarrow R + X^-$ in cyclohexane, extrapolated by a particular method to infinite alkyl halide concentration,[6] gave the result $G(\text{scavengable } e^-)^l_{extr} = 4.0$, whereas in gas-phase cyclohexane $G(\text{ionization})^g = 4.4$.[10]

(2) The decrease in hydrogen yield caused by the presence of nitrous oxide in a hydrocarbon during radiolysis is smaller than the nitrogen yield, *i.e.*, $G(N_2)/\Delta G(H_2) > 1.0$.[2-5,7,9] It has sometimes been assumed that each electron results in the formation of one molecule of hydrogen during the radiolysis of an alkane in the absence of nitrous oxide.

(3) A plot of $G(N_2)$ against nitrous oxide concentration does not reach a plateau value at high concentrations, but $G(N_2)$ continues a gentle increase. This might indicate that progressively more nitrogen is formed by secondary reactions as the nitrous oxide concentration is increased.[2-9]

(4) The reaction $O^- + N_2O \rightarrow N_2 + O_2^-$ had been reported to occur in a mass spectrometer[11] and seemed to be a reasonable candidate for the above-mentioned secondary reaction. It would supposedly follow $e^- + N_2O \rightarrow N_2 + O^-$.

(5) Nitrogen was formed when nitrous oxide solutions in alkanes were photolysed with 147-nm light,[12] thereby supporting a suggestion that the "extra nitrogen" in irradiated solutions might be formed by the reaction $RH^* + N_2O \rightarrow N_2 +$ products,[4] where RH* is a neutral, excited molecule.

Recent information leads one to examine the significance of each of the above points.

Radiation-induced electrical conductance measurements have shown that ionization yields in liquids can be much greater than those in the corresponding gases.[13] In argon, krypton, and xenon the ratios of the liquid- to gas-phase ionization yields were estimated to be 1.9, 3.2, and 3.0, respectively.[13] The fact that nitrogen yields from solutions of nitrous oxide in organic liquids can be ~1.3 times the gas-phase ionization yield in the same compound might simply indicate a larger ionization yield in the liquid phase.

The equation used to extrapolate organic halide scavenger results to infinite scavenger concentrations[6] is arbitrary and might not be correct. The observation that $G(\text{scavengable } e^-)^l_{extr} < G(\text{ionization})^g$ might not, therefore, imply that $G(\text{ionization})^l \leq G(\text{ionization})^g$.

When nitrous oxide was added to a number of normal, branched, and cyclic alkanes, the magnitude of $\Delta G(H_2)$ varied greatly from one hydrocarbon to another, while $G(N_2)$ varied relatively little.[7] The value of the ratio $G(N_2)/\Delta G(H_2)$ was greater than unity in all cases, and was greater in branched than in normal or cyclic alkanes. It has been demonstrated that only a portion of the neutralization reactions in branched alkanes lead to hydrogen formation in the absence of additive,[14,15] and the same might be true of other alkanes. The fact that $G(N_2)/\Delta G(H_2) > 1.0$ does not, therefore, imply that some of the nitrogen was formed by secondary reactions.

Points 3-5 are evaluated below, with reference to a study of the radiolysis of liquid nitrous oxide.[16]

Plateau Values of $g(N_2)_{HC}$

The present work is mainly concerned with the yield of nitrogen that results from energy initially absorbed in the hydrocarbon, $g(N_2)_{HC}$. The value of $G(N_2)$ from a solution includes the nitrogen formed by the direct radiolysis of nitrous oxide

$$G(N_2) = g(N_2)_{HC}\epsilon_{HC} + g(N_2)_N\epsilon_N \qquad (1)$$

where ϵ_{HC} and ϵ_N are the electron fractions of hydrocarbon and nitrous oxide, respectively, in solution, and $g(N_2)_N$ is the yield from the direct radiolysis of nitrous oxide in a liquid hydrocarbon solution. The value $g(N)_N = 10.4 \pm$

0.5 was recently found to be valid for many hydrocarbons.[16] Values of $g(N_2)_{HC}$ can now be obtained from previously published nitrogen yields.

In ethane[17] $g(N_2)_{HC}$ rises quickly with increasing nitrous oxide concentration, then flattens off and remains constant at 5.2 ± 0.2 over a 40-fold range of concentration (0.4–18 mol %, see Figure 1). Thus a plateau value of $g(N_2)_{HC}$ clearly exists in ethane. In this liquid secondary reactions do not generate progressively more nitrogen as the nitrous oxide concentration is increased.

In propane[17] the same plateau at $g(N_2)_{HC}$ = 5.2 was reached, but not until 5 mol % nitrous oxide had been added (Figure 1). A plateau was not observed in cyclopropane,[17] but the value $g(N_2)_{HC}$ = 5.2 was attained at 21 mol % nitrous oxide (Figure 1). It appears that a plateau near to 5.2 exists for cyclopropane.

Values of $g(N_2)_{HC}$ from cyclohexane solutions[7] are shown in Figure 2. A plateau in yield was reached at 5 mol % nitrous oxide, above which concentration $g(N_2)_{HC}$ = 5.1 ± 0.1. Yields obtained from results of Sato, *et al.*,[3] and Hatano, *et al.*,[9] parallel those in Figure 2, but are 0.3 units higher, which would indicate a plateau yield of 5.4. When other sets of results are normalized to the same nitrous oxide solubility coefficient in cyclohexane, α_{N_2O} = 2.62,[3] most of them[2,4,6] fall reasonably close to those of Sato[3] and Robinson,[7] but one set[5] is inexplicably 1.2 units higher than the average, along the entire concentration range. The best value for the plateau yield in cyclohexane is taken to be $g(N_2)_{HC}$ = 5.3 ± 0.2.

Yields in methylcyclopentane[14] plateaued above 4 mol % nitrous oxide at $g(N_2)_{HC}$ = 5.1 ± 0.1 (Figure 2).

In neopentane[18] a plateau had not been reached by 15 mol % nitrous oxide (Figure 2), but an extrapolation to be discussed later indicates that the plateau yield would be $g(N_2)_{HC}$ = 5.2 ± 0.3.

Thus, analysis of earlier results from dilute solutions of nitrous oxide in alkanes indicates that in each of the six liquids, from ethane at 183 K to cyclohexane and neopentane at 297 K, $g(N_2)_{HC}$ has a plateau value near 5.2. This agrees with the conclusion from a recent study of solutions of alkanes in liquid nitrous oxide that $g(N_2)_{HC}$ = 5.5 ± 0.5.[16]

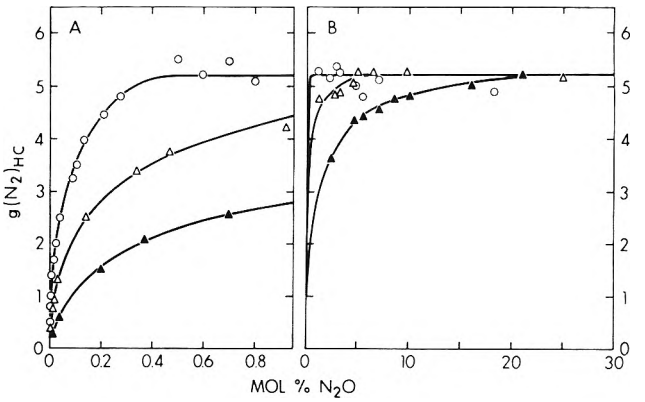

Figure 1. $g(N_2)_{HC}$ in ethane (○), propane (△), and cyclopropane (▲) calculated from eq 1 and results in ref 17 (temperature = 183 K). The curves in A are the front portions of those in B with the horizontal scale expanded 25-fold. The points in A are omitted in B to prevent conjestion, but the curves are the same.

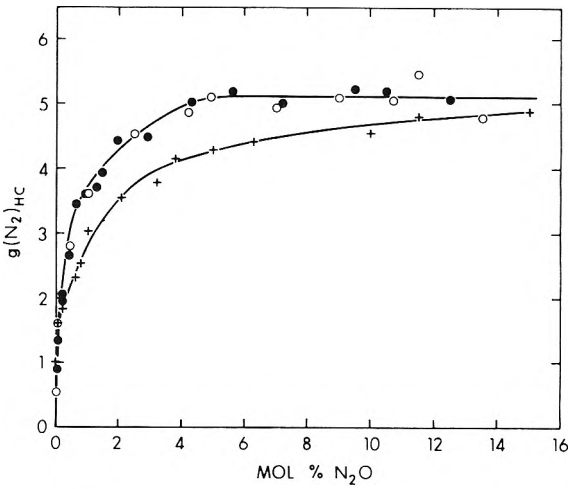

Figure 2. $g(N_2)_{HC}$ in cyclohexane (●), methylcyclopentane (○), and neopentane (+) calculated from eq 1 and results in ref 7, 14, and 18, respectively (temperature = 297 ± 1 K).

The Question of Secondary Reactions that Form Nitrogen

The gas-phase ionization yields in the above hydrocarbons are all in the range $g(\text{ionization})^g$ = 4.0–4.4, so at the plateau the nitrogen yield $g(N_2)^1_{HC}$ = (1.25 ± 0.05)$g(\text{ionization})^g$. Mechanisms that include the postulate that $g(N_2)_{max} = 2g(\text{ionization})$[6,8] are therefore improbable because they would require that $g(\text{ionization})^1 = 0.6g(\text{ionization})^g$.

A recent study of the radiolysis of liquid nitrous oxide[16] indicates that an average of 1.5 molecules of nitrogen result from each ionization in that liquid. Addition of 20 mol % or more of hydrocarbon to the nitrous oxide appears to reduce the number of nitrogen molecules resulting from each ionization to 1.0.[16] Secondary reactions of oxygen-containing anionic intermediates in nitrous oxide are completely scavenged by the presence of 10% hydrocarbon, but 20% is required to completely scavenge the N_2O^-.

When more than 10 mol % hydrocarbon is present in liquid nitrous oxide essentially the only oxygen containing product is water, with $g(H_2O) \approx g(N_2)$ at both 183 K[16] and ~298 K.[9] One may therefore extend a conclusion of Hatano[9] by stating that the possibility of nitrogen formation *via* secondary reactions of negative ions with nitrous oxide may be excluded for solutions containing less than 90 mol % nitrous oxide.

The solutions treated by Schuler and coworkers[6,8] contained only 0.01–5 mol % nitrous oxide. Their proposed reaction mechanism involved secondary reactions of anions that are now known to be improbable at the reactant concentrations in question. Their treatment should be reconsidered from the viewpoint that nitrogen results only from reactions of nitrous oxide with primary species.

It appears that when nitrous oxide is used as a scavenger in liquid hydrocarbons 1.0 molecule of nitrogen is formed for each primary species scavenged. All or most of these primary species appear to be electrons. A small contribution from neutral excited molecules cannot be ruled out. Independent attempts should be made to determine the total ionization yields in liquids to find whether in general, as in argon, krypton, and xenon, ionization yields are greater in the liquid than in the gas phase.

Scavenging Kinetics

A popularly used equation[6] leads one to expect that a plot of $(g(e^- \text{ scavenged}) - g_{fi})^{-1}$ against $[\text{scavenger}]^{-1}$[2]

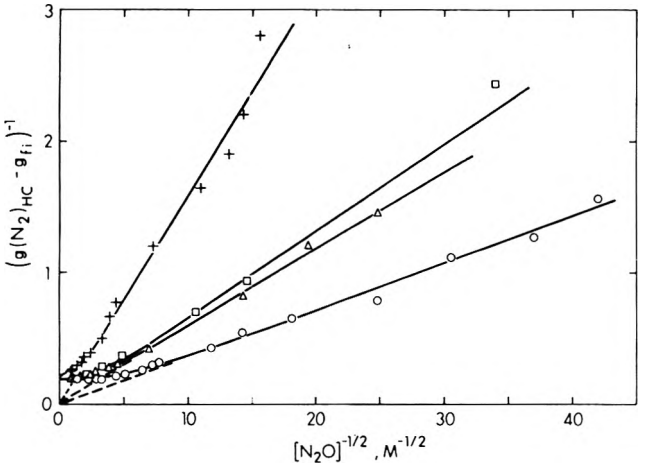

Figure 3. Plots of $(g(N_2)_{HC} - g_{fi})^{-1}$ against $[N_2O]^{-1/2}$ in ethane (O) and propane (△) at 183 K, and in methylcyclopentane (□) and neopentane (+) at 297 ± 1 K.

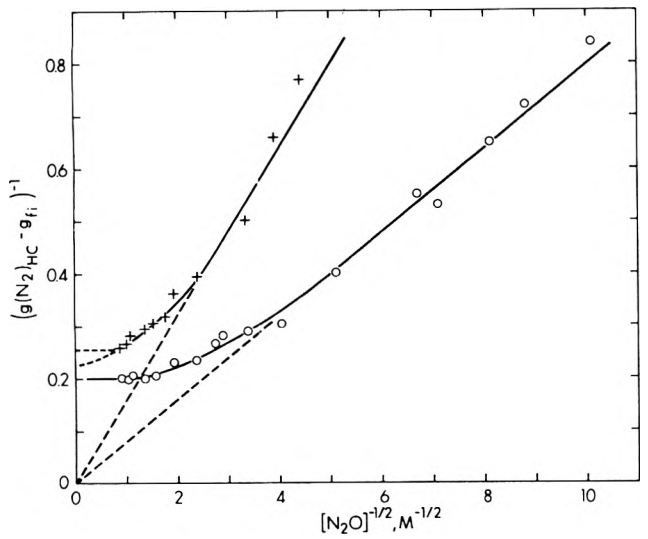

Figure 4. Plots of $(g(N_2)_{HC} - g_{fi})^{-1}$ against $[N_2O]^{-1/2}$ in cyclohexane (O) and neopentane (+) at 297 ± 1 K.

should be linear and have an intercept equal to $(g(\text{geminate ions}))^{-1}$. Such linear plots have been obtained for radical yields formed by the radiolysis of organic halide solutions.[6] However, the use of organic halides RX as electron scavengers suffers from complications such as the formation of the acid HX, which then competes with RX for electrons,[19] and the tendency of the transient ion RX^- to donate an electron to another scavenger than happens to be present.[19,20]

A plot of $(g(N_2)_{HC} - g_{fi})^{-1}$ against $[N_2O]^{-1/2}$ for ethane solvent is shown in Figure 3. The free ion yield is $g_{fi} = 0.13$.[21] The long, linear portion of the curve extrapolates to the origin, not to $(g(\text{geminate ions}))^{-1}$. The curve is not linear at $[N_2O]^{-1/2} < 10\ M^{-1/2}$, but levels out to have an intercept of 5 l^{-1}, which equals $(g(\text{scavengable primary species}) - g_{fi})^{-1}$, or $g(\text{scavengable primary species}) = 5.2$.

Analogous plots for the nitrogen yields from nitrous oxide solutions in propane, methylcyclopentane, and cyclohexane are similarly shaped (Figures 3 and 4), with linear portions that extrapolate to the origin, but which curve off at $[N_2O]^{-1/2} < 5\ M^{-1/2}$ to give intercepts at approximately 5.1^{-1}, indicating that $g(\text{scavengable primary species}) \approx 5.2$.

A similar treatment was given the yields from solutions in neopentane, which are shown in a normal plot in Figure 3 to determine the position of the curve and in expanded scale in Figure 4 to facilitate the extrapolation. One obtains $(g(\text{scavengable primary species}) - g_{fi}) = 4.2 \pm 0.3$, so $g(\text{scavengable primary species}) = 5.2 \pm 0.3$.

It has been demonstrated that in the low concentration portion of a $g(N_2)$ *vs.* $[N_2O]$ curve eq 2 applies[17]

$$g(N_2) - g_{fi} = K[N_2O]^{1/2} \qquad (2)$$

where K is a constant that depends on the solvent. The similar eq 3 describes the low concentration portion of an electron scavenging *vs.* scavenger concentration curve

$$g(\text{scavenged } e^-) - g_{fi} = K'[S]^{1/2} \qquad (3)$$

where [S] is the scavenger concentration. Equation 3 can be obtained by each of three different treatments of charge scavenging in spurs.[22-24]

The inverse of eq 2 describes the linear portions of the curves in Figures 3 and 4. The nitrogen yields are thus kinetically compatible with the suggestion that their sole radiolytic precursor in these solutions is electrons.

$$e^- + N_2O \longrightarrow N_2 + O^- \qquad (4)$$

or

$$e^- + N_2O \longrightarrow N_2O^- \qquad (5)$$

$$N_2O^- + RH^+ \longrightarrow N_2 + \text{products} \qquad (6)$$

By assuming that electrons are the sole radiolytic precursor of nitrogen one may estimate the relative electron scavenging efficiencies of nitrous oxide in several hydrocarbons. They are, taking that in ethylene as unity, ethylene, 1; propylene, 1; cyclopropane, 3; propane, 11; ethane, 40.[17] According to a simple stochastic model[22] the scavenging efficiencies are approximately proportional to the cube of the electron thermalization ranges. Relative ranges are given by the relative values of y_{min} in Table III[25] of ref 17: $(y_{min}^{RH}/y_{min}^{ethylene})^3 = 1.6$ in propylene, 2.8 in cyclopropane, 14 in propane, and 43 in ethane. The correlation between the above two sets of values seems to imply that, if an appreciable amount of nitrogen is formed by reaction 7, the competition between (7) and (8) also

$$RH^* + N_2O \longrightarrow N_2 + \text{products} \qquad (7)$$

$$RH^* \longrightarrow \text{products} \qquad (8)$$

correlates with the cube of the electron thermalization ranges. Such a correlation would seem surprising. It seems preferable to assume that the contribution of (7) is relatively small.

References and Notes

(1) Assisted financially by the National Research Council of Canada.
(2) G. Scholes and M. Simic, *Nature (London)*, **202**, 895 (1964).
(3) S. Sato, R. Yugeta, K. Shinsaka, and T. Terao, *Bull. Chem. Soc. Jap.*, **39**, 156 (1966).
(4) W. V. Sherman, *J. Chem. Soc. A*, 599 (1966).
(5) N. H. Sagert and A. S. Blair, *Can. J. Chem.*, **45**, 1351 (1967).
(6) J. M. Warman, K. -D. Asmus, and R. H. Schuler, *Advan. Chem. Ser.*, **No. 82**, 25 (1968).
(7) M. G. Robinson and G. R. Freeman, *J. Chem. Phys.*, **48**, 983 (1968).
(8) P. O. Infelta and R. H. Schuler, *Int. J. Radiat. Phys. Chem.*, **5**, 41 (1973).
(9) Y. Hatano, K. Takeuchi, and S. Takao, *J. Phys. Chem.*, **77**, 586 (1973).
(10) P. Alder and H. K. Bothe, *Z. Naturforsch. A*, **20**, 1700 (1965).
(11) B. P. Burtt and J. Henis, *J. Chem. Phys.*, **41**, 1510 (1964).
(12) R. A. Holroyd, *Advan. Chem. Ser.*, **No. 82**, 488 (1968).
(13) M. G. Robinson and G. R. Freeman, *Can. J. Chem.*, **51**, 641 (1973).

(14) E. D. Stover and G. R. Freeman, *J. Chem. Phys.*, **48**, 3902 (1968).
(15) G. R. Freeman and E. D. Stover, *Can. J. Chem.*, **46**, 3235 (1968).
(16) T. E. Sambrook and G. R. Freeman, *J. Phys. Chem.*, **78**, 32 (1974).
(17) M. G. Robinson and G. R. Freeman, *J. Chem. Phys.*, **55**, 5644 (1971).
(18) K. Horacek and G. R. Freeman, *J. Chem. Phys.*, **53**, 4486 (1970).
(19) S. M. S. Akhtar and G. R. Freeman, *J. Phys. Chem.*, **75**, 2756 (1971).
(20) S. R. Logan and P. B. Wilmot, *Chem. Commun.*, 558 (1966).
(21) M. G. Robinson, P. G. Fuochi, and G. R. Freeman, *Can. J. Chem.*, **49**, 3657 (1971).
(22) G. R. Freeman, *J. Chem. Phys.*, **43**, 93 (1965); **46**, 2822 (1967).
(23) A. Hummel, *J. Chem. Phys.*, **48**, 3268 (1968).
(24) A. Mozumder, *J. Chem. Phys.*, **55**, 3026 (1971).
(25) y_{min} = 12 Å in ethylene; the value 11 in Table III of ref 17 was a misprint.

Electron Spin Resonance Study of Photosensitized Radical Formation in *n*-Hexane by Benzoic Acid

Takuo Takeshita and Kozo Tsuji*

Central Research Laboratory, Sumitomo Chemical Co., Ltd., Takatsuki, Osaka, Japan *(Received July 30, 1973)*

Publication costs assisted by Sumitomo Chemical Co., Ltd.

Electron spin resonance and phosphorescence studies were performed in order to examine the effect of dimer formation of benzoic acid on photosensitized radical formation in *n*-hexane, and it was supposed that the dimer is more efficient for photosensitization of *n*-hexane decomposition.

Introduction

Photosensitized decomposition of paraffins by aromatic molecules has been reported by several authors,[1] and the mechanism involved is the biphotonic process through the excited triplet states. Benzoic acid is known to form a dimer by hydrogen bonding[2] and acts as a quencher of luminescent molecules.[3] Therefore it would be interesting to know whether benzoic acid sensitizes or suppresses the decomposition of paraffins by ultraviolet irradiation. In this investigation, esr and phosphorescence studies were performed to examine the effects of dimer formation of benzoic acid on the photosensitized radical formation in the solid solution of *n*-hexane with various benzoic acid concentration at −196°. For the purpose of comparison, several benzoates were also investigated.

Experimental Section

A spectrograde reagent of *n*-hexane was obtained from Merck Chemical Co. and used without further purification. Commercial benzoic acid was purified by zone refining (at least 50 zone passes) before use. Several kinds of benzoates were used without purification of the commercial samples. Gas chromatographic examination showed that small amount of impurities if present were other benzoates and we felt that it is not necessary to remove them for our study.

The esr apparatus was a JES-3BSX electron spin resonance spectrometer (Japan Electron Optics Lab.).[4] The ultraviolet light source was a super-high-pressure mercury lamp with a lamp house (Ushio Denki Co., Ltd., USH-500D). The distance between the lamp and the sample was about 60 cm, and a parallel light beam from the lamp house was focused on the sample by a quartz lens placed just outside the esr cavity. The phosphorescence measurements were made with a Model MPF-2A Hitachi fluorescence spectrophotometer at −196°.

Results

The uv light ($\lambda > 250$ nm) irradiation of pure *n*-hexane solid at −196° gave no observable esr signal. On the other hand, solid solutions of benzoic acid in *n*-hexane gave an apparent seven-line esr spectrum under the same experimental conditions, as is shown in Figure 1. This spectrum is similar to the one obtained after γ-irradiation of *n*-hexane solid at −196°[5] (*cf.*, Figure 8a in ref 5), and readily attributed to the alkyl radicals of the type $CH_3\dot{C}HCH_2CH_2CH_2CH_3$. Since this radical can not be derived from the added benzoic acid molecules, it is clear that benzoic acid sensitizes the photoinduced radical formation in *n*-hexane. Figure 2 shows radical growth curves measured by esr signal intensities for various benzoic acid concentrations. The radical yields after 30-min irradiation was plotted against benzoic acid concentration in Figure 3. The maximum yield was obtained for a solid solution of concentration of benzoic acid of about 10^{-4} *M*. These results were obtained from rapidly cooled samples.

In Figure 4, the radical yields are shown for rapidly cooled and slowly cooled solid solutions of concentration of about 10^{-4} *M* of benzoic acid in *n*-hexane. From this figure, it is seen that the rapidly cooled sample gave greater radical yield than the slowly cooled one. Figure 5 shows phosphorescence spectra of the rapidly and slowly cooled samples. In this case also, the rapidly cooled sample emitted stronger phosphorescence than the slowly cooled one. It should also be noticed here that the phosphorescence spectrum of the rapidly cooled sample is that of a dimeric form of benzoic acid, while the spectrum of the slowly cooled sample is predominantly the spectrum

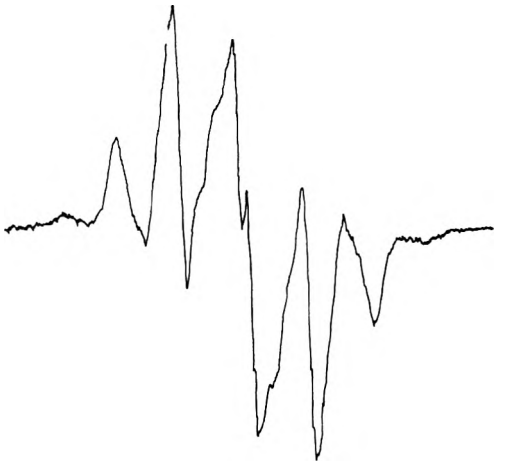

Figure 1. Esr spectrum of free radicals produced in *n*-hexane containing 10^{-4} *M* benzoic acid after ultraviolet irradiation at −196°.

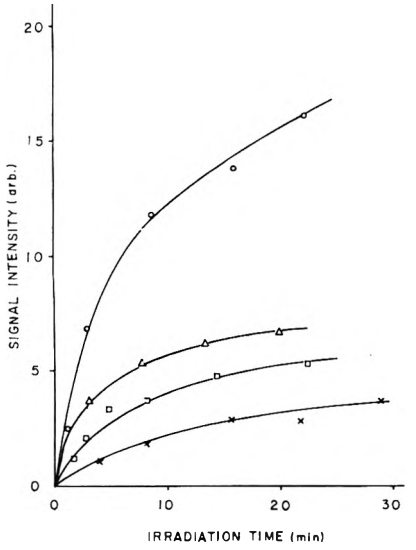

Figure 2. Dependence of esr signal intensity on irradiation time for the following benzoic acid concentrations (the rapidly cooled sample): ×, 1×10^{-2} *M*; △, 1×10^{-3} *M*; ○, 1×10^{-4} *M*; □, 1×10^{-5} *M*.

of the monomeric form of benzoic acid,[6] although some contribution from the dimer was also observed.

When benzoates such as methyl-, ethyl-, *n*-butyl-, and isopropylbenzoates were used as an additive instead of benzoic acid, the yield of the alkyl radical from *n*-hexane was small and a sharp singlet spectrum of $g \approx 2.001$ probably due to benzoyl radicals was also observed. The latter radicals are produced by the direct photolysis of the corresponding benzoates.

Discussion

From the facts that the alkyl radical yield depends on the rate of cooling of solutions and that the phosphorescence spectra also show different characteristic emissions for the rapidly and slowly cooled solid solutions, it is reasonable to assume that the efficiency of the photosensitization of *n*-hexane decomposition is greater for the dimer of benzoic acid than the monomer. This assumption is also supported by the observation that benzoates, which can not form a dimer, showed a much smaller yield of alkyl radicals.

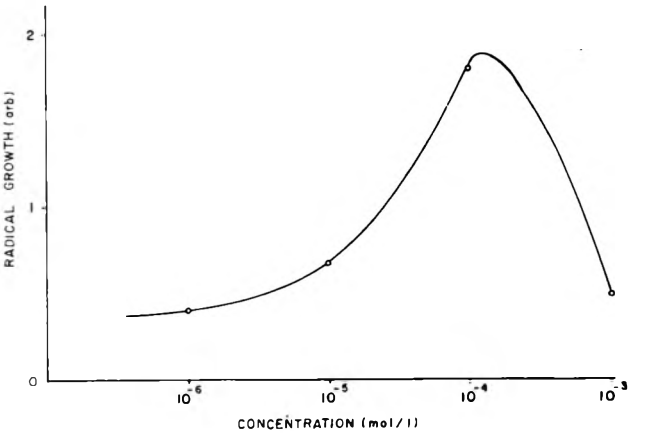

Figure 3. Dependence of radical yield after 30-min irradiation on benzoic acid concentration.

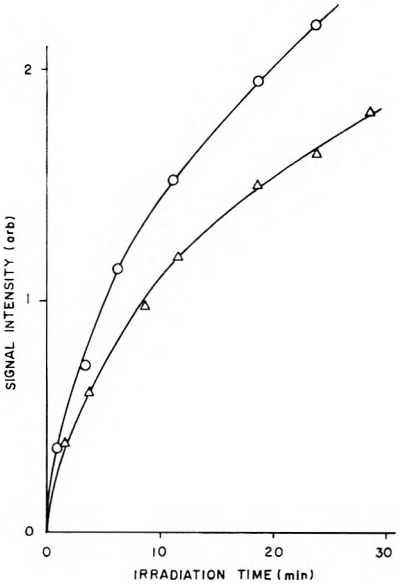

Figure 4. Effect of cooling rate on radical formation: △, slow cooling (the 10-cm long sample was gradually frozen in liquid nitrogen for 4 min); ○, rapid cooling (the sample of the same dimension was frozen at −196° rapidly).

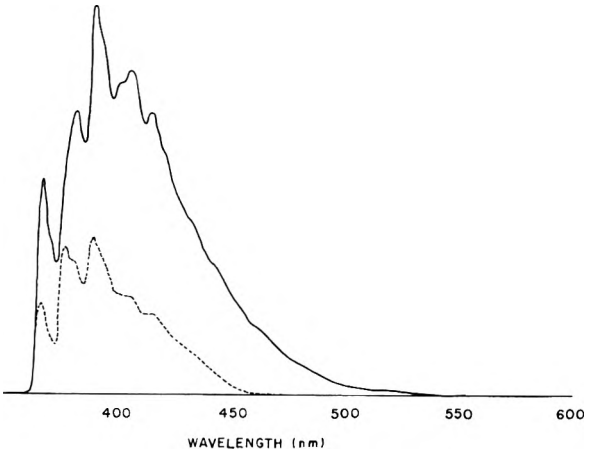

Figure 5. Effect of cooling rate on the phosphorescence spectrum of 10^{-4} *M* benzoic acid at −196°: solid line, rapid cooling; dotted line, slow cooling.

Dependence of radical formation on benzoic acid concentration may be interpreted as follows. At low concentration of benzoic acid, the dimer concentration is small, while at concentration greater than 10^{-4} M, some coagulation and the self-quenching of the excited states of benzoic acid might be responsible for smaller radical yield.

A correlation between the radical yields and the phosphorescence intensities in the slowly and rapidly cooled samples was obtained. This result might indicate that the triplet state of benzoic acid is responsible for the photosensitized radical formation in n-hexane. The monomer is known to give phosphorescence alone with a high quantum yield of 0.70,[7] while the dimer emits both phosphorescence (Φ_p = 0.46) and fluorescence (Φ_f = 0.25).[6] The lifetime of the first triplet state of the dimer (3.1 sec) is longer than that of the monomer (2.2 sec). Therefore the lower quantum yield of the first triplet state of the dimer compared with that of the monomer is compensated for by its longer lifetime as a sensitizer involving triplet states. Another possibility may involve nature of the triplet state, *i.e.*, $(n,\pi^*)^3$ or $(\pi,\pi^*)^3$. A further detailed study seems to be in order to clarify the nature of the excited states of the monomer and the dimer of benzoic acid.

The effect of the cooling rate of solutions on the phosphorescence spectrum of aromatic molecules in isooctane was reported.[8] Changes of the phosphorescence spectrum and the decay time of the triplet states were explained by the substantial difference of the crystal fields in which the impurity molecules are located. The same explanation may also be applicable to our present case. On the other hand, it is also reported that the equilibrium between the monomer and the dimer of benzoic acid inclines toward the monomer side at −196°.[6] In this case there is a possibility that the cooling rate can affect this equilibrium. In fact the phosphorescence spectrum of the rapidly cooled sample was that of the dimer, while the slowly cooled sample gave the spectrum mainly of the monomer with some contribution from the dimer (see Figure 5). These arguments also support our interpretation that the dimer of benzoic acid is more efficient than the monomer form in the photosensitized radical formation in n-hexane.

Acknowledgment. The authors are indebted to the Sumitomo Chemical Co. for permission to publish these results.

References and Notes

(1) V. E. Kholmogorov, *Russ. Chem. Rev.*, **38**, 164 (1969).
(2) M. Ito, *J. Mol. Spectrosc.*, **4**, 144 (1960).
(3) T. Miwa and M. Koizumi, *Bull. Chem. Soc. Jap.*, **38**, 529 (1965).
(4) T. Takeshita, K. Tsuji, and T. Seiki, *J. Polym. Sci., Part A-1*, **10**, 2315 (1972).
(5) T. Gillbro, P-O. Kinell, and A. Lund, *J. Phys. Chem.*, **73**, 4167 (1969).
(6) H. Baba and M. Kitamura, *J. Mol. Spectrosc.*, **41**, 302 (1972).
(7) J. B. Birks, "Photophysics of Aromatic Molecules," Wiley-Interscience, New York, N. Y., 1970.
(8) D. M. Grebenshchikov, N. A. Kovrizhnykh, and S. A. Kozlov, *Opt. Spectrosc.*, **31**, 214 (1971).

X-Ray Photoelectron Spectroscopic Study of the Reaction of Evaporated Metal Films with Chlorine Gas

Kosaku Kishi* and Shigero Ikeda

Department of Chemistry, Faculty of Science, Osaka University, Toyonaka, Osaka, Japan
(Received April 24, 1973; Revised Manuscript Received July 5, 1973)

The reaction of the evaporated metals iron, nickel, copper, palladium, silver, and gold with chlorine gas was investigated by X-ray photoelectron spectroscopy. Three types of chlorine species were observed on the surfaces as the surface reaction proceeded, namely the chlorine ion adsorbed at the metal surface, the ion of the surface metal chlorides, and Cl_2 or Cl adsorbed on the chlorides.

Introduction

Bonding character of adsorbent atoms on metal surfaces will vary as the localization of the atom from surrounding metal atoms in the course of a surface reaction. Investigation of such variations helps to elucidate the reaction mechanism and provides fundamental knowledge for analyses of corrosive, electrode, and catalytic reactions on metal surfaces.

X-Ray photoelectron spectroscopy (XPS or ESCA) is a useful tool for the investigation of chemical reactions of solid surfaces since the effective sampling depth by XPS is smaller than 100 Å. In our previous papers, the reactions of evaporated iron[1] and nickel[2] with O_2 and H_2O were studied by XPS. The surface oxides and the corresponding bulk oxides gave different photoelectron spectra and differed in their chemical reactivity with H_2O. Two kinds of oxygen ions were shown to exist in the surface oxides of these metals. Similar differences in chemical reactivity were also observed by uv absorption spectra when acetylacetone was exposed to iron and manganese surfaces and bulk oxides.[3]

In the present paper, the reactions of evaporated iron, nickel, copper, palladium, silver, and gold with chlorine gas (which has higher reactivity than oxygen to noble

metals) were investigated by XPS in a continuing effort to clarify the difference in chemical states between surface and bulk compounds.

Experimental Section

Metals were evaporated onto a stainless steel plate from an electrically heated tungsten filament at 10^{-6} Torr in a reaction chamber as described elsewhere.[1] The evaporated metal film on the plate was then transferred *in vacuo* into a sample chamber. After the spectrum of the metal was recorded, the surface was exposed to chlorine gas in the reaction chamber. Iron and nickel surfaces were exposed to the gas immediately after evaporation without recording the spectrum of the unreacted metal. The gas was then evacuated and the photoelectron spectra of the surface species formed were recorded. Copper was not used as a reaction chamber or sample holder material since the sample surface was covered immediately with CuCl sublimed from these copper surfaces after they were exposed to chlorine gas. During the measurement of the spectra, the vacuum of the sample chamber was maintained at 10^{-7} Torr.

Spectra were recorded in 0.1-eV steps on a KES-X2001 (Kokusai Electric Co.) electron spectrometer using Al Kα X-ray radiation. The instrument was calibrated so that the difference between the photoelectron peak of Cls observed in the background spectrum and the Fermi level of palladium was 285.0 eV. The Fermi level was taken as the inflection point of the steep low-energy edge of the 4d band from palladium according to Baer, *et al.*[4] Binding energies of other peaks were calculated using the Cls reference line. For the chlorides produced on the metals, charging effects were negligible under X-ray bombardment.

Results

The Cl 2p photoelectron lines from evaporated gold exposed to Cl_2 are shown in Figure 1. The background spectrum for gold in the Cl 2p region is indicated as (a). When gold was exposed to Cl_2 at a pressure of 0.5 Torr for 1 min, three peaks were observed at binding energies of 197.0, 199.4, and 201.1 eV as shown by (b). Chlorine 2p core levels appear as a doublet splitting at *ca.* 1.7 eV ($2p_{1/2}$ and $2p_{3/2}$ ratio 1:2) due to spin–orbit coupling. Line b can be resolved into two doublets when the profile is analyzed on the basis of the spectral line of the metal chlorides, in area ratio of *ca.* 5:4, the $2p_{3/2}$ of which are at 199.4 and 197.0 eV, respectively, as shown by dotted lines in the lower part of the figure. Gold was exposed, in succession, to Cl_2 at a pressure of 10 Torr for 2 min (c) and for 10 min (d). Lines e and f were obtained by subtracting (b) from (c), and (c) from (d), respectively, in order to clarify spectral variations for each reaction step. Both lines show two maxima, around 199.3 and 201.1 eV, with a weak shoulder around 197.6 eV.

When gold was exposed to Cl_2 at a pressure of 10 Torr for 10 min, the Au $4f_{5/2}$ and $4f_{7/2}$ lines appeared as very weak shoulders shifted +2.0 eV from those for the unreacted metal. In cases of milder reaction conditions the Au 4f lines were the same in shape as those for the fresh metal except for a decrease in counting rate.

The Cl 2p and the shifted Au 4f peaks decreased in intensity with time (during the spectral measurement), probably due to the decomposition of the surface species by X-ray irradiation. Therefore, the Cl 2p or Au 4f line

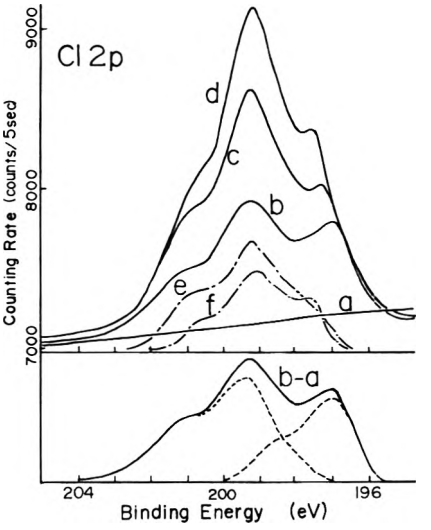

Figure 1. Cl 2p photoelectron lines from evaporated gold: (a) exposed to Cl_2; (b) 0.5 Torr, 1 min; (c) 10 Torr, 2 min; (d) 10 min; (e) c minus b; (f) d minus c. The lower figure shows two doublets.

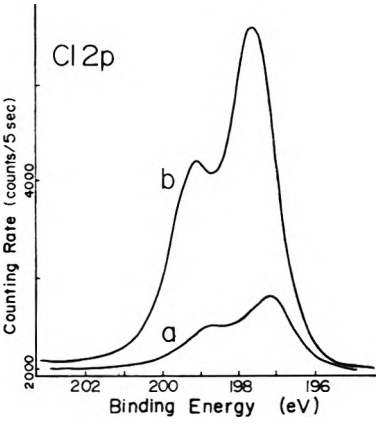

Figure 2. Cl 2p photoelectron lines from evaporated silver exposed to Cl_2: (a) 0.1 Torr, 1 min; (b) 1 Torr, 2 min.

was recorded, as quickly as possible (within 20 min) after starting X-ray irradiation. The order of measurement was either Cl 2p, Au 4f, Cl 2p, or Au 4f, Cl 2p, Au 4f. The spectra given in the figures are therefore the averaged ones. For the other metals described below, the same measurement procedure was used.

When evaporated silver was exposed to Cl_2 at a pressure of 0.1 Torr for 1 min, the Cl $2p_{1/2}$ and $2p_{3/2}$ peaks were located at 198.8 and 197.2 eV (Figure 2a). Silver was subsequently exposed to Cl_2 at a pressure of 1 Torr for 2 min. The Cl 2p peaks shifted +0.5 eV to higher binding energy. The silver 3d peaks shifted to lower binding energies on oxidation with chlorine and no new peak was observed.

When evaporated palladium was exposed to Cl_2 at a pressure of 0.5 Torr for 30 sec. Pd 3d peaks were the same in shape as those for the unreacted metal except for a 5% decrease in counting rate. The Cl 2p electrons gave two peaks at 197.8 and 199.3 eV with a shoulder on the higher binding energy side of the peaks (Figure 3a). The Cl 2p line was resolved into two doublets (dotted lines in the lower part of the figure) having the $2p_{3/2}$ peak maxima at 197.8 and 199.3 eV, respectively. The metal was subsequently exposed to Cl_2 at a pressure of 10 Torr for 1 min (b) and for 5 min (c). The Cl $2p_{3/2}$ peak at 199.0 eV was intensified, changing the peak area ratio of the two Cl 2p

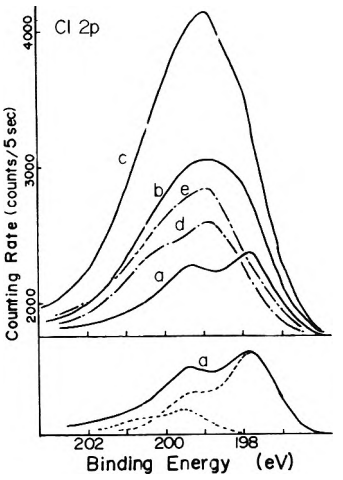

Figure 3. Cl 2p photoelectron lines from evaporated palladium exposed to Cl_2: (a) 0.5 Torr, 30 sec; (b) 10 Torr, 1 min; (c) 10 Torr, 5 min; (d) b minus a; (e) c minus b. The lower figure shows two doublets.

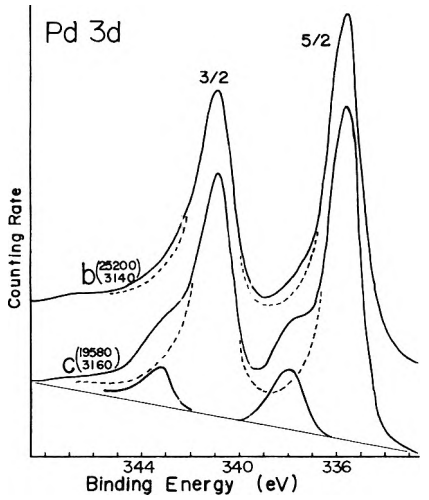

Figure 4. Pd 3d photoelectron lines from the same samples as Figure 3. Minimum and maximum counts/5 sec are written in parentheses.

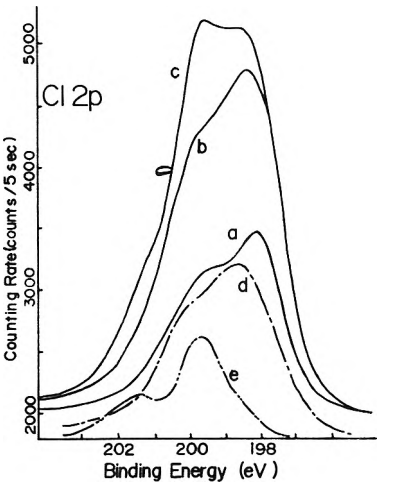

Figure 5. Cl 2p photoelectron lines from evaporated nickel exposed to Cl_2: (a) 0.5 Torr, 30 sec; (b) 10 Torr, 2 min; (c) 10 Torr, 10 min; (d) b minus a; (e) c minus d.

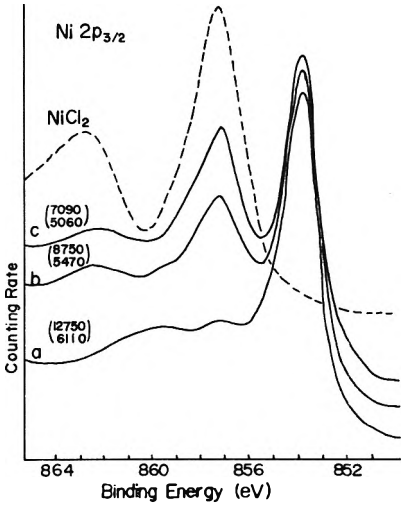

Figure 6. Ni $2p_{3/2}$ photoelectron lines from the same samples of Figure 5: - - -, $NiCl_2$. Minimum and maximum counts/5 sec are written in parentheses.

lines, and new Pd 3d peaks appeared, shifted +2.5 eV from the unreacted ones (Figure 4b,c).

When copper metal was exposed to Cl_2 at a pressure of 0.5 Torr for 10 sec, the Cl 2p electron counting rate became very high. A difference between maximum and minimum counts of 7900 counts/5 sec was observed, compared with about 2000 counts for other metals. The copper $2p_{3/2}$ peak did not shift and had the same peak width as the metal alone, while the spectrum in the valence electron region changed completely to that of CuCl.

Figures 5 and 6 were obtained from evaporated nickel exposed, in succession, to Cl_2 at a pressure of 0.5 Torr for 30 sec (a), 10 Torr for 2 min (b), and 10 Torr for 10 min (c). The Cl 2p line of (a) shows two maxima at 198.1 and 199.5 eV. The intensity of the left (199.5-eV) peak is too strong to consider the two peaks as a doublet for one kind of chlorine species, indicative of the presence of another doublet on the high-energy side. Lines d and e of Figure 5 were obtained by subtracting (a) from (b), and (b) from (c), respectively. The maximum of (d) is at 198.7 eV, being different from that for (e) at 199.7 eV and indicating adsorption of a different kind of chlorine species for the two reaction steps, in contrast to (e) and (f) of Figure 1 for gold where the two maxima are at the same binding energy of 199.3 eV. The Ni $2p_{3/2}$ lines of (a), (b), and (c) of Figure 6 indicate the appearance of a shifted peak (+3.3 eV from that for the metal). In (b) and (c), a satellite peak was observed at 862.3 eV which can be assigned to the peak due to "shake up" in nickel chloride. The peak at 859.8 eV in (a) is due to plasmon energy losses for metallic nickel.[4] The dotted curve shows the spectrum for $NiCl_2$ powder.

When evaporated iron was exposed to Cl_2 at a pressure of 10 Torr for 10 sec, a shifted Fe $2p_{3/2}$ peak appeared, +3.3 eV from the unreacted peak. The spectral variation in the Cl 2p lines were similar to that in the case of nickel.

The binding energies of the Cl $2p_{3/2}$ and the respective metal core electron peaks observed above are listed in part in Tables I and II, with the peak intensities (counts/5 sec) for Cl $2p_{3/2}$ obtained by subtracting the background counting rate from the peak maximum counting rate. The corresponding binding energies for the bulk compounds are also listed.

TABLE I: Binding Energies (eV) of Cl 2p$_{3/2}$ Peaks for Metals Exposed to Cl_2

	Fe	Ni	Cu	Pd	Ag	Au
After slight exposure to Cl_2	198.4 (800)[a]	198.1 (950)	198.0 (700)	197.8 (600) 199.4	197.2 (800)	197.0 (600) 199.4
After further exposure to Cl_2	199.0 (4700) 199.9	198.3 (3200) 199.7	198.6 (7900)	199.0 (2300) 197.8	197.7 (3600)	199.4 (2100) 197.0
Bulk compounds	199.0 ($FeCl_2$) 199.2 ($FeCl_3$)	198.5 ($NiCl_2$)	198.6 (CuCl) 199.6 ($CuCl_2$)	198.7 ($PdCl_2$)	197.9 (AgCl)	198.6 (AuCl) 199.0 ($NaAuCl_4$)

[a] Counting rates in the parentheses were obtained by subtracting minimum counts from maximum ones (counts/5 sec).

TABLE II: Chemical Shifts from Metals (eV)

	Fe 2p$_{3/2}$	Ni 2p$_{3/2}$	Cu 2p$_{3/2}$	Pd 3d$_{5/2}$	Ag 3d$_{5/2}$	Au 4f$_{7/2}$
Metals exposed to Cl_2	+3.3	+3.3	0	+2.5	−0.3	+2.0
Bulk compounds	+3.4 ($FeCl_2$) +4.7 ($FeCl_3$)	+3.6 ($NiCl_2$)	−0.3 (CuCl) +3.0 ($CuCl_2$)	+2.6 ($PdCl_2$)	−0.3 (AgCl)	+1.5 (AuCN) +2.3 (AuCl) +3.5 ($NaAuCl_4$)

Discussion

In the case of gold exposed to Cl_2, the appearance of the two Cl 2p doublets indicates the formation of two kinds of chlorine species on the surface. As the surface reaction proceeds, the shifted Au 4f peaks appear along with an increase in the intensity of the Cl 2p peak at merely higher binding energies as revealed by curves e and f of Figure 1, and these Au 4f and Cl 2p peaks are concluded to come from the same compound on the surface. The surface compound is either AuCl or an AuCl-like species since the shift in Au 4f peaks, +2.0 eV, is similar to those for Au(I) species, +2.3 eV for AuCl and +1.5 eV for AuCN, while the shift for Au(III) is +3.5 eV (for $NaAuCl_4$). The Cl 2p peak with lower binding energy and with almost constant intensity is discussed later along with the corresponding one for Pd and the peaks for other metals.

In the case of silver exposed to Cl_2, the binding energy of Cl 2p shifted +0.5 eV, with an increase in counting rate, toward that for AgCl powder. From the above results and the shift of Ag 3d, −0.3 eV, it was concluded that AgCl was formed on the surface as the reaction with chlorine proceeded. Binding energies of a peak from positively charged atoms are generally expected to be higher than those for the neutral atoms. The shift of the Ag 3d peak in AgCl is probably explained by the dominant effect of the crystal potential opposing the small shift due to the positive charge of the silver atom. The absence of a positive shift was also observed for the Cu 2p peak in Cu_2O and CuCl powder.

After longer (more than 30 min) exposure of AgCl powder to X-ray radiation, the presence of chlorine species such as Cl_2 or Cl occluded by AgCl was revealed by a new Cl 2p$_{3/2}$ peak around 200.1 eV. According to the effective charge–chemical shift relation, a peak from chlorine with zero charge is expected to appear around 200.0 eV[5] when the Cls line (285.0 eV) due to carbon contamination is used as a reference.

In the case of palladium exposed to Cl_2, two Cl 2p doublets also indicate the presence of two kinds of chlorine ions on the surface. With an increase in the concentration of the ion giving the Cl 2p$_{3/2}$ line around 199.0 eV, new Pd 3d peaks appeared which were shifted +2.5 eV from that for Pd metal, and these peaks were concluded to be due to the same Cl compound. The chemical shift for the Pd 3d peak, +2.5 eV, and the binding energy of the Cl 2p$_{3/2}$ peak, 199.0 eV, are almost the same as those for $PdCl_2$, indicative of the formation of $PdCl_2$ on the surface.

From the peak area ratio of the shifted and the unreacted Pd 3d peaks (0.05 and 0.2 for spectra c and d of Figure 3), the thickness of the surface compound formed was estimated as follows. The intensity of a photoelectron peak from a film of thickness d is represented by Klasson, *et al.*,[6] as

$$I_d = I_\infty(1 - \exp(-d/\Lambda))$$

where Λ is the escape depth, I_∞ is the intensity from a thick sample of the same material, and $\Lambda(E) = \text{const} \cdot E^{0.5}$ where E is the kinetic energy of the ejected electrons. The Λ values for E of 0.9 to 1.5 keV are smaller than 30 Å for the several samples reported, such as gold,[6] carbon,[7] alumina,[6] etc. For the surface chloride of thickness d, the intensity of Pd 3d is

$$I_c'\Lambda_c(1 - \exp(-d/\Lambda_c)); I_c'\Lambda_c = I_\infty(\text{chloride})$$

For the metal, the intensity of

$$I_m' \int_0^x \exp(-x/\Lambda_m)dx = I_m'\Lambda_m$$

is reduced to $I_m'\Lambda_m \exp(-d/\Lambda_c)$ due to the upper chloride layers. When assuming $I_m'/I_c' = 3$ (namely, an approximate value of the palladium atomic ratio per unit volume between the two phases) and the escape depth of 30 Å for the two phases (the real escape depth is expected not to exceed this value), thickness of the surface chloride layer can be estimated to be about 4 Å and 14 Å for cases c and d, respectively. When we take a smaller escape depth, the thickness is estimated to be less. The above values are rough but are probably accurate enough to estimate the upper limit.

Copper metal showed the highest reactivity with Cl_2 among the metals investigated. When copper was exposed to 0.5 Torr of Cl_2 for 10 sec, the spectrum in the valence electron region was identical with that for CuCl, indicating that multilayers of copper surface surveyed by XPS were entirely changed into CuCl.

In the case of nickel, the binding energy of Cl 2p shifted to higher values with an increase in intensity and with the appearance of a shifted Ni $2p_{3/2}$ peak. The chlorine $2p_{3/2}$ peak at 198.3 eV and nickel $2p_{3/2}$ at 857.2 eV indicate the formation of $NiCl_2$. However, from the different maxima for curves d and e of Figure 5, other types of chlorine species are expected to be adsorbed in the surface chloride. The maximum of curve e located at 199.7 eV is near that for Cl(0), indicating the adsorption of Cl_2 or Cl by the surface nickel chloride; that it does not result from decomposition of the nickel compound is indicated by a gradual decrease in its intensity during the spectral measurement. This suggests that an appreciable concentration of molecular chlorine is present after multilayers of surface chloride are formed.

In the case of iron, a reaction process was observed which was similar to that for nickel. On an iron surface, the formation of $FeCl_2$, not $FeCl_3$, was ascertained from the chemical shift of Fe $2p_{3/2}$, in contrast to the case for O_2 exposure, where Fe(III) was easily obtained.[1] Weakly adsorbed Cl_2 or Cl also exists in the surface iron chloride.

When the counting rate for the Cl 2p peak was less than 1000 counts/5 sec, the binding energies at the peak were lower for Fe, Ni, Cu, and Ag than after further surface reaction proceeded, and the difference was most distinct for Pd and Au (Table I). As the multilayers of surface chloride were formed, this peak became a shoulder of an intense peak at a higher binding energy in the cases of Au and Pd and became indistinct in the cases of Ag, Cu, Ni, and Fe. The counting rate of the former peak for Au and Pd varied only slightly, suggesting that the chloride ion giving the lower energy Cl 2p peak is limited in amount of thickness. In the case of Pd, the total area of the two Cl 2p lines for (b) of Figure 4 is two thirds of that for (c) where the chloride thickness was estimated to be smaller than 4 Å. From this, the chloride thickness for (b) can be considered to be less than 3 Å. In the case of Cu, the counting rate, 700 counts/5 sec, is one-eleventh that for the case where the copper was completely changed into CuCl to such a depth that the unreacted copper peak could not be detected by XPS. When assuming an escape depth of 30 Å for CuCl, 700 counts/5 sec corresponds to a surface chloride with a thickness of about 3 Å, that is, about one to two monolayers. The thickness of the surface chloride may be less if one considers the roughness factor of the surface and a smaller escape depth of CuCl. The above results show that the Cl 2p peak with about 700 counts/5 sec corresponds to a chloride whose thickness is about one layer. Thus, the chloride ion giving the lower binding energy for the Cl 2p peak is considered to be at the very surface when detected at a low counting rate, as illustrated by Figure 7a.

The lower binding energy of the Cl 2p peak from the chlorine ion at the very surface may be interpreted by a smaller crystal potential effect on the ion compared to that which would apply to the ion located within the reaction product surface layer and/or by the difference in bonding nature of the ion to the metals. The binding energies of the Cl 2p at low counting rate is in the order

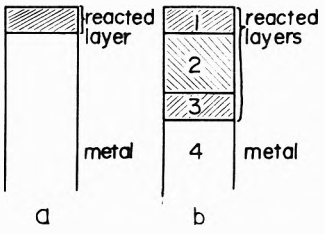

Figure 7. Surface chloride layers.

Fe > Ni > Cu > Pd > Ag > Au. The order is coincident with the oxidation-reduction potential of metals. A smaller negative charge at the chlorine ion is observed for metals with lower oxidation potential. The donor $p\pi$ strength of a chlorine ion is usually greater than the acceptor $d\pi$ strength in complexes of a high valence metal ion, and the acceptor strength becomes greater in zero valent complexes. In the cases of Fe, Ni, and Cu, the binding energy of the Cl 2p peak is near those for $FeCl_2$, $NiCl_2$, or CuCl (198.4, 198.1, and 198.0 eV, respectively), suggesting a strongly donating chlorine ion. This also suggests that the adsorbent metal atoms on the bulk metal were easily oxidized to Fe(II), Ni(II), or Cu(I) and localized largely from the metal phase. In the case of Au, the binding energy of the Cl 2p peak is much lower (197.0 eV), indicating a high negative charge on the chlorine and differing by −2.4 eV from that for the higher binding energy peak. Such highly negative chlorine is expected to bond with stronger $d\pi$ acceptor action to the adsorbent atom which is still strongly bonded to the metal phase with larger resistance to oxidation. The Pd and Ag are located between the above two classes.

Of the above two factors being considered to contribute to the shift of the binding energy, crystal potential variance and difference in bonding nature, the latter seems to be more important at present when considering the large energy difference (2.4 eV) in the shift for Au in contrast to the smaller differences (about 0.5 eV) for Cu and Ag. In the case of chlorine adsorption on nickel, the work function decreases at low surface coverage but as surface coverage $\theta \rightarrow 1.0$ the work function increases.[8] The lowering of the work function is attributed to chlorine ion penetration, resulting in the surface nickel being polarized slightly positively, which seems to correspond to the lower valency of the gold atom described above. A more negatively charged chlorine ion bonding to such a slightly positive metal may be observed even in the case of nickel if an experiment is carried out under higher vacuum to lessen oxidation by oxygen and under milder reaction conditions than the present work.

When a surface chloride multilayers thick was formed, the higher binding energy peak of the Cl 2p peak was intensified, but the lower one still remained without increasing in intensity in the cases of Au and Pd. In the case of other metals, the lower binding energy peak may be obscured by the intense higher energy peak because of the small energy differences. In these reaction stages, the chlorine ion giving the lower peak is expected to be at (3) of Figure 7b rather than at (1) according to the above discussion.

Acknowledgments. The authors wish to thank Dr. Y. Yokoyama and Mr. I. Watanabe, Osaka University, for assistance in carrying out the experiments.

กรมวิทยาศาสตร์

References and Notes

(1) K. Kishi and S. Ikeda, *Bull. Chem. Soc. Jap.*, **46**, 341 (1973).
(2) K. Kishi and S. Ikeda, *Chem. Lett.*, 245 (1972).
(3) K. Kishi and S. Ikeda, *J. Phys. Chem.*, **73**, 15 (1969).
(4) Y. Baer, P. F. Heden, J. Hedman, M. Klasson, C. Nordling, and K. Siegbahn, *Phys. Scr.*, **1**, 55 (1970).
(5) K. Siegbahn, *et al.*, "ESCA; Atomic, Molecular and Solid State Structure Studied by Means of Electron Spectroscopy," Almqvist and Wiksells, Uppsala, 1967.
(6) M. Klasson, J. Hedman, A. Berndtsson, R. Nilsson, C. Nordling, and P. Melnik, *Phys. Scr.*, **5**, 93 (1972).
(7) R. G. Steinhardt, J. Hudis, and M. L. Perlman, *Phys. Rev., B*, **5**, 1016 (1972).
(8) J. R. Anderson, *J. Phys. Chem. Solids*, **16**, 291 (1960); J. R. Anderson and N. J. Clark, "Proceedings of the 1st Australian Conference on Electrochemistry," Sydney, 1965.

Optical Spectra and Reactivities of Radical Anions of 4-Nitrobenzyl Compounds Produced by Pulse Radiolysis of Acetonitrile Solutions

H. D. Burrows[1] and Edward M. Kosower*

Department of Chemistry, Tel-Aviv University, Ramat-Aviv, Tel-Aviv, Israel, and Department of Chemistry, State University of New York, Stony Brook, New York, 11790

(Received June 25, 1973)

Electronic absorption spectra are reported for transients formed on pulse radiolysis of acetonitrile solutions of aromatic nitrobenzyl compounds and are assigned to the solute radical anions. Decay of the transients is fairly rapid but is markedly slower in the presence of tetraethylammonium formate. It is suggested that the $\cdot CH_2CN$ radical is responsible for the rapid decay and that formate ion scavenges this species. With 4-nitrobenzyl chloride, the decay of the transient is observed to be second order, in contrast to electrochemical experiments where first-order decay is observed. With 4-nitrobenzyl fluoride or alcohol, decay of the initially formed transient is accompanied by formation of a new species absorbing at longer wavelength. Identification of the 4-nitrobenzyl chloride anion is supported by first-order decay of the species in water with $k = 4 \times 10^3$ sec^{-1} (found by Hayon and Madhavan).

Introduction

Radical anions of 4-nitrobenzyl compounds $O_2NC_6H_4CH_2X$ have been shown by chemical[2] and electrochemical[3-9] methods to be unusually reactive. Where the CH_2–X bond is weak, as in the case of the halides,[3-9] cyanide,[7] and thiocyanate,[7] the predominant fate of the radical anion appears to be the unimolecular decomposition.

$$O_2NC_6H_4CH_2X\cdot^- \longrightarrow O_2NC_6H_4CH_2\cdot + X^- \qquad (1)$$

Electrochemical studies indicate that the rate of this reaction roughly parallels the CH_2–X bond energies,[5-8] although the absolute rate constants for this decomposition are not certain. Thus, "single-sweep" cyclic voltammetry of 4-nitrobenzyl chloride in acetonitrile containing 0.1 *M* tetra-*n*-butylammonium perchlorate indicated a rate constant for the decomposition of the radical anion of approximately 50 sec^{-1},[7,10] while other cyclic voltammetric measurements and chronoamperometry suggest the rate constant to be at least 4×10^3 sec^{-1}.[6] The failure to obtain consistent results by these procedures may indicate their limitations in studying very fast reactions.

The technique of pulse radiolysis has been shown to be a valuable method for studying short-lived species. Consequently, we have used this procedure to obtain further information on the anion radicals of 4-nitrobenzyl compounds, and attempt to resolve this discrepancy in their decomposition rates.

In addition to providing a suitable solvent for the electrochemical studies, acetonitrile has been shown upon radiolysis to produce a species capable of reducing anthracene to its radical anion in high yield (G = 1.55[11]) and thus provides a good medium for the pulse radiolysis investigation.

The primary step in the radiolysis of acetonitrile can be written

$$CH_3CN \longrightarrow CH_3CN^* + CH_3CN\cdot^+ + e^- \qquad (2)$$

Pulse radiolysis studies on liquid acetonitrile using naphthalene as an acceptor indicate that the yield of excited states (including excited states formed by solute ion recombination) is low, but detectable ($G(^3N)$ = 0.30).[11] The nature of the reducing species present in the radiolysis of CH_3CN is not clear at present. An initial report[12] that a solvated electron, $\lambda_{max} \sim 700$ nm, $t_{1/2} \sim 5$ μsec, was produced has been questioned by Hayon,[11] who was unable to detect any absorption in the range 280–800 nm with a time resolution of 100 nsec.

The oxidizing species formed initially, $CH_3CN\cdot^+$, may be expected to deprotonate to give $\cdot CH_2CN$ radicals

$$CH_3CN\cdot^+ + CH_3CN \longrightarrow \cdot CH_2CN + CH_3CNH^+ \qquad (3)$$

Evidence for the presence of $\cdot CH_2CN$ radicals comes from steady-state studies,[13] and also from the observation of a weak absorption at wavelengths shorter than 280 nm assigned to this species on pulse radiolysis of liquid acetonitrile.[11] We describe the pulse radiolysis of acetonitrile so-

lutions of 4-nitrobenzyl compounds, and indicate the reactivities of the resultant species.

Experimental Section

Materials. 4-Nitrobenzyl fluoride, chloride, and bromide and 4-nitrotoluene were purified as described previously.[8] 4-Nitrobenzyl iodide was prepared by the method of Finkelstein[14] and was purified by one recrystallization from ethanol, followed by sublimation (in the absence of light): pale yellow crystals, mp 125.5–127° (lit.[14] 127°). 4-Nitrobenzyl acetate was prepared as described by Reid[15] and was recrystallized twice from aqueous ethanol: white crystals, mp 76–77° (lit.[15] 78°). 4-Nitrobenzyl alcohol was obtained by hydrolysis of the acetate[16] and was recrystallized three times from water: white crystals, mp 92.5–93.5° (lit.[16] 96–97°). Further recrystallization did not affect the melting point. Acetonitrile was purified by two procedures. Merck Uvasol grade was dried by standing over molecular sieves and was redistilled from fresh molecular sieves. Fluka purum grade acetonitrile was purified by the method of O'Donnell, *et al.*[17] No difference was found between the results obtained using these different samples.

Tetraethylammonium ferrocyanide was prepared by neutralizing a cold aqueous solution of hexacyanoferric acid[18] with tetraethylammonium hydroxide. Water was removed under reduced pressure, and the salt crystallized as pale yellow needles. Light was excluded from all manipulations with this compound which was very photosensitive. The salt was added to argon-saturated solutions immediately prior to pulse radiolysis as it was oxidized in the presence of oxygen in acetonitrile. Tetraethylammonium dibenzyl phosphate was prepared by neutralizing hydrogen dibenzyl phosphate[19] in 60% aqueous methanol with tetraethylammonium hydroxide. Excess solvent was removed under reduced pressure. The salt was obtained as an oil. Nmr indicated the presence of 20% water. Tetraethylammonium formate was prepared by neutralizing formic acid with tetraethylammonium hydroxide. Excess water was removed under reduced pressure. The product was obtained as an oil. Nmr (D_2O) indicated peaks at δ 8.64 (s, 1 formate hydrogen), 5.03 (s, water), 3.7–3.2 (q, 8 methylene hydrogens), 1.8–1.25 (three overlapping triplets, 12 methyl hydrogens). The nmr indicated the presence of *ca.* 30% (w/w) water. The observation of overlapping methyl triplets strongly suggests ion pairing in the salt. Strong ion pairing has been clearly demonstrated by infrared spectroscopy in the related compound, triethylammonium acetate.[20] On preparing solutions containing tetraethylammonium formate for pulse radiolysis, a small amount of precipitation occurred. Consequently, solutions were filtered immediately before each experiment. This precipitate was not characterized, but it is possibly tetraethylammonium carbonate.

Procedure. Pulse radiolysis experiments were carried out using 0.05–1.5-μsec, 5-MeV, 200-mA pulses from the electron linear accelerator at the Hebrew University of Jerusalem. The pulses were of up to 2-krad dose. The irradiation cell was 4 cm long with multipass optics such that the analyzing light traveled three times through the cell. The details of the experimental setup have been described elsewhere.[21] Dosimetry was performed using the absorption of the solvated electron in deaerated ethanol at 600 nm, as described by Land, *et al.*[22] Extinction coefficients of radical anions were estimated assuming $G = 1.55$ for the reducing species in acetonitrile, with complete scavenging of this species by the solute.

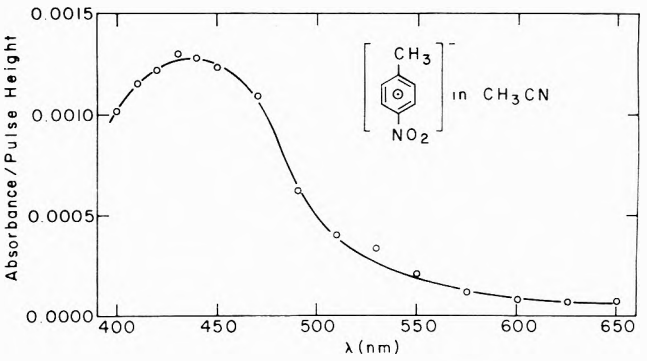

Figure 1. End of pulse spectrum for degassed acetonitrile solution of 4-nitrotoluene.

Solutions were degassed by bubbling argon through them prior to radiolysis, and they were protected from photolysis by the monitoring light by insertion of a filter cutting off wavelengths just below the relevant transient absorption.

Results

Spectra. Pulse radiolysis of a solution of 4-nitrotoluene (6×10^{-3} *M*) in acetonitrile resulted in an absorption with λ_{max} 440 (±10) nm, ϵ_{max} ~1800 M^{-1} cm^{-1} (Figure 1) which was completely formed at the end of a 1.5-μsec pulse. A similar absorption was obtained upon pulse radiolysis of 4-nitrotoluene in 10% acetone–water. This absorption was very similar to the reported spectra of the radical anion of 4-nitrotoluene obtained by electrolysis in dimethylformamide (λ_{max} 460 nm),[23] by pulse radiolysis in water at pH 3 (λ_{max} 440 nm, ϵ_{max} 400 M^{-1} cm^{-1}),[24] and by γ radiolysis in 4-methyltetrahydrofuran at 77 K (λ_{max} 470 nm, ϵ_{max} 3500 M^{-1} cm^{-1}),[25] and is accordingly assigned to this species. The reason for this large difference in extinction coefficients is not at present clear. An earlier report[26] that the radical anion (obtained by reduction by potassium in tetrahydrofuran) possessed absorption bands at 302, 607, and 875 nm must be viewed with some caution, as has been previously indicated by Sioda and Kemula.[23] An identical but more intense absorption was observed on pulse radiolysis of an acetonitrile solution of 4-nitrotoluene in the presence of tetraethylammonium formate (0.1 *M*). An absorption of similar character, although rather broader and weaker, was observed on pulse radiolysis of a solution of 4-nitrotoluene in the presence of Tris (5×10^{-4} *M*) in 95% acetonitrile–water.

Pulse radiolysis of a solution of 4-nitrobenzyl fluoride (2×10^{-3} *M*) in acetonitrile yielded a species absorbing at 490 (±10) nm ϵ_{max} ~1600^{-1} cm^{-1} (Figure 2, circles). The species responsible for this absorption is rapidly replaced ($t_{1/2}$ ~10 μsec) by a new species absorbing at *ca.* 625 nm (Figure 2, triangles). This new species eventually decays, leaving a permanent absorption below 410 nm. The initially formed species is assigned to the radical anion by analogy with 4-nitrotoluene. Assignment of the second absorption is more problematical (see Discussion section for a consideration of possible candidates). Similar behavior was observed on pulse radiolysis of solutions of 4-nitrobenzyl fluoride in the presence of tetraethylammonium dibenzyl phosphate (5×10^{-4} *M*) tri-*n*-butylamine (5×10^{-4} *M*), or tetraethylammonium formate (0.1 *M*). Pulse radiolysis of a solution of 4-nitrobenzyl fluoride in 95% ac-

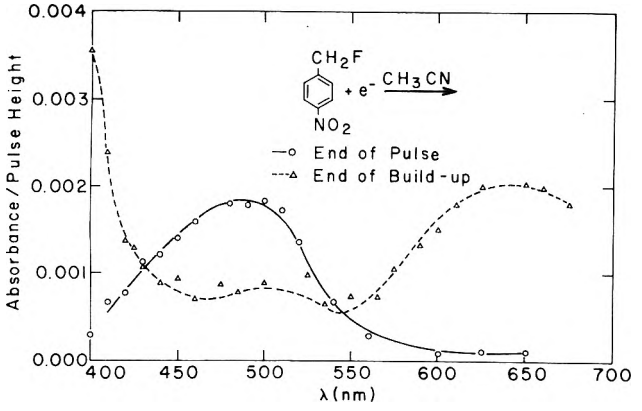

Figure 2. Transients observed upon pulse radiolysis of degassed acetonitrile solution of 4-nitrobenzyl fluoride: ——O——, end of pulse; - - -Δ- - -, end of buildup of long wavelength absorption.

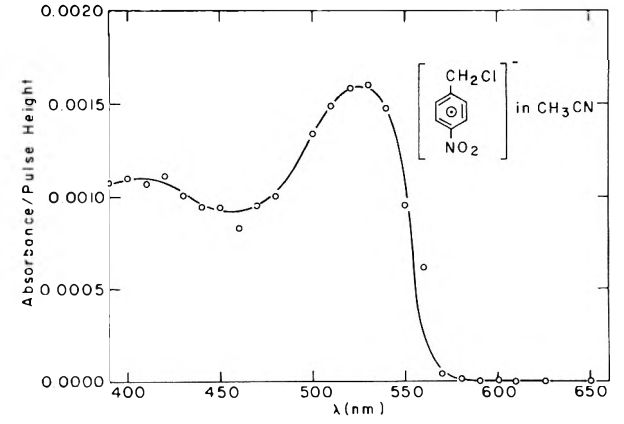

Figure 3. End of pulse spectrum for degassed acetonitrile solution of 4-nitrobenzyl chloride.

etonitrile–water in the presence of tris (2×10^{-4} *M*) gave a similar, but rather broader and weaker spectrum.

Tetraethylammonium salts were used because of their solubility in organic media. Ferrocyanide was used as a non-nucleophilic reducing agent, dibenzyl phosphate as a non-nucleophilic proton donor, and formate as a weakly nucleophilic hydrogen atom donor.

Pulse radiolysis of solutions of 4-nitrobenzyl chloride (4×10^{-3} *M*), bromide (2.5×10^{-3} *M*), and iodide (2.5×10^{-3} *M*) gave rather similar behavior for all three halides, with an absorption at 530 (±5) nm, ϵ_{max} ~1900 M^{-1} cm^{-1}, and a shoulder at *ca.* 420 nm. The spectrum of 4-nitrobenzyl chloride is illustrated in Figure 3. With the chloride and bromide, similar but rather broader and weaker absorptions were observed in the presence of Tris (2×10^{-4} *M*) in 95% acetonitrile–water.

Pulse radiolysis of a solution of 4-nitrobenzyl chloride with tetraethylammonium ferrocyanide (5×10^{-3} *M*) and water (2 *M*) gave a similar but broader and weaker absorption which decayed to give a permanent absorption below 460 nm. The absorption was identical in the presence of tetraethylammonium dibenzyl phosphate (5×10^{-4} *M*), and similar but more intense in the presence of tetraethylammonium formate (0.1 *M*).

Pulse radiolysis of a solution of 4-nitrobenzyl acetate (2×10^{-3} *M*) in acetonitrile yielded an absorption at the end of the pulse at 460 (±10) nm, ϵ_{max} ~1700 M^{-1} cm^{-1} (Figure 4). An identical but more intense spectrum was obtained in the presence of tetraethylammonium formate (0.1 *M*).

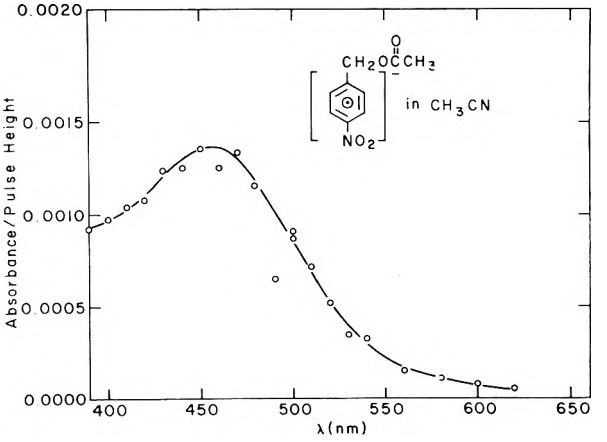

Figure 4. Absorption at end of pulse for degassed acetonitrile solution of 4-nitrobenzyl acetate.

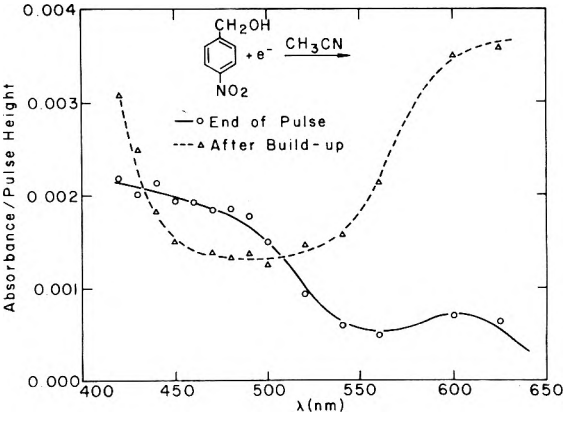

Figure 5. Transients observed upon pulse radiolysis of degassed acetonitrile solution of 4-nitrobenzyl alcohol with tetraethylammonium formate (0.1 *M*): ——O——, end of pulse; - - -Δ- - -, end of buildup.

Pulse radiolysis of a solution of 4-nitrobenzyl alcohol (2×10^{-3} *M*) in acetonitrile yielded an absorption at *ca.* 450 nm. Pulse radiolysis in the presence of tetraethylammonium formate (0.1 *M*) yielded a similar absorption, λ *ca.* 450 nm, ϵ_{450} ~1250 M^{-1} cm^{-1} which also decayed to give a new species absorbing at λ > 625 nm (Figure 5).

Kinetics. One aim of this work has been to obtain information on the lifetimes of radical anions of 4-nitrobenzyl compounds. However, in the study of the kinetics of the transient absorptions observed on pulse radiolysis of acetonitrile solutions of these compounds it became apparent that the species were decaying by a reaction with one of the primary products of the radiolysis of acetonitrile. Thus 4-nitrotoluene, which is known from electrochemical studies to yield a stable radical anion[7] on pulse radiolysis in acetonitrile yielded a species λ_{max} 440 nm, which decayed *via* complex kinetics over a period of hundreds of microseconds. The rate of decay depended upon the pulse size. Similarly, the species observed on pulse radiolysis of 4-nitrobenzyl, chloride, bromide, iodide, acetate, and alcohol decayed fairly rapidly, the decay rate being dependent upon the pulse size. Of the products produced on radiolysis of acetonitrile, $CH_3CN^{\cdot+}$, $\cdot CH_2CN$, and H^+ appear the most likely candidates for reacting with the radical anions. Accordingly, compounds were added to trap these species. Tetraethylammonium ferrocyanide was found to have little effect on the decay rate of the species

obtained from the chloride, although after radiolysis a new absorption was observed below 460 nm, due to the ferricyanide. Thus $CH_3CN\cdot^+$ was probably not the reactive species. Similarly, tetraethylammonium dibenzyl phosphate, Tris, or tri-*n*-butylamine did not markedly affect the decay rate, suggesting protonation was not responsible for the rapid decay. In the radiation chemistry of water, formate ions have been used to trap the oxidizing hydroxyl radical.[27] With $\cdot CH_2CN$, formate ion might be expected to transfer a hydrogen atom to yield $CO_2\cdot^-$, a reducing species. If $\cdot CH_2CN$ is responsible for the short lifetime of the species obtained on pulse radiolysis, then formate ion may be expected to slow down the decay. Further, as a reducing species is produced, if the absorbing species produced on radiolysis of acetonitrile solutions of 4-nitrobenzyl compounds is the radical anion, or some species derived from it, then the concentration of this species may be expected to be increased on pulse radiolysis in the presence of formate. Pulse radiolysis of acetonitrile solutions of tetraethylammonium formate (0.1 *M*) revealed only a very weak absorption at wavelengths shorter than 425 nm. Pulse radiolysis of a solution of 4-nitrotoluene in the presence of tetraethylammonium formate (0.1 *M*) with 2-krad pulses yielded an absorption which was identical in shape, but of about double the intensity of that observed in the absence of the formate. There was a small (less than 10%) decrease in the absorption at 440 nm, and a corresponding small increase in absorption at 420 nm over period of 100 μsec. However, after this time, the absorption was long lived (decayed in greater than 20 msec). Similar behavior was observed with 4-nitrobenzyl acetate. A likely explanation for this behavior is that the formate ion scavenges most, but not all, of the $\cdot CH_2CN$ species. Due to problems of solubility, it was not possible to go to higher formate concentrations, however, when smaller pulses (*ca.* 900 rads) were used there was no decay of the absorption in times less than 20 msec. 4-Nitrobenzyl bromide and iodide appeared to react with the formate in acetonitrile. Pulse radiolysis of 4-nitrobenzyl chloride in the presence of tetraethylammonium formate yielded an absorption identical in shape but enhanced in intensity. With large (2-krad) pulses, fairly complex decay kinetics were observed for the first 30 μsec. After this time, however, the decay followed a second-order rate law to greater than 3 half-lives. As with the 4-nitrotoluene and 4-nitrobenzyl acetate radical anions, the initial decay probably arises from reaction of $\cdot CH_2CN$ with the radical anion. With smaller pulses (<1 krad) only the second-order decay was observed. This showed a slight (25%) decrease in the decay rate for a greater than tenfold decrease in pulse size. A mean value of 14.4 ($\pm$2.3) $\times 10^5$ cm sec^{-1} was obtained for k/ϵ. Employing the estimated extinction coefficient, the second-order rate constant for the decay is approximately 2.7×10^9 M^{-1} sec^{-1}. Under the conditions of pulse radiolysis where there are comparatively high (10^{-6} to 10^{-7} *M*) concentrations of radical anions it would appear that a second-order reaction (possibly radical coupling) is the main fate of this species. This contrasts with the behavior in electrochemical experiments[8] where, possibly because of the radical concentration, unimolecular decay is the favored reaction.

With 4-nitrobenzyl bromide and iodide it was not possible to scavenge the $\cdot CH_2CN$ radicals in the same way, as the tetraethylammonium formate very rapidly reacted with the halides in acetonitrile solution, probably *via* nucleophilic substitution, yielding 4-nitrobenzyl formate. However, a lower limit of 70 μsec could be set for the lifetimes of the radical anions from the slowest decays.

The decays of the radical anions from 4-nitrobenzyl fluoride and alcohol differed from those of the other derivatives in that new absorptions were observed to grow in on a time-scale similar to the loss of the absorptions assigned to the radical anions. In both these cases the decay appeared to be first-order with rate constants 10^4–10^5 sec^{-1} for *ca.* 2×10^{-3} *M* solute. With the fluoride, however, the rate of interconversion showed a dependence on 4-nitrobenzyl fluoride concentration. This reaction was not investigated further.

Discussion

The objective of this study has been to characterize the radical anions of 4-nitrobenzyl compounds, both with regard to their optical spectra and reactivities. It is perhaps surprising that few reports exist on the spectroscopic characterization of these species in view of the large number of studies on reductions of 4-nitrobenzyl compounds in which they are claimed as intermediates. With 4-nitrotoluene, characterization of the radical anion optical spectrum has been achieved by electrochemical,[23] pulse radiolysis,[24] and γ-radiolysis[25] studies. Our work supports these previous assignments and indicates that in acetonitrile this species has an absorption λ_{max} 440 nm. This radical anion has also been observed in esr experiments.[28,29,31] Few other reports of spectra of anion radicals of 4-nitrobenzyl compounds exist in the literature.[29-33]

We tentatively assign the initial spectra observed upon pulse radiolysis of acetonitrile solutions of 4-nitrobenzyl fluoride, 4-nitrobenzyl chloride, 4-nitrobenzyl bromide, 4-nitrobenzyl iodide, 4-nitrobenzyl alcohol, and 4-nitrobenzyl acetate to the corresponding radical anions on the basis of the known radiation chemistry of acetonitrile and the behavior observed with 4-nitrotoluene. With the alcohol, acetate, and fluoride similar spectra were observed with a progressive shift of the maxima to lower energies, possibly resulting from a σ–π interaction similar to the examples reported by Traylor, *et al.*[34] Assignment of the absorptions observed with the chloride, bromide, and iodide is less certain as, although these all possessed a band at longer wavelength than the other derivatives as expected on the basis of σ–π interactions, the spectra were very similar for these three compounds.

A possible alternative assignment of the absorption which must be considered is the 4-nitrobenzyl radical, formed by dissociative electron capture (4) as has been

$$RX + e^- \longrightarrow R\cdot + X^- \qquad (4)$$

suggested to occur in the reduction of benzyl chloride by hydrated electrons.[35] This process may be expected to be less important with 4-nitrobenzyl chloride than with benzyl chloride. Further, the decay of the absorbing species is second order. If the 4-nitrobenzyl radical were produced, one might anticipate that hydrogen abstraction from the tetraethylammonium formate would be an important decay pathway for this species. Finally, although in the electrochemical studies there is disagreement over the absolute rate of cleavage of the 4-nitrobenzyl halide radical anions, all workers are agreed that these are actual intermediate species.[5,6,8,9] Unless, therefore, different factors are important in the electrochemical and radiation chemi-

cal reductions, we feel that the observed behavior can be best explained by assignment of these absorptions to the corresponding radical anions.

Further evidence in favor of this assignment comes from a study of the pulse radiolysis of 4-nitrobenzyl chloride in aqueous solution (Hayon and Madhavan, unpublished results). A transient is observed both on pulse radiolysis of 4-nitrobenzyl chloride in water in the presence of *tert*-butyl alcohol and on reduction of 4-nitrobenzyl chloride by $(CH_3)_2COH$ radical in water. The spectrum of this species is dependent upon the pH, clearly demonstrating an acid–base property. Further, the observed pK_a (3.5 ± 0.1) is close to that for other substituted nitrobenzene radical anions.[24] The most reasonable explanation for this behavior is that the transient formed initially upon pulse radiolysis of 4-nitrobenzyl chloride in water is the radical anion, which in acidic solution protonates at the nitro group. If the 4-nitrobenzyl chloride radical anion is sufficiently long-lived in water to permit direct observation by pulse radiolysis (k_1 = 4.1 ± 0.6 × 10^3 sec^{-1} for decay of species in water at pH 9.3), it is hardly likely that in acetonitrile the species will decay in a time shorter than that of the first observation (~1 μsec). Thus, we feel that the transients observed upon radiolysis of the 4-nitrobenzyl halides in acetonitrile are the radical anions.

Analysis of the decay kinetics of the radical anions, under conditions in which the species did not react with solvent-derived radicals (*i.e.*, using low doses, with 0.1 *M* tetraethylammonium formate) indicated that while the radical anions of 4-nitrotoluene and 4-nitrobenzyl acetate were long-lived (lifetime greater than 20 msec) the species from the 4-nitrobenzyl chloride decayed by a second-order process with rate constant *ca.* 3 × 10^9 M^{-1} sec^{-1}. This reaction may be either dimerization of disproportionation of the radical anion and is in marked contrast to the electrochemical experiments where, possibly as a result of the lower radical concentrations, unimolecular decay predominates. With 4-nitrobenzyl bromide and iodide, it was only possible to set a lower limit of *ca.* 70 μsec for the lifetime of these radical anions.

A plausible scheme for the second-order disappearance of the 4-nitrobenzyl chloride radical anion can be formulated on the following principles: (1) π radicals can interact to form dimer complexes, which we have termed π-mers;[36] (2) reversible electron transfer, forming 4-nitrobenzyl chloride and 4-nitrobenzyl chloride dianion (the dianion would surely lose chloride ion extremely quickly); or (3) simultaneous loss of two chloride ions with formation of a covalent bond between the two rings in the π-mer. Charged π radicals are well known to form π-mers, *e.g.*, dimethylbipyridylium cation radical[37] and tetracyanoquinodimethane radical anion[38] (reactions 5–7).

4-Nitrobenzyl fluoride and 4-nitrobenzyl alcohol showed rather different behavior from the other compounds investigated. The radical anions were observed to convert to a new species possessing an absorption at *ca.* 625 nm. Furthermore, in the case of the 4-nitrobenzyl fluoride the rate of this interconversion was found to depend upon the solute concentration. Hawley and coworkers[5] observed similar electronic spectra on electroreduction of 4,4′-dinitrobibenzyl or 4-nitrobenzyl chloride in acetonitrile, suggesting that an anionic species derived from dinitrobibenzyl may be responsible for the absorptions. This assignment would explain the observed dependence of the interconversion on the solute concentration in the case of 4-nitrobenzyl fluoride. However, a firm proposal for the structure of the 625-nm absorbing material requires further work.

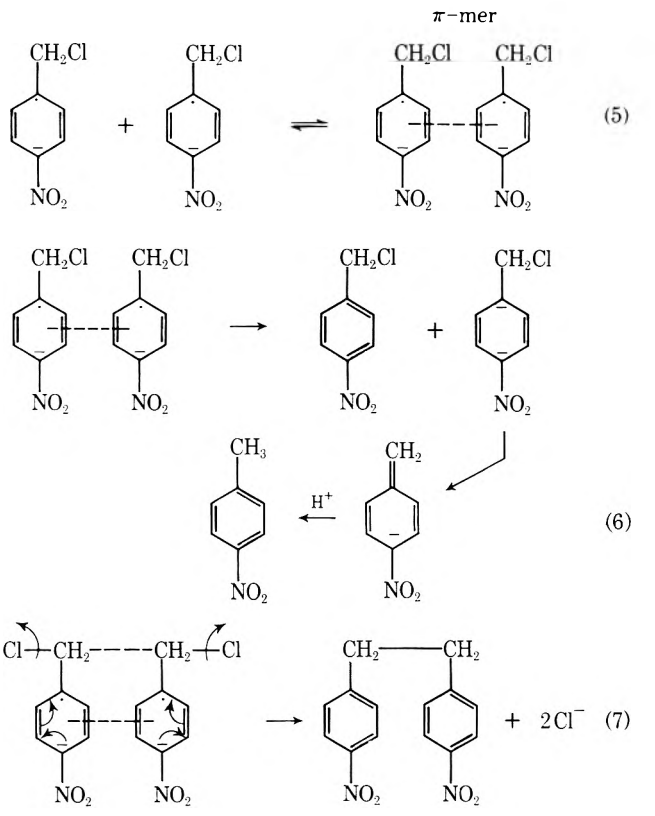

Acknowledgments. We thank Professor G. Czapski and the linac group at the Hebrew University of Jerusalem for access to their facilities, and we are particularly grateful to Mr. J. Ogdan for maintenance of the accelerator and electronic equipment. Professor E. Hayon and V. Madhavan (U. S. Army Natick Laboratories) were kind enough to send us their results on 4-nitrobenzyl chloride. We are grateful to the Petroleum Research Fund of the American Chemical Society for financial support.

References and Notes

(1) Universidade de Coimbra, Laboratório Químico da Faculdade de Ciências, Coimbra, Portugal.
(2) L. Weisler and R. W. Helmkamp, *J. Amer. Chem. Soc.*, **67**, 1167 (1945); H. B. Hass and M. L. Bender, *ibid.*, **71**, 1767, 3482 (1949); R. C. Kerber, G. W. Urry, and N. Kornblum, *ibid.*, **87**, 4520 (1965); N. Kornblum, R. E. Michel, and R. C. Kerber, *ibid.*, **88**, 5660 (1966); G. A. Russell and W. C. Danen, *ibid.*, **88**, 5663 (1966).
(3) G. Klopman, *Helv. Chim. Acta*, **44**, 1908 (1961).
(4) J. Grimshaw and J. S. Ramsay, *J. Chem. Soc. B*, 60 (1968).
(5) J. G. Lawless, D. E. Bartak, and M. D. Hawley, *J. Amer. Chem. Soc.*, **91**, 7121 (1969).
(6) D. E. Bartak and M. D. Hawley, *J. Amer. Chem. Soc.*, **94**, 640 (1972).
(7) M. Mohammad, J. Hajdu, and E. M. Kosower, *J. Amer. Chem. Soc.*, **93**, 1792 (1971).
(8) M. Mohammad and E. M. Kosower, *J. Amer. Chem. Soc.*, **93**, 2713 (1971).
(9) P. Peterson, A. K. Carpenter, and R. F. Nelson, *J. Electroanal. Chem. Interfacial Electrochem.*, **27**, 1 (1970).
(10) In a preliminary report[7] this value was given as approximately 10–20 sec^{-1}. More detailed electrochemical analysis gives a value of 50 sec^{-1}; M. Mohammad, unpublished work.
(11) E. Hayon, *J. Chem. Phys.*, **53**, 2353 (1970).
(12) A. Singh, H. D. Gesser, and A. R. Scott, *Chem. Phys. Lett.*, **2**, 271 (1968).
(13) D. Bradley and J. Wilkinson, *J. Chem. Soc. A*, 53 (1967).
(14) H. Finkelstein, *Chem. Ber.*, **43**, 1531 (1910); *Chem. Abstr.*, 2441 (1910).
(15) E. E. Reid, *J. Amer. Chem. Soc.*, **39**, 124 (1917).
(16) W. W. Hartman and E. J. Rahrs, "Organic Syntheses," Coll. Vol.

III, Wiley, New York, N. Y., 1955, p 652.
(17) J. F. O'Donnell, J. T. Ayres, and C. K. Mann, *Anal. Chem.*, **37**, 1161 (1965).
(18) Prepared according to H. Lux, "Handbook of Preparative Inorganic Chemistry," 2nd ed, G. Brauer, Ed., Academic Press, New York, N. Y., 1965, p 1509.
(19) F. R. Atherton, H. T. Howard, and A. R. Todd, *J. Chem. Soc.*, 1111 (1948).
(20) G. M. Barrow and E. A. Yerger, *J. Amer. Chem. Soc.*, **76**, 5211 (1954).
(21) Internal Report of the Accelerator Laboratory, Hebrew University, Jerusalem, Israel; N. N. Lichtin, J. Ogdan, and G. Stein, *Biochim. Biophys. Acta*, **263**, 14 (1972).
(22) E. J. Land, J. T. Richards, and J. K. Thomas, *J. Phys. Chem.*, **76**, 3805 (1972).
(23) R. E. Sioda and W. Kemula, *J. Electroanal. Chem. Interfacial Electrochem.*, **31**, 113 (1971).
(24) W. Gruenbein, A. Fojtik, and A. Henglein, *Z. Naturforsch.* **24b**, 1336 (1969).
(25) T. Shida and S. Iwata, *J. Phys. Chem.*, **75**, 2591 (1971).
(26) A. Ishitani, K. Kuwata, H. Tsubomura, and S. Nagakura, *Bull. Chem. Soc. Jap.*, **36**, 1357, (1973).
(27) See, for example, E. J. Land and A. J. Swallow, *Biochim. Biophys. Acta*, **162**, 327 (1968).
(28) A. H. Maki and D. H. Geske, *J. Amer. Chem. Soc.*, **83**, 1852 (1961).
(29) P. L. Kolker and W. A. Waters, *J. Chem. Soc.*, 1136 (1964).
(30) W. M. Gulick and D. H. Geske, *J. Amer. Chem. Soc.*, **88**, 2928 (1966).
(31) P. B. Ayscough, F. P. Sargent, and R. Wilson, *J. Chem. Soc.*, 5418 (1963).
(32) G. A. Russell and W. C. Danen, *J. Amer. Chem. Soc.*, **90**, 347 (1968).
(33) W. E. Griffiths, G. F. Longster, J. Myatt, and P. F. Todd, *J. Chem. Soc. B*, 1130 (1966).
(34) W. Hanstein, H. J. Berwin, and T. G. Traylor, *J. Amer. Chem. Soc.*, **92**, 829 (1970).
(35) J. P. Mittal and E. Hayon, *Nature (London), Phys. Sci.*, **240**, 20 (1972), and references therein.
(36) E. M. Kosower and J. Hajdu, *J. Amer. Chem. Soc.*, **93**, 2534 (1971).
(37) E. M. Kosower and J. L. Cotter, *J. Amer. Chem. Soc.*, **86**, 5524 (1964).
(38) R. H. Boyd and W. D. Phillips, *J. Chem. Phys.*, **43**, 2927 (1965).

Electron Paramagnetic Resonance Study of Radicals Formed from Allyl Compounds[1]

P. Smith,* R. A. Kaba,[2] and P. B. Wood

Paul M. Gross Chemical Laboratory, Department of Chemistry, Duke University, Durham, North Carolina 27706

(Received August 27, 1973)

Using the $TiCl_3$-H_2O_2 radical-generating method within a continuous-flow system at *ca.* 25°, we have carried out a comprehensive epr study of the radicals formed from $CH_2{=}C(CH_3)CH_2OH$ and 14 allyl compounds, *viz.*, $(CH_2{=}CHCH_2)_2O$ and $CH_2{=}CHCH_2X$ with -X equal to -OH, -OOCH, $-OOCCH_3$, $-OOCCH_2CH_3$, $-OOCCH_2CH_2CH_3$, $-OOCC_6H_5$, -CN, $-NH_2$, $-NHCONH_2$, -COOH, $-OCH_2CH_2OH$, $-OCH_2CH_3$, and $-OCH_2\underline{CHCH_2}O$. Generally, water was the reaction solvent. However, the aromatic compound was not sufficiently soluble in this medium and so was run in water mixed with acetone. Each $CH_2{=}CHCH_2X$ compound gave only the $HOCH_2\dot{C}HCH_2X$, **1** (-X), and $\cdot CH_2CH(OH)CH_2X$, **2** (-X), radicals, except that $CH_2{=}CHCH_2OH$ also yielded $CH_2{\cdots}\dot{C}H{\cdots}CHOH$. The $CH_2{=}C(CH_3)CH_2OH$ and $(CH_2{=}CHCH_2)_2O$ each gave only one radical, of structure analogous to **1** (-X), although the spectrum formed from the ether was broadlined and might contain other radicals. To help characterize some of the **1** (-X) and **2** (-X) radicals, we have carried out a similar investigation where we replaced the H_2O_2 in the $TiCl_3$-H_2O_2 system with NH_2OH, five $CH_2{=}CHCH_2X$ compounds being so examined, *viz.*, with -X equal to -OH, -OOCH, $-OOCCH_2CH_2CH_3$, $-NH_2$, and $-OCH_2\underline{CHCH_2}O$. Each of these compounds gave only the $H_2NCH_2\dot{C}HCH_2X$ radical, except that $CH_2{=}CHCH_2OH$, when run at high enough concentrations, also produced a signal assignable to a polymeric radical.

Introduction

The reaction between titanous chloride and hydrogen peroxide in the presence of a reactive organic substrate within an aqueous continuous-flow system is the basis of a well known method of generating transient free radicals in electron paramagnetic resonance, epr, spectroscopic investigations.[3,4] In an earlier paper,[5] we reported the results of an epr spectroscopic study of the radicals observed to be formed from allyl alchohol, $CH_2{=}CHCH_2OH$ or AOH, as substrate with the use of this method. We found this substrate to yield the two conceivable addition radicals $HO\dot{C}H_2CHCH_2OH$, **1**, and $\cdot CH_2CH(OH)CH_2OH$, **2**, as the major products. Also observed was the allylic radical $\cdot CH_2CH{=}CHOH \leftrightarrow CH_2{=}CHCHOH$, **3**, and, when the allyl alcohol concentration was sufficiently high, there was noticed a signal attributable to a polymeric addition radical. On the other hand, when the photodecomposition of hydrogen peroxide is employed as the radical-generating reaction, only radical **3** is observed.[6,7]

The present paper represents an extension of our previous investigation to the study of other allyl compounds with the use of the $TiCl_3$-H_2O_2 method. In general, our results with these allyl compounds are similar to those of our earlier work.[5] However, for no allyl compound except allyl alcohol did we readily observe a signal attributable to an allylic radical and, consequently, we made no attempt to pursue this aspect. Also, for each allyl compound studied, the concentration was low enough that we did not observe a polymeric radical spectrum.[5] The resolution we could obtain under optimum conditions proved to be much better than before, thus allowing, for example, a more complete characterization of radical **1** and the observation of an ϵ-proton coupling in several ether radicals.

Experimental Section

The experimental arrangement and procedures were essentially as detailed before[8] except that the continuous-flow system was of the two-stream type employed in several of our previously reported[5,9-14] investigations. The epr cell was constructed of Suprasil to the Borg mix-and-flow design.[11,15] Spectra were recorded as the first derivative and g values taken as before against aqueous potassium peroxylamine disulfonate.[8]

Fresh samples of the following substrates were examined without further purification: allyl alcohol, allyl acetate, allylamine, allyl formate, and 1-allylurea (Eastman, reagent grade), methallyl alcohol (Eastman, practical grade), allyl benzoate and allyl propionate (Calbiochem), allyl cyanide, allyl n-butyrate, diallyl ether, and allyl ethyl ether (Borden), allyl 2-hydroxyethyl ether (Borden and K & K), vinylacetic acid (K & K), and allyl glycidyl ether (Aldrich).

Unless specified otherwise, the following reaction conditions were employed: the reducing stream, 0.004 and 0.2 M in titanous chloride and sulfuric acid, respectively; and the oxidizing stream, 0.1 M in hydrogen peroxide with no added sulfuric acid; total flow rate, 2–4 ml sec^{-1} divided equally between the two streams; the reaction temperature, 25 ± 2°. For allyl alcohol and methallyl alcohol, both streams were 0.1 M with respect to substrate. Otherwise, substrates were included only in the hydrogen peroxide stream, their concentrations being as follows: allyl acetate, 0.01 M; 1-allylurea, 0.02 M; allyl formate and allylamine, 0.03 M; allyl n-butyrate and allyl propionate, 0.04 M; allyl 2-hydroxyethyl ether, 0.05 M; vinylacetic acid, 0.06 M; allyl benzoate, allyl glycidyl ether, and allyl cyanide, 0.09 M. For allyl benzoate, due to its limited solubility in aqueous solutions, the substrate stream was made up with CP acetone as the solvent. As the titanous chloride stream was left unchanged, the resulting reaction mixture was *ca.* 50 v/v% acetone. This procedure does not appear to be of general applicability as it failed with several other water-insoluble allyl compounds.

Throughout this study basically two different types of epr machine settings were used, denoted low-resolution and high-resolution conditions. In the former, the power and modulation amplitude, respectively, were *ca.* 60 mW and 300 mG, while in the latter, these were *ca.* 20 mW and 70 mG. Under high-resolution conditions, peak-to-peak line widths of *ca.* 0.1 G were generally obtained.

In addition, several typical substrates, *viz.*, allyl alcohol, allyl formate, allyl n-butyrate, allylamine, and allyl glycidyl ether, were run using the titanous chloride–hydroxylamine hydrochloride radical-generating system.[13] For these experiments, the reducing stream was 0.008 and 0.2 M in titanous chloride and sulfuric acid, respectively, and the oxidizing stream was 1 M in $NH_2OH \cdot HCl$ (Eastman, reagent grade) with no added sulfuric acid. Also, the substrate was included only in the hydroxylamine stream with concentrations as follows: allyl alcohol, 0.1 to 1 M; allyl n-butyrate, 0.08 M; allyl glycidyl ether, 0.09 M; allylamine, 0.1 M; and allyl formate, 0.12 M. Spectra were run only under low-resolution conditions with this radical-generating system, there being no advantage in working at high-resolution conditions since the line widths were so large.

Results

Alcohols. Under low-resolution conditions, allyl alcohol was found to give the radicals 1–3 observed earlier,[5] the spectrum consisting of a sextet (1:5:10:10:5:1), a triplet (1:2:1) of doublets (1:1), and a quartet (1:3:3:1) of small doublets (1:1) from the radicals **1**, **2**, and **3**, respectively. However, under conditions of high resolution the spectra from radicals **2** and **3** were reduced in intensity and that from radical **1** predominated and could be further resolved consistent with $a_{\alpha\text{-H}}$ being slightly less than $a_{\beta\text{-H}}$. Furthermore, the spectrum from **1** was more complicated than a quintet (1:4:6:4:1) of doublets (1:1) because the second-order splittings[16] from the four equivalent methylene protons were essentially resolved, as illustrated in Figure 1.

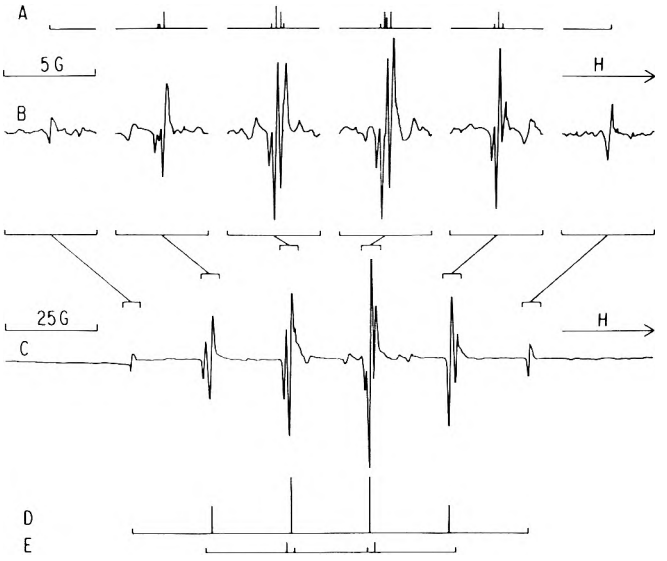

Figure 1. Epr spectrum for the substrate allyl alcohol: tp 25°; $[TiCl_3]$ 0.004 M and $[H_2SO_4]$ 0.2 M in the reducing stream; $[H_2O_2]$ in the oxidizing stream 0.1 M; $[CH_2{=}CHCH_2OH]$ 0.1 M in both streams; total flow rate 3 ml sec^{-1} equally divided between the two streams. A, Second-order stick plot for $HOCH_2\dot{C}HCH_2OH$ appropriate to the spectrum in B, for a first-order quintet (1:4:6:4:1) of doublets (1:1). B, Epr spectrum for the substrate allyl alcohol under high-resolution conditions. C, Epr spectrum for the substrate allyl alcohol under low-resolution conditions and similar to that reported previously.[5] D, First-order stick plot for $HO\dot{C}H_2CHCH_2OH$ appropriate to the spectrum in C, a sextet (1:5:10:10:5:1). E, First-order stick plot for $\cdot CH_2CH(OH)CH_2OH$ appropriate to the spectrum in C, a triplet (1:2:1) of doublets (1:1).

Methallyl alcohol, $CH_2{=}C(CH_3)CH_2OH$, gave rise to a spectrum which was analyzed as a quintet (1:4:6:4:1) of quartets (1:3:3:1) consistent with the single radical $HOCH_2\dot{C}(CH_3)CH_2OH$, **4**. Under high-resolution conditions additional lines were observed. These lines were found to be the result of second-order splittings from both the four equivalent β-CH_2 protons and the three equivalent β-CH_3 protons, these splittings being fully resolved only where one of these two groups of protons would be expected to give rise to second-order effects.

Table I lists the coupling constants and g values we observed for radicals **1–4** with the most comparable data from previous investigations.[5,6,17-20] It will be seen that, where comparison is possible, our present results agree reasonably well with those reported previously.

Carboxylic Esters. Each of the five allyl carboxylic esters, AOOCR,[21] studied (formate, acetate, propionate, n-butyrate, and benzoate) gave spectra which could be analyzed in terms of two radicals, these being analogous to **1** and **2**, respectively, $HOCH_2\dot{C}HCH_2X$, **1** (-X), and $\cdot CH_2CH(OH)CH_2X$, **2** (-X), where -X is the variable group.[22] For each **1** (-OOCR)[21] radical save radical **1**

TABLE I: Coupling Constants and *g* Values for Radicals from Allyl and Methallyl Alcohol

Radical	$a_{\alpha\text{-H}}$, G	$a_{\beta\text{-H}}$, G	*g* Value	Ref
$HOCH_2\dot{C}HCH_2OH$	21.85	21.85	2.0024	*a,b*
	21.46	21.70	2.0024	*a,c*
	21.78	21.78	...	5[a]
	21.8	21.8	...	19[d]
$\cdot CH_2CH(OH)CH_2OH$	22.27	24.50	2.00245	*a,b*
	22.14	24.39	...	5[a]
	22.1	24.4	...	19[d,e]
$CH_2{=}\dot{C}HOH$	13.62[f]	3.45	2.0029	*a,b*
	13.33,13.86[g]	3.16	2.00287	6[h]
	13.82[f]	3.43	...	5[a,i]
$HOCH_2\dot{C}(CH_3)CH_2OH$	...	16.13,[j] 23.59[k]	2.00245	*a,c*

[a] At 25 ± 2°; *g* values have a maximum uncertainty of 0.0001. [b] Present work, low-resolution conditions; the maximum uncertainty of the *a* values is estimated as being 0.1 G. [c] Present work, high-resolution conditions; the maximum uncertainty of the *a* values is estimated to be 0.1 G, but for the difference between two nearly equal values, this is 0.05 G. [d] In water, pH 9, probable tp *ca.* 15°. [e] Also see ref 20. [f] For three protons, $a_{\alpha\text{-H}}$ equals $a_{\gamma\text{-H}}$ in the formula given. [g] The 13.33- and 13.86-G couplings are for one and two protons, respectively, and were unassigned. [h] In allyl alcohol containing 0.5% hydrogen peroxide, 29°. Two isomers were found, the data for the more abundant being given as they match ours more closely. [i] Using the $TiCl_3$–*t*-C_4H_9OOH method, we have obtained comparable data. [j] $a_{\beta\text{-H}}^{CH_2OH}$. [k] $a_{\beta\text{-H}}^{CH_3}$.

(-OOCH), the spectrum comprised a triplet (1:2:1) of triplets (1:2:1) of doublets (1:1) consistent with the two sets of β-CH_2 protons and the α-CH proton being nonequivalent. A typical spectrum taken with the use of allyl acetate is shown in Figure 2. However, the spectrum from radical **1** (-OOCH) showed this same pattern of lines but, in addition, there was a small doublet (1:1) splitting, 2.8 G, which was of necessity assigned to the formyl proton. This small doublet splitting was unexpected, the only other analogous δ splittings of which we are aware being in quite different structures.[23] However, recently we have found other examples of this type of splitting in related radicals.[24]

For each **2** (-OOCR)[21,22] radical, the spectrum consisted of a triplet (1:2:1) of doublets (1:1) with the coupling constants being similar in size to those of **2**, see Figure 2.

For allyl benzoate the reaction mixture was *ca.* 50 v/v% acetone (see Experimental Section). When acetone is examined as substrate at room temperature in dilute aqueous solution with the use of the $TiCl_3$–H_2O_2 method only the radical $\cdot CH_2COCH_3$, **5**, is observed;[9,25] on the other hand, with the use of photo-flow radical-generating methods and acetone-rich reaction mixtures at room temperature, two radicals are reported, *viz.*, **5** together with the $\cdot CH_3$ radical present as a minor product.[26] Consequently, it is not altogether surprising that in our present investigation we found a total of four radicals, these being, in descending order of concentration, **5**, **1** (-$OOCC_6H_5$), **2** (-$OOCC_6H_5$), and $\cdot CH_3$. It seems unlikely that the spectra assigned to **1** (-$OOCC_6H_5$) and **2** (-$OOCC_6H_5$) were largely from other addition radicals (see the Discussion).

Nitrogen Compounds. Allyl cyanide, allylamine, and 1-allylurea, ACN, ANH_2, and $ANHCONH_2$, respectively, each gave spectra analyzable in terms of the two radical analogs of **1** and **2**. The spectrum for radical **1** (-CN) consisted of a quartet (1:3:3:1) of triplets (1:2:1) indicating that one set of β-CH_2 protons and the α-CH proton are equivalent. That for **1** (-NH_2) showed a similar absorption pattern together with an extra triplet (1:1:1) splitting from the amino nitrogen. Our attempts to resolve this apparent equality of the β-CH_2 protons and the α-CH in these two radicals failed, the line widths remaining virtually unchanged under all experimental conditions employed. Radical **1** (-NH_2) has been observed earlier[17] by both hydroxyl radical addition to allylamine and amino

Figure 2. Epr spectrum for the substrate allyl acetate: tp 25°; [$TiCl_3$] 0.004 *M* and [H_2SO_4] 0.2 *M* in the reducing stream; [H_2O_2] 0.1 *M* and [$CH_2{=}CHCH_2OOCCH_3$] 0.01 *M* in the oxidizing stream; total flow rate 3 ml sec^{-1} equally divided between the two streams. A, First-order stick plot for $HOCH_2CHCH_2OOCCH_3$, a triplet (1:2:1) of triplets (1:2:1) of doublets (1:1). B, First-order stick plot for $\cdot CH_2CH(OH)CH_2OOCCH_3$, a triplet (1:2:1) of doublets (1:1).

radical addition to allyl alcohol, the results of this study and our present investigation being in good agreement. 1-Allylurea gave a spectrum which was poorly resolved because the lines were broad (*ca.* 1 G peak to peak). However, radical **1** (-$NHCONH_2$) was successfully analyzed as a triplet (1:2:1) of triplets (1:2:1) of doublets (1:1) of small triplets (1:1:1).

Radicals **2** (-CN), **2** (-NH_2), and **2** (-$NHCONH_2$) had splitting patterns similar to **2** and **2** (-OOCR),[21] *i.e.*, a triplet (1:2:1) of doublets (1:1). In order to show the presence of **2** (-CN) it was necessary to use intensity measurements of the spectrum from **1** (-CN) because there was severe overlap of the lines from each radical. The presence of **2** (-CN) satisfactorily explains the anomalous intensities observed in the spectrum of **1** (-CN). Radical **2** (-NH_2) was not observed in the earlier study[17] of allylamine. A representative spectrum of the results obtained with the use of allylamine is shown in Figure 3.

Ethers. Diallyl ether, allyl 2-hydroxyethyl ether, allyl ethyl ether, and allyl glycidyl ether. AOA, $AOCH_2CH_2OH$, $AOCH_2CH_3$, and $AOCH_2\underline{CHCH_2}O$, respectively, were studied. Diallyl ether gave a spectrum of broad (*ca.* 2 G) lines that could not be further resolved. However, by comparison of this spectrum with those obtained from other allyl compounds, we conclude the major radical present to be **1** (-$OCH_2CH{=}CH_2$). The remaining ethers each gave spectra analyzable in terms of two radicals, these being analogous to **1** and **2**. The spectrum from

radical 1 ($-OCH_2\dot{C}H_2OH$) under low-resolution conditions was analyzed as a sextet (1:5:10:10:5:1), indicating the apparent equivalence of all four β-CH_2 protons and the α-CH proton. One set of β-CH_2 protons and the α-CH proton in 1 ($-OCH_2\dot{C}HCH_2O$) are apparently equivalent, under low resolution, as evidenced by the splitting pattern observed, *i.e.*, a quartet of (1:3:3:1) of triplets (1:2:1). The low-resolution spectrum of 1 ($-OCH_2\dot{C}HCH_2O$) was analyzed as a triplet (1:2:1) of triplets (1:2:1) of doublets (1:1). Compared with their low-resolution spectra, the high-resolution spectra of both 1 ($-OCH_2\dot{C}H_2OH$) and 1 ($-OCH_2\dot{C}H_3$) were of low intensity and very complicated, whereas that from 1 ($-OCH_2\dot{C}HCH_2O$) was decreased in both intensity and line width but exhibited no further hyperfine structure. Therefore, interest was centered on the high-field end lines of 1 ($-OCH_2\dot{C}H_2OH$) and 1 ($-OCH_2\dot{C}H_3$). With the use of high-resolution conditions and time-averaging techniques,[8] we found the end line of 1 ($-OCH_2\dot{C}H_2OH$) to be a small (*ca.* 0.3 G) triplet of (1:2:1) and that of 1 ($-OCH_2\dot{C}H_3$), a small (*ca.* 1.0 G) quartet (1:3:3:1). These small couplings can be explained in terms of a through-space coupling with the ϵ-CH_2 and ϵ-CH_3 protons, respectively, as illustrated in Figure 4. As with the case of the long-range δ-CH coupling in 1 (-OOCH), these ϵ splittings were unexpected.

Radicals 2 ($-OCH_2\dot{C}H_2OH$), 2 ($-OCH_2\dot{C}H_3$), and 2 ($-OCH_2\dot{C}HCH_2O$) all gave rise to the expected pattern, *viz.*, a triplet (1:2:1) of doublets (1:1).

Vinyl Acetic Acid. For vinyl acetic acid, ACOOH, two radicals were observed, 1 (-COOH) and 2 (-COOH), their spectra being very similar to those found for 1 and 2, respectively. Under low-resolution conditions, radical 1 (-COOH) gave a spectrum consisting of a sextet (1:5:10:10:5:1). Under high-resolution conditions, the spectrum of radical 2 (-COOH) was reduced in intensity while that of radical 1 (-COOH) predominated and yielded further hyperfine structure analyzable as a quintet (1:4:6:4:1) of doublets (1:1) with second-order splittings[16] evident. These second-order effects could be better resolved than in the analogous case of radical 1 because of slight numerical differences in the coupling constants of 1 and 1 (-COOH). On the basis of our results for other allyl compounds, the equality of the two sets of β-CH_2 protons in 1 (-COOH), as evidenced by observable second-order effects appropriate for four equivalent protons, was unexpected. The spectrum from radical 2 (-COOH) was a triplet (1:2:1) of doublets (1:1) similar to the patterns observed for radicals 2 and 2 (-X).

Tables II and III give the coupling constants and g values we observed for 1 (-X) and 2 (-X) radicals with the most comparable data from previous studies.[17,27] Where comparison is possible, it will be seen that our data are in reasonable accord with those of past workers.

Amino Radical Addition. Allyl alcohol, formate, *n*-butyrate, amine, and glycidyl ether were each subjected to amino radical addition. In general, the only spectrum observed was from the head-addition radical $H_2N\dot{C}H_2CHCH_2X$, 6 (-X),[28] this being similar to that of the corresponding 1 (-X) radical save for the presence of the expected[17] additional γ-nitrogen splitting in the former, this being in the range 5.2–6.2 G. In the case of radical 6 (-OH), the spectrum was as for this same radical, 1 ($-NH_2$), when formed from allylamine, except the line widths were larger (see Experimental Section). Unlike the other substrates, allyl alcohol was run over a range of concentrations, 0.1–1 M. At low concentrations only the spectrum from radical 6 (-OH) was observed. As the concentration of allyl alcohol was raised, extra lines became increasingly evident, their pattern being a quartet (1:3:3:1) of triplets (1:2:1). On the basis of our previous work[5] with allyl alcohol with the use of the $TiCl_3$–H_2O_2 system, these lines can be assigned to a polymer radical[29] such as $YCH_2\dot{C}HCH_2OH$, 7, with Y most likely being 6 (-OH).

TABLE II: Coupling Constants and g Values for $HOCH_2\dot{C}HCH_2X$ Radicals[a]

-X	$a_{\alpha\text{-H}}$, G	$a_{\beta\text{-H}}$, G[b]	Other, G	g Value
-OOCH	21.75	17.96 23.40	2.80[c]	2.0024
$-OOCCH_3$	21.68	18.46 23.07	...	2.00245
$-OOCCH_2CH_3$	21.69	18.54 23.14	...	2.0024
$-OOCCH_2CH_2CH_3$	21.78	18.44 23.27	...	2.0024
$-OOCC_6H_5$[d,e]	21.64	18.64 24.33	...	2.0026
-CN[d,f]	22.27	22.27 23.16	...	2.0025
$-NH_2$[d,g]	21.67	21.67 24.38	6.17[h]	2.0025
$-NHCONH_2$[d]	21.56	20.49 25.00	4.30[h]	2.0025
-COOH[i]	21.80	22.26	...	2.0026
$-OCH_2CH_2OH$[d,j]	21.93	21.93	0.29[k,l]	2.0025
$-OCH_2CH_3$[d,j]	21.46	21.46 22.14	1.04[l,m]	2.0025
$-OCH_2CHCH_2O$[j]	21.35	20.86 22.46	...	2.0025

[a] At 25 ± 2°; all g values have a maximum uncertainty of 0.0001. Unless specified differently, all were data taken under high-resolution conditions, the maximum uncertainty of the a values being as given in Table I, footnote c. [b] When two values are given, the upper and lower values are assigned to the β-CH_2OH and $-CH_2X$ protons, respectively, except for 1 ($-OCH_2CH_3$) where assignment was not possible; when a single value is given, both pairs of protons are equivalent. [c] $a_{\delta\text{-H}}^{OOCH}$. [d] Low-resolution conditions, the maximum uncertainty in the a values being 0.1 G except where given differently. [e] Low-intensity spectrum, maximum uncertainty 0.15 G. [f] Poorly resolved, maximum uncertainty 0.15 G. [g] By procedures like ours, $a_{\alpha\text{-H}}^{CH}$, $a_{\beta\text{-H}}^{CH_2OH}$, $a_{\beta\text{-H}}^{CH_2X}$, and $a_{\gamma\text{-N}}$ have been found[17] to be 21.72, 21.72, 24.27, and 6.13 G, respectively; probable tp *ca.* 15°. [h] $a_{\gamma\text{-N}}$. [i] Fischer[27] has reported $a_{\alpha\text{-H}}^{CH}$ and $a_{\beta\text{-H}}^{CH_2}$ as 21.75 and 22.52 G, respectively; in water, at 300°K. [j] For 1 ($-OCH_2C(CH_2OH)_2CH_2CH_3$), $a_{\alpha\text{-H}}^{CH}$, $a_{\beta\text{-H}}^{CH_2OH}$, and $a_{\beta\text{-H}}^{CH_2X}$ have been found[30] to be 22.0 G; by procedures like ours, 20 ± 2°. [k] $a_{\epsilon\text{-H}}^{CH_2OH}$. [l] Maximum uncertainty 0.05 G. [m] $a_{\epsilon\text{-H}}^{CH_3}$.

TABLE III: Coupling Constants and g Values for $\cdot CH_2CH(OH)CH_2X$ Radicals[a]

-X	$a_{\alpha\text{-H}}$, G	$a_{\beta\text{-H}}$, G	g Value
-OOCH	22.25	24.52	2.0024
$-OOCCH_3$	22.09	24.50	2.0024
$-OOCCH_2CH_3$	22.25	24.60	2.0025
$-OOCCH_2CH_2CH_3$	22.40	24.77	2.00235
$-OOCC_6H_5$	21.99[b]	24.78[b]	2.0025
-CN	22.10[c]	24.02[c]	2.0025
$-NH_2$	22.37	23.82	2.00245
$-NHCONH_2$	22.19	24.29	2.0025
-COOH	21.91	23.56	2.0024
$-OCH_2CH_2OH$[d]	22.34	25.02	2.0025
$-OCH_2CH_3$	22.16	24.62	2.0025
$-OCH_2CHCH_2O$[d]	22.17	24.62	2.0025

[a] At 25 ± 2°, low-resolution conditions; the maximum uncertainties of the a and g values are 0.1 G and 0.0001, respectively, unless specified otherwise. [b] Low-intensity spectrum, maximum uncertainty 0.15 G. [c] Poorly resolved, maximum uncertainty 0.15 G. [d] For 2 ($-OCH_2C(CH_2OH)_2CH_2CH_3$), $a_{\alpha\text{-H}}^{CH_2}$ and $a_{\beta\text{-H}}^{CH}$ have been found[30] to be 22.5 and 25.2 G, respectively; by procedures like ours, 20 ± 2°.

TABLE IV: Coupling Constants and g Values for $H_2NCH_2\dot{C}HCH_2X$ Radicals[a]

-X	$a_{\alpha\text{-H}}$, G	$a_{\beta\text{-H}}$, G[b]	Other, G	g Value
-OH[c]	21.67	24.38	6.17[d]	2.0025
		21.57		
-OOCH	22.39	19.64	2.78[e]	2.0024
		22.39	5.56[d]	
$-OOCCH_2CH_2CH_3$	22.10	20.31	5.63[d]	2.0024
		22.54		
$-NH_2$[f]	21.87	23.54	5.23[d]	2.0025
$-OCH_2\underline{CHCH_2}O$	22.00	23.39	5.82[d]	2.0026
		22.00		

[a] At 25 ± 2°, low-resolution conditions; the maximum uncertainties of the a and g values are 0.1 G and 0.0001, respectively. [b] When two values are given, the upper and lower values are assigned to the β-CH_2NH_2 and $-CH_2X$ protons, respectively; when a single a value is given, both pairs of protons are equivalent. [c] Data for **1** ($-NH_2$) in Table II as this is from spectra better resolved than those taken by the $TiCl_3$–NH_2OH–AOH_2 procedure, see Table II, footnote *d*. [d] $a_{\gamma\text{-N}}$. [e] $a_{\delta\text{-H}}^{OOCH}$. [f] With the use of procedures similar to those of this present work, $a_{\alpha\text{-H}}^{CH}$, $a_{\beta\text{-H}}^{CH_2NH_2}$, and $a_{\gamma\text{-N}}^{NH_2}$ have been found[17] to be 22.54, 23.69, and 5.29 G, respectively; probable tp *ca.* 15°.

The quartet splitting, indicating a chance equivalence of the α-proton with one set of β-CH_2 protons, was *ca.* 21.3 G, whereas the triplet splitting was *ca.* 24.4 G, these values being in good agreement with the corresponding data obtained in our previous study.[5]

Table IV lists the coupling constants and g values observed for the **6** (-X) radicals with the comparable data in the literature.[17] It will be seen that, where comparison is possible, our data agree tolerably well with those of others.

Discussion

I. The Radicals Observed. Every allyl compound but methallyl alcohol underwent both head and tail hydroxyl radical addition, the head-addition radical always having the higher concentration. Also, the relative molar proportion of these addition radicals was qualitatively similar for each such substrate. However, with methallyl alcohol, only the head-addition radical was observed. As in our previous study of allyl alcohol with the use of the $TiCl_3$–H_2O_2 radical-generating system,[5] the spectrum of radical **3**, was observed and, although this spectrum was less intense than that for either of the addition radicals, it could be resolved and characterized. Only a few of the other substrates, *viz.*, the ethers and the *n*-butyrate, gave evidence of signals other than those from the two addition radicals when treated with this same radical-generating system, but these signals proved to be too faint to be characterized. This is perhaps not too surprising, for of all the substrates examined, only the ethers might be expected to be reactive enough at the allylic position to give results comparable to that from allyl alcohol.[5,25,30] It will be noted that none of the allyl substrates were found to give clear evidence of polymeric addition radicals with the use of the $TiCl_3$–H_2O_2 radical-generating system. This observation is in line with our earlier, analogous $TiCl_3$–H_2O_2 system investigation of allyl alcohol[5] which showed such radicals to be readily observed only for substrate concentrations considerably larger than those employed here.

The few allyl compounds investigated with the use of the $TiCl_3$–NH_2OH radical-generating method each gave only one observable monomeric addition radical, this being the head amino radical addition product, and no evidence of an allylic radical. For a given substrate and in comparison with the $TiCl_3$–H_2O_2 system, the $TiCl_3$–NH_2OH system gave signals of lower intensity and greater complexity. This may be a reason that only one such radical product could be detected with the use of the latter system. However, for the $TiCl_3$–NH_2OH system investigation of allyl alcohol, by extending the study to substrate concentrations much larger than for the other substrates, a signal attributable to a polymeric addition radical was also observed, as would be expected on the basis of our earlier work[5] referred to already.

Our results for the relative proportion of 1-, 2-, and 3-type radicals observed with the use of these two radical-generating methods cannot be reliably discussed on a kinetic basis because, for example, their detailed dependence on the reaction conditions was not investigated.[5] Nevertheless, they are qualitatively similar to the results of all comparable studies of which we are aware.[31]

II. $HOCH_2\dot{C}HCH_2X$ Radicals. The α-proton coupling constants of these radicals, including **1** or **1** (-OH), are approximately equal, all such values (see Tables I and II) ranging between 21.4 and 22.3 G, the average being 21.7 G. This result is expected because the π-electron spin density at the α-C, $\rho_{\alpha\text{-C}}^{\pi}$, in all these radicals should not be very dependent on -X.[32,33] The value of $\rho_{\alpha\text{-C}}^{\pi}$[$HOCH_2\dot{C}HCH_2OH$] may be calculated to be 0.876 on the assumption that it equals[33,34] $\rho_{\alpha\text{-C}}^{\pi}$[$HOCH_2\dot{C}(CH_3)CH_2OH$]/(0.919) where, for the radical $HOCH_2\dot{C}(CH_3)CH_2OH$

$$a_{\beta\text{-H}}^{CH_3} = Q_H^{CCH_3}\rho_{\alpha\text{-C}}^{\pi} \quad (1)$$

with $Q_H^{CCH_3}$ equal to 29.3 G.[33,34] Hence, for this same radical, the value of $|Q_H^{CH}|$ in the McConnell equation[35]

$$a_{\alpha\text{-H}}^{CH} = Q_H^{CH}\rho_{\alpha\text{-C}}^{\pi} \quad (2)$$

equals 24.5 G, which is within the range expected.[32,33] Also, this estimate for $\rho_{\alpha\text{-C}}^{\pi}$[$HOCH_2\dot{C}HCH_2OH$] leads to a value for $\Delta(-CH_2OH)$ of 0.064, which is somewhat less than that reported by Fischer,[32,33] 0.079, but in reasonable agreement, for example, with those which may be derived from the $a_{\beta\text{-H}}^{CH_3}$ data[36] for $CH_3\dot{C}HCH_2OH$ and $(CH_3)_2\dot{C}CH_2OH$, 0.061 and 0.058, respectively.

In radical **4**, $a_{\beta\text{-H}}^{CH_2}$ was substantially less than $a_{\beta\text{-H}}^{CH_3}$ and also $a_{\beta\text{-H}}^{CH_2}$[1], probably on account of the likely increased restriction to rotation about the $\cdot C\text{–}CH_2OH$ bond in **4** relative to **1**.[32] In radicals **1** (-X) there were generally two sets of inequivalent β-CH_2 couplings which were both similar in size to those in **1**. For each **1** (-X) radical, these couplings can be reasonably assigned to the two sets of chemically equivalent CH_2 protons. Radicals **1** (-COOH) and **1** ($-OCH_2CH_2OH$) were the two seeming exceptions to the above generalization. For the former, the two sets of CH_2 protons were so close to magnetic equivalence that second-order splitting[16] effects could be completely resolved. In the case of the latter, the magnetic equivalence was less close so that, although the nonequivalence did not show up under low-resolution conditions, under high-resolution conditions it appeared to be present but could not be analyzed.

For the most of the **1** (-X) radicals, tentative assignments of the β-CH_2 couplings can be made by comparison of these couplings to those of previously reported radicals, as follows. For the radical **6** ($-NH_2$) we have found $a_{\beta\text{-H}}^{CH_2}$ to be 23.5 G, whereas in **1**, $a_{\beta\text{-H}}^{CH_2}$ is 21.7 G. Therefore, the larger of two β-couplings in **1** ($-NH_2$) can be assigned to the $-CH_2NH_2$ group and the smaller one to the $-CH_2OH$ group (see Table II). On the basis of this assignment for **1** ($-NH_2$), it would seem reasonable to assign

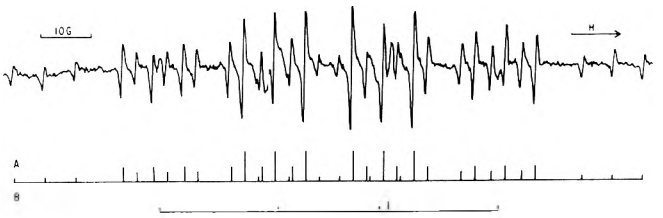

Figure 3. Epr spectrum for the substrate allylamine: tp 25°; $[TiCl_3]$ 0.004 *M* and $[H_2SO_4]$ 0.2 *M* in the reducing stream; $[H_2O_2]$ 0.1 *M* and $[CH_2{=}CHCH_2NH_2]$ 0.03 *M* in the oxidizing stream; total flow rate 3 ml sec^{-1} equally divided between the two streams. A, First-order stick plot for $HOCH_2\dot{C}HCH_2NH_2$, a quartet (1:3:3:1) of triplets (1:2:1) of triplets (1:1:1). B, First-order stick plot for $\cdot CH_2CH(OH)CH_2NH_2$, a triplet (1:2:1) of doublets (1:1).

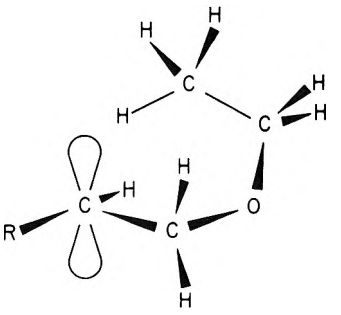

Figure 4. A possible conformation for the proposed cyclic radical $HOCH_2\dot{C}HCH_2OCH_2CH_3$, where -R equals $-CH_2OH$, with the ϵ-CH_3 protons interacting with the $2p_z$ orbital by a through-space mechanism.

the larger of the two β-CH_2 couplings in both **1** (-CN) and **1** ($-NHCONH_2$) to the CH_2 group adjacent to the nitrogen containing -X group, for these β-CH_2 couplings are considerably closer to $a_{\beta\text{-}H}^{CH_2NH_2}$[$H_2NCH_2\dot{C}HCH_2NH_2$] than to $a_{\beta\text{-}H}^{CH_2OH}$[$HOCH_2\dot{C}HCH_2OH$], whereas for the smaller β-CH_2 coupling the reverse holds.

For the radicals **1** (-OOCR)[21] the two sets of β-CH_2 coupling constants are unequal and fall into two distinct groupings (see Table II). The smaller β-CH_2 couplings are in the range of 18.0–18.6 G whereas the larger couplings fall in the range 23.1–24.3 G.[37] A tentative assignment can be made by comparison with the radical $\cdot CH_2CH_2OOCCH_3$, **8**, formed by hydrogen atom abstraction from ethyl acetate[9] for which $a_{\alpha\text{-}H}^{CH_2}$ and $a_{\beta\text{-}H}^{CH_2}$ are 22.2 and 25.2 G, respectively. Based on the work of Ōki and Nakanishi,[38-40] who have investigated the conformation of carboxylic acid esters in the liquid phase, we may suppose that the ester groups in radicals **8** and **1** (-OOCR) exist in the *s-trans* form which for the latter may be illustrated

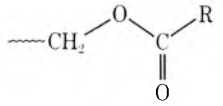

Thus the larger β-CH_2 coupling in **1** (-OOCR) can be reasonably assigned to the $-CH_2OOCR$ group on the basis of its being closer to the size of $a_{\beta\text{-}H}^{CH_2}$[**8**]. Moreover, if we assume that the sole effect on $a_{\beta\text{-}H}^{CH_2OOCCH_3}$ of substituting a $-CH_2OH$ group for an α-H atom in **8** would be from the resultant change in $\rho_{\alpha\text{-}H}^{\pi}$, it follows that $a_{\beta\text{-}H}^{CH_2OOCCH_3}$[**1**(-$OOCCH_3$)] should equal 23.6 G, based on the previously given values for $a_{\beta\text{-}H}^{CH_3}$[**8**] and $\Delta(-CH_2OH)$, 25.2 G and 0.64, respectively. The experimental value of $a_{\beta\text{-}H}^{CH_2OOCCH_3}$[**1**(-$OOCCH_3$)] is 23.1 G, in reasonable agreement with expectation. Consequently, the smaller β-CH_2 coupling in **1** (-OOCR) is assigned to the $-CH_2OH$ methylene protons.

For the **1** ($-OCH_2CH_3$) and **1** ($-OCH_2\underline{CHCH_2O}$) radicals it does not seem readily possible to assign the β-CH_2 couplings. However, in the case of the latter, an attempt to do so is given in section IV. Radical **1** ($-OCH_2CH_2OH$) appears to have two inequivalent sets of β-CH_2 protons but, because of the complexity of the high-resolution spectra, it was impossible to show this inequivalence clearly. The interesting feature of these ether radicals is the ϵ-proton splitting. We have suggested already that this coupling might arise from the formation of a six-membered cyclic structure (see Figure 4). This idea is supported by the decrease of $a_{\epsilon\text{-}H}$ with increasing steric bulkiness of the -X group, *viz.*, from *ca.* 1.0 G in **1** ($-OCH_2CH_3$) to *ca.* 0.3 G in **1** ($-OCH_2CH_2OH$) and finally to less than the line width (*ca.* 0.1 G) in **1** ($-CH_2\underline{CHCH_2O}$). The broad lines attributed to **1** ($-OCH_2CH{=}\underline{CH_2}$) when diallyl ether was the substrate might perhaps be explained by the formation of such a cyclic radical in which there would be spin delocalization into the double bond. The cyclic radical concept proposed here is similar, for example, to the intramolecular hydrogen transfer *via* transient-ring-formation hypothesis put forth by Roedel[41,42] to account for short-chain branching in the radical polymerization of ethylene. However, the secondary radicals, $HOCH_2CH_2$-$CH_2OCH_2\dot{C}HOH$ and $HOCH_2CH_2CH_2OCH_2\dot{C}H_2$ from allyl 2-hydroxyethyl ether and allyl ethyl ether, respectively, expected from such a process, were not observed.

III. $\cdot CH_2CH(OH)CH_2X$ *Radicals.* The α- and β-proton coupling constants for radicals **2** (-X), including **2** or **2** (-OH), are of very similar size with $a_{\alpha\text{-}H}^{CH_2}$, $a_{\beta\text{-}H}^{CH}$, and their difference falling in the ranges 21.9–22.4, 23.6–25.0, and 1.4–2.9 G, respectively. This similarity is not unexpected as, in each radical, the -X group is far removed from the unpaired electron in the $2p_z$ orbital. If the comparison is restricted to a series of like radicals, these variation ranges are smaller, *e.g.*, **2** (-OOCR) radicals excluding **2** ($-OOCC_6H_5$).

IV. $H_2NCH_2\dot{C}HCH_2X$ *Radicals.* As noted previously, except for the presence of a γ-nitrogen coupling, the spectrum of each **6** (-X) radical is similar to that of the corresponding **1** (-X) radical. However, the analogous proton coupling constants for each **6** (-X)/**1** (-X) pair show differences. First, $a_{\alpha\text{-}H}$[**6** (-X)] is slightly greater than $a_{\alpha\text{-}H}$[**1** (-X)], their difference being about the size expected. For we would expect this difference to be determined primarily by $\rho_{\alpha\text{-}H}^{\pi}$[**6** (-X)]/$\rho_{\alpha\text{-}C}^{\pi}$[**1** (-X)] which may be put equal to $[1\text{-}\Delta(-CH_2NH_2)]/[1\text{-}\Delta(-CH_2OH)]$;[17,32,33] and, assuming $\Delta(-CH_2NH_2)$ and $\Delta(-CH_2OH)$ to be 0.043[43] and 0.064, respectively, gives the latter ratio as 1.02. Secondly, we have already pointed out that $a_{\beta\text{-}H}^{CH_2}$[**6** ($-NH_2$)] is greater than $a_{\beta\text{-}H}^{CH_2}$[**1**] and have used this inequality to assign the larger β-CH_2 proton coupling in **1** ($-NH_2$), or **6** (-OH), to the $-CH_2NH_2$ group. The two sets of β-CH_2 couplings for each **6** (-OOCR)/**1** (-OOCR) pair appear to show a similar kind of effect, *viz.* the smaller value of $a_{\beta\text{-}H}^{CH_2}$[**6** (-OOCR)] is greater than the smaller value of $a_{\beta\text{-}H}^{CH_2}$[**1** (-OOCR)], whereas the reverse holds for the larger values of $a_{\beta\text{-}H}^{CH_2}$[**6** (-OOCR)] and $a_{\beta\text{-}H}^{CH_2}$[**1** (-OOCR)]. This effect seems consistent with and tends to support our previous assignment of the two sets of β-CH_2 proton couplings in the **1** (-OOCR) radical series. Also it leads to our tentatively assigning the smaller β-CH_2 proton coupling in the **6** (-OOCR) radicals to the $-CH_2NH_2$ group.

Earlier we noted that **1** or **1** (-OH) and the head-addition radicals from the ethers were similar with respect to coupling constants. From this knowledge and by comparing **1** ($-NH_2$) or **6** (-OH) with **6** ($-OCH_2\underline{CHCH_2}O$), we may tentatively assign the larger $a_{\beta\text{-}H}^{CH_2}$[**6** ($-OCH_2\underline{CHCH_2}O$)] value to the $-CH_2NH_2$ group. On the basis of these assignments and omitting consideration of the ether radical, it is seen that the range of values of $\{a_{\beta\text{-}H}^{CH_2NH_2}[\mathbf{6}\ (-X)] - a_{\beta\text{-}H}^{CH_2OH}[\mathbf{1}\ (-X)]\}$ is 1.6–2.7 G and that of $\{a_{\beta\text{-}H}^{CH_2X}[\mathbf{1}\ (-X)] - a_{\beta\text{-}H}^{CH_2X}[\mathbf{6}\ (-X)]\}$ is 0.0–1.0 G. On the basis of these two ranges, we may now attempt to assign the two $a_{\beta\text{-}H}^{CH_2}$[**1** ($-OCH_2\underline{CHCH_2}O$)] values, the smaller being assigned to the $-CH_2OH$. If the assignments were reversed the two $a_{\beta\text{-}H}^{CH_2}$ difference ranges would have to be extended. No attempts were made to extend this tentative argument to the other ether $HOCH_2\dot{C}HCH_2X$ type radicals as their $a_{\beta\text{-}H}^{CH_2}$ values are less different.

Acknowledgment. The hydrogen peroxide used was a gift from FMC Corp., Inorganic Chemicals Division.

References and Notes

(1) This work was supported by U. S. Public Health Service Grant GM 07653, Division of General Medical Sciences, and National Science Foundation Grants GP-7534 and GP-17579.
(2) National Defense Education Act Predoctoral Fellow.
(3) R. O. C. Norman, "Essays in Free-radical Chemistry," Special Publication No. 24, The Chemical Society, London, 1970, Chapter 6.
(4) G. Czapski, A. Samuni, and D. Meisel, *J. Phys. Chem.* **75**, 3271 (1971).
(5) P. Smith and P. B. Wood, *Can. J. Chem.*, **45**, 649 (1967).
(6) R. Livingston and H. Zeldes, *J. Chem. Phys.*, **44**, 1245 (1966).
(7) R. Livingston and H. Zeldes, *J. Amer. Chem. Soc.*, **88**, 4333 (1966).
(8) P. Smith, R. D. Stevens, and R. A. Kaba, *J. Phys. Chem.*, **75**, 2048 (1971).
(9) P. Smith, J. T. Pearson, P. B. Wood, and T. C. Smith, *J. Chem. Phys.*, **43**, 1535 (1965).
(10) J. T. Pearson, P. Smith, and T. C. Smith, *Can. J. Chem.*, **42**, 2022 (1964).
(11) P. Smith and P. B. Wood, *Can. J. Chem.*, **44**, 3085 (1966).
(12) P. Smith, J. T. Pearson, and R. V. Tsina, *Can. J. Chem.*, **44**, 753 (1966).
(13) P. Smith and W. M. Fox, *Can. J. Chem.*, **47**, 2227 (1969).
(14) P. Smith, W. M. Fox, D. J. McGinty, and R. D. Stevens, *Can. J. Chem.*, **48**, 480 (1970).
(15) D. C. Borg, *Nature (London)*, **201**, 1037 (1964).
(16) R. W. Fessenden, *J. Chem. Phys.*, **37**, 747 (1962).
(17) C. Corvaja, H. Fischer, and G. Giacometti, *Z. Phys. Chem. (Frankfurt am Main)*, **45**, 1 (1965).
(18) W. T. Dixon and R. O. C. Norman, *J. Chem. Soc.*, 3119 (1963).
(19) R. O. C. Norman, P. M. Storey, and P. R. West, *J. Chem. Soc., B*, 1087 (1970).
(20) A. L. Buley, R. O. C. Norman, and R. J. Pritchett, *J. Chem. Soc., B*, 849 (1966).
(21) -R equals -H, $-CH_3$, $-CH_2CH_3$, $-CH_2CH_2CH_3$, and $-C_6H_5$.
(22) In the rest of the paper, head- and tail-addition radicals of type **1** and **2**, respectively, will be denoted **1** (-X) and **2** (-X) where -X is the variable group.
(23) *E.g.*, D. Kosman and L. M. Stock, *Chem. Commun.*, 551 (1968).
(24) R. A. Kaba and P. Smith, unpublished work.
(25) W. T. Dixon, R. O. C. Norman, and A. L. Buley, *J. Chem. Soc.*, 3625 (1964).
(26) H. Zeldes and R. Livingston, *J. Chem. Phys.*, **45**, 1946 (1966).
(27) H. Fischer in "Landolt-Bornstein," Vol. 1, K.-H. Hellwege, Ed., New Series, Group II, Springer-Verlag, Berlin, 1965, p 27.
(28) This nomenclature is similar to that defined in ref 22.
(29) At the same time, the epr cell became clogged with organic solid, presumably polymeric.
(30) Y. Doi and B. Rånby, *J. Polym. Sci., Part C*, **31**, 231 (1970).
(31) *E.g.*, see (a) I. Izumi and B. Rånby, "Esr Applications in Polymer Research," P.-O. Kinell, B. Rånby, and V. Runnstrom-Reio, Ed., Wiley, New York, N. Y., 1973, p 43, and (b) P. Smith, same reference, p 50.
(32) H. Fischer, *Z. Naturforsch.*, **19a**, 866 (1964).
(33) H. Fischer, *Z. Naturforsch.*, **20a**, 428 (1965).
(34) R. W. Fessenden and R. H. Schuler, *J. Chem. Phys.*, **39**, 2147 (1963).
(35) H. M. McConnell and D. B. Chesnut, *J. Chem. Phys.*, **28**, 107 (1958).
(36) W. J. Maguire and P. Smith, unpublished work, by the $TiCl_3$-H_2O_2 method and with the appropriate alkene in aqueous solution at 25 ± 2°.
(37) These two ranges become 18.0–18.4 and 23.1–23.4 G if the data are restricted to where the solvent was water, *i.e.* if **1** ($-OOCC_6H_5$) is excluded. In the light of the arguments which follow this reference, that $a_{\beta\text{-}H}^{CH_2OH}$ [**1** ($-OOCC_6H_5$)] equals 18.6 G is good evidence for identity of the radical taken as **1** ($-OOCC_6H_5$) for, if the added radical were **5** or $\cdot CH_3$ and not $\cdot OH$, this β-CH_2 coupling would likely be significantly different from 18.6 G; see ref 17, 32, 33, and H. Fischer and G. Giacometti, *J. Polym. Sci., Part C*, **16**, 2763 (1967). Although the spectrum attributed to **2** ($-OOCC_6H_5$) is not out of line with those of the other **2** (-OOCR) radicals, it is relatively uninformative; see section III. However, it seems likely that this is the correct assignment if that for **1** ($-OOCC_6H_5$) is valid.
(38) M. Ōki and H. Nakanish, *Bull. Chem. Soc. Jap.*, **43**, 2558 (1970).
(39) M. Ōki and H. Nakanish, *Bull. Chem. Soc. Jap.*, **44**, 3144 (1971).
(40) M. Ōki and H. Nakanish, *Bull. Chem. Soc. Jap.*, **44**, 3197 (1971).
(41) M. J. Roedel, *J. Amer. Chem. Soc.*, **75**, 6110 (1953).
(42) *E.g.*, see also J. C. Bevington, "Radical Polymerization," Academic Press, London, 1961, Chapter 5; M. Julia, *Accounts Chem. Res.*, **4**, 386 (1971); D. J. Edge and J. K. Kochi, *J. Amer. Chem. Soc.*, **94**, 7695 (1972).
(43) Based on the $a_{\beta\text{-}H}^{CH_3}$ values for $CH_3\dot{C}HCH_2NH_2$ and $(CH_3)_2\dot{C}CH_2NH_2$ in aqueous solution at 25 ± 2° [W. J. Maguire and P. Smith, unpublished work by the $TiCl_3$-NH_2OH method] $\Delta(-CH_2NH_2)$ is 0.040 and 0.047, respectively.

Carbon-13 Chemical Shifts of the Carbonyl Carbon. VII. The Phenol–Acetone System

Thomas T. Nakashima, Daniel D. Traficante, and Gary E. Maciel*

Department of Chemistry, Colorado State University, Fort Collins, Colorado 80521 *(Received July 13, 1973)*

Publication costs assisted by the National Science Foundation

^{13}C chemical shifts were determined for 1:1 acetone–phenol solutions in carbon tetrachloride. Solute concentrations were varied from 6.5 to 0.0098 *m* and the temperature was varied from 258 to 324°K. Equilibrium constants for the formation of the phenol–acetone complex and ^{13}C chemical shift values of the pertinent individual species were obtained at each temperature by iterative least-squares approaches at two levels. In the more complete treatment, phenol and acetone self-association were included. Data on self-association were obtained in separate ^{13}C nmr studies of phenol in carbon tetrachloride and acetone in carbon tetrachloride. Thermodynamic data were also obtained from the self-association data. It appears that carbonyl ^{13}C shifts are well suited to detailed analysis of hydrogen-bonding systems, but that the ^{13}C resonances of phenolic carbons may not be as promising.

Introduction

During the past few years there has been a large volume of ^{13}C nmr data accumulated on a variety of compounds. A large portion of the ^{13}C investigations have been at least partially devoted to the characterization of the shifts of a carbonyl carbon.[1] Carbon-13 nmr solvent studies by Maciel and Natterstad[2] on the ^{13}C chemical shifts of the carbonyl carbon in a variety of carbonyl containing compounds, including acetone, have shown the shifts to be especially sensitive to solvents that are hydrogen-bonding acids, but relatively insensitive to aprotic solvents. Similar ^{13}C nmr solvent studies by Maciel and James[3] on the ^{13}C chemical shifts of phenol have shown that the induced solvent shifts were dependent upon the basicity of the solvent system, and that as the basicity of the solvent increases, the induced shifts tend to increase in magnitude. In both of these earlier ^{13}C nmr solvent studies, the observed shifts were interpreted in terms of the formation of intermolecular hydrogen-bonded complexes between the solute and solvent. The sensitivities of the carbonyl and phenolic ^{13}C chemical shifts to the acidic or basic nature of the solvent found in these earlier investigations[2,3] point to the possible use of the ^{13}C chemical shift parameter in studying intermolecular hydrogen bonding.

The present study was undertaken in order to establish in greater detail the utility of the ^{13}C chemical shift parameter to characterize intermolecular hydrogen bonding. The acetone–phenol system was chosen, focusing attention on the carbonyl carbon of acetone and the substituted carbon of phenol. Thermodynamic data for this system have been determined previously on the basis of other methods, *e.g.*, infrared and ^{1}H nmr,[4,5] providing a check on the thermodynamic values obtained by ^{13}C nmr.

Experimental Section

The ^{13}C nmr spectra were obtained at a frequency of 22.628 MHz on solutions containing equimolar concentrations of phenol and acetone in a solvent which consisted of 5% (by volume) C_6H_{12} (Eastman, spectrograde) and 95% carbon tetrachloride (Fisher, spectrograde) and was stored over Linde molecular sieves (Union Carbide, 3 Å). The ^{13}C resonance of C_6H_{12} served as the internal reference. Field/frequency stabilization was achieved by locking on the ^{19}F resonance signal of 1,1,2-trichloro-3,3,3-trifluoro-1-propene (PCR, Inc.) contained in a 2-mm (o.d.) capillary centered concentrically with Teflon spacers in a 10-mm sample tube. The spectrometer employed was a Bruker HFX-90, interfaced to a Digilab FTS/NMR-3 data system and pulse unit. The combinations of acquisition time and number of data points were chosen such that the accuracy of all shifts determined is better than ±0.05 ppm.

Phenol (Baker, reagent grade) and acetone (Fisher, spectrograde) were purified by distillation from Linde molecular sieves (3 Å) to remove any water contained in the compounds. The samples were prepared in a drybox, charged with dry nitrogen, by weighing or syringing phenol, acetone, and the 5% C_6H_{12}–CCl_4 solvent to make what is formally a 6.5 *m* solution of the 1:1 acetone–phenol complex. Dilutions were also carried out in the drybox and spectra were obtained on natural abundance samples prepared in this manner at concentrations ranging down to (and including) 0.2 *m*. Samples of formal acetone–phenol concentrations of 0.2 *m* and below were prepared with ^{13}C-enriched phenol (1-^{13}C 50%, see below) and carbonyl-labeled acetone (2-^{13}C 50%, Merck Chemical Co.). These compounds were purified also by vacuum distillation from molecular sieves, 3 Å. With ^{13}C-enriched solutes, spectra were obtained at concentrations down to 0.0098 *m*.

The phenol-1-^{13}C was prepared by the dehydrogenation of carbonyl-labeled cyclohexanone, carried out nearly quantitatively by passing the cyclohexanone vapors at about 350° through a Pd/charcoal column.[6] The cyclohexanone-1-^{13}C was prepared by the pyrolysis of the barium salt of heptanedioic-1,7-^{13}C acid, prepared *via* hydrolysis of the dicyanide obtained by treating 1,5-dibromopentane with K^{13}CN, according to the procedure described by Murray and Williams.[7]

^{13}C spectra were obtained for each solution over a temperature range of about 258 to 324°K, covered in increments of about 11°.[8] The Bruker ST-100/700 temperature control unit was calibrated for the specific characteristics of these experiments and the temperature of the sample is reported with an accuracy of ±1°.

Results and Discussion

A. Overall Trends. ^{13}C chemical shifts were determined on the carbonyl carbon of acetone and on the substituted

carbon of phenol as a function of temperature (258–324°K) and the formal concentration of the 1:1 acetone–phenol complex (0.0098–6.5 *m*) in CCl_4. Data on the other phenol carbons and on the methyl carbon of acetone were obtained in the concentration range 0.20–6.5 *m*. Figure 1 summarizes the results for the carbonyl shifts at concentrations of 0.722 *m* and below.

Several trends can be noted upon examination of Figure 1. As the temperature is decreased for a given concentration, the shielding of the carbonyl carbon of acetone decreases. As the formal concentration of the complex is decreased, the carbonyl carbon of acetone becomes more shielded.

Examination of the data on the shifts of phenol carbons revealed that they are not very sensitive to a 66° temperature variation nor to a 20-fold variation in concentration.[8] Because of this low sensitivity, plots similar to those given in Figure 1 are not shown for the phenol results.

Of the carbons in this system, the chemical shift that is most sensitive to changes in temperature and/or concentration is that of the carbonyl carbon of acetone. At the highest phenol–acetone concentration investigated, the total change in shielding of the carbonyl carbon of acetone for a temperature variation of 66° is approximately 1.5 ppm (to lower shielding as the temperature is reduced). The sensitivity of the shielding of the carbonyl carbon to variation in temperature increases as one proceeds to the lower concentrations, and is a maximum at about 0.039 *m* (3.24 ppm change in shielding for a 66° temperature variation) and then decreases below this concentration. At a given temperature, as the concentration decreases, the shielding of the carbonyl carbon increases; the sensitivity of the shielding to a concentration change increases at the lower concentrations. Comparing the sensitivity of the carbonyl carbon at various temperatures, it is seen from Figure 1 that at the lower concentrations the change in shielding with concentration change is greater at the lower temperatures; *i.e.*, the slope $\Delta\delta^{13}C/\Delta m$, where Δm represents the changes in molality of the complex, is greater for the lower temperatures.

The observed shielding variations with temperature or concentration for the other carbons within this system are much lower in magnitude than those found for the carbonyl carbon. It was felt before initiating this work that the shielding of the substituted carbon of phenol would also show sufficient sensitivity to changes in concentration and temperature to provide an additional useful probe; however, this hope was not realized experimentally.

A reality that must be considered in interpreting these results is that the shifts observed in this investigation are partly due to changes in the position of an equilibrium between monomeric and dimeric or polymeric species, *i.e.*, formation of aggregates of acetone and/or phenol. To explore this possibility, experiments were carried out to determine the effects of variations of concentration (0.02–6.5 *m*) and temperature (258–321°K) on the carbonyl carbon shielding of acetone in the absence of phenol and on the shielding of the substituted carbon of phenol in the absence of acetone.

For the acetone case, as the concentration of acetone is reduced at a given temperature the carbonyl carbon becomes more shielded. For a given concentration, as the temperature is reduced by 63° the carbonyl carbon becomes less shielded by about 1 ppm for any of the nine concentrations investigated. Comparing these results and those obtained for the shielding of the carbonyl carbon of

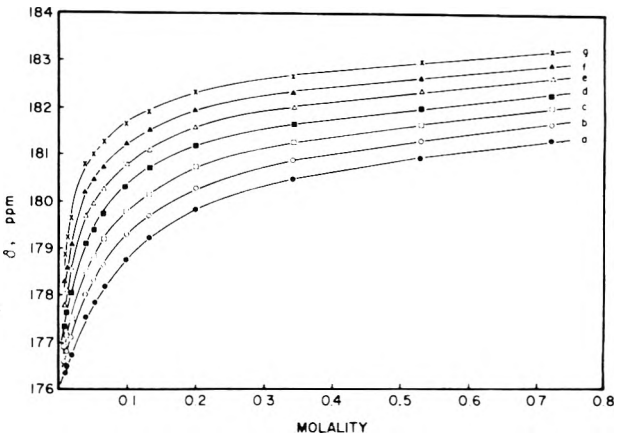

Figure 1. ^{13}C chemical shifts of the carbonyl carbon of acetone in 1:1 acetone–phenol solutions as a function of concentration and temperature. Increasing δ values correspond to decreasing shielding (given with respect to cyclohexane). Temperatures given by a = 324°K, b = 314°K, c = 302°K, d = 291°K, e = 280°K, f = 269°K, g = 258°K.

acetone in the presence of phenol reveals the following: (1) for a given concentration and temperature, the carbonyl carbon of acetone is less shielded in the presence of phenol than in the absence of phenol; (2) for any concentration, the sensitivity of the carbonyl carbon shielding of acetone in the absence of phenol to a temperature variation is virtually a constant value of 1 ppm over a 63° range; however, the sensitivity of the carbonyl shielding in the *presence* of phenol to temperature variation changes with concentration, with a maximum sensitivity occurring at a concentration of about 0.039 *m* for the complex; (3) at a given temperature, the shielding of the carbonyl carbon of acetone is not very sensitive to variation in concentration in the absence of phenol, while the shielding of the carbonyl carbon of acetone in the *presence* of phenol is very sensitive to variation of concentration, and approaches at the lowest concentrations that value obtained in the absence of phenol at the lowest concentration investigated.

For a given concentration, as the temperature is decreased the substituted carbon of phenol (C-1) becomes more shielded. For a given temperature, as the concentration is decreased the substituted carbon becomes less shielded. At the lowest concentrations the sensitivity of the C-1 shielding to a temperature variation is small. Comparing these results with the shieldings obtained for the substituted carbon of phenol in the presence of acetone reveals the following patterns: (1) for a given concentration and temperature, the substituted carbon of phenol is less shielded in the presence of acetone than in the absence of acetone; (2) for any concentration the sensitivity to temperature variation of the C-1 shielding of phenol is somewhat higher *without* acetone present; (3) at a given concentration the temperature sensitivity of the C-1 shielding of phenol in the presence of acetone or in the absence of acetone appears to be of roughly the same order of magnitude, but in the opposite sense; empirically, this accounts for the general pattern of insensitivity of the C-1 shielding of phenol in the phenol–acetone case; (4) the C-1 shielding of phenol, extrapolated to infinite dilution, tends toward the same value whether or not acetone is present.

The composite picture of the ^{13}C data described above indicates that the shifts obtained in the acetone–phenol system in CCl_4 reflect two types of equilibria. Thus, the

observed shifts depend upon the following: (1) changes in the position of an equilibrium between unassociated phenol and acetone molecules and those that are hydrogen bonded, and (2) changes in the position of equilibria between monomeric and polymeric species of each component. There are at least two approaches by which the acetone–phenol data can be analyzed to extract the equilibrium constant for hydrogen-bond formation. In one approach one simply ignores changes in the shieldings of acetone and phenol due to factors (*e.g.*, self-association) other than changes in the hydrogen bond equilibrium between acetone and phenol. In such an approach one either assumes that self-association effects are negligible in comparison to the influence of acetone–phenol interactions, or assumes that the errors implicitly introduced by neglecting self-association are largely self-cancelling. Or, at essentially the same level, one can qualitatively visualize the equilibrium between the acetone–phenol complex and non-hydrogen-bonded acetone and phenol, without regard to the detailed states of microscopic aggregation of the non-hydrogen-bonded species. A somewhat more sophisticated approach attempts to use the observed shifts directly to analyze the data by taking self-association of acetone and of phenol explicitly into account (to the dimer level, in this particular treatment). Each of these methods is discussed in greater detail in the next section.

B. Analysis of the Data. Method I. Neglecting self-association, we focus upon the equilibrium expression for the dissociation of the hydrogen-bonded acetone–phenol complex. Assuming a 1:1 complex, the equilibrium can be represented as

$$AP = A + P \tag{1}$$

where AP represents the 1:1 hydrogen-bonded complex, and A and P represent acetone and phenol monomers, respectively. The equilibrium expression for this process is

$$K = [A][P]/[AP] \tag{2}$$

where the brackets represent the equilibrium activities of the indicated species (in the present investigation we have employed the ideal dilute solution assumption, using molalities). For a fast exchange process between two sites, the observed acetone resonance position corresponds to a weighted average signal of the two types of A species (monomer and hydrogen-bonded complex), with a chemical shift that is given by the usual type of expression

$$\delta_{obsd} = \frac{[A]}{[AP] + [A]}\delta_A + \frac{[AP]}{[AP] + [A]}\delta_{AP} \tag{3}$$

In eq 3, δ_{obsd}, δ_A, and δ_{AP} represent the observed weighted average chemical shift value and the chemical shifts of monomer A and of A in the complex AP, respectively, with respect to an internal reference. The problem is to extract K, the equilibrium constant for dissociation of the hydrogen-bonded complex, from the experimental data. This was accomplished as follows.

The solutions were all prepared initially with equimolar quantities of A and P, so that eq 2 becomes

$$K = [A]^2/[AP] \tag{4}$$

which can be written as

$$K = [A]^2/(C_T - [A]) \tag{5}$$

where

$$C_T = [AP] + [A] \tag{6}$$

Solving for [A] and [AP] in eq 5 and 6, respectively, and substituting the resulting expressions into eq 3, yields

$$\delta_{obsd}(N) = \frac{-K + \sqrt{K^2 + 4KC(N)}}{2C(N)}\delta_A + \frac{2C(N) + K - \sqrt{K^2 + 4KC(N)}}{2C(N)}\delta_{AP} \tag{7}$$

where $C(N)$ and $\delta_{obsd}(N)$ represent values of C_T and δ_{obsd} for the Nth experiment in a series of experiments in which C_T is varied. The known quantities in eq 7 are $\delta_{obsd}(N)$ and $C(N)$. The unknowns are δ_A, δ_{AP}, and K. To solve eq 7 for δ_A, δ_{AP}, and K, an iterative least-squares computer program was employed.[9] The results of this analysis for the data obtained on the carbonyl carbon are summarized in Table I for all the temperatures employed.

TABLE I: Calculated Values of K, δ_A, and δ_{AP} Using Acetone Shifts and Method I

Temp[a]	K	δ_{AP}[b]	δ_A[c]	$1/K$[d]
324	0.0918	183.81	175.54	10.89
314	0.0669	183.81	175.60	14.59
302	0.0463	183.81	175.61	21.60
291	0.0318	183.81	175.67	31.45
280	0.0239	183.94	175.82	41.84
269	0.0180	184.03	175.98	55.56
258	0.0145	184.16	176.39	68.97

[a] Temperature in degrees Kelvin. [b] Least-squares evaluated shift of the carbonyl carbon of acetone in the associated (AP) molecule. [c] Least-squares evaluated shift of the carbonyl carbon of acetone as the unassociated molecule. [d] Association constant for formation of the acetone–phenol complex.

The values of δ_{obsd} computed for the acetone carbonyl carbon by method I agreed extremely well with those determined experimentally. A plot that demonstrates this agreement for a particular temperature is shown in Figure 2. Agreement of similar quality was obtained for each temperature studied. The association constants ($1/K$) for hydrogen bond formation determined by method I from the acetone shifts are also in rough qualitative agreement with those reported in the literature, but are generally higher. Employing an infrared study of the phenol-OH stretching line, Gramstad[10] has determined the hydrogen-bond association constant of phenol and acetone in carbon tetrachloride at two temperatures. The values he obtained are $(1/K)^{293} = 12.31(M^{-2})$ and $(1/K)^{323} = 6.01(M^{-1})$. Also based upon infrared methods, Joesten and Drago,[4a] Widom and coworkers,[11] Heinen,[12] and Mizushima and coworkers[13] have reported $(1/K)^{298} = 13.5(M^{-1})$, $(1/K)^{297.5} = 8.5(M^{-1})$, $(1/K)^{296} = 12.3(M^{-1})$, and $(1/K)^{303} = 8.35(M^{-1})$, respectively, for the acetone–phenol system. Based upon ^{1}H nmr experiments, Nakano and coworkers[14] report $10.7(M^{-1})$ for $(1/K)^{298}$.

Values of ln $(1/K)$ determined by method I for each temperature from the acetone carbonyl data were plotted *vs.* $1/T$. The plot is shown in Figure 3; the slope at 298°K is 2.63×10^3 deg, from which a $\Delta H°_{298}$ value of -5.2 kcal/mol is derived for the formation of the phenol–acetone complex. This is in fairly good agreement with the values reported previously for the same system, -7.0,[11] -5.1,[4b] -5.34,[15] and -3.3 ± 0.5,[4a] all based upon infrared studies. A value of -11.3 eu was obtained for $\Delta S°_{298}$. Values of -6.2 and -12.9 eu have been reported for the acetone–phenol[4a] and the 2-butanone–phenol[15] complexes, respectively, based on other methods.

The association constants ($1/K$) determined by method I from the phenol data showed large deviations from a monotonic trend as temperature is varied. This is probably due to the generally small chemical shift variation ob-

served for the phenol case as temperature and concentration were varied; with such small shift variation, any complicating factors, *e.g.*, instrument variation or failure of the model, could preclude a straightforward analysis of the data. Hence, the phenol chemical shift data are not considered further in this paper.

Method II. In this method, *self*-association to the *dimer* level is included explicitly in the weighted-average chemical shift expression. Inclusion of this term in eq 3 yields

$$\delta_{obsd} = \frac{[A]}{[AP] + [A] + 2[A_2]}\delta_A + \frac{2[A_2]}{[AP] + [A] + 2[A_2]}\delta_{A_2} + \frac{[AP]}{[AP] + [A] + 2[A_2]}\delta_{AP} \quad (8)$$

Three simultaneous equilibria are pertinent in analyzing the data in terms of this model. These are

$$A + A = A_2, \qquad [A_2]/[A]^2 = a \quad (9)$$

$$A + P = AP, \qquad [AP]/[A][P] = c \quad (10)$$

$$P + P = P_2, \qquad [P_2]/[P]^2 = p \quad (11)$$

where A_2 and P_2 represent dimers of acetone and phenol, respectively, and a and p represent the *association* constants for acetone and phenol, respectively.

Defining A_T as the total concentration of species A in any form and P_T as the total concentration of species P in any form, eq 9-11 can be solved for [A], [AP], and $[P_2]$. Combining these results and the definitions of A_T and P_T, yields

$$A_T = [A] + 2a[A]^2 + c[A]\left\{\frac{-(1 + c[A]) \pm \sqrt{(1 + c[A])^2 + 8pP_T}}{4p}\right\} \quad (12)$$

Algebraic rearrangement, noting that for the present study $A_T = P_T$, yields the quartic equation

$$a(4a - c/p^2)[A]^4 + (4a - c/2p^2 - ac/p)[A]^3 + (1 - c/2p - 4aA_T)[A]^2 + (2A_Tc/4p - 1)[A] + A_T^2 = 0 \quad (13)$$

Using eq 9-11 and the definition of A_T in eq 8, one obtains

$$\delta_{obsd} = \frac{[A]}{A_T}\delta_A + \frac{2a[A]^2}{A_T}\delta_{A_2} + \frac{A_T - [A] - 2a[A]^2}{A_T}\delta_{AP} \quad (14)$$

We seek now the solutions of eq 13 and 14 that give the best account of δ_{obsd}, *i.e.*, the best agreement between calculated and experimental values for each experiment (each A_T and temperature). This requires values of the dimerization constants, a and p.

The values of a and p and of δ_A and δ_{A_2} were obtained from experiments on acetone in carbon tetrachloride and on phenol in carbon tetrachloride, analyzed *via* a simple modification of the iterative least-squares approach outlined in method I. Equation 7 for the monomer-dimer model becomes, for the acetone case

$$\delta_{obsd}(N) = \frac{-K_A/2 + \sqrt{K_A^2/4 + 2K_AA_T(N)}}{2A_T(N)}\delta_A + \frac{2A_T(N) + K_A/2 - \sqrt{K_A^2/4 + 2K_AA_T(N)}}{2A_T(N)}\delta_{A_2} \quad (15)$$

where $K_A = 1/a$.

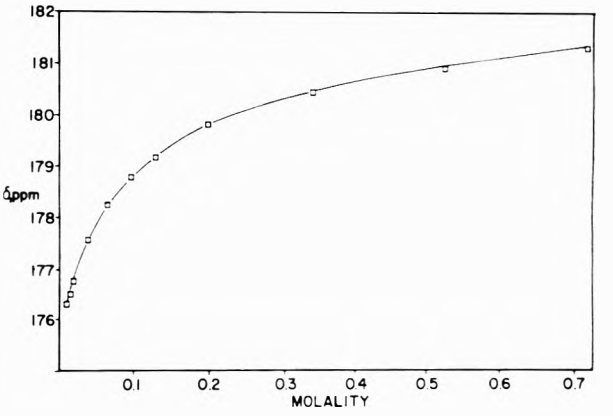

Figure 2. Experimental points and calculated line for δ_{obsd} *vs.* formal acetone-phenol concentration (C_T), using method I for carbonyl carbon shifts of acetone at 324°K. Increasing δ values correspond to decreasing shielding (given with respect to cyclohexane).

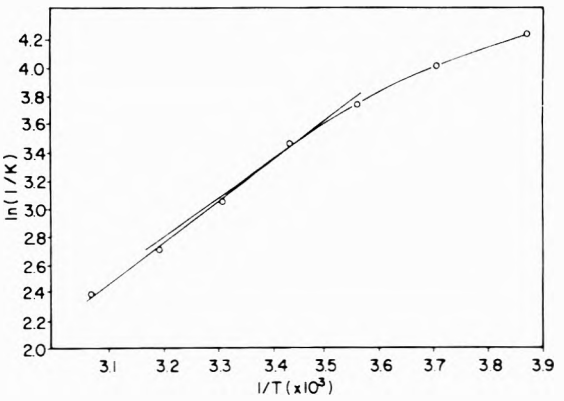

Figure 3. Plot of ln $(1/K)$, determined for acetone-phenol complex formation by method I from the acetone carbonyl carbon shifts, *vs.* $1/T$. Slope at 298°K is 2.63×10^3 deg

TABLE II: Calculated Values of the Dimerization Constant (a), δ_A, and δ_{A_2} for Acetone[a]

Temp[b]	a	δ_{A_2}[c]	δ_A[d]	K_A[e]
321	0.186	178.76	174.34	5.38
311	0.189	178.97	174.49	5.28
300	0.213	179.01	174.63	4.70
290	0.231	179.20	174.78	4.33
279	0.256	179.23	174.93	3.90
269	0.284	179.26	175.11	3.52
258	0.330	179.28	175.29	3.03

[a] Calculated on the basis of a least-squares fit to the experimental data, using eq 15. [b] Temperature in degrees Kelvin. [c] Values of the shift of the carbonyl carbon in a dimer complex, calculated as described in footnote *a*. [d] Values of the shift of the carbonyl carbon as the monomer, calculated as described in footnote *a*. [e] The dissociation constant of the acetone dimer, $K_A = 1/a$.

A similar expression may be written for the phenol case in terms of p. Using the observed shifts for acetone in carbon tetrachloride (in the absence of phenol) as a function of concentration in an iterative computer program based upon this equation, values of δ_A, δ_{A_2}, and a were determined for each temperature; these values are summarized in Table II. Values of δ_P, δ_{P_2}, and p were determined in the same manner from the data on phenol in carbon tetrachloride in the absence of acetone; these values are summarized in Table III. The agreement between the experimental values of δ_{obsd} and the values calculated using the

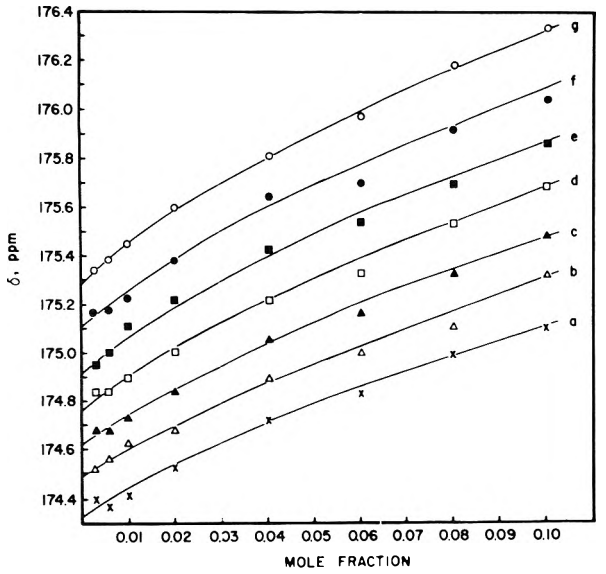

Figure 4. The dependence of ^{13}C chemical shift of the carbonyl carbon of acetone (with respect to cyclohexane) upon concentration in carbon tetrachloride (in the absence of phenol). The curves for each temperature were computed according to eq 15 in terms of molality, but are given here with respect to mole fractions. Experimental points indicated. Temperatures given by a = 321°K, b = 311°K, c = 300°K, d = 290°K, e = 279°K, f = 269°K, g = 258°K.

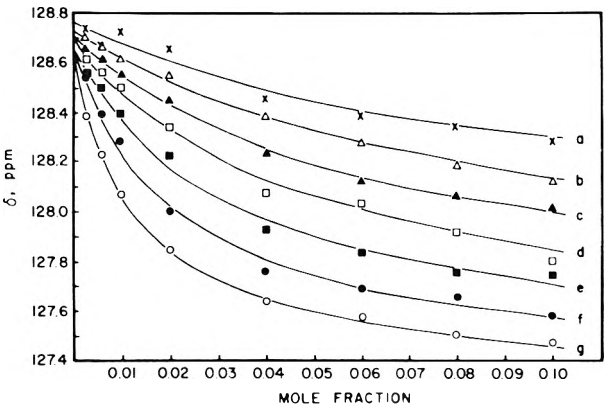

Figure 5. The dependence of the ^{13}C chemical shift of the substituted carbon of phenol upon concentration in carbon tetrachloride (in the absence of acetone). The curves for each temperature were computed according to the analog of eq 15 in terms of molality, but are given here with respect to mole fractions. Experimental points indicated. Temperatures given by a = 321°K, b = 311°K, c = 300°K, d = 290°K, e = 279°K, f = 269°K, g = 258°K.

parameters given in Tables II and III is shown for acetone and phenol in Figures 4 and 5, respectively.

Plots of ln (a) and ln (p) *vs.* $1/T$ yield values of $\Delta H°$ for the self-associations of acetone and of phenol, respectively. The $\Delta H°$ of self-association is found to be −8.3 kcal/mol for phenol and −1.6 kcal/mol for acetone. Previously reported values of $\Delta H°$ of dimerization of phenol are −5.12[15] and −4.35 kcal/mol[16] based upon other types of experiments. Values of −27.9 and −8.4 eu were obtained for the self-association $\Delta S°_{298}$ values for phenol and acetone, respectively.

The importance of phenol trimers in carbon tetrachloride solutions has been discussed by Bogachev and coworkers, based upon ^1H nmr studies.[17] While trimer contributions may introduce uncertainties into the precise meaning of the phenol association results given here, the

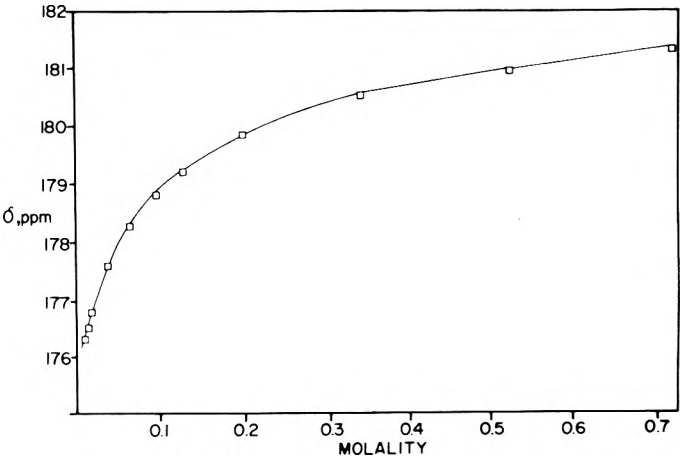

Figure 6. Experimental points and curve computed by method II for the carbonyl shift of acetone *vs.* formal concentration of the acetone–phenol complex at 324°K. Increasing δ values correspond to decreasing shielding (given with respect to cyclohexane). Parameters used are δ_A = 175.54, δ_{A_2} = 178.76, a = 0.174, c = 11.0, δ_{AP} = 184.2, p = 0.319.

TABLE III: Calculated Values of the Dimerization Constant p, δ_P, and δ_{P_2} for Phenol[a]

Temp[b]	p	δ_{P_2}[c]	δ_P[d]	K_P[e]
321	0.694	127.53	128.77	1.44
311	0.699	127.18	128.74	1.43
300	0.901	127.00	128.72	1.11
290	1.52	127.02	128.72	0.66
279	2.50	127.01	128.72	0.40
269	4.44	127.00	128.73	0.23
258	9.09	127.03	128.77	0.11

[a] Calculated on the basis of a least-squares fit to the experimental data using the analog of eq 15. [b] Temperature in degrees Kelvin. [c] Values of the shift of the substituted carbon of phenol in the dimer complex, calculated as described in footnote *a*. [d] Values of the shift of the substituted carbon of phenol in the monomer, calculated as described in footnote *a*. [e] The dissociation constant of the phenol dimer, $K_P = 1/p$.

main purpose in treating the phenol association was to provide more realistic values for the phenol monomer concentration for use in eq 10 than would be available if phenol self-association were completely neglected. The fact that the dimer model accounts satisfactorily for the phenol association data summarized in Figure 5 provides support for the use of this model in the present special case.

Still remaining is the primary task of obtaining the value of the acetone–phenol association constant, c, which yields the best fit to the experimental data according to eq 13 and 14. A computer-aided iterative approach was taken.[9] For a given c, the roots of A in eq 13 were determined for values of A_T ranging from 0.722 to 0.0098 m. This process was carried out for a series of c values ranging between 0 and 200.

For a given temperature, using values of a, δ_A, and δ_{A_2} listed in Table II, p values from Table III, and a series of trial c values and δ_{AP} values, the agreement between experimental values of δ_{obsd} and values calculated by eq 14 for acetone was generally poor. However, it was found that if the δ_A and c values calculated from method I (and summarized in Table I) and the δ_{A_2} values summarized in Table II are used, an excellent fit is obtained for the δ_{obsd} values calculated according to eq 14. This agreement between calculated and experimental dependence of δ_{obsd} on concentration is illustrated for one temperature in Figure 6. The agreement between the computed and observed shielding was very good at all the temperatures. For each

TABLE IV: Parameters Used in Method II

	Input[a]		Output[b]	
Temp[c]	a	p	δ_{AP}	c
324	0.174	0.319	184.2	11.0
314	0.186	0.496	184.1	15.0
302	0.206	0.860	184.0	22.0
291	0.230	1.490	184.1	32.0
280	0.256	2.560	184.4	42.0
269	0.289	4.960	184.6	56.0
258	0.329	9.490	184.8	69.0

[a] Association constants of acetone and phenol interpolated for the temperatures of interest from plots of ln a and ln p *vs.* $1/T$, based on the a and p values of Tables II and III, respectively. [b] The values of δ_{AP} and c obtained by a best fit criterion of calculated and experimental plots of δ_{obsd} *vs.* A_T by method II. [c] Temperature in degrees Kelvin.

temperature the best agreement between the experimental points and those computed by method II turns out to be given by a value of c that is approximately the $1/K$ value obtained by method I, using the δ_A value obtained in method I, the δ_{A_2} value computed by the use of eq 15, and a and p values derived from Tables II and III, respectively. The optimized values of δ_{AP} are slightly different from those obtained directly by method I. The results are summarized in Table IV. The thermodynamic parameters appropriate to these method II results are essentially the same as those given above for method I.

The excellent agreement between the experimental values of δ_{obsd} and those calculated by using method I, in which we have not explicitly included self-association effects, may be accounted for by the following arguments. First, the concentration of A_2 is small in all of the acetone–phenol–CCl_4 solutions. Also, both of the terms in which acetone self-association (method II) enters in eq 14 are almost equal, but of opposite sign. This near cancellation leaves an expression for δ_{obsd} which is nearly identical with that used in method I, so it is not surprising that both methods should require almost the identical c and $1/K$ parameters to obtain the best agreement between calculated and experimental δ_{obsd}. Furthermore, it is not entirely surprising that the simpler method would give a fit equally as good as that of method II, because in method I the δ_A parameter is free-running (chosen for the best fit).

The fact that the δ_A values derived from method I differ from those obtained by eq 15 and that method II is far more successful when employing the former set than when using the latter set, can be rationalized in the following manner. A dimer–monomer model is, of course, an oversimplification of acetone self-association. To the extent that this model deviates from physical reality, an analysis of the data that is based on it can give distortions in the parameters employed in an iterative fitting procedure. For example, in attempting to fit the acetone self-association data (no phenol present) at high acetone concentrations, where dimerization may not account for a more complicated self-association, the fitting procedure may yield parameters that would distort the δ_{obsd} *vs.* A_T curve at very low concentrations (where the monomer–dimer model might be more appropriate). Such distortions would not be apparent from our data, which are limited to concentrations of 0.02 m and higher; however, these distortions could lead to an incorrect extrapolation of δ_A. Such distortions might not occur in the acetone–phenol system, where the effects of the formation of the AP complex would dominate over those of acetone self-association at high A_T values; and since A_2 (or A_n) species would not occur in appreciable concentrations in this system, their presence could not, therefore, distort the fitting procedure in the manner described above. If this is the case, the δ_A value obtained by method I, in which a minimum of acetone concentration of 0.01 m was employed, would be more correctly identified with an acetone monomer than a δ_A value obtained by eq 15. Indeed, it appears from these data that acetone self-association could be left out of the analysis of phenol–acetone complexation.

To conclude, it appears that the observed ^{13}C shifts in the acetone–phenol system can be accounted for in terms of three independent equilibria, the self-association of acetone, the self-association of phenol, and the formation of a hydrogen-bonded complex between acetone and phenol; the first of these is relatively unimportant. The results obtained from the ^{13}C nmr approach using the carbonyl carbon are quite satisfactory; however, the ^{13}C shieldings of phenolic carbons do not appear to be as promising for detailed studies of hydrogen-bonding equilibria.

Acknowledgment. The authors are grateful to the National Institute of Neurological Diseases and Stroke for support of this work on Grant No. NS-08900-02 BBCB and for the support of National Science Foundation Grant No. GP-33429. They also acknowledge equipment grants from the National Science Foundation for funds toward the purchase of the nmr spectrometer and data system.

Supplementary Material Available. Tables of chemical shift as a function of concentration and temperature will appear following these pages in the microfilm edition of this volume of the journal. Photocopies of the supplementary material from this paper only or microfiche (105 × 148 mm, 24× reduction, negatives) containing all of the supplementary material for the papers in this issue may be obtained from the Journals Department, American Chemical Society, 1155 16th St., N.W., Washington, D. C. 20036. Remit check or money order for $3.00 for photocopy or $2.00 for microfiche, referring to code number JPC-74-124.

References and Notes

(1) J. B. Stothers, "Carbon-13 NMR Spectroscopy," Academic Press, New York, N. Y., 1972, Chapter 8.
(2) G. E. Maciel and J. J. Natterstad, *J. Chem. Phys.*, **42**, 2752 (1965).
(3) G. E. Maciel and R. V. James, *J. Amer. Chem. Soc.*, **86**, 3893 (1964).
(4) (a) M. D. Joesten and R. S. Drago, *J. Amer. Chem. Soc.*, **84**, 3817 (1962); (b) T. D. Epley and R. S. Drago, *ibid.*, **89**, 5770 (1967).
(5) C. M. Huggins, G. C. Pimentel, and J. N. Shoolery, *J. Phys. Chem.*, **60**, 1311 (1956).
(6) Syntheses of labeled substances were carried out at the University of California, Davis.
(7) A. Murray, III, and D. L. Williams, "Organic Synthesis with Isotopes, Part I," Interscience, New York, N. Y., 1958, p 823.
(8) See paragraph at end of paper regarding supplementary material.
(9) The computer program was adapted from that employed by D. C. Hofer, Ph.D. Dissertation, University of California, Davis, 1967.
(10) T. Gramstad, *Spectrochim. Acta.*, **19**, 497 (1963).
(11) J. M. Widom, R. J. Philippe, and M. E. Hobbs, *J. Amer. Chem. Soc.*, **79**, 1383 (1957).
(12) W. Heinen, *Recl. Trav. Chim. Pays-Bas.* **82**, 859 (1963).
(13) S. Mizushima, M. Tsuboi, T. Shimanouchi, and Y. Tsuda, *Spectrochim. Acta.*, **7**, 100 (1955).
(14) M. Nakano, N. I. Nakano, and T. Higuchi, *J. Pnys. Chem.*, **71**, 3954 (1967).
(15) D. L. Powell and R. West, *Spectrochim. Acta.* **20**, 983 (1964).
(16) M. M. Maguire and R. West, *Spectrochim. Acta.* **17**, 369 (1961).
(17) Y. S. Bogachev, L. K. Vasianina, N. N. Shapet'ko, and T. L. Alexuva, *Org. Magn. Resonance.* **4**, 453 (1972).

Activation Parameters for the Restricted Rotation of the Hydroxyl Group in the Duroquinol Cation Radical as Determined from the Electron Spin Resonance Spectra

Daniel G. Ondercin and Paul D. Sullivan*

Department of Chemistry, Ohio University, Athens, Ohio 45701 *(Received August 20, 1973)*

Publication costs assisted by the Petroleum Research Fund and the Ohio University Research Institute

The esr spectra of the duroquinol and duroquinol-d_2 cation radicals have been reinvestigated in various oxidant-solvent systems. In contrast to previous work the isomer ratio at low temperatures is found to be 70:30 in favor of the trans form. Using a calculation based on density matrix theory the spectra have been simulated and matched throughout the temperature range studied and activation parameters have been obtained. The new value for the barrier to rotation of the hydroxyl proton in duroquinol is *ca.* 7 kcal/mol, this now compares favorably with the value obtained by considering only the temperature dependence of the hydroxyl proton splitting constant. The effect of solvent and deuterium substitution on the activation parameters is also discussed.

Introduction

Duroquinol (DQ, 1,4-dihydroxy-2,3,5,6-tetramethylbenzene) cation radical was one of the first examples studied which showed the phenomenon of line width alternation in the electron spin resonance (esr) spectrum.[1] The effect was attributed to the restricted rotation of the hydroxyl groups which thus modulated the splittings of the methyl protons. The initial experiments were carried out in concentrated sulfuric acid solution in the temperature range 10–50°. Further work[2] in aluminum chloride–nitromethane extended the measurements down to −90°. At these low temperatures the spectra were interpreted in terms of cis and trans isomers in agreement with earlier predictions[1] and a four-jump model was used to explain the variation in the spectra with temperature. Calculations of the spectra were made using the solution of the modified Bloch equations assuming a 50:50 ratio of cis and trans isomers. An activation energy for the hydroxyl group rotation was then obtained as 4.2 ± 0.6 kcal/mol.

Further work on the DQ system was initiated for several reasons; first in our earlier investigation[2] the agreement between the simulated and experimental spectra at low temperatures left something to be desired. This disagreement could have been due to several factors; line width asymmetries are present in the experimental spectra but were not taken into account in the simulated spectra; the isomer ratio may not be 50:50, in fact, there was a slight possibility that only one isomer was present at low temperatures. Second, the barrier to rotation of the hydroxyl group has been estimated from the temperature dependence of the hydroxyl proton splitting constant as 6.6 ± 1.5 kcal/mol,[3] and also some preliminary studies of the deuterated duroquinol cation radical suggested that the barrier to rotation of the OD group was *ca.* 6.5 kcal/mol.[4] This latter result by itself would be interesting if shown to be true and was therefore worthy of further investigation. Finally, the availability of a general line shape program using density matrix theory[5] made it possible to carry out the required calculations in a reasonable amount of computer time.

In order to resolve some of the questions raised above it was therefore decided to carefully reexamine the spectra of DQ^+ in several oxidant-solvent systems and to obtain where possible the corresponding deuterated DQ^+ spectra. Particular interest was focussed on how different solvents and oxidizing agents and deuterium substitution would affect the splitting constants and activation energies.

Experimental Section

Duroquinol was a commercially available sample. The cation radical was prepared under vacuum using either sulfuric acid or aluminum chloride as oxidant and nitromethane, methylene chloride, or nitrobenzene as solvent. The deuterated duroquinol spectra were obtained by oxidizing duroquinol with dideuteriosulfuric acid followed by addition of nitromethane or nitrobenzene. Isolation of d_2-DQ was attempted so that it could be oxidized with aluminum chloride, but a mixture of DQ, d-DQ and d_2-DQ was always obtained. The esr spectra were measured on a Varian E-15 spectrometer using a sample of the perylene radical anion as a secondary standard. The temperature of the sample was varied using a Varian temperature controller which was calibrated against a thermocouple and the temperature was regularly checked during the course of our experiments. The least-squares analyses of the experimental spectra were carried out as previously described.[6] The density matrix program was that described by Heinzer[5] and a print-out of the program was kindly supplied by Dr. Heinzer.

Results and Discussion

Low-Temperature Spectra. As stated above, at low temperatures one expects the spectrum of DQ^- to be resolvable into two isomers. Previously in $AlCl_3$–CH_3NO_2[2] some ambiguities were present at low temperatures, therefore, it was decided to try other solvents in order to resolve the difficulties. Methylene chloride proved to be a good solvent using aluminum chloride as oxidant (system I). The spectra in this system (Figures 1-3) were better resolved and simpler in appearance than those in $AlCl_3$–CH_3NO_2 (see Figure 1 in ref 2 for comparisons). The simplification in the spectrum is caused by the accidental degeneracy of certain lines due to the 2:1 ratio of the splittings of the methyl groups in the trans isomer[6] (see Table

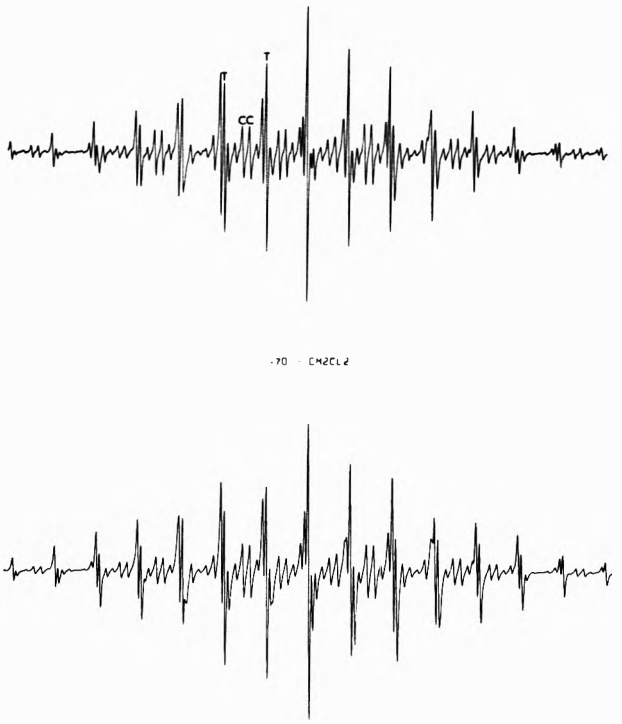

Figure 1. Esr spectrum (upper) of duroquinol in $AlCl_3$–CH_2Cl_2 at −70°. The lines indicated with T are from the trans isomer only, the lines indicated with C are from the cis isomer only. The lower spectrum is the matched simulated spectrum with $k = 1.8 \times 10^4$ sec^{-1}.

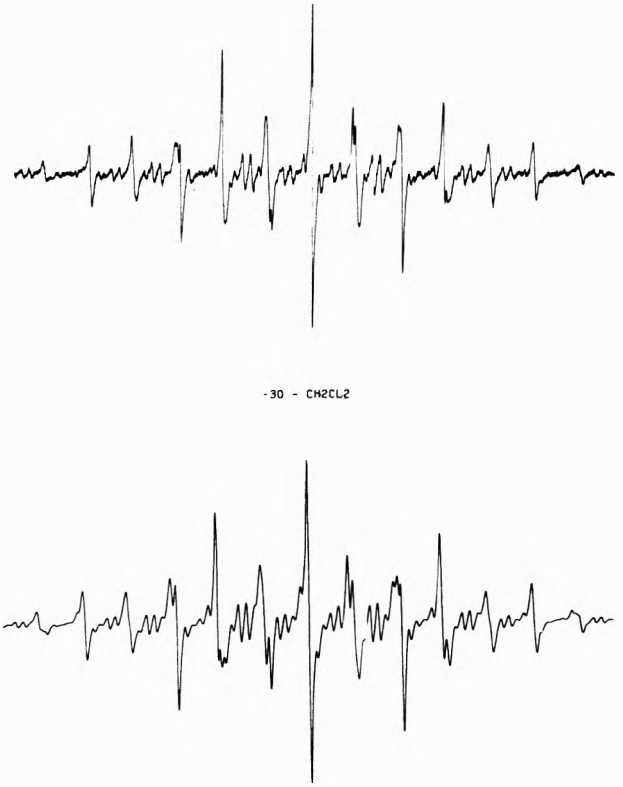

Figure 2. Esr spectrum of duroquinol in $AlCl_3$–CH_2Cl_2 at −30°. The lower spectrum is the matched simulated spectrum with $k = 1.5 \times 10^5$ sec^{-1}.

I). Because of this degeneracy the presence of two isomers is readily verified; one also observes that the relative intensities of the isomers is not 50:50. Figure 1 indicates

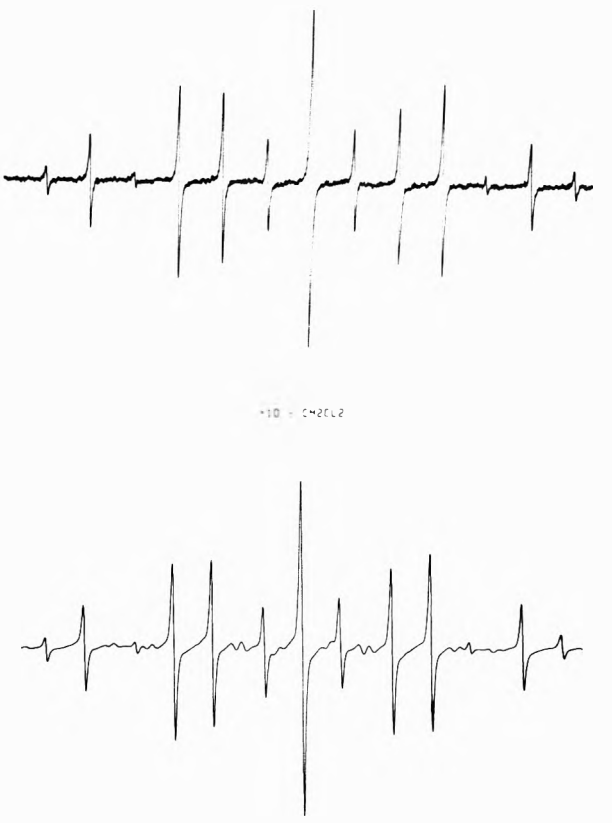

Figure 3. Esr spectrum of duroquinol in $AlCl_3$–CH_2Cl_2 at 10°. The lower spectrum is the matched simulated spectrum with $k = 1.18 \times 10^6$ sec^{-1}.

four lines, two from the cis and two from the trans isomers, which should be of approximately equal intensity if the isomers are present in equal amounts. Since they are not equally intense, one can estimate the relative isomer ratio as 70:30 in favor of the trans isomer. This corresponds to a free energy difference between the two isomers of *ca.* 375 cal/mol.

In $AlCl_3$–CH_3NO_2 (system II) spectra were obtained at low temperatures as previously described[2,7] and the splitting constants for the cis and trans isomers are shown in Table I. As can be seen in Table I, on changing solvents from CH_3NO_2 to CH_2Cl_2 there is a large change in the splitting constants of the trans isomer only. The isomer ratio in CH_3NO_2 is again as far as one can ascertain approximately 70:30 in favor of the trans form.

Low-temperature spectra in H_2SO_4–CH_3NO_2 (system III) were generally somewhat inferior to the two previous systems. Line width asymmetries were particularly severe at low temperatures and these caused difficulties in the simulations (see later). The splitting constants in H_2SO_4–CH_3NO_2 were the same as those in $AlCl_3$–CH_3NO_2 within experimental error.

In D_2SO_4–CH_3NO_2 (system IV) the spectra take on a different appearance (Figures 4–6) due to the substitution of two deuterium atoms for the hydroxyl protons. The low-temperature spectrum (Figure 4) is readily analyzed by analogy with the protonated systems and the splitting constants of the cis and trans isomers, as shown in Table I, are only slightly changed over those of the protonated form. The ratio $a_{OH}{}^{H}/a_{OD}{}^{D}$ is ~6.10 ± 0.05, considerably less than the ratio of the magnetogyric ratios. This is, however, what one would expect when the torsional oscillations of the O–D *vs.* the O–H group are taken into ac-

TABLE I: Summary of Low-Temperature Measurements of Splitting Constants

Isomer		Oxidizing system		
		$AlCl_3$–CH_3NO_2 (−70°)	$AlCl_3$–CH_2Cl_2 (−70°)	D_2SO_4–CH_3NO_2 (−60°)
Cis	$a_{CH_3}^{H}$(2,3)	2.151 ± 0.006	2.171 ± 0.006	2.168 ± 0.008
	$a_{CH_3}^{H}$(5,6)	1.903 ± 0.005	1.931 ± 0.005	1.895 ± 0.007
Trans	$a_{CH_3}^{H}$(2,5)	2.483 ± 0.006	2.785 ± 0.005	2.524 ± 0.005
	$a_{CH_3}^{H}$(3,6)	1.571 ± 0.005	1.389 ± 0.003	1.587 ± 0.006
	a_{OH}^{H}	2.730 ± 0.007	2.887 ± 0.006	0.447 ± 0.006[a]
	g	2.00330 ± 0.00002	2.00342 ± 0.00003	2.00346 ± 0.00002
Temperature dependence of OH splitting constant		−1.40 ± 0.04[b]	−1.29 ± 0.05	−0.46 ± 0.04

[a] Deuterium splitting. [b] mG/deg.

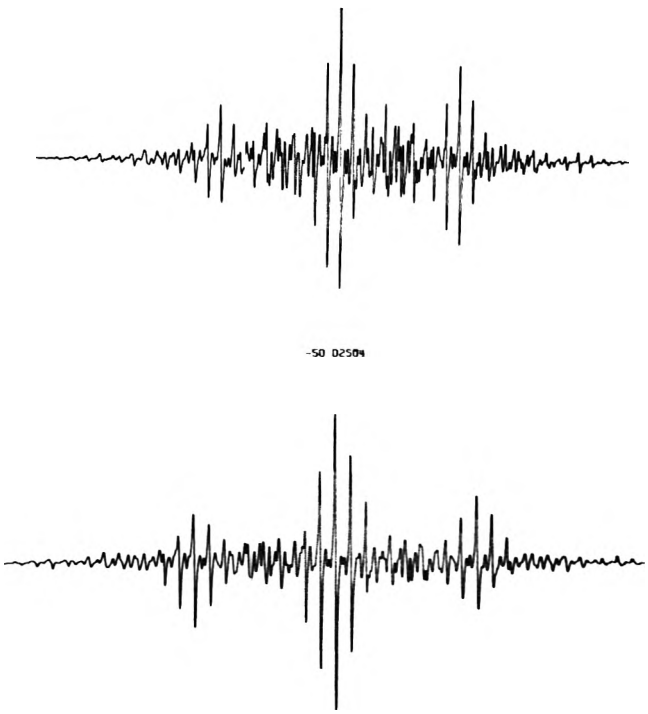

Figure 4. Esr spectrum of dideuterioduroquinol in D_2SO_4–CH_3NO_2 at −50°. The lower spectrum is the matched simulated spectrum with $k = 2.5 \times 10^4$ sec^{-1}.

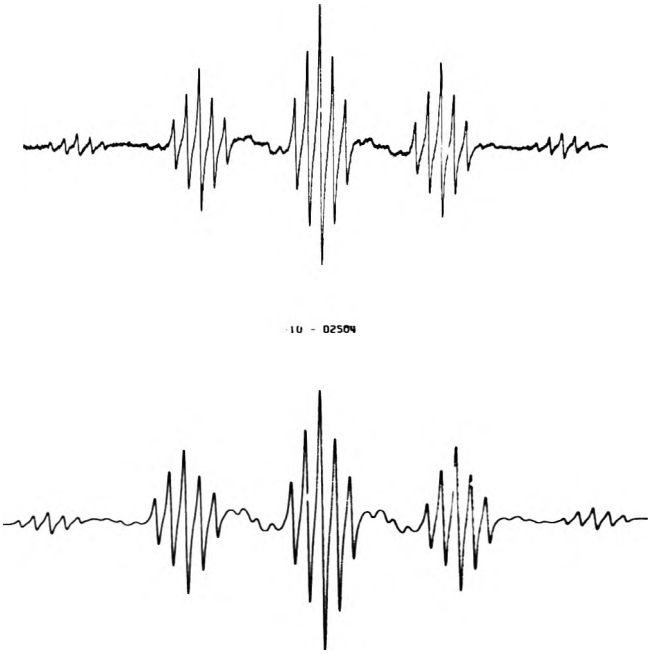

Figure 5. Esr spectrum of dideuterioduroquinol in D_2SO_4–CH_3NO_2 at −10°. The lower spectrum is the matched simulated spectrum with $k = 1.08 \times 10^6$ sec^{-1}.

count. For this system the line width asymmetries were not as pronounced at low temperatures as for system III and fewer difficulties were encountered in fitting the simulated to the experimental spectra.

Density matrix calculations on systems I–IV were carried out using a four-jump model, but in contrast to earlier work the isomer ratio was set to coincide with the experimentally measured value of 70:30. This was done in practice by letting the rate of the trans → cis exchange be ⅔ that of the cis → trans exchange rate. Care was also taken to keep the residual line width in agreement with the experimentally measured line widths at each temperature. The calculated spectra were fitted to the experimental spectra over the whole range from fast to slow exchange (see Figures 1–5). In the regions between fast and intermediate exchange certain lines change in intensity very rapidly and accurate rates are obtainable. In the intermediate to slow range the changes in the spectra are not so pronounced and the fitting is less precise. Additionally, in systems II–IV line width asymmetries at low temperatures contribute to a further uncertainty of the estimated rates. This manifests itself in the estimated errors for the activation parameters of these systems as shown in Table II. System I did not suffer so severely from the line width asymmetries and hence the activation parameters for this system may be considered more reliable than for the others.

High-Temperature Spectra. As noted above in the fast to intermediate region of exchange certain lines broaden and change in intensity very rapidly with temperature. Four further systems were studied under these exchange conditions, these were 98% H_2SO_4 (system V), H_2SO_4–$C_6H_5NO_2$ (system VI), 98% D_2SO_4 (system VII), and D_2SO_4–$C_6H_5NO_2$ (system VIII). Since the slow exchange spectra are not obtained in these systems in order to carry out simulations it was assumed that the parameters for the slow exchange limit would be the same as those found above for systems II and III. An additional approximation is also made that the isomer ratio remains constant at 70:30. This is certainly not true since the ratio should change with temperature, however, over the temperature range studied the effects are expected to be small.

Activation Parameters. The activation parameters were calculated in the usual way from least-squares fits of plots of log k *vs.* $1/T$ and ln (k/T) *vs.* $1/T$ utilizing the values of k obtained from the fitted spectra. The results for the

TABLE II: Summary of Activation Parameters

System	E_a, kcal/mol	Log A	ΔH^*, kcal/mol	ΔS^*, eu	ΔG^*_{273}, kcal/mol	$k(300)^a$
$AlCl_3$–CH_2Cl_2(I)	6.12 ± 0.08[b]	10.75 ± 0.07	5.65 ± 0.08	10.93 ± 0.10	2.66 ± 0.10	1.8×10^6
$AlCl_3$–CH_3NO_2(II)	7.70 ± 1.00	13.84 ± 0.90	5.77 ± 1.0	1.73 ± 0.60	5.33 ± 0.70	22.0×10^6
H_2SO_4–CH_3NO_2(III)	8.40 ± 0.6	12.98 ± 0.50	7.88 ± 0.55	0.87 ± 0.40	7.65 ± 0.55	9.5×10^6
H_2SO_4(V)	6.37 ± 0.10	11.10 ± 0.07	5.73 ± 0.11	9.86 ± 0.09	3.04 ± 0.25	2.9×10^6
H_2SO_4–$C_6H_5NO_2$(VI)	6.39 ± 0.37	11.67 ± 0.28	5.64 ± 0.46	7.64 ± 0.31	3.55 ± 0.37	11.0×10^6
D_2SO_4–CH_3NO_2(IV)	6.99 ± 0.48	11.68 ± 0.41	6.44 ± 0.48	6.76 ± 0.31	4.60 ± 0.40	5.0×10^6
D_2SO_4(VII)	7.62 ± 0.21	11.90 ± 0.15	7.01 ± 0.21	6.12 ± 0.10	5.34 ± 0.16	2.3×10^6
D_2SO_4–$C_6H_5NO_2$(VIII)	8.62 ± 0.44	12.78 ± 0.31	8.02 ± 0.44	2.06 ± 0.07	7.46 ± 0.32	3.5×10^6

[a] This is the rate constant in sec^{-1} for the trans to cis exchange at 300°K. [b] The error limits quoted represent the standard deviation of the result from a least-squares fit of the data.

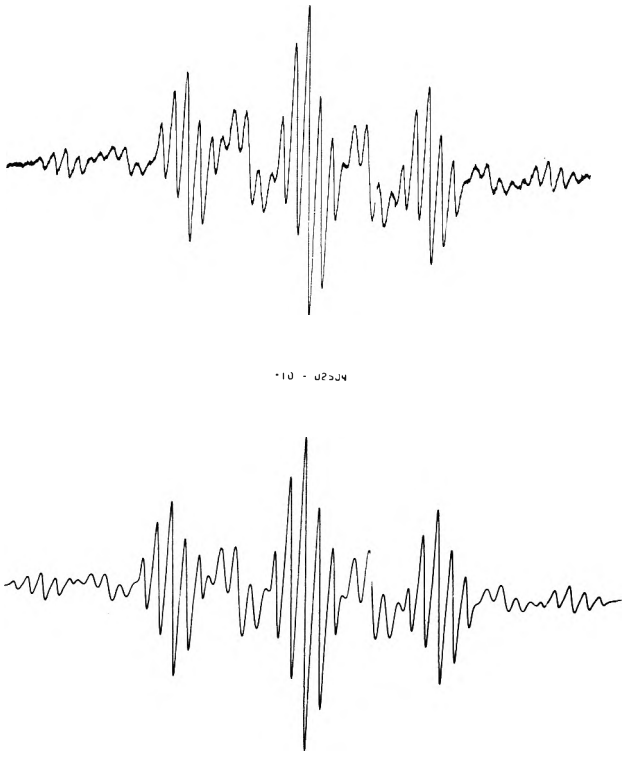

Figure 6. Esr spectrum of dideuterioduroquinol in D_2SO_4–CH_3NO_2 at 10°. The lower spectrum is the matched simulated spectrum with $k = 2.44 \times 10^6$ sec^{-1}.

eight systems studied are shown in Table II. A general conclusion to be drawn from Table II is that the activation energy is not particularly different for all of the systems studied. This indicates that the properties of the solvents themselves (*i.e.*, viscosity) do not contribute significantly to the kinetics of the dynamic process in contrast to the results found for a series of nitroxide radicals.[8] There are, however, significant differences in the activation parameters due to solvent effects. The results for systems I and II indicate the changes between nitromethane and methylene dichloride as solvents when the oxidant remains the same. The most obvious difference between the two systems is in the entropy of activation which decreases by ~9 eu on changing from methylene chloride to nitromethane. This difference manifests itself most obviously in the appearance of the esr spectra (and hence in the rates of the rotations) around +10°. At this temperature the spectrum in I is in the region of maximum broadening (intermediate rate of exchange, see Figure 1) while that in II is already into the region of rapid exchange. This is indicated in Table II by a factor of 12 difference in the relative rates at 300°K. Other differences between systems I and II were mentioned earlier and are shown in Table I. These are a change in the splitting constants of the trans isomer in particular and also an increased value of the hydroxyl proton splitting constant in I over that in II. These latter effects are explained if it is assumed that the hydroxyl group is more nearly in the plane containing the benzene ring in methylene chloride solutions than in nitromethane solutions, presumably arising from the poorer solvating power of CH_2Cl_2 as compared to CH_3NO_2.

The effect of a change in oxidant, and hence the counterion in solution, should be provided by comparing systems II and III. However, due to the uncertainties in the activation parameters for these systems, no significant differences can be ascertained. Interestingly when systems I and IV are compared no significant differences are again observed in the activation parameters, although both the solvent and counterion have been changed.

The effect of substituting deuterium for the hydroxyl protons is shown by comparing systems III with IV, V with VII, and VI with VIII. As already noted the effect of deuterium at low temperatures is to perturb the spin density distributions slightly in the cis and trans isomers (see Table I). The effects on the activation parameters are somewhat unclear. A comparison of systems III and IV for which the activation parameters were determined from spectra over the whole range of rates showed a decrease in the activation energy, the frequency factor and the rate constant at 300°K on deuterium substitution. The errors involved in the activation parameters for these systems are, however, quite large due to uncertainties in the determination of the rates at low temperatures caused by line width asymmetries. A comparison of systems V with VII and VI with VIII showed that for these systems the activation energy and frequency factors increased and the rate at 300°K decreased on deuterium substitution. (The activation parameters for these systems were determined from high-temperature spectra only and the relative values between different systems are thought to be more reliable.) These latter changes are what one would have expected to occur on deuterium substitution[9,10] and the relative changes are such that quantum mechanical tunnelling does not seem to be significant for the rotation of the hydroxyl group in duroquinol.

In conclusion the activation parameters in Table II indicate that the barrier to rotation of the hydroxyl group in duroquinol is *ca.* 7.0 kcal/mol. This result is somewhat higher than a previous value[2] but is probably more reliable because of the fact that the isomer ratio has been determined and taken into account in this paper. This new calculation is now in good agreement with a value of 6.5 ± 1.5 kcal/mol determined from the temperature dependence of the hydroxyl proton splitting constant.[3]

Acknowledgments. Acknowledgment is made to the donors of the Petroleum Research Fund, administered by the American Chemical Society, and to the Research Corporation for partial support of this research. The authors also thank Dr. J. Heinzer for a copy of his computer program ESREXN.

References and Notes

(1) J. R. Bolton and A. Carrington, *Mol. Phys.*, **5**, 161 (1962).
(2) P. D. Sullivan, *J. Amer. Chem. Soc.*, **89**, 4294 (1967).
(3) P. D. Sullivan, *J. Phys. Chem.*, **75**, 2195 (1971).
(4) P. D. Sullivan and J. R. Bolton, *Advan. Magn. Resonance*, **4**, 39 (1970).
(5) J. Heinzer, *Mol. Phys.*, **22**, 167 (1971).
(6) The splittings are assigned to the cis and trans isomers by comparison with the splittings in the 2,3- and 2,5-dimethylhydroquinone cation radicals.
(7) In the course of remeasuring the spectra in $AlCl_3$–CH_3NO_2 it was found that the temperatures reported previously were somewhat in error.
(8) L. Jonkman and J. Kommandeur, *Chem. Phys. Lett.*, **5**, 579 (1970).
(9) E. F. Caldin, *Chem. Rev.*, **69**, 135 (1969).
(10) Note Added in Proof. In a recent publication A. I. Prokof'ev, N. N. Bubnov, S. P. Solodovnikov, and M. I. Kabachnik, *Tetrahedron Lett.*, 2479 (1973), have measured a kinetic isotope effect in the intramolecular hydrogen migration within the 2-oxy-3,6-di-*tert*-butylphenoxy radical. Their measured act vation energies show $E_D - E_H = 1.6$ kcal/mol, in good agreement with our results.

Interaction of Matrix-Isolated NiF_2 and $NiCl_2$ with CO, N_2, NO, and O_2 and of CaF_2, CrF_2, MnF_2, CuF_2, and ZnF_2 with CO in Argon Matrices[1]

D. A. Van Leirsburg and C. W. DeKock*

Department of Chemistry, Oregon State University, Corvallis, Oregon 97331 *(Received August 10, 1973)*

The infrared spectra of matrix-isolated NiF_2 and $NiCl_2$ with CO, N_2, NO, and O_2 and of CaF_2, CrF_2, MnF_2, CuF_2, and ZnF_2 with CO in argon matrices have been observed. Perturbation of the frequencies of both the small molecules and metal halides are found to occur and these have been tabulated. The perturbed CO frequencies are all above the gas-phase frequency. The high-frequency band is correlated to the strength of the electric field of the metal ion at the carbon nucleus. A good correlation is found for the isotropic metal ions while ligand field arguments are involved to explain the deviations for those ions with anisotropic electron distribution. Evidence for a D_{2h} planar fluoride bridged dimer structure for $(NiF_2)_2$ and $(CrF_2)_2$ is also given.

Although the infrared spectra of a large number of matrix-isolated fourth period metal dihalides have been extensively studied,[2-10] no work has appeared on the interaction of these coordinately unsaturated molecules with other reactive species. In this paper we report the interaction of matrix-isolated NiF_2 and $NiCl_2$ with CO, N_2, NO, and O_2 and of CaF_2, CrF_2, MnF_2, CuF_2, and ZnF_2 with CO. Some of the transitions which we assign to the interacting species NiF_2N_2, NiF_2CO, $NiCl_2N_2$, and $NiCl_2CO$ were noted by earlier workers[2] but were not identified. A preliminary communication of part of this work has appeared.[11]

Experimental Section

The matrix-isolation technique is well known and our experimental apparatus is described elsewhere.[12] The major change from the previous equipment is that cooling is now provided by a Model DE-202 Displex helium refrigerator made by Air Products and Chemicals, Inc., which allows deposits to be made at ~14°K.

The argon was doped with CO, N_2, NO, or O_2 using a very low flow-rate valve into a tee in the argon line or in a few cases with CO by passing the reactive gas into the furnace chamber. Doping concentrations were as low as 1/500 to as high as 1/50 depending on the experiment. The infrared spectra were recorded from 4000 to 200 cm^{-1} using a Perkin-Elmer 180 spectrophotometer. The absolute uncertainty of the spectra is of the order of ±0.2 cm^{-1} while the isotopic frequency differences are known to ±0.1 cm^{-1}. Optimum resolution used for these experiments was 0.5 cm^{-1}.

The analytical reagent grade $NiCl_2 \cdot 6H_2O$ (Mallinckrodt Corp.) was dehydrated at 400° under a stream of HCl and then sublimed under HCl. The anhydrous NiF_2 (A. D. McKay Corp.) and CrF_2 (D. F. Goldsmith Co.) were further dried at 800° under a stream of SiF_4. The CuF_2 and MnF_2 (both anhydrous 99%) were purchased from Research Inorganic-Research Organic Co. and were used without further purification. The anhydrous ZnF_2 was prepared by heating $ZnCO_3$ with 50% excess NH_4HF_2 for 4 hr at 200° and then subliming off the excess NH_4HF_2 at 250°. The CaF_2 was B and A reagent grade and was used without further purification. Gases used were as follows: prepurified N_2 and USP O_2 from the NCG division of the Chemtron Corp.; chemically pure NO and CO and ultrapure Ar from the Matheson Co.; ^{13}CO, enriched to 90% ^{13}C, from the Monsanto Research Corp.; and $^{18}O_2$, enriched at 94% ^{18}O, from Miles Laboratories.

All samples were outgassed within 10° of the deposition temperature for at least 30 min prior to deposition. During the outgassing period the furnace walls were also heated with a heat gun to outgas the furnace chamber thoroughly. This effectively eliminated "impurity transitions" with the exception of HF. Deposits were made from nickel

Knudsen cells or for CuF_2 and ZnF_2 from platinum cells and CaF_2 from tantalum cells at temperatures corresponding to 10^{-4} to 10^{-5} atm vapor pressure. Deposition times from as short as 0.5 hr to as long as 4 hr were employed.

Results

We assume that the interaction of the metal halides with small molecules is a diffusion-controlled process. In order to obtain reasonable concentrations of the species of interest one either allows diffusion to occur by warming the matrix or else uses a high concentration of reactive species in the matrix. The first method leads to severe complications for these molecules because the metal halides dimerize very readily when the matrix is warmed.

The second method, used in this study, was carried out with a relatively high concentration of reactive small molecules (CO, N_2, NO, or O_2 ($1/50$)) and a rather low concentration of MX_2. High concentrations of MX_2 had to be avoided due to dimer formation. However, in many cases due to concentrations needed to observe complex formation some weak transitions attributable to dimers or higher polymer species were observed. An additional complication with this method is that the metal halide small molecule complex sometimes appears to be in more than one matrix site—apparently a result of the mixed matrix. If more than one frequency for the complex was observed, the higher frequency was always more intense and was taken to be the frequency in a pure argon matrix. These values are shown in Tables I–V with the additional sites shown in brackets.

The nickel halide small molecule interactions were the first to be studied. Accordingly, they were studied in depth both with respect to different small molecules (N_2, O_2, CO, and NO) and as a function of the nickel halide concentration. These results will be discussed first. The remaining metal fluorides were studied only with CO because in the nickel halide work only the perturbed CO stretch was easily observed and CO perturbations appeared to give the most information concerning the nature of the interaction. In addition, no metal fluoride concentration studies were carried out with the other systems.

Our interest in this paper is primarily centered upon the new transitions observed when a small molecule is doped into the argon matrix. In general, our undoped results are in very good agreement with literature values and therefore these references[2-10] may be consulted for more elaboration on the spectra of the isolated metal halide monomer or polymers in pure argon.

A. CO. Leroi, *et al.*,[13] Davies and Hallam,[14] and Maki[15] have deposited CO in Ar and all obtained three transitions at 2148, 2142, and 2138 cm^{-1}. The 2148-cm^{-1} transition was assigned to monomeric CO in Ar while the 2142 and 2138 cm^{-1} transitions were assigned to polymeric CO. It is also of interest to this study that when CO is codeposited with HCl in an argon matrix a new band appears at 2155 cm^{-1} with a shoulder at 2157 cm^{-1} in addition to the usual CO transitions.[16]

B. Nickel Halides. 1. NiF_2. The spectrum of pure NiF_2 is shown in Figure 1a. No absorptions other than those between 765 and 780 cm^{-1} are observed. These are readily assigned to ν_3 of NiF_2 with the individual absorptions due to the various nickel isotopes (see Table I). This spectrum is in complete agreement with those previously published[2,4] and confirms the assignment by Margrave, *et al.*,[4] of a 152° bond angle for NiF_2.

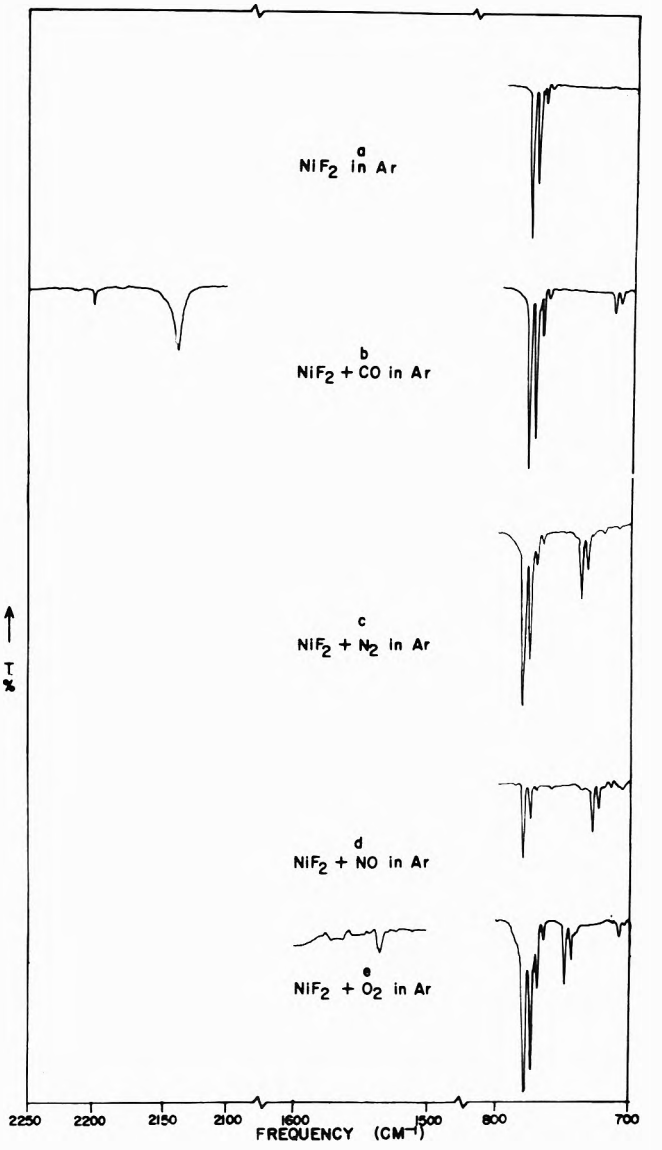

Figure 1. Infrared absorption spectra of NiF_2 in (a) Ar, (b) Ar–CO, (c) Ar–N_2, (d) Ar–NO, and (e) Ar–O_2 matrices.

2. NiF_2CO. Figure 1b shows the spectrum of NiF_2 in an Ar–CO matrix. New absorptions appear at 713 and 2200 cm^{-1} together with the usual CO absorptions. (With high concentrations of CO an additional matrix site for these transitions is present at 2195 and 694 cm^{-1}; see Table I.) Figure 1b clearly shows the strong similarity between the 713- and 780-cm^{-1} absorptions and allows the 713-cm^{-1} absorption to be assigned to the F–Ni–F asymmetric stretch of an NiF_2CO complex. Table I shows the fit obtained for the 713-cm^{-1} transition using the isotope relation for the asymmetric stretch of free NiF_2 with a 150° bond angle. The 2179-cm^{-1} absorption is assigned to an $(NiF_2)_2CO$ complex (*vide infra*).

3. NiF_2N_2. The spectrum of NiF_2 isolated in Ar–N_2 matrices is shown in Figure 1c. A 736.2-cm^{-1} absorption now grows in strongly which from its isotopic structure is assigned to an F–Ni–F asymmetric stretch of an NiF_2N_2 complex. A careful search in the 1900–2600-cm^{-1} region revealed no evidence of an N–N stretch.

NiF_2 was also deposited in a pure nitrogen matrix in an attempt to observe the N–N stretch. A new very weak absorption was observed at 2327 cm^{-1} which was not ob-

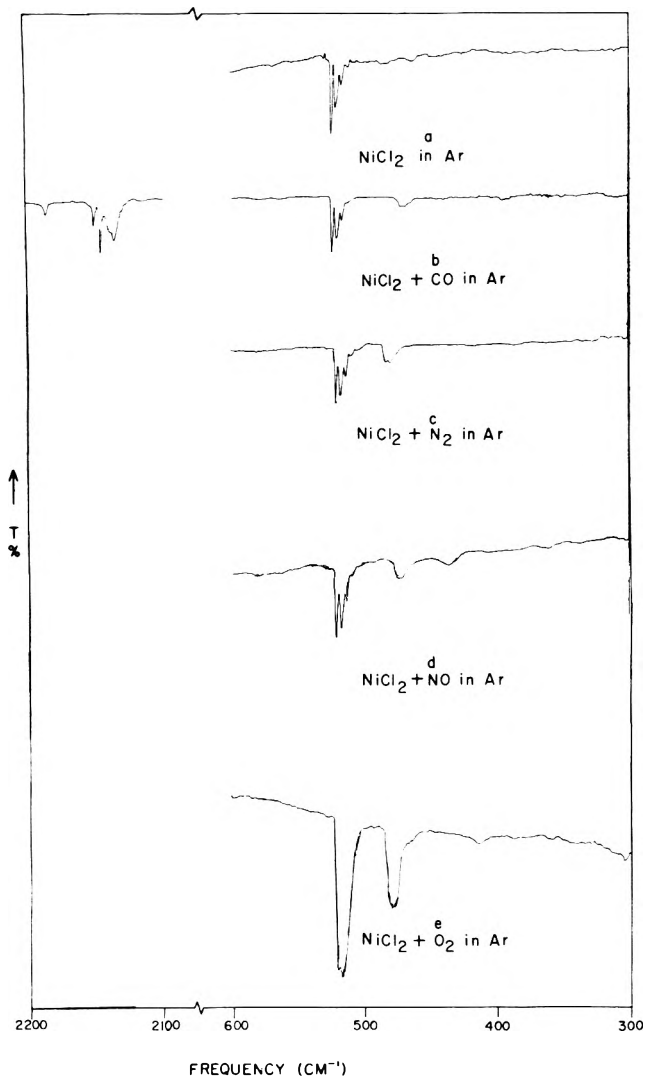

Figure 2. Infrared absorption spectra of $NiCl_2$ in (a) Ar, (b) Ar–CO, (c) Ar–N_2, (d) Ar–NO and (e) Ar–O_2 matrices.

served in the Ar–N_2 matrix. However, this same weak transition is observed for $NiCl_2$ in N_2 which casts some doubt upon the N–N stretch assignment. Impurities, particularly a new site for CO_2 in nitrogen, may also be responsible.

ν_3 for NiF_2 in nitrogen is at 706 cm^{-1}. The stretching force constant, $f_r - f_r'$, for NiF_2 in N_2 and Ar is 3.46 and 4.22 mdyn/Å, respectively, indicating that N_2 is a strongly interacting matrix.

4. NiF_2NO. Figure 1d shows the spectrum of NiF_2 in an Ar–NO matrix. A new absorption observed at 727.7 cm^{-1} and recorded in Table I may clearly be assigned to the asymmetric F–Ni–F stretch of a nickel fluoride–nitric oxide complex which will be written as $NiF_2(NO)_x$. It is not possible to characterize this complex more carefully since a number of transitions were observed in the N–O stretching region which could be assigned to monomeric and dimeric NO (both *cis* and *trans*), as well as N_2O.[17,18] The N_2O was apparently an impurity in the NO. In addition a whole series of transitions which were in all cases considerably weaker than those assigned to *cis* or *trans* $(NO)_2$ or NO appeared between 1800 and 1850 cm^{-1} even in the absence of NiF_2. These are apparently higher polymers of NO arising from the relatively high concentration

TABLE I: Observed and Calculated Infrared Frequencies for NiF_2 and NiF_2 Small Molecule Complexes

	NiF_2		NiF_2CO			NiF_2N_2		NiF_2NO		NiF_2O_2	
	Obsd	Calcd	Obsd		Calcd	Obsd	Calcd	Obsd	Calcd	Obsd	Calcd
$^{58}NiF_2$	779.3	(779.3)	713.6 [694.6]		(713.6 [694.6])	736.2 [719.1]	(736.2 [719.1])	727.7 [705.1]	(727.7 [705.1])	748.6 [708.2]	(748.6 [708.2])
$^{60}NiF_2$	774.2	774.3	708.9 [690.6]		709.0 [690.2]	731.3 [714.2]	731.4 [714.5]	723.4 [701.1]	723.0 [700.6]	743.7 [703.6]	743.8 [703.6]
$^{61}NiF_2$	771.9	771.9	.....		706.9	.....	729.2	721.4 (sh)	720.9	741.6	741.6
$^{62}NiF_2$	769.5	769.6	704.4		704.7	727.3	727.0	718.6	718.7	739.1 [699.6]	739.3 [699.6]
$^{64}NiF_2$	765.1	765.3	700.4		700.6	.....	723.0	.....	714.6	.....	735.1
^{12}CO			2200.4 [2195.5]		(2200.4 [2195.5])						
^{13}CO			2151.1 [2146.6]		2151.4 [2146.6]						
$^{16}O_2$										1534.5	(1534.5)
$^{18}O_2$										1448.2	1446.7

TABLE II: Observed and Calculated Frequencies for $NiCl_2$ and $NiCl_2$ Small Molecule Complexes

	$NiCl_2$		$NiCl_2CO$		$NiCl_2N_2$		$NiCl_2NO$		$NiCl_2O_2$	
	Obsd	Calcd	Obsd	Calcd	Obsd	Calcd	Obsd	Calcd	Obsd	Calcd
$^{58}Ni^{35}Cl_2$	520.7	(520.7)	468.6	(468.6)	483.1	(483.1)	474.9	(474.9)	[a]	
$^{58}Ni^{35}Cl^{37}Cl$	517.5	517.5	465.4	465.7	480.0	480.2	472.2	471.8		
$^{60}Ni^{35}Cl_2$	516.1	516.0	...	464.3	478.7	478.6	471.1	470.7		
$^{58}Ni^{37}Cl_2$	513.9	514.2	...	462.8	476.9	477.1	468.4	468.8		
$^{60}Ni^{35}Cl^{37}Cl$	512.7	512.6	461.8	461.5	475.7	475.8	466.8	467.6		
$^{62}Ni^{35}Cl_2$	511.4	511.4	...	460.2	...	474.4	466.8	466.6		
$^{60}Ni^{37}Cl_2$	509.4	509.4	458.4	458.4	472.9	472.7	464.0	464.5		
$^{62}Ni^{35}Cl^{37}Cl$	508.2	508.1	...	457.2	472.0	471.6	462.6	463.4		
$^{64}Ni^{35}Cl_2$	507.3	507.1	...	456.4	...	470.5	...	462.6		
$^{64}Ni^{35}Cl^{37}Cl$	504.1	504.0	...	453.4	...	467.5	...	459.6		
^{12}CO			2189.2	(2189.2)						
^{13}CO			2140.2	2140.5						

[a] Broad absorption centered at 480.2 cm^{-1}.

TABLE III: Observed and Calculated Frequencies for ν_{12} of the Dimer $(NiF_2)_2$ and $(CrF_2)_2$

Species	% Natural abundances	Obsd energy, cm^{-1}	Calcd energy, cm^{-1}
$(^{58}NiF_2)_2$	46.1	670.8	(670.8)
$^{58}Ni^{60}NiF_4$	35.6	669.1	669.3
$(^{60}NiF_2)_2$	6.9		667.9
		667.6	
$^{58}Ni^{62}NiF_4$	5.0		668.1
$^{58}Ni^{64}NiF_4$	1.5		666.9
		666.9	
$^{60}Ni^{62}NiF_4$	1.9		666.6
$^{50}Cr^{52}CrF_4$	7.4	631.8	631.7
$(^{52}CrF_2)_2$	69.6	630.1	(630.1)
$^{52}Cr^{53}CrF_4$	16.0	629.3 (sh)	629.3

(1/50) of NO needed for complex formation. Therefore, no new N–O stretch was observed which could be assigned to an $NiF_2(NO)_x$ complex; however, this is not surprising since it may well have been hidden under the existing $(NO)_x$ transitions.

5. NiF_2O_2. The spectrum of NiF_2 isolated in an Ar–O_2 matrix is shown in Figure 1e and is recorded in Table I. The additional stretching frequency observed beginning at 748.6 cm^{-1} is assigned to the F–Ni–F asymmetric stretch of an NiF_2O_2 complex. A very weak transition at 1534.5 cm^{-1} grew in with the transition at 748.6 cm^{-1}. Deposition of NiF_2 with Ar–$^{18}O_2$ led to a weak transition at 1448.2 cm^{-1} (calculated 1446.7) leading to its assignment as an O–O stretch of the NiF_2O_2 complex.

6. $NiCl_2$. Figure 2a shows the spectrum of pure $NiCl_2$ in an Ar matrix. The spectrum is identical with that previously reported for $NiCl_2$[2,3,6] except that the 483- and 468-cm^{-1} absorptions are now absent. Heavier deposits of $NiCl_2$ show an additional broad transition at 440 cm^{-1} which has previously been assigned to dimeric $NiCl_2$.[2,3] Bond angle calculations for the monomer from the observed isotopic shifts indicate that a 180° model fits the observed frequencies very well, which is in good accord with molecular beam experiments of Büchler, Stauffer, and Klemperer[19] and electron diffraction experiments of Hedberg and Eddy.[20]

7. $NiCl_2CO$. Addition of $NiCl_2$ to an Ar–CO matrix gives the spectrum shown in Figure 2b. A new transition is observed at 468 cm^{-1} which from its isotopic structure may clearly be assigned to a Cl–Ni–Cl asymmetric stretch of an $NiCl_2CO$ species. Formation of such a species is clearly indicated by the ^{12}CO frequency observed at 2189 cm^{-1} which shifts to 2141 cm^{-1} on addition of ^{13}CO. Occasionally another ^{12}CO frequency is observed at 2153 cm^{-1} in addition to the usual ^{12}CO absorptions at 2148, 2142, and 2138 cm^{-1}. The 2153-cm^{-1} absorption occurs only when some HCl is present due to hydrolysis of $NiCl_2$.

TABLE IV: Observed and Calculated Isotopic Frequencies for ν_3 of CaF_2, CrF_2, MnF_2, CuF_2, and ZnF_2 in Ar and CO–Ar Mixtures and ^{12}CO and ^{13}CO Frequencies

		MF_2		MF_2CO	
		Obsd	Calcd	Obsd	Calcd
A.	$^{40}CaF_2$	557.8		552.2	
				547.6	
	^{12}CO			2178.0	
B.	$^{50}CrF_2$	659.8	659.8	...	643.2
	$^{52}CrF_2$	654.4	(654.4)	637.8	(637.8)
	$^{53}CrF_2$	652.7 sh	652.6	...	635.2
	$^{54}CrF_2$	649.5	649.1	...	632.6
	^{12}CO			2188.4	
	^{13}CO			2139.1	2139.8
	^{12}CO			2186.6	
	^{13}CO			2137.7	2138.1
	^{12}CO			2184.9	
	^{13}CO			2136.0	2136.4
	^{12}CO			2183.7	
	^{13}CO			2133.7	2133.3
	^{12}CO			2181.7	
	^{13}CO			...	2131.0
	^{12}CO			2167.8[a]	
	^{13}CO			2118.0[a]	2119.7
	^{12}CO			2165.2[a]	
	^{13}CO			2114.0	2117.1
C.	$^{55}MnF_2$	699.4		675.9	
	^{12}CO			2183.2	
	^{12}CO			2181.0	
D.	$^{63}CuF_2$	743.5	(743.5)	704.2	(704.2)
	$^{65}CuF_2$	739.6	739.3	700.2	700.2
	$^{63}CuF_2$	[736.5]	[(736.5)]		
	$^{65}CuF_2$	[732.6]	[732.3]		
	^{12}CO			2210.4	
	^{13}CO			2160.9	2161.3
E.	$^{64}ZnF_2$	762.5	(762.5)	728.1	(728.1)
	$^{66}ZnF_2$	758.0	758.3	724.1	724.1
	$^{67}ZnF_2$	756.2	756.2	...	722.1
	$^{68}ZnF_2$	754.4	754.2	720.4	720.2
	$^{70}ZnF_2$	750.2	750.4	...	716.5
	^{12}CO			2185.9	
	^{13}CO			...[b]	2137.4
	^{12}CO			2183.8	
	^{13}CO			...[b]	2135.5

[a] CO frequencies perturbed by $(CrF_2)_2$. [b] ^{13}CO perturbed hidden by ^{12}CO.

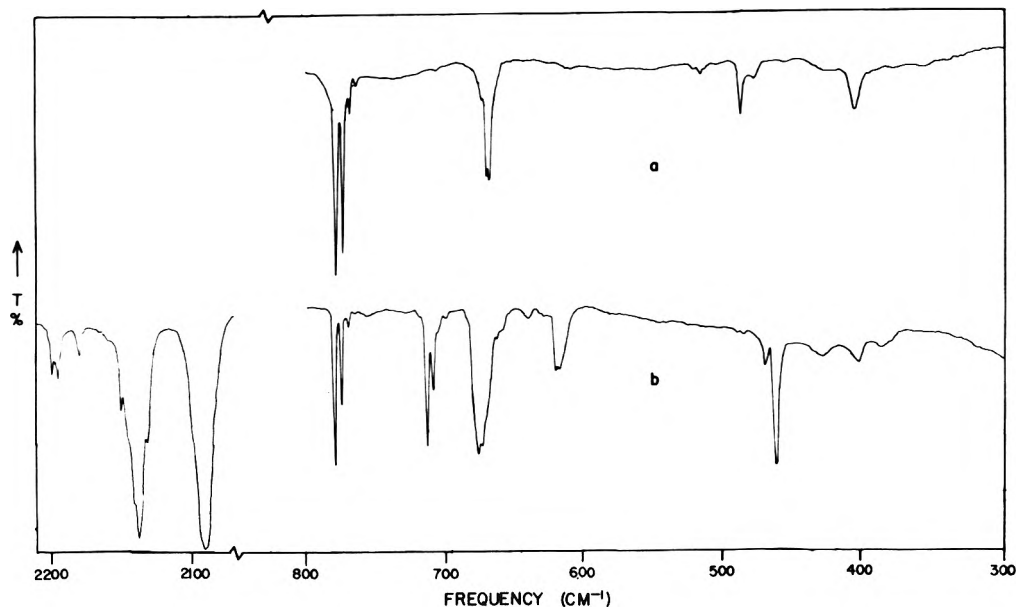

Figure 3. Infrared absorption spectra of NiF_2 and $(NiF_2)_2$ in (a) Ar and (b) $Ar-{}^{12}CO-{}^{13}CO$ matrices.

TABLE V: Observed and Calculated Frequencies for ν_3 of CrF_3 Assuming D_{3h} Symmetry

Species	% Natural abundance	Obsd	Calcd
$^{50}CrF_3$	4.4	754.7	754.6
$^{52}CrF_3$	83.5	749.3	(749.3)
$^{53}CrF_3$	9.6	746.9	746.8
$^{54}CrF_3$	2.6	744.4	744.4

This transition is due to CO perturbed by HCl as shown by Barnes, *et al.*[16]

8. $NiCl_2N_2$. Figure 2c shows the spectrum of $NiCl_2$ in an $Ar-N_2$ matrix. The absorption at 483 cm^{-1} is assigned to the Cl-Ni-Cl asymmetric stretch of an $NiCl_2N_2$ complex. No transitions are observed which may definitely be assigned to an N-N or a Ni-N stretch.

When $NiCl_2$ is deposited in a N_2 matrix it is found that the Cl-Ni-Cl absorption shifts to 428 cm^{-1}. The very large shift in the force constant, $f_r - f_r'$, for $NiCl_2$ in N_2 and Ar, 1.78 and 2.63 mdyn/Å, shows that nitrogen interacts strongly with $NiCl_2$. A very weak transition at 2327 cm^{-1} was observed for $NiCl_2$ in N_2 which may be an N-N stretch (see (see NiF_2N_2).

9. $NiCl_2NO$. The spectrum of $NiCl_2$ in an Ar-NO matrix is shown in Figure 2d. A new absorption is observed at 475 cm^{-1} which is assigned to a Cl-Ni-Cl asymmetric stretch of a $NiCl_2(NO)_x$ species from the isotopic structure. Because of the complexity of the NO stretching region no N-O stretches belonging to this species could be definitely assigned.

10. $NiCl_2O_2$. The spectrum of $NiCl_2$ in an $Ar-O_2$ matrix is shown in Figure 2e. A new absorption grows in at 480 cm^{-1} which may be assigned to the Cl-Ni-Cl asymmetric stretch of $NiCl_2O_2$. No definite O-O or Ni-O stretches were seen.

11. $(NiF_2)_2$. The infrared spectrum of monomer and dimer in the region 800-300 cm^{-1} is shown in Figure 3a. Dimer transitions are located at 671, 486, and 405 cm^{-1} and grow in when the matrix is warmed or when concentrated deposits are made.

The proposed dimer for MX_2 species has invariably been the halogen bridged form, that is a four-membered planar diamond-shaped ring and two additional halogen atoms located on the M-M axis outside the ring.[21] The symmetry of the structure is D_{2h} for which there are twelve normal vibrational frequencies. Of these, six are infrared active—$2B_{1u}(\nu_7, \nu_8)$, $2B_{3u}(\nu_9, \nu_{10})$, and $2B_{3u}(\nu_{11}, \nu_{12})$. Following McNamee,[22] the ν_7 and ν_8 modes may be described as out-of-plane ring-bending motions; ν_{10}, as an outer-bond bending in the plane; ν_9 and ν_{11}, as bridge-bond stretching; and ν_{12}, as an outer-bond stretching. The stretching motions are expected to have higher energies than the bending motions, with the terminal stretch, ν_{12}, having the highest energy and therefore assigned to the 671-cm^{-1} transition.

Excellent support for this assignment and structure comes from the agreement between the observed and calculated nickel isotopic frequencies of the 671-cm^{-1} transition. The G matrix elements for both B_{3u} modes (ν_{11} and ν_{12}) are $\mu_{Ni} + \mu_F$. The product rule requires[23]

$$\frac{\nu_{11} \cdot \nu_{12}}{\nu'_{11} \cdot \nu'_{12}} = \frac{\mu_{Ni} + \mu_F}{\mu'_{Ni} + \mu'_F}$$

However, because no isotopic splitting could be resolved for either the 486- or 404-cm^{-1} transitions,[24] the product rule was ignored and the isotopic frequency shifts were calculated from

$$\frac{\nu_{12}}{\nu'_{12}} = \sqrt{\frac{\mu_{Ni} + \mu_F}{\mu'_{Ni} + \mu'_F}}$$

This approximation is equivalent to assuming that the terminal stretch is independent of the bridge stretch. Good agreement is obtained as shown in Table III.

The 486- and 405-cm^{-1} transitions are assigned to the bridge stretches, ν_9 and ν_{11}. It is not possible from present information to make an unambiguous assignment of these two stretches. The bond bending modes are expected to lie below 200 cm^{-1}, the limit of the instrument.

Additional evidence for this model comes from a simplified normal coordinate analysis patterned after that by Büchler[25] and McNamee.[22] They assumed that the bridge bonds form a square structure and that the potential energy is completely specified by the force constant f_r for the terminal stretch, the constant f_d for the bridge-bond

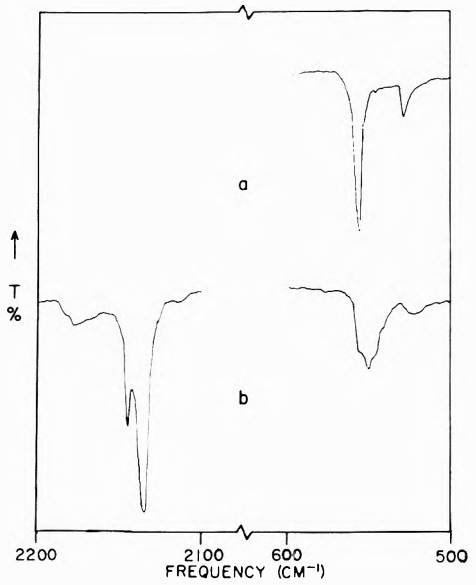

Figure 4. Infrared absorption spectra of CaF_2 in (a) Ar and (b) Ar–CO matrices.

stretch, and the constant f_α/r^2 for the terminal bend. These assumptions give simple expressions for the B_{3u} and B_{2u} representations.

The additional assumptions they made are that f_r is equal to the force constant derived from ν_3 of the monomer and that $f_d = \frac{1}{2}f_r$ and $f_\alpha/r^2 = \frac{1}{10}f_r$. These assumptions give the following values : ν_{12}, 717 cm^{-1}; ν_{11}, 463 cm^{-1}; ν_9, 454 cm^{-1}. The observed values are 671, 486, and 405 cm^{-1}.

12. $(NiF_2)_2CO$. Depositions were usually carried out with a low concentration of NiF_2 to prevent dimer formation, and a reasonably high, 1/50, concentration of the XY molecule. In a few instances involving CO both $(NiF_2)_2$ and the CO concentrations were reasonably high and frequencies attributable to dimer complexes were observed.

Closely spaced absorptions at 2180 cm^{-1} are present when ^{12}CO is deposited with dimeric NiF_2. This transition grows in when a matrix containing NiF_2, CO, and NiF_2CO is warmed allowing diffusion to occur. These results are shown in Figure 3b. Lower frequencies which grow in with 2180 cm^{-1} are located at 680, 622, 470.4, 440, and 404 cm^{-1}. The 470.4-cm^{-1} frequency is carbon dependent because substitution of ^{13}CO shifts the absorption to 463.5 cm^{-1}. The nature of this transition is unclear. It does not appear to be an Ni–C stretch because no Ni isotopic structure is observed and frequencies this high are not expected for these relatively weak interactions.

C. CaF_2. 1. CaF_2 in Ar. The spectrum of CaF_2 above 500 cm^{-1} is shown in Figure 4a and recorded in Table IV. Transitions grow in at 557.8 and 529.2 cm^{-1} which following earlier workers[8,9] are assigned to ν_3 of CaF_2 and dimeric CaF_2, respectively. Additional weak transitions were also observed at 484.8 and 368.1 cm^{-1} and are assigned to ν_1 and dimeric CaF_2, respectively, following the previous workers.

2. CaF_2CO. Figure 4b shows the spectrum of CaF_2 in an Ar–CO matrix. The new transitions observed here are recorded in Table IV. When Ar is doped with CO the 557.8 cm^{-1} transition broadens and shoulders grow in at 552.2 and 547.6 cm^{-1}. A new broad CO transition at 2178 cm^{-1} grows in at the same rate as the 552.2- and 547.6-cm^{-1} shoulders. No changes were observed for the ν_1 mode or the polymer modes.

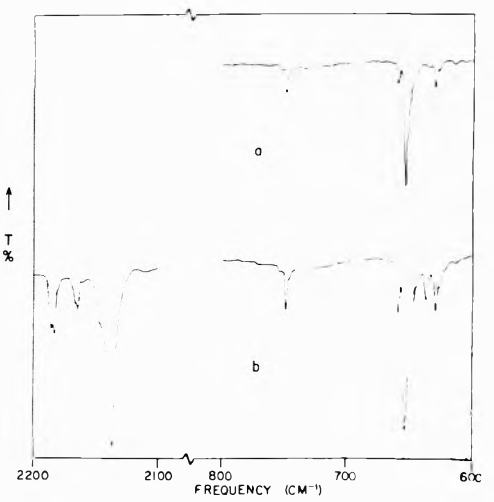

Figure 5. Infrared absorption spectra of CrF_2 in (a) Ar and (b) Ar–CO matrices.

D. 1. CrF_2 in Ar. The spectrum of CrF_2 in argon above 600 cm^{-1} is shown in Figure 5a and the ν_3 region is recorded in Table IV. The isotopic structure of the intense transition at 654 cm^{-1} is assigned to ν_3 for CrF_2 with 180° bond angle. The isotopic structure of the weaker transition at 750 cm^{-1} is consistent with assignment ν_3 of CrF_3 assuming 120° bond angle and is recorded in Table V. Apparently the CrF_2 was slightly contaminated with CrF_3. These assignments for both ν_3 of CrF_2 and of CrF_3 are the same as those made earlier by Linevsky.[10] In addition, weak transitions grow in together at 630, 472, and 395 cm^{-1} which by the isotopic structure on the 630 cm^{-1} transition may be assigned to CrF_2 dimer. (See Table III.)

2. CrF_2CO. Figure 5b shows the spectrum of CrF_2 in an Ar–CO matrix. The new transitions observed here are recorded in Table IV. Transitions in the 2180 and 2190 region grow in with a new transition at 637.8 cm^{-1}. The 637.8-cm^{-1} transition is assigned to ν_3 of CrF_2 perturbed by CO. Isotopic proof of this assignment is lacking due to the small abundance of ^{50}Cr, ^{53}Cr, and ^{54}Cr and overlap of the weak dimer transition at 630 cm^{-1}.

A weak series of transitions also appear between 2160 and 2170 cm^{-1} which have ^{13}CO counterparts between 2110 and 2120 cm^{-1} with no intermediate transitions. These are assigned to CO perturbed by CrF_2 dimer by analogy with $(NiF_2)_2$ CO transitions.

E. 1. MnF_2 in Ar. Figure 6a shows the spectrum of MnF_2 in the stretching region in argon and the results are recorded in Table IV. The intense transition at 699.4 cm^{-1} is assigned to ν_3 in agreement with Hastie, *et al.*[26] In addition, with heavier deposits weak transitions are observed at 615, 602, 433, 426, and 376 cm^{-1} which are assigned to MnF_2 dimer and polymer species.

2. MnF_2CO. Figure 6b shows the spectrum of MnF_2 in an Ar–CO matrix. The new transitions which appear here are recorded in Table IV. Two transitions at 2183.2 and 675.9 cm^{-1} grow in simultaneously and the 675.9-cm^{-1} transition is assigned to ν_3 of MnF_2 perturbed by CO. The transition observed at 2159 cm^{-1} is CO perturbed by HF (*vide infra*).

F. 1. CuF_2 in Ar. The spectrum of CuF_2 in the stretching region is shown in Figure 7a and is recorded in Table IV. The doublet observed at 743.5 and 739.6 cm^{-1} is assigned to ν_3 of $^{63}CuF_2$ and $^{65}CuF_2$, respectively, in agree-

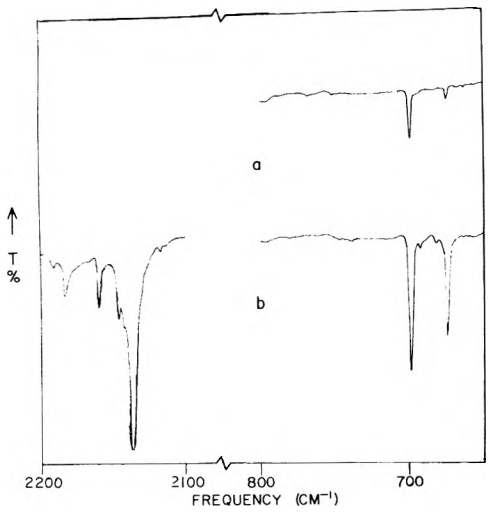

Figure 6. Infrared absorption spectra of MnF_2 in (a) Ar and (b) Ar–CO matrices.

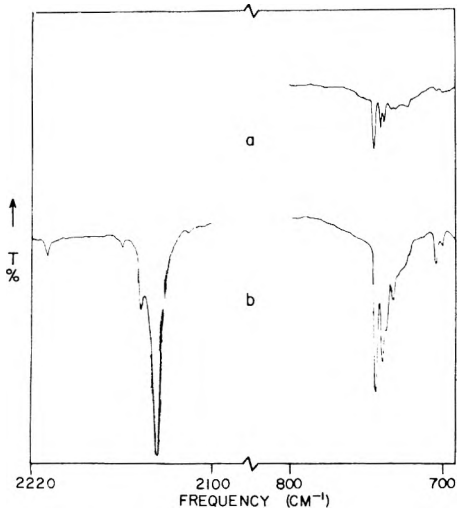

Figure 7. Infrared absorption spectra of CuF_2 in (a) Ar and (b) Ar–CO matrices.

ment with earlier workers.[4] A weaker doublet with the same isotopic structure at 736.5 and 732.6 cm^{-1} is assigned to ν_3 of CuF_2 in a different matrix site.

In addition, weaker transitions were observed at 660, 487, and 395 cm^{-1} and are assigned to CuF_2 dimer by analogy with the other difluorides studied here.

2. *CuF_2CO.* Figure 7b shows the spectrum of CuF_2 in an Ar–CO matrix. The new transitions observed here are recorded in Table IV. A new doublet grows in at 704.2 and 700.2 cm^{-1} together with a CO transition at 2210.4 cm^{-1}. The isotopic structure of the doublet is consistent with its assignment as ν_3 for CuF_2 perturbed by CO. The weak transition at 2159 cm^{-1} is again CO perturbed by HF.

G. 1. ZnF_2 in Ar. Figure 8a shows the spectrum of ZnF_2 in the stretching region in Ar and the results are recorded in Table IV. A series of transitions are observed beginning at 762.5 which in accordance with earlier workers[4,7] may be assigned to ν_3 of ZnF_2 with 165° bond angle. In addition, previously assigned dimer modes were also observed at 661, 458, and 400 cm^{-1}.

2. *ZnF_2CO.* Figure 8b shows the spectrum of ZnF_2 in an Ar–CO matrix and the new transition at 2185.9 cm^{-1} grows in together with a new series of transitions beginning at 728.1 cm^{-1}. The isotopic structure of the latter

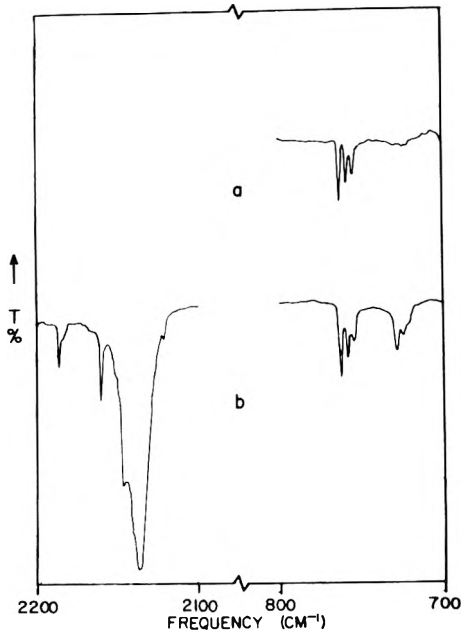

Figure 8. Infrared absorption spectra of ZnF_2 in (a) Ar and (b) Ar–CO matrices.

transitions is consistent with ν_3 of ZnF_2 perturbed by CO. The 2159-cm^{-1} transition is due to CO perturbed by HF.

H. ^{13}CO Experiments. For CrF_2, NiF_2, $NiCl_2$, CuF_2, and ZnF_2 experiments using isotopically enriched ^{13}CO were done. In all cases both for 90:10 and 50:50, $^{13}CO/^{12}CO$ enrichment only the pure ^{12}CO or ^{13}CO frequencies were observed. No mixed frequencies were ever observed proving the absence of species of the type $MX_2(CO)_x$ where x is 2 or greater.

I. HF and HF Perturbed Transitions. The most common impurity observed in these experiments was HF. It was often observed in the spectra of MnF_2, NiF_2, CuF_2, and ZnF_2 and apparently resulted from the hydrolysis of the MF_2 compounds by traces of water present in the samples. In addition to the usual HF transitions in the 3800–4000 cm^{-1} region, transitions were observed at 681, 560, and 445 cm^{-1} apparently caused by HF because these transitions were also observed when only HF was deposited in the matrix. HF also complicated the CO spectrum giving rise to a transition at 2159 cm^{-1} which is observed for MnF_2, CuF_2, and ZnF_2. This transition is present only when both CO and HF are present and is assigned to CO perturbed by HF in argon. This is close to 2155 and 2157 cm^{-1} which have been observed for CO perturbed by HCl.[16]

Discussion

All the perturbed CO frequencies observed in this study are above those of free CO. There are a number of studies in the literature in which this effect is observed.[27] In general these are systems in which CO is physically adsorbed on solids, particularly metal oxides. Of direct interest to the present work is a study by Angell and Schaffer[28] on CO adsorbed to zeolites in which the unipositive cation was replaced by dipositive cations. They report CO stretches up to 2217 and 2214 cm^{-1} for Ni^{2+} and Zn^{2+} cation exchanged zeolites, respectively. Most significantly, they were able to correlate the frequency of these CO absorptions with the strength of the electric field near the cation. Thus they showed unambiguously that the high-

frequency absorption was due to CO adsorbed to the metal ion.

The present study also indicates that the CO is definitely attached to the metal ion. This conclusion may be drawn because the isotopic structure of the CO perturbed ν_3 stretch is of exactly the same form as for free MX_2. If the CO coordinated to the halogen, the two M-X bonds would be nonequivalent and two MX frequencies would be observed. Also the coupling between the two MX bonds would be destroyed and the isotopic structure of these species would be different than that expected for uncoordinated MX_2 or MX_2 coordinated to CO through the metal.

In order to understand the CO perturbed frequencies it is necessary to establish the nature of the MX_2 molecules. CuF_2 has been shown to be ionic by Kasai, *et al.*,[29] from an esr study of CuF_2 in argon. This conclusion is based on the fact that there was very little coupling between the unpaired electron on the copper and the magnetic moment on the ^{19}F nucleus. It is assumed that the other metal dihalides used here are also ionic.

Turning now to the model used by Angell and Schaffer,[28] we have correlated the perturbed CO frequency with the electric field of the cation at the carbon nucleus and this correlation is shown in Figure 9. It is assumed here that the CO is attached to the metal ion through the carbon nucleus, the negative end of the dipole. The electric field strength at the carbon nucleus was calculated from the equation

$$|\epsilon| = \frac{|F|}{q_2} = \frac{q_1}{4\pi\epsilon_0(r_M + r_c)^2}$$

where ϵ is the electric field strength at the carbon nucleus, q_1 is the charge on the cation, assumed to be +2 in all cases, r_M is the Pauling ionic radius of the cation, r_c = 1.5 Å was chosen to be the van der Waals radius of carbon on CO, and ϵ_0 is the permittivity of the medium assumed to be that of a vacuum. F is the coulombic force of attraction between the ion and the dipole and q_2 is the charge on the carbon.

The correlation shown in Figure 9 shows that a straight line may be drawn through the points for CaF_2, MnF_2, and ZnF_2 and that the intercept occurs at 2148 cm^{-1}, the frequency of free monomeric CO in argon. These results may be easily understood from the fact that electron density is being removed from the 5σ orbital of CO by the positive metal ion. Huo,[30] from *ab initio* calculations, has shown that the 5σ orbital of CO is weakly antibonding and located principally on the carbon atom. This removal leads to an increase in bond strength and the observed frequency increase. This effect is also observed from the stretching frequency of CO^+.[31] Removal of a 5σ electron from the CO molecule raises the stretching frequency (from 2143 cm^{-1} for CO(g) to 2184 cm^{-1} in CO^+ (g)).

Figure 9 exhibits a double-humped curve strongly suggestive of ligand field effects. It is just those ions, Cr^{2+}, Ni^{2+}, and Cu^{2+}, which have anisotropic d electron configurations which do not lie on the line. Furthermore, it may be observed that the CO frequencies for NiF_2 and CuF_2 deviate farther from the correlation than CrF_2. A simple crystal field model for the M^{2+} ion in MF_2 compounds places the energy levels in the order $\delta g < \pi g < \sigma g^+$ for a linear MF_2 compound.[29] Qualitatively then, it is expected that the σg^+ is the least filled orbital and it has the correct symmetry to overlap with the $5\sigma g$ orbital of CO. Therefore it is just these ions, Cr^{2+}, Ni^{2+} and Cu^{2+},

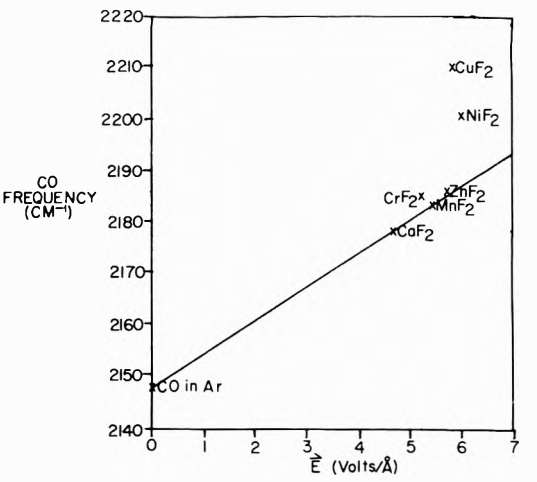

Figure 9. Stretching frequency of CO *vs.* electric field at carbon nucleus due to various fourth-period dipositive metal ions.

which would appear to the CO to have a higher positive charge than those with an isotopic distribution of electrons leading to the observed extra frequency increase. In addition, Cu^{2+} and Ni^{2+} are expected to have a greater effect than Cr^{2+} because as the nuclear charge increases the 3d orbitals become more stable across the series. Calculations show that the 5σ of CO is below the 3d orbitals of the transitions metal ions.[32] Therefore as the 3d level drops across the series a greater interaction is expected between the 5σ of CO and the σg of the transition metal ion yielding the observed results.

The model also accounts for the frequency difference of CO adsorbed to NiF_2 *vs.* $NiCl_2$ (2200 *vs.* 2189 cm^{-1}). $NiCl_2$ is expected to be more covalent than NiF_2 leading to a smaller electric field strength for Ni^{2+} in $NiCl_2$ than NiF_2 and a consequent decrease in CO frequency.

Our results are also consistent with recent semiempirical calculations of Politzer and Kasten[33] on the interaction of CO with Ni^0, Ni^+, Ni^{2+}, and Ni^{3+}. Their findings for CO adsorbed to Ni^{n+} species show that the CO is bound to metal or metal ion through the carbon and that the CO bond strength increases as n increases due to a greater σ charge transfer as n increases. Their calculations also show π back bonding but this is relatively small for Ni^{2+} and Ni^{3+} species and their results clearly show that the σ donation contributes to the observed CO frequency increase.

Little can be said about the CO perturbed by the dimer species in $(NiF_2)_2$ and $(CrF_2)_2$ other than to note that the lower CO frequency compared to the monomer species is probably due to the lower metal ion charge in the dimers.

We now turn to the results of NiX_2 with N_2, O_2, and NO. No perturbed N-N or N-O stretch was observed for either of these molecules with NiX_2. A weak O-O stretch was observed for NiF_2 at 1535 cm^{-1}. Hatzenbuhler and Andrews[34] report the stretching frequency of O_2 in Ar as 1551 cm^{-1} by Raman spectroscopy and of O_2^- as 1074 cm^{-1} as in LiO_2. Herzberg[31] reports the stretching frequency of O_2^+(g) at 1835 cm^{-1}. Therefore the O_2 frequency observed here is essentially like molecular oxygen. Because O_2 is more electronegative than CO it is not unreasonable to assume it to be a poorer σ donor and better π acceptor than CO. These two effects combined could lead to the observed result.

All that may be definitely said for NO is that the perturbed frequency is not in the NO^+ region, that is above

1900 cm^{-1}, because this region was clear in our spectra. Because NO is a better π acceptor than CO the σ donation from the nitrogen may be offset by the back π bonding to the NO from the metal again resulting in an NO-like frequency. This is consistent with Politzer and Kasten's[33] calculations which show that even Ni^{2+} and Ni^{3+} do back bond to CO and therefore may be expected to do so to an even greater extent with NO.

The lowering of the asymmetric X-Ni-X stretch frequency upon interaction with the small molecule is also consistent with this model. It is well known that the stretching force constant increases with increasing oxidation state of the metal. For both nickel halides the asymmetric stretch decreases in the order $O_2 > N_2 > (NO)_x >$ CO suggesting an order for the electron donor ability of these molecules.

Conclusions

The present work indicates that the matrix isolation technique may be used to study the interaction of small molecules such as CO, N_2, O_2, and NO with ionic compounds. The advantage of the technique is that the ionic species is precisely known in contrast to the infrared studies of adsorbed molecules on various other solid supports in which more than one type of active center may be present. This study also shows that small concentrations of these molecules often lead to unexplained transitions in matrix isolation studies and special care must be taken to exclude such effects. For example, it may be that these types of interactions are responsible for some of the unclassified transitions in the infrared spectra of the matrix isolated mercuric halides.[35]

Acknowledgments. We wish to thank the U. S. Atomic Energy Commission for support of this research and the National Science Foundation for providing funds for the purchase of the Perkin-Elmer 180 infrared spectrophotometer.

References and Notes

(1) (a) Presented in part at the 27th Northwest Regional Meeting of the American Chemical Society, June 15, 1972. (b) Based on the thesis presented by D. A. Van Leirsburg to the Graduate College of Oregon State University, Corvallis, Ore., in partial fulfillment of the requirement for the Ph.D. degree, 1973.
(2) D. E. Milligan, M. E. Jacox, and J. D. McKinley, *J. Chem. Phys.*, **42**, 902 (1965).
(3) K. R. Thompson and K. D. Carlson, *J. Chem. Phys.*, **49**, 4379 (1968).
(4) J. W. Hastie, R. H. Hauge, and J. L. Margrave, *High Temp. Sci.*, **1**, 76 (1969).
(5) M. E. Jacox and D. E. Milligan, *J. Chem. Phys.*, **51**, 4143 (1969).
(6) J. W. Hastie, R. H. Hauge, and J. L. Margrave, *High Temp. Sci.*, **3**, 257 (1971).
(7) A. Loewenschuss, A. Ron, and O. Schnepp, *J. Chem. Phys.*, **49**, 272 (1968).
(8) V. Calder, D. E. Mann, K. S. Seshadri, M. Allavena, and D. White, *J. Chem. Phys.*, **51**, 2093 (1969).
(9) A. Snelson, *J. Phys. Chem.*, **70**, 3208 (1966).
(10) M. J. Linevsky, U. S. Government Research and Development Report AD-670-626 (1968).
(11) C. W. DeKock and D. A. Van Leirsburg, *J. Amer. Chem. Soc.*, **94**, 3235 (1972).
(12) R. D. Wesley and C. W. DeKock, *J. Chem. Phys.*, **55**, 3866 (1971).
(13) G. E. Leroi, G. E. Ewing, and G. C. Pimentel, *J. Chem. Phys.*, **40**, 2298 (1964).
(14) J. B. Davies and H. E. Hallam, *J. Chem. Soc., Faraday Trans. II*, 509 (1972).
(15) A. G. Maki, *J. Chem. Phys.*, **35**, 931 (1961).
(16) A. J. Barnes, H. E. Hallam, and G. F. Scrimshaw, *Trans. Faraday Soc.*, **65**, 3172 (1969).
(17) W. G. Fateley, H. A. Bent, and B. Crawford, Jr., *J. Chem. Phys.*, **31**, 204 (1959).
(18) W. A. Guillory and C. E. Hunter, *J. Chem. Phys.*, **50**, 3516 (1969).
(19) A. Buchler, J. L. Stauffer, and W. E. Klemperer, *J. Chem. Phys.*, **42**, 902 (1964).
(20) K. Hedberg and L. Eddy, private communication.
(21) See, for example, ref 3 and 7 and references therein.
(22) R. W. McNamee, Jr., Ph.D. Dissertation, University of California at Berkeley, 1962; also issued as Univ. of Calif. Radiation Lab. Dept. UCRL-10451. See also ref 3 for agreement of this model with a number of 3d transition metal dichloride dimers.
(23) E. B. Wilson, Jr., J. C. Decius, and P. C. Cross, "Molecular Vibrations," McGraw-Hill Book Co., Inc., New York, N. Y., 1955.
(24) The maximum resolution attainable in the 400-cm^{-1} region was 1 cm^{-1}. The calculated splitting between $(^{58}NiF_2)_2$ and $^{58}Ni^{60}NiF_4$ is 1.2 cm^{-1} for the 486-cm^{-1} transition. This transition is sufficiently broad to encompass all the isotopic structure.
(25) A. Buchler, Ph.D. Dissertation, Harvard University, 1960.
(26) J. W. Hastie, R. Hauge, and J. L. Margrave, *Chem. Commun.*, 1452 (1969).
(27) L. H. Little, "Infrared Spectra of Adsorbed Species," Academic Press, London, 1966, pp 67-74.
(28) C. L. Angell and P. C. Schaffer, *J. Phys. Chem.*, **70**, 1413 (1966).
(29) P. H. Kasai, E. B. Whipple, and W. Weltner, Jr., *J. Chem. Phys.*, **44**, 2581 (1966).
(30) W. M. Huo, *J. Chem. Phys.*, **43**, 624 (1965).
(31) G. Herzberg, "Spectra of Diatomic Molecules," D. Van Nostrand Co., Inc., Princeton, N. J., 1950.
(32) M. B. Hall and R. F. Fenske, *Inorg. Chem.*, **11**, 1619 (1972).
(33) P. Politzer and S. D. Kasten, *Surface Sci.*, **36**, 186 (1973).
(34) D. A. Hatzenbuhler and L. Andrews, *J. Chem. Phys.*, **56**, 3398 (1972).
(35) A. Loewenschuss, A. Ron, and O. Schnepp, *J. Chem. Phys.*, **50**, 2502 (1969).

Liquid Ammonia Solutions. XI. A Raman Study of the Nature of Solutions Containing Alkali and Alkaline Earth Cations

K. R. Plowman and J. J. Lagowski*

Department of Chemistry, The University of Texas at Austin, Austin, Texas 78712 *(Received June 4, 1973)*

The Raman spectra of ammonia solutions of the alkaline earth and some alkali metal salts are discussed in terms of ion–solvent interaction. The fundamental vibrational frequencies of liquid ammonia are perturbed primarily by anion interaction with one exception, the symmetric bending mode (ν_2) which exhibits a strong cation dependence. Low-frequency bands which are assigned to the symmetric stretching mode of the solvated cation are observed for Li^+, Na^+, Mg^{2+}, Ca^{2+}, Sr^{2+}, and Ba^{2+} at 241, 194, 328, 266, 243, and 215 cm^{-1}, respectively. The observed frequencies are discussed on the basis of an electrostatic model for the cation–solvent interaction.

Introduction

The spectroscopic properties of liquid ammonia have been studied extensively using many different spectroscopic methods. In our laboratory, solutions in liquid ammonia of many salts, primarily ammonium and alkali metal salts, have been extensively investigated using near-infrared spectroscopy for the vibrational overtone region and Raman spectroscopy for the fundamental and low-frequency regions of the infrared. In all of these solutions the observed solvent spectra, with the exception of the symmetric bending mode, can be interpreted on the basis of an anion interaction with the solvent without introducing any cation-dependent perturbation.[1,2] This investigation concerns itself with the cation-dependent nature of the solvent spectrum in solutions of salts of the more highly charged alkaline earth cations as well as those of the alkali metal cations.

There is a great deal of interest in the nature of the cationic species in solution. The low-frequency vibrational region where ion–solvent interactions should be observed is discussed in detail. An ionic model for such interactions, which has been investigated extensively in water solutions in regard to interaction energy calculations,[3-5] is used to interpret the low-frequency spectra and to support the assignment of the fundamental vibrations observed in this region.

Experimental Section

The presence of small quantities of water in the salt solutions would greatly complicate the interpretation of the observed spectra. Small amounts of water in liquid NH_3 cause shifts in the frequency positions of the ammonia fundamental vibrations and would prevent an unambiguous assignment of any bands which might be observed in the low-frequency region. For these reasons great care was taken to exclude water from these solutions. The nitrate and perchlorate salts of Ca, Sr, and Ba were prepared *via* a simple acid–base reaction between the metal, dissolved in liquid ammonia, and previously dried ammonium nitrate or perchlorate dissolved in liquid NH_3. Anhydrous magnesium perchlorate and $Mg(NO_3)_2 \cdot 6H_2O$ were recrystallized from liquid NH_3 and the products were subjected to lengthy evacuation; this process was repeated until infrared analysis indicated that water was absent. The alkali metal salts were dissolved in liquid NH_3 with subsequent evaporation of the solvent followed by evacuation; this was repeated twice. All ammonia which was used in the salt and sample preparations had been previously dried and stored over sodium and was dried again immediately before use by condensing onto sodium metal. All glassware was first oven dried and then heated under vacuum.

The solutions were prepared by placing an amount of salt in the solution preparation arm of the sample cell[2] under an inert atmosphere. The cell was subsequently evacuated and ammonia was condensed onto the salt after which the cell was sealed by means of a pressure stopcock. After the cell had warmed to ambient temperature and the salt had dissolved, the solution was passed through a glass frit to the cell in which the spectra were taken. The weights of salt and ammonia involved were determined by difference.

All spectra were recorded at ambient temperature on a Cary Model 82 Raman spectrophotometer using as an exciting line the 5145-Å line of the argon ion laser (Coherent Radiation Laboratories Model 53A). Resolution of the observed spectra was accomplished with the use of RESOL, a non-linear least-squares computer program.[6]

Results and Discussion

This section is divided into four subdivisions, the NH_3 fundamental vibrations, the anion fundamental vibrations, the low-frequency region, and a general discussion applying an ionic model to these systems.

Ammonia Fundamental Vibrations. The 3300-cm^{-1} region of liquid ammonia at 25°, which is shown in Figure 1, consists of a broad envelope which clearly exhibits three band maxima which are assigned as follows: the asymmetric stretch, ν_3, is at 3385 cm^{-1}; the symmetric stretch, ν_1, is at 3300 cm^{-1}; and the first overtone of the asymmetric bend, $2\nu_4$, is at 3215 cm^{-1}.[2,7] Wave number (cm^{-1}) is used to mean δ wave number relative to the exciting line of the laser source. Some authors feel the assignment of ν_1 and $2\nu_4$ should be reversed.[8] The disagreement over the assignment of ν_1 and $2\nu_4$ has been discussed in a previous paper as has the experimental evidence which supports the four band resolution.[2] This very broad band which is centered at 3270 cm^{-1} in the pure liquid is primarily due to the symmetric stretch of an ammonia molecule associated through one of its hydrogen atoms,

TABLE I: Frequencies of the Fundamental Vibrations of Ammonia

Solution	ν_3	ν_1	$\nu_1(C_s)$	ν_4	ν_4	ν_2	Concn[a]
$Ba(ClO_4)_2$	3387	3304	3280	3218	1640	1086	27
$Sr(ClO_4)_2$	3385	3304	3282	3217	1640	1088	24
$Ca(ClO_4)_2$	3384	3303	3283	3217	1640	1094	26.7
$Mg(ClO_4)_2$	3386	3302	3280	3216	1640	1097	Sat. 35
NH_3	3385	3300	3270	3214	1640	1046	

[a] In moles of ammonia per mole of salt.

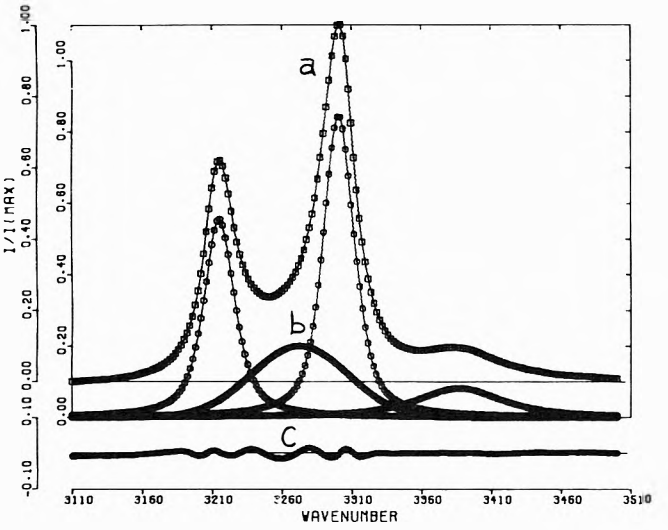

Figure 1. Resolved Raman spectrum of the N–H stretching region of NH_3 at 25°: (a) experimental curve, (b) resolved bonds, (c) error curve.

i.e., an ammonia molecule with C_s symmetry. In salt solutions ammonia molecules interacting through their hydrogen atoms with an anion also contribute intensity to this band.

The resolution of this region was accomplished using RESOL, a non-linear least-squares computer program; the band functions allowed in this program are Gaussian, Lorentzian, or a linear combination of Gaussian and Lorentzian functions.[6] A linear combination of functions gave the best fit in the statistical sense based on the *R*-factor significance tests of Hamilton.[9] The positions of the resolved ammonia fundamentals in solutions of the alkaline-earth salts are shown in Table I; the same information for the pure liquid is shown for reference. The band positions for solutions of alkali metal salts are reported in the literature.[2,10] The changes which occur—the increase frequency of ν_1 and ν_1 of C_s ammonia molecules—can be explained by the influence of the perchlorate ion and show no consistent dependence on the cation. There is however a large change in ν_2, the symmetric bending mode of ammonia; the frequency is shifted approximately 50 wave numbers to higher energy, a direction opposite that expected for the effect of perchlorate ion.[1] This frequency shift, which is proportional to the charge density of the cation, was shown earlier by Corset using infrared data[11] and indicates a relatively strong ammonia–cation interaction.

Anion Fundamental Vibrations. Perturbation of the anion through its interaction with other molecules often gives information about those interactions. With this in mind, an analysis of the anion fundamentals is presented. The perchlorate fundamental frequencies are not changed from those observed in solutions of ammonium perchlorate, indicating little or no direct cation–anion interaction. However the nitrate ion fundamentals, ν_3 (the asymmetric stretching mode) and ν_4 (the in-plane bending mode), are perturbed in all nitrate solutions. Table II lists the frequencies of the nitrate ion fundamental vibrations. The asymmetric stretch which is split in ammonium nitrate solutions is also split in the metal nitrate solutions; the splitting, which appears to show a small cation dependence, can only be compared qualitatively since there is a variation of concentration.

TABLE II: Frequencies of the Nitrate Ion Fundamental Vibrations

	V_1, cm^{-1}	V_3, cm^{-1}	V_4, cm^{-1}	Concn[a]
NH_4NO_3[b]	1044	1340, 1380	712	7
$LiNO_3$[b]	1045	1340, 1385	711, 719	6
$NaNO_3$[b]	1044	1347, 1390	709, 719	6
$CaNO_3$	1044	1350, 1380	708, 730	19
$SrNO_3$	1044		708, 723	37
$BaNO_3$	1044	1345, 1390	709, 719	Sat.

[a] In moles of ammonia per mole of salt. [b] Reference 10.

The in-plane bend of nitrate ion is also split as is shown in Figure 2. In water solutions the splitting of nitrate ion ν_4 has been attributed to contact ion pair formation.[12] Our results show that the amount of splitting is cation dependent and that the depolarization ratios are the same for each peak, both being depolarized. These observations indicate the presence of two kinds of nitrate environments in the solutions rather than a lifting of the degeneracy of the nitrate ion ν_4 mode of vibration. The concentration dependence of the splitting has been studied in the sodium nitrate–ammonia system. The splitting remains constant as the relative intensity of the two components changes with the concentration of $NaNO_3$.[10] The results of conductance experiments suggest that most ions in liquid ammonia are closely associated with their counter ions[13] to form ion aggregates.

On the basis of this evidence and the frequency position of ν_4 (714 cm^{-1}) of nitrate ion in ammonium nitrate solutions as well as dilute metal nitrate solutions, the high-frequency component is assigned to a nitrate ion in a contact ion pair.

Low-Frequency Region. All of the bands observed in the low-frequency region occur on the Rayleigh wing, and therefore an approximate baseline function was needed for any attempt to resolve these bands to obtain accurate positions and half-widths. While the correlation theory of light scattering developed by Fabelinski and Starunov[14,15] results in a complex description of the Rayleigh wing, most authors use a simple exponential function to describe the baseline.[16,17] In liquid ammonia the situation is further complicated by the presence of a very broad, low-intensity band centered at approximately 300 cm^{-1}.[2] In this work an exponential background function is used for pragmatic reasons. Attempts at resolution of the bands using more complex background functions did not result in statistically better fits.

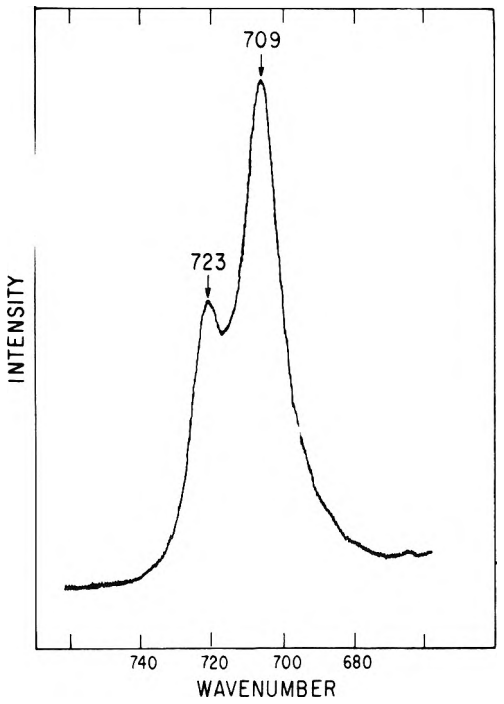

Figure 2. Raman spectrum of nitrate ion ν_4 in a solution of $Sr(NO_3)_2$.

TABLE III: Positions of Bands Observed in Salt Solutions in the Low-Frequency Region

Salt	Position, cm^{-1}	Width, cm^{-1}	Concn[a]
$Ba(ClO_4)_2$	215	65	27
$Sr(ClO_4)_2$	243	60	24
$Sr(NO_3)_2$	237	80	37
$Ca(ClO_4)_2$	266	50	27
$Ca(NO_3)_2$	263	91	19
$Mg(ClO_4)_2$	328	33	Sat.
$LiClO_4$	241	33	6
$LiNO_3$	242	36	6
Li(SCN)	240	37	6
$NaClO_4$	194		7.5

[a] In moles of ammonia per mole of salt.

One broad low-intensity band was observed in each solution of the metal perchlorates and in solutions of nitrates of metal cations with high charge density. The resolved low-frequency spectrum of a barium perchlorate solution is shown in Figure 3; the positions and half-widths observed in all of the solutions studied are shown in Table III. The band parameters were obtained using a linear combination of Gaussian and Lorentzian functions for the band shape and an exponential background function in a non-linear least-squares program. All of the observed bands are polarized.

The half-widths of the low-frequency bands are anion dependent. A comparison of the half-widths of the perchlorates with those of the corresponding nitrates reveals that the half-widths of the bands in the nitrate solutions are considerably larger than those in the corresponding bands in perchlorate solutions. The low-frequency band in a lithium thiocyanate solution is also slightly broader than that of the corresponding solution of lithium perchlorate. Figure 4 demonstrates the broadening and intensity effect of the anion. Though experimental parameters were kept as constant as possible, intensity arguments are questionable; however, a qualitative decrease in intensity

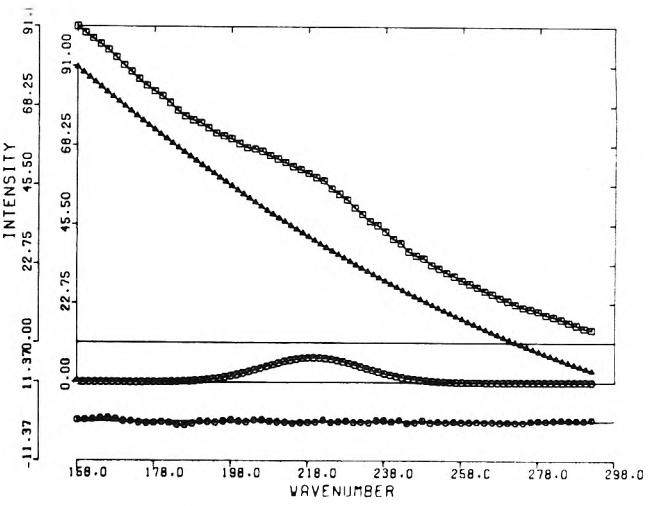

Figure 3. Resolved low-frequency spectrum of a solution of $Ba(ClO_4)_2$.

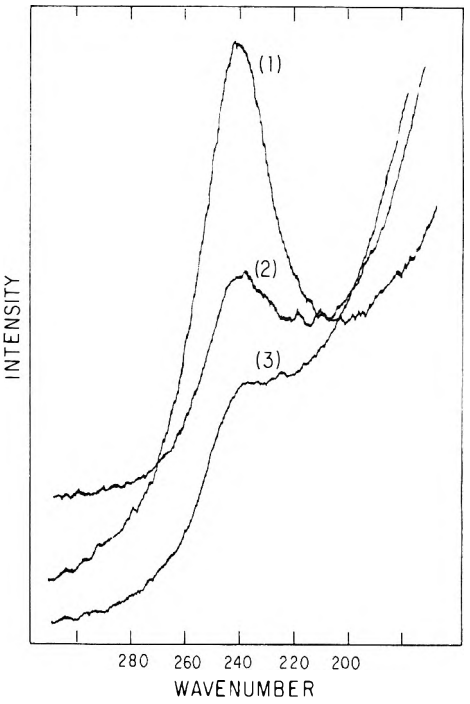

Figure 4. A portion of the low-frequency spectra of solutions of (1) $LiClO_4$, (2) $LiNO_3$, (3) LiSCN.

in the nitrate and thiocyanate solutions is observed in the data of Figure 4. The broadening is attributed to stronger solvated cation–anion interaction and the decrease in intensity is attributed to a lower concentration of the completely solvated species, which is in agreement with the higher tendency of nitrate and thiocyanate toward anion association, as shown in conductance work,[13] and the corresponding cation-dependent perturbation of the anion fundamentals.

Discussion

The low-frequency bands are assigned to the symmetric stretching mode of the solvated cation, presumably arising from interaction of the first solvation sphere. A short summary of the supporting experimental evidence follows. The cation-dependent shift to higher energy of the symmetric bend of ammonia indicates a strong solvent–cation

interaction. While it is possible for an ion pair to give rise to the low-frequency band, it is highly improbable that ion pairs with different anions would give rise to the same frequency. The small changes which do occur appear to be due to an anion perturbation of the solvated cation. The polarization data which indicate that all bands are polarized suggest that the vibrations which give rise to them are totally symmetric.

The remaining discussion centers on an ionic model for the ammonia-cation interaction. It is generally accepted that interactions of this type are primarily ionic in character. The low intensity (low molar scattering factor) of the observed bands is consistent with low covalent character even though a small amount of covalent character probably exists. With these limiting statements in mind an attempt to qualitatively and quantitatively describe the cation-solvent interaction on the basis of an ionic model was undertaken.

The model chosen was originally developed for aqueous solutions but is apparently applicable to other solvents. In this model, ion-dipole, ion-quadrupole, dipole-dipole, dipole-quadrupole, and quadrupole-quadrupole interactions are considered.[3] Conceptually the cation is surrounded by solvent molecules in either a tetrahedral or octahedral geometry depending upon the coordination number. The solvent dipoles are directed along the radius vector of the cation. This model yielded expressions which give the *in vacuo* interaction energy of a cation in an octahedral or tetrahedral cage of water molecules. The model explicitly takes into account the induced dipole produced by the cation and the other molecules in the primary solvation sphere. While a similar derivation may be carried out for both symmetries only the equations (eq 1-3) for the tetrahedral symmetry are discussed here where μ is the permanent dipole moment of the solvent molecule, θ is its quadrupole moment, e is the fundamental charge of the electron, and R is the distance between the cation center (point charge) and the center of the solvent dipole.[3] Equation 1 describes the field at one solvent position produced by the cation and the other three solvent molecules. Equation 2 describes the total electrostatic interaction energy. The induced dipole, μ_i, is obtained by setting μ in eq 1 equal to $\mu + \mu_i$, multiplying by α, the polarizability, and solving the resulting equation for μ_i. All calculations of the energy (U) are then accomplished by substituting $\mu + \frac{1}{2}\mu_i$ for μ and $\mu(\mu + \mu_i)$ for μ^2.[3]

$$F = \frac{e}{R^2} - \frac{15\sqrt{6}\mu}{32R^3} + \frac{45\sqrt{6}\theta}{128R^4} \quad (1)$$

$$U = \frac{-4\mu e}{R^2} + \frac{4\theta e}{R^3} + \frac{15\sqrt{6}\mu^2}{16R^3} - \frac{45\sqrt{6}\mu\theta}{32R^4} + \frac{45\sqrt{6}\theta^2}{64R^5} \quad (2)$$

$$\mu_i = \left[\frac{\alpha e}{R^2} - \frac{15\sqrt{6}\alpha\mu}{32R^3} + \frac{45\sqrt{6}\theta\alpha}{128R^4}\right] \Big/ \left[1 + \frac{15\sqrt{6}\alpha}{32R^3}\right] \quad (3)$$

Calculations were carried out for ammonia molecules in the primary solvation sphere, and the plot of energy *vs.* R is shown in Figure 5 for both mono- and divalent cations in both octahedral and tetrahedral solvent shells. The dipole and quadrupole moments of ammonia were taken to be 1.47×10^{-18} and 0.6×10^{-26} esu,[18] respectively; however it is found that the energy is much less sensitive to these constants than it is to the value of R. Examination of Figure 5 indicates that for both types of cations, the octahedral symmetry is energetically favored if only this interaction is considered. In the case of divalent cations the energy difference is so large ($\approx$70 kcal/mol) that it is unlikely that other factors will cause tetrahedral solvation to be favored. For the alkali cations, however, the energy difference is only 10–15 kcal/mol. If one considers entropy differences and the need to break additional hydrogen bonds in the octahedral case, it may be likely that a tetrahedral geometry is energetically favored for monovalent cations.

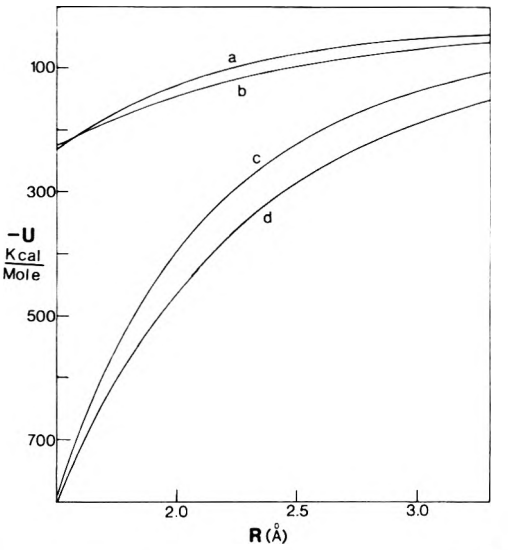

Figure 5. Plot of energy as a function of R: (a) T_d, $Z = 1$; (b) O_h, $Z = 1$; (c) T_d, $Z = 2$; (d) O_h, $Z = 2$.

The problem now is to relate the electrostatic model to the observed vibrational frequencies which requires the calculation of the vibrational force constant. In the harmonic oscillator approximation the force constant is given by the second derivative of the potential function evaluated at the equilibrium internuclear distance. This distance must be the internuclear separation at the minimum of the potential energy. Figure 5 demonstrates that the electrostatic energy, U, does not have a minimum at separations which are reasonable for intermolecular distances in the liquid state. The short-range repulsive energy terms which must dominate at distances smaller than the equilibrium distance are not considered. Near the potential minimum the approximation is made that the second derivative of the short-range repulsion terms is equal to zero. This is a hard-sphere approximation which may be interpreted as a steep potential wall originating from repulsive forces which are very strong relative to the long-range electrostatic forces. This pragmatic assumption of course introduces a large degree of anharmonicity.

A normal coordinate analysis in tetrahedral symmetry shows that the force constant for the totally symmetric stretch is composed of a linear combination of internal force constants, $F_1 + 3F_2$. F_1 is the force constant due to stretching along one bond and F_2 is the force constant due to interaction of one bond stretch with another. If the harmonic oscillator approximation (*viz.* that the force constant is given by the second derivative with respect to R of the potential function) is assumed, F_1 may be calculated from the first two terms of eq 2.

The second force constant, F_2, is conceptually more difficult. The last two terms of eq 1 describe the field at one solvent position produced by the other three. If we consid-

TABLE IV: Experimental and Calculated Values of the Vibrational Frequency and the Total Energy

Cation	Symmetry	R^a, Å	ν_{calcd}	$U_{calcd}^{a,b}$	ν_{obsd}	ΔH_{exp}^c	R', Å	U_{calcd}^b
Li^+	T_d	2.16	182	−107	241	−133.3	1.91	−140
Na^+	T_d	2.46	135	−80	194	−105	2.10	−114
Mg^{2+}	O_h	2.14	268	−401	328		1.94	−494
Ca^{2+}	O_h	2.47	196	−291	266	−402.7	2.15	−399
Sr^{2+}	O_h	2.60	175	−259	243	−370.2	2.24	−363
Ba^{2+}	O_h	2.82	146	−214	215	−335.7	2.37	−321

[a] Values calculated from the sum of hard sphere radii. [b] Energies are in units of kcal/mol. [c] Reference 20.

er that this field interacts with the dipole and quadrupole of one ammonia molecule, we obtain the energy of the interaction between that ammonia molecule and the other three. The second derivative with respect to R of the resulting expression is equal to $3F_2$. The sign is positive because an increase in the bond length of one solvent molecule increases the strength of the other three bonds since the dipole–dipole repulsion decreases. The force constant equations for the totally symmetric mode of both tetrahedral and octahedral symmetry are shown below. These equations give the F^{19} matrix element for the totally symmetric mode of vibration.

$$K_{A_1} = \frac{6Ze\mu}{R^4} - \frac{12Ze\theta}{R^5} + \frac{45\sqrt{6\mu^2}}{8R^5} - \frac{225\sqrt{6\mu\theta}}{16R^6} \quad T_d \tag{4}$$

$$K_{A_{1g}} = \frac{6Ze}{R^4} - \frac{12e}{R^5} + \frac{3(1+6\sqrt{2})}{2R^5} - \frac{15(1+6\sqrt{2})}{2R^6} \quad O_h \tag{5}$$

The corresponding G^{19} matrix elements which describe the kinetic energy of the vibration are easily determined. One finds for the totally symmetric stretch in a cubic symmetry that the vibrational frequency depends only on the inverse mass of the coordinating molecule or atom. As applied here the G matrix elements for both symmetries considered are equal to the inverse mass of the coordinating molecule. There is no frequency dependence on the mass of the cation.

The appropriate force constant in eq 6 permits the calculation of the vibrational frequency of interest. Figure 6 shows the vibrational frequency as a function of R for a mono- or divalent cation interaction with ammonia; the curves for both tetrahedral and octahedral solvation spheres are shown.

$$\bar{\nu}(\text{cm}^{-1}) = (1/2\pi c)\sqrt{K_{A_1}/M_{NH_3}} \tag{6}$$

Application of these equations to the experimental data is difficult because accurate values for R, the distance from the ion center to the center of the dipole, are not available. A possible approximation for R might be the sum of the hard-sphere radius of ammonia and the crystallographic radius of the cation. This leads to qualitative agreement with the experimental data in that (1) the observed and calculated frequencies increase in an orderly fashion as the cation radius decreases and that (2) the differences between the observed and calculated values for each cation are relatively constant.

A strategy which involves a self-consistent argument is available. The experimental ammonation enthalpy for a number of cations has been determined by Senozan from the heats of solution of salts and metals in liquid ammonia.[20] Either the ammonation enthalpy or the vibrational frequency can be used to estimate a value of an effective radius, R', for this model which should yield the other quantity to confirm the model. Since the vibrational

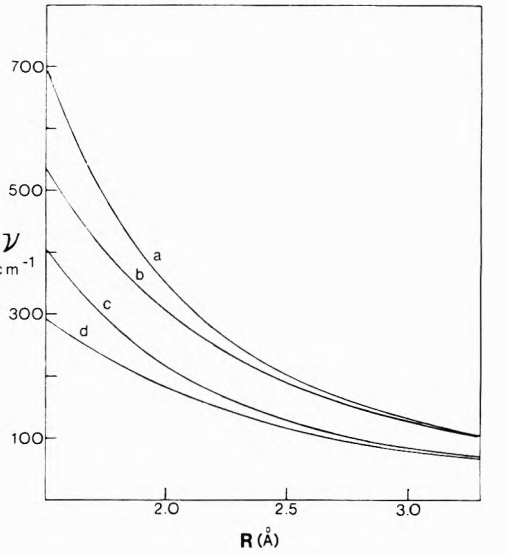

Figure 6. Plot of vibrational frequency as a function of R: (a) T_d, $Z = 2$; (b) O_h, $Z = 2$; (c) T_d, $Z = 1$; (d) O_h, $Z = 1$.

frequencies are more accurately determined than the ammonation enthalpy, they were used to calculate R' which was then used to estimate the ammonation enthalpy. Table IV gives the results of these calculations.

The following process was employed to determine the solvation symmetry. Given the observed frequency, the energy which most closely matched the experimental values indicated the proper symmetry. Using lithium as an example, the energies are −140 and −185 kcal/mol respectively for tetrahedral and octahedral symmetries. The choice based on a comparison with the experimental value (−133.3 kcal/mol) is clearly four coordinate tetrahedral symmetry.

It was earlier stated that several general limitations of the ionic model in regard to covalent bond character should be considered. Comparison of the energy values, which have an estimated error of ±6 kcal/mol obtained from a thermodynamic approach, with those calculated from the ionic model indicates that these bonds must be predominantly ionic. The difference between the calculated values of R and the sum of hard-sphere radii is rather large; however, because the ammonia molecule has nonspherical symmetry the hard-sphere radius of ammonia is probably too large for interactions through the lone pair. Substracting the cationic radius from the corresponding intermolecular distance gives the "effective" dipole radius along the C_3 axis of ammonia. This radius varies linearly with the total dipole moment from 1.28 Å for solvation of the most polarizing cation, magnesium, to 1.03 Å for solvation of barium, the least polarizing cation. The lengthening of the dipole radius with increasing cationic charge density and the linear dependence of the di-

pole on this radius is consistent with an electrostatic interaction.

In summary, the frequencies of all the observed low-frequency bonds are consistent with an ionic interaction model if assigned to the symmetric stretch of the primary solvation sphere of the cation. The primary solvation sphere of the cations of the alkali metals consists of four ammonia molecules and that of cations of the alkaline earth metals consists of six. A method, with the limitations of the ionic model, is developed by which the value of R and the ammonation enthalpies of spherical cations can be determined.

Acknowledgment. We wish to thank the National Science Foundation and the Robert A. Welch Foundation for financial support.

References and Notes

(1) J. R. Roberts and J. J. Lagowski in "Electrons in Fluids," Proceedings of Colloque Weyl III, J. Jortner and N. R. Kestner, Ed., Springer-Verlag, Berlin, in press.
(2) A. T. Lemley, J. H. Roberts, K. R. Plowman, and J. J. Lagowski, *J. Phys. Chem.*, **77**, 2185 (1973).
(3) D. K. Ross, *Aust. J. Phys.*, **21**, 597 (1968).
(4) R. M. Noyes, *J. Amer. Chem. Soc.*, **84**, 513 (1962).
(5) A. D. Buckingham, *Discuss. Faraday Soc.*, **24**, 151 (1957).
(6) P. F. Rusch, Dissertation, University of Texas at Austin, 1971.
(7) B. de Bettignies and F. Wallart, *C. R. Acad. Sci., Ser. B*, **271**, 640 (1970).
(8) T. Birchall and I. Drummond, *J. Chem. Soc. A*, 1859 (1970).
(9) W. C. Hamilton, *Acta Crystallogr.*, **18**, 502 (1965).
(10) A. T. Lemley, private communication.
(11) J. Corset, Thesis, Universite de Bordeaux, 1967.
(12) D. E. Irish, A. R. Davis, and R. A. Plane, *J. Chem. Phys.*, **50**, 2262 (1969).
(13) J. J. Lagowski, G. A. Moczygemba in "The Chemistry of Non-Aqueous Solvents," J. J. Lagowski, Ed., Vol. II, Academic Press, London, 1967.
(14) L. Fabelinski, "Molecular Scattering of Light," Plenum Press, New York, N. Y., 1968, pp 133–139.
(15) V. S. Starunov, *Opt. Spectrosc.*, **18**(2), 165 (1965).
(16) S. L. Shapiro and H. P. Broida, *Phys. Rev.*, **154**, 129 (1967).
(17) J. P. McTague, P. A. Aeury, and P. B. DuPre, *Phys. Rev.*, **188**, 303 (1969).
(18) The reported quadrupole moment of ammonia varies from approximately 1.3×10^{-26} to 0.14×10^{-26} esu. Since the energy and frequency are not highly sensitive to μ an average value of those reported was used.
(19) E. B. Wilson, J. C. Decius, and P. C. Cross, "Molecular Vibrations," McGraw-Hill, New York, N. Y., 1955.
(20) N. M. Senozan, *J. Inorg. Nucl. Chem.*, **35**, 727 (1973).

On the Behavior of the Excess Electron in Methane

Shingo Ishimaru, Tokio Yamabe, Kenichi Fukui,*

Department of Hydrocarbon Chemistry, Kyoto University, Kyoto, Japan

and Hiroshi Kato

Department of General Education, Nagoya University, Nagoya, Japan *(Received July 24, 1973)*

The electronic state of the trapped electron in methane is calculated by the use of the INDO-UHF method and the minimum lifetime of the electron is also estimated from the above result. Consequently, it is concluded that (1) the traps in methane do not play a substantial role in the motion of the excess electron, (2) the absorption spectra of the excess electron in methane will be difficult to obtain or quite broad, if detected, and (3) the present molecular orbital treatment is expected to lead to reasonable results for other hydrocarbons in which the trapped electron is more stable than in methane.

Introduction

There are many theoretical investigations[1-7] which confirm the existence of trapped electrons in cavities in polar solvents. For example, in previous papers,[7] the present authors have shown with the aid of the semiempirical Hartree-Fock method that, using the cavity model, it is possible to interpret not only the thermal and optical but also the magnetic properties of the solvated electron.

On the other hand, several authors[8-11] suggest that electrons in liquid hydrocarbons are also trapped in cavities which are formed by the fortuitous aggregation of molecules. From the standpoint of electron trapping by cavities in such nonpolar solvents, the following may be easily conjectured: the electron-trap potential in hydrocarbons, unlike the cases of polar solvents, will be generally weak at attraction and mainly caused by the repulsion between the excess electron and the electron cloud of molecules. Hence the potential will not always be enough to create the stable, bound state of the excess electron. If the electron cannot be bound, it will stay quasistationarily for the trap time τ until removed to the outside of the trap thermally or by tunnelling. In case τ is so small that the above collective effect of molecules plays only a trivial role, the electron will be "quasifree" and its property may be understood by considering the transport phenomena of an electron with thermal velocity among molecules.[12-16]

Thus it is probable that one of the factors which dominate the behavior of the excess electron in hydrocarbon will be the electronic state of the electron in the cavity. Therefore, we investigate in the present paper the electronic state of the trapped electron in a hydrocarbon, selecting the simplest case which is that of methane, with the use of the hypothetical cavity model and the Hartree-Fock method as before. The lifetime of the trapped electron is also discussed based on that result.

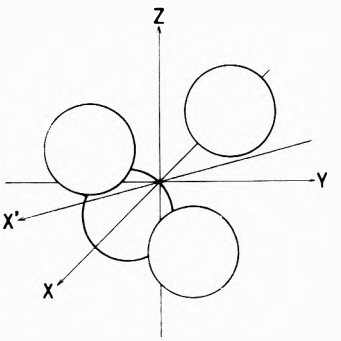

Figure 1. Four methane molecules in a tetrahedral array. X' axis lies on X–Y plane and intersects X axis with a 45° angle.

Model and Method

The trap is assumed to be composed of four methane molecules coordinating tetrahedrally with respect to the carbon atoms of each toward the center (Figure 1). The distance from the cavity center to the carbon atom R is set at 1.5, 2.0, and 2.5 Å, the second of which is a rough estimation based on the structure of solid methane.[17]

The calculation is performed by the unrestricted Hartree-Fock method[18] with INDO approximation.[19] Then, in the same way as the cases of polar solvents,[7] the additional two groups of hydrogen-like atomic orbitals (AO) located at the cavity center are used in addition to valence AO's of solvent molecules because as was shown in our previous paper,[7] such a treatment makes it very easy to describe the state of an excess electron, if it is localized in the cavity. For the sake of simplicity of calculation, moreover, the ground and excited states of an excess electron are obtained separately with the additional 1s AO for the former state and the 2s and three 2p AO's for the latter state, respectively (method 2 in ref 7). The orthogonalization condition between the above two states will be approximately satisfied, if an excess electron is localized in the additional AO's. Parameters concerned with the additional two groups of AO's are analogous to those used in ref 7; the orbital exponents, ζ, are set at 0.2, 0.3, and 0.4 au^{-1}, all the bonding parameters are set at −4.5 eV, and the Mulliken-type electronegativities are set so that core integrals for the ground and excited states of an excess electron become nearly 0.0 and 4.0 eV. This last value is about 0.5 eV higher than that of method 3 in ref 7, according to which the excitation energies obtained were most reasonable.

Besides, because the UHF wave function is not a pure spin multiplet,[20,21] we examine the effect of spin contamination with the aid of the single annihilation method of Amos and Snyder,[22] although the resulting correction will be small when an excess electron is localized in the additional AO's.

Results and Discussion

At first, we will discuss the electronic state of the trapped electron. Table I shows the total energies of the trap with an excess electron in the ground state, $E(e_M^-)$, for three values of R; in parentheses, the values after annihilation are cited only when they are varied[23] by this manipulation. The result seems to indicate the anion state is most stable when R = 2.0 Å. Hence, in the following discussion, only the case of R = 2.0 Å is treated. In Table II, ΔE[24] represents the stabilization energy given by

TABLE I: The Total Energies of the Trap with an Excess Electron in the Ground State[a]

	$E(e_M^-)$		
R, Å	ζ = 0.2	ζ = 0.3	ζ = 0.4
1.5	−1049.638	−1042.425	−1044.027
	(−1049.618)		(−1044.025)
2.0	−1076.756	−1078.202	−1079.836
2.5	−1073.804	−1075.209	−1076.440
	(−1073.803)		(−1076.439)

[a] In parentheses, the values after annihilation are cited, only when they are varied by the manipulation.

TABLE II: The Calculated Results for the Trapped Electron in Methane[a]

ζ, au^{-1}	ΔE, eV	ϵ_{HO}^{α}, eV	$h\nu$, eV	ρ_H
0.2	−0.254	−2.094	4.441	0.007
0.3	0.578	0.030	0.252	0.017
			(0.253)	(0.016)
0.4	0.234	0.357	−4.316	0.025
			(−4.312)	(0.023)

[a] In parentheses, the values after annihilation are cited, only when they are varied by the manipulation.

the difference between the energy of the anion radical group and the neutral group which is calculated using the same basis set as that for the open shell system, ϵ_{HO}^{α} is the energy of the highest occupied molecular orbital (with α spin), $h\nu$ is the energy of the first excitation, and ρ_H is the inside proton spin density. The values after annihilation are cited in parentheses only when they are varied by the manipulation. Since the excess electron in liquid methane has been found (from the mobility data[25,26]) to be quasifree, the positive ΔE for ζ = 0.3 and 0.4, meaning that the excess electron in the cavity cannot be stabilized, will be reasonable.[27] In these cases, ϵ_{HO}^{α} is also positive and small. It is to be noted that the highest occupied molecular orbitals are dominated by the additional 1s AO[28] like those for polar solvents;[7] *i.e.*, the coefficients of this AO before annihilation are 0.964 (ζ = 0.2), 0.947 (ζ = 0.3), and 0.933 (ζ = 0.4), respectively. Concerning the excitation energy and the proton spin density, there has been no observation because of the high mobility in this liquid,[25,26] but $h\nu$ in methane will presumably be smaller than 0.6 eV since the maximum absorption probably occurs at wavelengths $\lambda \gtrsim 2000$ nm in liquid propane.[29] Moreover, accepting the tetrahedral model, ρ_H would be expected to be of the order of 0.01 in terms of the values of the epr line width ΔH in other hydrocarbons at 77°K[30-32] and the formula by Kip, *et al.*[33] According to the present calculation, the excess electron in the lowest excited state is localized in 2p MO and the value of $h\nu$ at ζ = 0.3 seems to be most appropriate. Besides, it is noticeable that all of $|\rho_H|$ are of the same order as those of other hydrocarbons and that ρ_H is positive contrary to the result for polar solvents.[7] The latter result is ascribed to the relatively large contribution of the spin delocalization term, which was negligibly small in the cases of polar solvents.[7] It should be remarked that, like the cases of polar solvents,[34] ρ_H is mainly determined by the pair-wise interaction between a methane molecule and a localized electron, because according to the calculation of this system using the valence AO's of a methane molecule and the 1s AO (ζ = 0.3 and its center is 2.0 Å distant from the carbon atom), ρ_H after annihilation is 0.016 and coincides with the corresponding

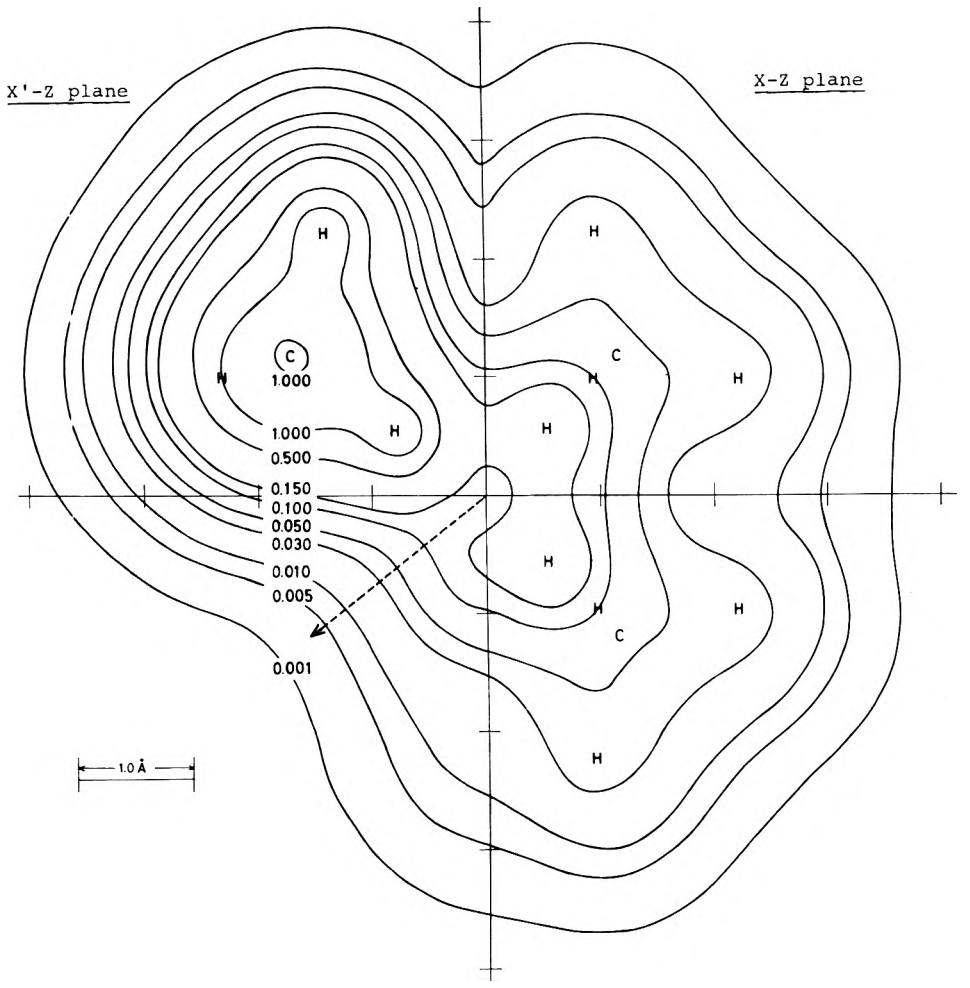

Figure 2. The electron distribution of methane molecules (ζ = 0.3). The atoms are projected on two planes.

value in Table II. It is probable that, in the present case of nonpolar solvent, the influence of molecules outside the first coordination shell will be not greater than that of adjacent molecules in this shell and that therefore the former influence will be also insignificant for ρ_H.

As is easily expected from the result that an excess electron in both the ground and excited states is localized in the additional AO's, the effect of spin contamination is negligibly small on the whole. In fact, the values of $\langle S^2 \rangle$ are 0.750 both before and after annihilation except in the case of the excited state with ζ = 0.4, even in which case the value is 0.752.

Summarizing the above results, the most appropriate ζ seems to be 0.3. In Table III, the calculated charge densities and the dipole moments, none of which changes by annihilation, are shown. From this result, it is supposed that at the first stage when only methane molecules aggregate instantaneously with the approximate vibrational period of 10^{-13} sec, the distortion of each molecule is small (the dipole moment D = 0.039 D outward from the cavity), secondly, that if an excess electron comes into the system and is localized in the cavity, these molecules are further polarized to have D = 0.406 D in each one toward the cavity center in a time less than 10^{-15} sec (electronic polarization time), and finally, that thereby the electron itself is stabilized[35] compared with its initial state in the cavity. Figure 2 shows the electron distribution of four methane molecules obtained without the additional 1s AO; the atoms are projected on X-Z and X'-Z planes. In the cavity, there is a place surrounded by the electron cloud of methane and a very shallow depression of the distribution exists near the center (compare this with our previous result for water[7]). It may be natural to consider that the excess electron will most probably go out along the direction combining the carbon atom of a methane molecule and the cavity center, which is shown with a broken line in Figure 2. In Figure 3, the potential felt by an electron moving along this direction, which is approximated by ΔE (ζ = 0.3) as in our previous work, is shown by a solid line; on the horizontal axis, the distance from the cavity center is indicated. It should be stressed that, even in this direction, there is a peak with a height of 1.13 eV at a distance of 1.65 Å from the center though ΔE is always positive. Hence an electron which has come into this cavity will be expected to stay for a time and to go outward thermally or by tunnelling. In the following, assuming electron tunnelling, we will estimate the trap lifetime of the electron by the use of the above potential which gives the minimum value of the lifetime.

For convenience, we approximate the curve of ΔE by the function[36]

$$V(x) = a - v\cosh^2 \mu\{\tanh|(x-b) - \mu| + \tanh \mu\}^2 \quad (1)$$

where x is the coordinate in the horizontal axis and a, b, v, and μ are parameters determined as follows: (1) $V(x)$ has the maximum value, a, at $x = b$; hence a = 1.13 and

TABLE III: The Charge Densities and the Dipole Moments of Methane[a]

Charge densities[b]				Dipole moment of each molecule, D[c]	Induced dipole moment, D[c]
q_H	q_C	$q_{H'}$	q_{1s}		
0.817	4.184	0.991	1.111	+0.406[d]	+0.445
(0.996)	(3.977)	(1.009)	(...)	(−0.039)	

[a] These results are not varied by annihilation. [b] The subscripts H, C, H′, and 1s indicate the inside hydrogen, the carbon, the outside hydrogen, and the additional 1s AO (ζ = 0.3), respectively. Values in parentheses are those for the neutral state calculated without the additional 1s AO. [c] The positive sign indicates the direction toward the cavity center and vice versa. [d] In each of the molecules, the sum of the net charges is not zero, but the absolute value of the positive charge is very small ($\lesssim$0.03) and so the dipole moment can be approximately estimated.

b = 1.65. (2) At $x \to +\infty$, $V(x)$ gives the asymptotic value, $a - v\exp(2\mu)$, which is zero in the present case. (3) At $x \to -\infty$, $V(x)$ gives the asymptotic value, $a - v\exp(-2\mu)$, which is put equal to ΔE at x = 0, *i.e.*, 0.578.[37] (4) From (2) and (3), v = 0.790 and μ = 0.179. The concrete form of $V(x)$ thus obtained is shown in Figure 3 with a broken line (the part for $x < 0$ is abbreviated). The coincidence in $x \lesssim 2.0$ Å is good, but in the outer region there is some discrepancy between two curves. However, such a discrepancy may be permissible, because the excess electron will diffuse in this region and hence the real electron-trap potential will be lower than the curve of ΔE. The Schrödinger equation for an electron moving in the field of $V(x)$ is exactly solved,[36] giving the wave function which represents a transmitted beam at $x = +\infty$ and an incident and reflected beam at $x = -\infty$ under the condition that the kinetic energy of the electron is positive for all x. The resulting transmissivity is[36]

$$T = \frac{2\sinh(\pi k_+)\sinh(\pi k_-)}{\cosh[\pi(k_+ + k_-)] + \cosh(\pi\beta)} \qquad (2)$$

where

$$k_+ = \sqrt{(2m/\hbar^2)[\epsilon - (a - v\exp(2\mu))]}$$
$$k_- = \sqrt{(2m/\hbar^2)[\epsilon - (a - v\exp(-2\mu))]} \qquad (3)$$
$$\beta = \sqrt{(8m/\hbar^2)\, v\cosh^2\mu - 1}$$

in which ϵ is the energy of the electron, m is the mass of an electron, and $\hbar = h/2\pi$ (h is Planck's constant). Then the trap lifetime τ is roughly estimated by[38]

$$\tau \sim \frac{r}{T(p/m)} \qquad (4)$$

where r is the coordinate of the inside turning point with regard to the curve of ΔE and p/m corresponds to the velocity of the electron. The result is listed in Table IV. The transmissivity is near unity for the electron with the kinetic energy of 0.1 ~ 0.5 eV and is 0.328 even for the electron with the small kinetic energy of 0.01 eV which is of the order of kT (k is Boltzmann's constant and T is the absolute temperature); accordingly, the lifetimes are quite short (10^{-15} to 10^{-16} sec). Therefore, the incident electron has probably no sooner polarized the methane molecules than it goes outward from the cavity. It is to be noted that as already mentioned the lifetimes obtained are the minimum values because in other directions the repulsive potential will be higher and thicker and so the transmissivity will decrease.

Thus, the following may be concluded from the above result. (1) The traps formed fortuitously do not play a substantial role in the motion of the excess election in methane. That is, the excess electron in methane will be quasifree as pointed out by several authors.[25,26,39] (2) The absorption spectra of the excess electron in methane will

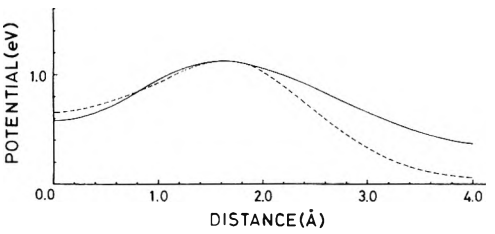

Figure 3. The shape of the trap potential (ζ = 0.3) in the direction of the broken line in Figure 2. The solid line is the potential approximated by ΔE and the broken line is the result of eq 1.

TABLE IV: The Calculated Properties of the Excess Electron in Methane

Kinetic energy, eV	Velocity × 10^8 cm/sec	Transmissivity, T	Lifetime × 10^{-15} sec
0.010	0.059	0.328	0.723
0.100	0.188	0.704	0.348
0.200	0.265	0.812	0.342
0.300	0.325	0.864	0.303
0.400	0.375	0.894	0.316
0.500	0.419	0.915	0.344

be difficult to obtain or quite broad, if detected, as easily expected from the uncertainty principle, $\Delta\epsilon \gtrsim \hbar/\tau \sim 0.7$ eV. (3) In view of the calculation of the electronic state of the trapped electron in methane, it is probable that the present molecular orbital treatment will lead to reasonable results for other hydrocarbons in which the trapped electron is more stable than in methane.

Further theoretical investigations seem to be needed in order to clarify the nature of the trapped electron in hydrocarbons.

Acknowledgment. The authors wish to thank Professor K. Fueki for his valuable suggestions. It is a pleasure to express our gratitude to the Data Processing Center, Kyoto University, for its permission to use the Facom 230-60 computer. S. Ishimaru gratefully acknowledges the financial support of the Japanese Society for the Promotion of Science.

References and Notes

(1) J. Jortner, *J. Chem. Phys.*, **27**, 823 (1957); **30**, 839 (1959).
(2) M. Natori and T. Watanabe, *J. Phys. Soc. Jap.*, **21**, 1573 (1966); M. Natori, *ibid.*, **24**, 913 (1968).
(3) K. Iguchi, *J. Chem. Phys.*, **48**, 1735 (1968).
(4) D. A. Copeland, N. R. Kestner, and J. Jortner, *J. Chem. Phys.*, **53**, 1189 (1970).
(5) K. Fueki, Da-Fei Feng, and L. Kevan, *J. Phys. Chem.*, **74**, 1976 (1970); K. Fueki, Da-Fei Feng, L. Kevan, and R. E. Christoffersen, *ibid.*, **75**, 2297 (1971).
(6) G. Howat and B. C. Webster, *J. Phys. Chem.*, **76**, 3714 (1972).
(7) S. Ishimaru, H. Kato, T. Yamabe, and K. Fukui, *Chem. Phys. Lett.*, **17**, 264 (1972); *J. Phys. Chem.*, **77**, 1450 (1973).
(8) G. R. Freeman and J. M. Fayadh, *J. Chem. Phys.*, **43**, 86 (1965).
(9) J. M. Buchanan and F. Williams, *J. Chem. Phys.*, **44**, 4377 (1966).
(10) W. F. Schmidt and A. O. Allen, *J. Chem. Phys.*, **52**, 4788 (1970).
(11) R. M. Minday, L. D. Schmidt, and H. T. Davis, **54**, 3112 (1971); *J. Phys. Chem.*, **76**, 442 (1972).

(12) J. Jortner, N. R. Kestner, S. A. Rice, and M. H. Cohen, *J. Chem. Phys.*, **43**, 2614 (1965).
(13) K. Hiroike, N. R. Kestner, S. A. Rice, and J. Jortner, *J. Chem. Phys.*, **43**, 2625 (1965).
(14) J. Lekner, *Phys. Rev.*, **158**, 130 (1967).
(15) M. H. Cohen and J. Lekner, *Phys. Rev.*, **158**, 305 (1967).
(16) B. E. Springett, J. Jortner, and M. H. Cohen, *J. Chem. Phys.*, **48**, 2720 (1968).
(17) H. M. James and T. A. Keenan, *J. Chem. Phys.*, **31**, 12 (1959).
(18) J. A. Pople and R. K. Nesbet, *J. Chem. Soc.*, **22**, 571 (1954).
(19) J. A. Pople, D. L. Beveridge, and P. A. Dobosh, *J. Chem. Phys.*, **47**, 2026 (1967).
(20) P.-O. Löwdin, *Advan. Chem. Phys.*, **2**, 207 (1959).
(21) K. F. Berggren and R. F. Wood, *Phys. Rev.*, **130**, 198 (1963).
(22) T. Amos and L. C. Snyder, *J. Chem. Phys.*, **41**, 1773 (1964).
(23) To three decimal places.
(24) This refers to the "corrected stabilization energy" in ref 7.
(25) P. G. Fuochi and G. R. Freeman, *J. Chem. Phys.*, **56**, 2333 (1972).
(26) W. F. Schmidt and G. Bakale, *Chem. Phys. Lett.*, **17**, 617 (1972).
(27) However, it is to be noticed that the destabilization may be partly attributed to the overestimated charge density of the hydrogen atom of methane in the INDO calculation; for example, according to the *ab initio* calculation, the charge density of the hydrogen atom of isolated methane is 0.867 with a C–H bond length of 1.094 Å (see W. E. Palke and W. N. Lipscomb, *J. Amer. Chem. Soc.*, **88**, 2384 (1966)); nevertheless, the INDO calculation with a C–H bond length of 1.090 Å gives 1.009 for the value. Therefore, ΔE was also recalculated by correcting the electronegativity of the hydrogen atom so that it might give a reasonable charge density for this atom, 0.867. ΔE consequently obtained is −1.868 eV, which seems to be too low and to have errors caused by the collapse of the consistency of parametrization. Hence we will maintain further discussions, keeping in mind that ΔE will probably be slightly lowered by more accurate calculations.
(28) Such a molecular orbital is called 1s MO.
(29) H. A. Gillis, N. V. Klassen, G. G. Teather, and K. H. Lokan, *Chem. Phys. Lett.*, **10**, 481 (1971).
(30) A. Ekstrom and J. E. Willard, *J. Phys. Chem.*, **72**, 4599 (1968).
(31) K. Tsuji, H. Yoshida, and K. Hayashi, *J. Chem. Phys.*, **46**, 810 (1967).
(32) K. Tsuji and T. Williams, *J. Amer. Chem. Soc.*, **89**, 1526 (1967).
(33) A. F. Kip, C. Kittel, R. A. Levy, and A. M. Portis, *Phys. Rev.*, **91**, 1066 (1953).
(34) S. Ishimaru, H. Kato, H. Tomita, T. Yamabe, and K. Fukui, *Chem. Phys. Lett.*, in press.
(35) According to the results that $|\rho_H| \ll 1$ and that q_{1s} is near unity, the correlation energy may be considered to be small.
(36) P. H. Morse and H. Feshbach, "Methods of Theoretical Physics," McGraw-Hill, New York, N. Y., 1953, p 1659.
(37) Hence the transmissivity for the electron with the energy near ΔE at $X = 0$ will slightly be overestimated.
(38) D. Bohm, "Quantum Theory," Prentice-Hall, New York, N. Y., 1951, Chapter 12.
(39) H. Fueki, *Can. J. Chem.*, **50**, 3379 (1972).

On the Mechanism of Ion Exchange in Crystalline Zirconium Phosphates. X. Calorimetric Determination of Heats of Na^+–H^+ Exchange[1a]

A. Clearfield* and L. H. Kullberg[1b]

Department of Chemistry, Clippinger Graduate Research Laboratories, Ohio University, Athens, Ohio 45701

(Received July 23, 1973)

Publication costs assisted by the National Science Foundation

The heats of Na^+–H^+ exchange on three samples of zirconium phosphate of widely different crystallinities have been determined calorimetrically. For the crystalline sample the first 50% of exchange is exothermic with $\Delta H^\circ = -6.90 \pm 0.10$ kcal/mol. The second half of the reaction is endothermic with $\Delta H^\circ = +6.45 \pm 0.15$ kcal/mol. The corresponding entropies accompanying these reactions are -31.0 ± 0.1 and 0.0 ± 0.1 eu. In the case of a gelatinous, nearly amorphous, exchanger the reaction is initially exothermic but then the heat function passes through a broad maximum and becomes progressively more endothermic. The overall reaction is endothermic with $\Delta H^\circ = 2.0 \pm 0.2$ kcal/mol and $\Delta S^\circ = -14.8 \pm 1.3$ eu. The semicrystalline exchanger exhibited heat effects surprisingly similar to those of the fully crystalline exchanger. Qualitative explanations for the observed results are presented.

Introduction

The ion-exchange behavior of zirconium phosphate has been described by several authors and measurements of distribution and selectivity coefficients have been reported in many papers. This literature is summarized in two recent reviews.[2,3] Free energies of exchange of alkali metal ions have been calculated from measured selectivity coefficients and enthalpies have been determined from the temperature dependence of the selectivity coefficients. These data are collected in Table III of ref 2.

It is now recognized that there are at least a dozen known crystaline zirconium phosphates as well as gelatinous and semicrystalline varieties.[3] The most common form is α-zirconium phosphate (α-ZrP) which is zirconium bis(monohydrogen orthophosphate) monohydrate, $Zr(HPO_4)_2 \cdot H_2O$. This compound is prepared by refluxing zirconium phosphate gels in phosphoric acid.[4] By suitable variation of the acid concentration and time of reflux it is possible to obtain products with crystallinities ranging from almost totally amorphous to fully crystalline.[5,6] The crystallinity of the exchanger has a marked effect upon ion-exchange behavior. Another problem arises in that appreciable amounts of hydrolysis may occur either during preparation and washing of the exchanger or during the ion-exchange reaction. Thus, it is of the utmost importance when reporting thermodynamic data that the exchanger phase be well characterized as to composition and crystallinity and that the exchange reaction be correctly defined.

Still a further problem stems from the uncertainty in defining the exchange capacity of amorphous and semi-

TABLE I: Standard Integral Functions of Na^+–H^+ Exchange[a]

	$\Delta G°$, kcal/mol	$\Delta H°$, kcal/mol	$T\Delta S°$, kcal/mol	$\Delta S°$, eu	ΔS_{EX}, eu
On 0.5:48	6.4 ± 0.3[b]	2.00 ± 0.2	−4.4 ± 0.4	−14.8 ± 1.3	
On crystalline ZrP up to half exchange	2.33 ± 0.06[c]	−6.90 ± 0.10	−9.23 ± 0.12	−31.0 ± 0.1	−25.9
On crystalline ZrP half-fully exchanged	6.45 ± 0.03[c]	6.45 ± 0.15	0.00 ± 0.15	0.0 ± 0.1	5.1

[a] All values are calculated in kcal/mol of Na^+. [b] From ref 5. [c] From ref 12 in which $\Delta H°$ = −5.88 ± 0.81 and +3.95 ± 0.67 kcal/mol for the first and second steps, respectively.

crystalline exchanger samples. In such exchangers the uptake of ions is pH dependent and at moderately high pH values some hydrolysis of phosphate groups occurs making the determination of the true capacity difficult.[7] Thus in some instances capacities were determined empirically for given electrolyte solutions.[8-11] In other cases the theoretical capacity was chosen.[5,12] Since the value of ion exchange equilibrium constants and hence any thermodynamic values derived from them depend upon the choice of exchange capacities, it is important that this point be clarified. For these reasons the thermodynamic data collected in Table III of ref 2 may be of limited value.

In earlier papers of this series careful attention was given to the points mentioned above. Exchanger samples were characterized by analysis, X-ray patterns, water content, and dehydration behavior.[5,12] Exchange isotherms for Na^+–H^+ exchange were obtained covering the entire composition range. Equilibrium constants were determined from these isotherms on an exchanger of low crystallinity[5] and also for the fully crystalline α-ZrP.[12] In the latter case it was shown that exchange occurs in two steps, one of them covering the range of 0 to 50% Na^+ uptake and the other from 50% to full exchange.[4,13] Enthalpy values were determined from the variation of equilibrium constants with temperature in the range 25–55°. These data are presented in Table I. For the exchanger of low crystallinity a single isotherm over the entire composition range was observed.

A better insight into the exchange process can often be achieved from a precise knowledge of free energies, enthalpies, and entropies. Direct calorimetric measurements present the best means of accurately determining ΔH values. In this paper we report on such measurements for Na^+–H^+ exchange on three samples of α-ZrP possessing widely different crystallinities.

Experimental Section

Chemicals. All chemicals used were of reagent grade. The sodium hydroxide solutions were standardized by titration against weighed amounts of NBS potassium biphthalate and then used to standardize the hydrochloric acid solutions. The sodium chloride solution was analyzed by exchange of Na^+ for H^+ on a strong acid resin followed by titration of the released acid. THAM (Fisher, certified primary standard) was dried at 80° for 24 hr followed by vacuum treatment for an additional 24 hr and stored over anhydrous $CaSO_4$. Care was taken to avoid CO_2 contamination of the NaOH solutions by preparing and storing them under nitrogen atmospheres. Only freshly prepared NaOH solutions were used. Distilled, deionized water was used throughout. The water was boiled to remove CO_2 when used for the preparation of NaOH solutions. The zirconium phosphate samples used were the same as those prepared and analyzed earlier.[5,12] Water contents of the gels were redetermined as loss of weight on ignition to 800–900°.

Calorimetric Apparatus and Procedure. All the thermochemical measurements were made using an LKB 8721-1 reaction solution calorimeter.[14] This calorimeter is of the constant temperature environment type with associated thermostat, temperature sensing device (including a thermistor), and calibration apparatus. The calorimeter consists of an outer chromium plated brass can and a 100-cm^3 inner reaction vessel made of glass. This reaction vessel contains a 2000-Ω thermistor temperature sensor, a 50-Ω *manganin* wire heater and a combined stirrer-ampoule holder. Standard LKB ampoules made of thin-walled Pyrex glass were used. After filling the ampoules were sealed by melting off an attached filling tube or by closing the ampoule shaft with a tightly fitting silicon rubber stopper which was then covered with a thin layer of *microwax*.

The experiments were performed over approximately equal intervals on either side of 25.00° except when the reactions were slow. In the latter case the reaction was initiated at such a temperature as to give a nonsloping after period of the calorimetric curve. However the deviation of the mean temperature of the experiment from 25.0° was never larger than 0.2°. Electrical calibrations were made over the same temperature range as in the main experiment, both before and after the reaction had taken place. These agreed usually very well (Δ < 0.1%) and the mean value for each experiment was used to compute the corresponding enthalpy value which thus refers to 25.0°.

For the main experiments the resistance changes were computed by extrapolating the linear portions of the fore and after parts of the calorimetric curve to the time corresponding to ~63% of the heat evolution (Dickinson's extrapolation method).[15] For the electrical calibrations, extrapolations were taken to the time corresponding to 50% of the heat evolution. From the thermistor resistance change, ΔR, obtained in an experiment, the total heat, Q, was calculated by the expression $Q = (\Delta R/R_m)E$ where R_m is the mean resistance value in the reaction experiment. The value for the calibration constant, E, was calculated from the expression $E = Q_c R_{m,c}/\Delta R_c$ where Q_c is the electrical energy introduced in the calibration experiment, ΔR_c is the change in thermistor resistance, and $R_{m,c}$ is the mean resistance.

Testing of the Calorimeter. To test the overall performance of the calorimeter, the enthalpy of solution of THAM in 0.1 *M* HCl was measured. This reaction is a suitable test reaction for rapid, moderately exothermic reactions.[16] Varying amounts of THAM (0.26–0.43 g) were dissolved in 100.0 ml of 0.1000 *M* HCl. For eight measurements the mean value of $-\Delta H$ was (7.123 ± 0.007) kcal/mol. The error is given as the single standard deviation of the mean, $(\Sigma\delta^2/n(n-1))^{1/2}$. Our value is in good agreement with previously reported values, of which the best is thought to be 7.110 kcal/mol.[17]

Heats of Ion Exchange. Measurements were made on three α-ZrP preparations of different crystallinities,

namely, crystalline (12:330), semicrystalline (4.5:48), and amorphous (0.5:48).[5] These samples were prepared by refluxing a precipitated ZrP in a specific concentration of H_3PO_4 for a given length of time as specified by the numbers in parentheses.

A quantity (0.1–0.4 g) of the exchanger in its pure hydrogen form was weighed into an ampoule. In order to avoid heats of wetting during the experiment 0.5 ml (0.5–0.8 ml for gel 4.5:48) of a 0.1000 *M* NaCl solution was added to the exchanger in the ampoule. For gel 0.5:48 deionized H_2O was used instead of 0.1 *M* NaCl since in this case an appreciable amount of sodium ion exchange would occur in the ampoule. The sealed ampoule was put into the calorimeter where it was held by a four-pronged stirrer which could be lowered to break the ampoule on a sapphire-tipped glass pin without interrupting the stirring. The maximum stirring rate (500 rpm) was used.

To check that no further heats of wetting took place when the ampoule contents came into contact with the solution in the reaction vessel experiments were performed where the reaction vessel was filled with 100.0 ml of H_2O. No heat effects were obtained for α-ZrP crystals or gel 4.5:48 while a small heat release (~0.02 cal) accompanied the breaking of an ampoule containing 0.4 g of gel 0.5:48. Since in all cases less than 0.4 g of gel 0.5:48 was used this heat release could be neglected since it is less than the experimental error.

For measurements of the heats of exchange the reaction vessel was filled with 100.0 ml of a solution consisting of 0.1000 *M* NaCl + C m*M* NaOH where $0 \leq C \leq 10$. After filling, the reaction vessel was put into its place in the calorimeter and the temperature was brought to just under 25°. It was then sealed in its jacket and immersed in the 25.00° thermostat. When a steady-state temperature drift was reached in the stirred solution (the solution was stirred for at least 2 hr to ensure thermal equilibrium) a split second stopwatch was started. Readings of resistance of thermistor and time were taken at constant intervals of resistance or time. A prerating resistance–time curve was plotted over a period of 5–7 min. At a preselected time the stirrer was lowered and the ampoule broken. The thermal effects due to the reaction were usually completed within 5 min. For gel 0.5:48, however, the reactions especially at higher sodium ion loadings were much slower and equilibrium was not attained until 20–30 min after ampoule breaking. Readings of resistance and time were continued for a time after equilibration in order to plot the post-rating curve. After each calorimetric determination the solution was analyzed to establish the amount of exchange that had occurred. The hydrogen ion concentration of the solution was obtained from pH measurement with an Orion potentiometer Model 801 equipped with a Corning combination electrode with Ag|AgCl internal and glass electrode external. After determining pH, the solid was filtered off and a 50-ml sample of the filtrate was taken out and potentiometrically titrated with 0.1 *M* NaOH. If the pH of the filtrate was higher than *ca.* 4, 0.1 *M* HCl was added. From a compilation of ionization constants of phosphoric acid,[18] pK_{ai} values of 2.0, 6.7, and 11.7 for $i = 1, 2$, and 3, respectively, have been chosen as the "best" ones at an ionic strength of 0.1 *M* and 25°. Thus at pH 5.0 most of the phosphate is in the form of $H_2PO_4^-$ and at pH 8.3 the phosphate is mainly in the form of HPO_4^{2-}. Then the amount of NaOH required to change pH from 5.0 to 8.3 corresponds to the total phosphate content in the solution. By knowing the hydrogen ion concentration, the total phosphate concentration, and the pK_{ai} values, the amount of each phosphate species in a particular solution could be obtained by simple stoichiometry. Thus, assuming the phosphate being washed out as H_3PO_4, the amount (milliequivalents) of deprotonized H_3PO_4 can be calculated. The hydrogen released by the exchange is given by the milliequivalents of OH^- added, plus the milliequivalents of hydrogen ion in solution at equilibrium, minus the milliequivalents of deprotonized H_3PO_4.

Calculations and Interpretation of Thermochemical Results

The standard heat of partial exchange, ΔH°_x, may be defined as the heat involved in the exchange

$$H_2Zn_s^{H}H_2O(s) + \infty H_2O + 2X\text{NaCl (aq)} \longrightarrow Na_{2X}H_{2-2X}Zn_s^{M}H_2O(s) + (\infty + n_s^{H} - n_s^{M})H_2O + 2X\text{HCl (aq)} \quad (1)$$

where Z represents one formula weight of the anionic framework of the exchanger.

In this equation one formula weight of mixed exchanger containing $2X$ equivalents of Na^+ is formed from 1 mol of zirconium phosphate in its pure hydrogen form. All reactants and products are in their standard states, *i.e.*, the mixed exchanger is in equilibrium with an infinitely dilute (∞H_2O) solution of NaCl and HCl in their correct proportions to maintain the composition of the exchanger while the exchangers in pure hydrogen, H_2Z, and pure sodium, Na_2Z, forms are in equilibrium with infinitely dilute solutions of HCl and NaCl, respectively. n_s^H denotes the number of moles of water in one formula weight of H_2Z; n_s^M denotes this number in the mixed exchanger. When $X = 1$, we obtain the standard heat of complete exchange, ΔH°.

The experimentally measured heats do not correspond with either ΔH° or ΔH°_x since sodium hydroxide was used in order to neutralize the HCl and thus achieve as high a sodium ion loading as possible. The actual reaction taking place can be written

$$H_2Zn_s^{H(v)}H_2O(s) + 2N\text{NaCl (aq)} + 2Y\text{NaOH (aq)} + VH_2O \longrightarrow Na_{2X}H_{2-2X}Zn_s^{M'}H_2O(s) + (V + n_s^{H(v)} - n_s^{M'} + 2Y)H_2O + 2(N - X + Y)\text{NaCl (aq)} + 2(X - Y)\text{HCl (aq)} \quad (2)$$

where $n_s^{H(v)}$ and $n_s^{M'}$ are the numbers of moles of water in one formula weight of exchanger before and after the exchange, respectively.

The heat content, H'_{liq}, of the reactant solution in the calorimeter containing $2N$ moles of NaCl and $2Y$ moles of NaOH in V moles of water is

$$H'_{liq} = 2N\Phi^{M'}_{NaCl} + 2Y\Phi^{M'}_{NaOH} + VH^\circ_s \quad (3)$$

where $\Phi^{M'}_{NaCl}$ is the apparent molar heat content of NaCl at a molality M'_{NaCl}, $\Phi^{M'}_{NaOH}$ the same quantity for NaOH at a *molality* M'_{NaOH} and H°_s the standard heat content of water at 1 atm and 25°. In eq 3 the apparent molar heat contents of the components in the mixture are assumed equal to those of the unmixed components at the same ionic strength (Young's rule).[19]

In the same way the heat content H''_{liq} of the resultant solution after exchange is given by

$$H''_{liq} = 2(N - X + Y)\Phi^{M''}_{NaCl} + 2(X - Y)\Phi^{M''}_{HCl} + (V + n_s^{H(v)} - n_s^{M'} + 2Y)H^\circ_s \quad (4)$$

where M''_{NaCl} and M''_{HCl} are the molalities of NaCl and HCl, respectively, after the reaction is completed.

The heat content, $H^\circ_{H_2Z}$, of one formula weight of exchanger in the standard state (immersed in water at 25°) is

$$H^\circ_{H_2Z} = \Phi^\circ_{H_2Z} + n_s{}^H H^\circ_s \quad (5)$$

Before reaction the exchanger (0.1–0.3 g) is in contact with 0.5–0.8 ml of 0.1 M NaCl in an ampoule. The heat content, $H^v_{H_2Z}$, of one formula weight of exchanger in the ampoule can be written

$$H^v_{H_2Z} = \Phi^\circ_{H_2Z} + n_s{}^{H(v)} H^\circ_s \quad (6)$$

However, breaking of ampoules with exchanger + 0.1 M NaCl (H_2O) in 100 ml of H_2O gave no measurable heat effects. This means that

$$H^\circ_{H_2Z} \cong H^v_{H_2Z} \quad (7)$$

The heat content, $H^\circ_{(Na,H)Z}$, of one formula weight of mixed exchanger in its standard state is

$$H^\circ_{(Na,H)Z} = \Phi^\circ_{(Na,H)Z} + n_s{}^M H^\circ_s \quad (8)$$

The heat content, $H^{M'}_{(Na,H)Z}$, of one formula weight of mixed exchanger after reaction was written

$$H^{M'}_{(Na,H)Z} = \Phi^\circ_{(Na,H)Z} + n_s{}^{M'} H^\circ_s \quad (9)$$

Here also tests showed that breaking of ampoules, containing partially exchanged zirconium phosphate and 0.5 ml of H_2O, in a solution containing the correct equilibrium ratio of the two ions in the exchanger gives negligible heat effects. Thus we can assume

$$H^\circ_{(Na,H)Z} \cong H^{M'}_{(Na,H)Z} \quad (10)$$

If the heat content of reactants in eq 2 is H_R and that of products H_P then the heat of exchange, ΔH_X, corresponding to an amount of reaction involving one formula weight of exchanger is

$$\Delta H_X = H_P - H_R \quad (11)$$

where

$$H_P = H^{M'}_{(Na,H)Z} + H''_{liq} \quad (12)$$

and

$$H_R = H^v_{H_2Z} + H'_{liq} \quad (13)$$

Inserting the results of eq 3–5, 7, 8, 10, 12, and 13 into eq 11 gives

$$\Delta H_X = \Phi^\circ_{(Na,H)Z} - \Phi^\circ_{H_2Z} + 2(N - X + Y)\Phi^{M''}_{NaCl} + 2(X - Y)\Phi^{M''}_{HCl} - 2Y\Phi^{M'}_{NaOH} + 2YH^\circ_s - 2N'_{NaCl} \quad (14)$$

In eq 14 $X \cong Y$ (in many cases $X = Y$) and $N \gg X, Y$. Thus $(N - X + Y)$ can be set equal to N with very good approximation. This implies that $\Phi^{M''}_{NaCl} \cong \Phi^{M}_{NaCl}$ and inserting this result in eq 14 yields

$$\Delta H_X = \Phi^\circ_{(Na,H)Z} - \Phi^\circ_{H_2Z} + 2(X - Y)\Phi^{M''}_{NaCl} + 2(X - Y)\Phi^{M''}_{HCl} - 2Y\Phi^{M'}_{NaOH} + 2YH^\circ_s \quad (15)$$

The neutralization reaction between NaOH and HCl at infinite dilution can be written

$$NaOH(\infty) + HCl(\infty) \longrightarrow H_2O + NaCl(\infty) \quad (16)$$

The heat of this reaction, ΔH°_N, is given by

$$\Delta H^\circ_N = H^\circ_s + \Phi^\circ_{NaCl} - \Phi^\circ_{NaOH} - \Phi^\circ_{HCl} \quad (17)$$

where Φ°_{NaCl}, Φ°_{NaOH}, and Φ°_{HCl} are the apparent molar heat contents at infinite dilution of NaCl, NaOH, and HCl, respectively.

The standard heat of partial exchange, ΔH°_X, for reaction 1 can be shown to be

$$\Delta H^\circ_X = \Phi^\circ_{(Na,H)Z} - \Phi^\circ_{H_2Z} + 2X\Phi^\circ_{HCl} - 2X\Phi^\circ_{NaCl} \quad (18)$$

Combination of eq 15, 17, and 18 gives

$$\Delta H_X - 2Y\Delta H^\circ_N - \Delta H^\circ_X = 2(X - Y)(\Phi^{M''}_{HCl} - \Phi^\circ_{HCl}) - 2(X - Y)(\Phi^{M''}_{NaCl} - \Phi^\circ_{NaCl}) - 2Y(\Phi^{M'}_{NaOH} - \Phi^\circ_{NaOH}) \quad (19)$$

The function $(\Phi^{M''}_{HCl} - \Phi^\circ_{HCl})$ is the relative apparent molar heat content, $\Phi_L(M''_{HCl})$, of HCl at a molality M''_{HCl} at 1 atm and 25°, and similarly for NaCl and NaOH. Making these substitutions into eq 19 and rearranging gives

$$\Delta H^\circ_X = \Delta H_X - 2Y\Delta H^\circ_N - 2(X - Y)\Phi_L(M''_{HCl}) + 2(X - Y)\Phi_L(M''_{NaCl}) + 2Y\Phi_L M'_{NaOH} \quad (20)$$

Thus from experimentally determined values of ΔH_X it is possible to obtain ΔH°_X since the relative apparent molar heat contents of the components are tabulated,[20] and as ΔH°_N the heat of neutralization at 25° and at infinite dilution has been thoroughly established.[21,22] The "best" value of ΔH°_N seems to be -13.34 kcal mol^{-1}.

In the determination of ΔH_X heat effects due to phosphate release had to be considered. In the ampoules where the pH was between 3 and 4 nearly all the phosphate in solution is in the form of $H_2PO_4^-$. This means that the hydrolysis reactions taking place at the ampoule breaking are either

$$H_2PO_4^- + H_2O \longrightarrow HPO_4^{2-} + H_3O^+ \quad (21)$$

or

$$H_2PO_4^- + H_3O^+ \longrightarrow H_3PO_4 + H_2O \quad (22)$$

The enthalpy changes for these two reactions have been found to be 0.8 and 1.9 kcal mol^{-1}, respectively.[23] As the amounts of the different phosphate species in the solutions (after reaction) are determined we are able to make calculations and thus corrections for heat effects due to these reactions. For crystalline α-ZrP there was no phosphate release and for sample 4.5:48 the corrections were all quite negligible. Even for sample 0.5:48 the correction terms were in most cases within the experimental errors and they were in no case larger than 0.035 cal.

The ΔH_X values were subsequently calculated by dividing the corrected heat effects, *i.e.*, the measured heat effects corrected for heat effects due to phosphate release, by the amount of water free exchanger.

The sum of the three last terms in eq 20 made only small positive contributions to ΔH°_X and never exceeded 0.09 kcal mol^{-1}. The term $2Y\Delta H^\circ_N$, on the other hand, is significantly large. As, however, both the amount of base added, $2Y$, and the value of ΔH°_N are known with high accuracy, this correction should not noticably affect the precision of the value of ΔH°_X. This is corroborated by the fact that points at low sodium loadings, where no base was added, fit well to the same curves as points at higher sodium loadings where base addition was required (see Figures 1–3).

The mole fraction of sodium ion in the exchanger, $\bar{X}_{Na}$, has been calculated by dividing the hydrogen ion released by the theoretical exchange capacity of zirconium phosphate, 7.54 mequiv/g, based on anhydrous ZrP, *i.e.*, ZrP_2O_7. This procedure is justified since it has been found previously that sodium exchange on α-ZrP is a perfect ion

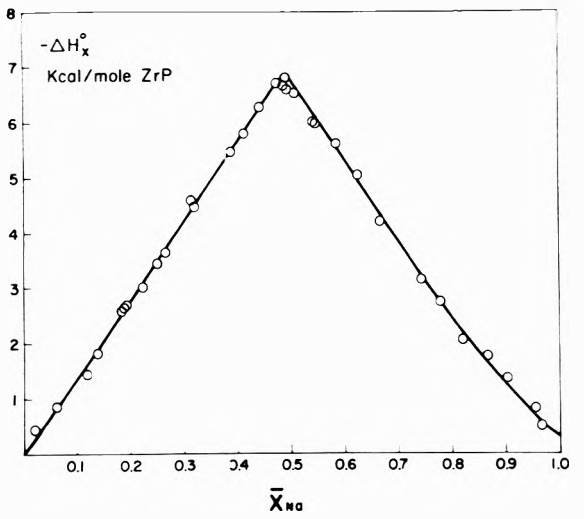

Figure 1. Standard heats of partial exchange as a function of sodium ion loading for crystalline α-ZrP.

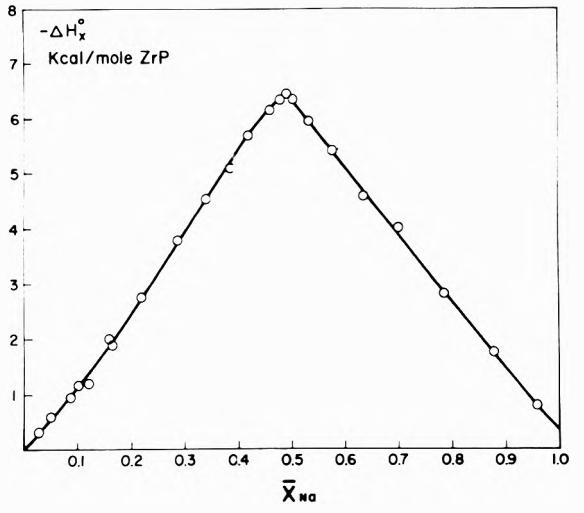

Figure 2. Standard heats of partial exchange as a function of sodium ion content for semicrystalline α-ZrP (4.5:48).

exchange, *i.e.*, the sodium uptake and the hydrogen release are equal.[5]

For crystalline and amorphous (0.5:48) α-ZrP the sodium exchange has been shown to be reversible.[5,12] Corrected selectivity coefficients have been determined as functions of the extent of exchange. From these data thermodynamic equilibrium constants have subsequently been calculated. In these cases it is possible to gain information about the dependence of the heats and entropies of exchange on the composition of the exchanger from the differential free energies, heats, and entropies. The differential free energy, $\Delta\bar{G}_X$, is obtained from the corrected selectivity coefficient, K_H^{Na}, by the relation

$$-\Delta\bar{G}_X = RT \ln K_H^{Na} \quad (23)$$

The differential heat of exchange, $\Delta\bar{H}_X$, is obtained from

$$\Delta\bar{H}_X = (\Delta H^\circ_X)/\delta X \quad (24)$$

finally from the relation

$$\Delta\bar{G}_X = \Delta\bar{H}_X - T\Delta\bar{S}_X \quad (25)$$

it is possible to calculate the differential entropy of exchange, ΔS_X.

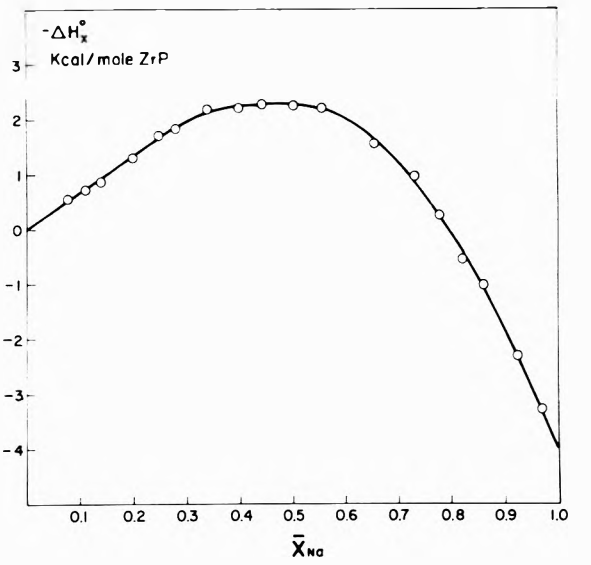

Figure 3. Standard heats of partial exchange as a function of sodium ion loading for an almost amorphous α-ZrP (0.5:48).

Standard free energies, heats, and entropies of full exchange were calculated from the corresponding thermodynamic equilibrium constants and the data of Figures 1 and 3. These values, collected in Table I, are given in kcal per mole of Na^+ while ΔH°_X are given in kcal per mole of exchanger. This means that the mole ratio sodium–exchanger had to be considered for the evaluation of the standard heats of full exchange from the ΔH°_X curves.

Results

Crystalline Sample. ΔH°_X for sodium exchange on crystalline α-ZrP plotted as a function of $\bar{X}_{Na}$, Figure 1, show unambigously, in agreement with earlier theories,[12,13] that the reaction proceeds in two distinct and separate steps. The first step, going from 0 to 50% of exchange, is exothermic while the second one, from half to full exchange, is endothermic. The interception of the two almost linear parts of the curve in Figure 1 is not exactly at $\bar{X}_{Na} = 0.500$ but rather at $\bar{X}_{Na} = 0.490$ indicating that the real exchange capacity for this ZrP is a little lower (*ca.* 2%) than the theoretical one. As there are two distinct steps upon exchange it is thermodynamically justified to treat them separately.

It has previously been shown that the exchange reaction from 0 to 50% of exchange exhibits microscopic reversibility,[12] thus allowing equilibrium expressions to be formulated. The differential quantities of exchange, expressed in kcal per mole of Na^+, for the first stage are plotted in Figure 4. For calculation of $\Delta\bar{G}_X$ from eq 23 corrected selectivity coefficients from Figure 3 in ref 12 were used. The $\Delta\bar{H}_X$ values were calculated, by eq 24 from data in Figure 1, assuming that the first exchange step is completed at $\bar{X}_{Na} = 0.49$, *i.e.*, $\bar{X}_{Na} = 1.00$ in Figure 4 corresponds to $\bar{X}_{Na} = 0.49$ in Figure 1. It should be recognized that for this reaction the mole ratio exchanger:sodium ions is 1:1. The results in Figure 4 show that the differential heats of exchange are independent of composition. The small smooth increase in $-\Delta\bar{G}_X$ during the exchange is caused by a similar increase in $T\Delta\bar{S}_X$. The standard integral functions of exchange are given in Table I. From the results it may be observed that the agreement between our ΔH° value and the corresponding one determined earlier by the temperature coefficient method

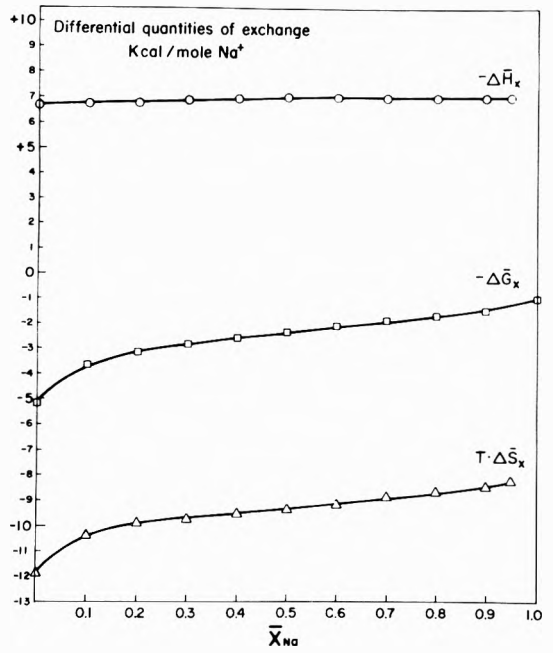

Figure 4. Differential thermodynamic quantities of exchange as a function of sodium ion loading for the first 50% of exchange of crystalline α-ZrP.

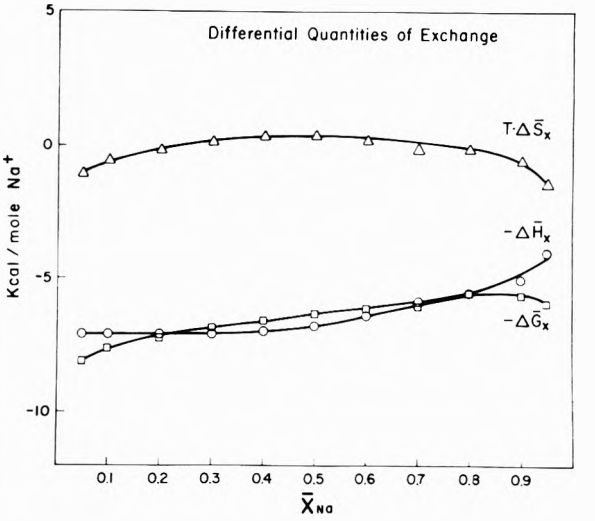

Figure 5. Differential thermodynamic quantities of exchange as a function of sodium ion loading for the second 50% of exchange on crystalline α-ZrP.

(-5.88 kcal mol^{-1}) is very good, considering the uncertainty in the latter method.

Results for the second stage, 50 to 100% of exchange, are collected in Figures 1, 5, and Table I. This stage was assumed to take place between $\bar{X}_{Na} = 0.49$ and $\bar{X}_{Na} = 0.98$. The standard integral heat of exchange was consequently obtained from $(\Delta H^\circ_{0.98} - \Delta H^\circ_{0.49})$, since the mole ratio exchanger:sodium is 1:1 for this reaction step also. The differential heats of exchange are independent of composition up to $\bar{X}_{Na} = 0.5$. The small and smooth increase in $-\Delta\bar{H}_X$ at higher loadings does not indicate any drastic structural change of the exchanger.

Sample 4.5:48. The heat of exchange for this sample, characterized as semicrystalline,[5] is strikingly similar to that for crystalline α-ZrP (compare Figures 1 and 2). Even for this ZrP the ΔH°_X function, consisting of two approximately linear parts, exhibits a definite break at half-exchange, $\bar{X}_{Na} = 0.49$, indicative of two distinct exchange reactions. The linearity of ΔH°_X means that the heat changes upon exchange are independent of exchanger composition (within each step) just as was the case for the crystalline sample.

A comparison between Figures 1 and 2 shows that for the first step the crystalline sample exhibits slightly higher exothermic values than the semicrystalline. Thus at half-exchange the difference is *ca.* 0.5 kcal mol^{-1}. At full exchange, on the other hand, the values of ΔH°_X for the two samples are essentially the same (-0.45 kcal mol^{-1}). Consequently during the second step the exchange reaction on the crystalline sample is a little more endothermic than the exchange on the semicrystalline one. Under the assumption that exchange with sample 4.5:48 also exhibits microscopic reversibility we can treat the exchange data in a similar fashion as for crystalline α-ZrP and make a comparison of the thermodynamic functions of sodium ion exchange on the two different exchangers. Up to half-exchange the Na^+–H^+ selectivity decreases slightly when going from a crystalline to a semicrystalline sample.[5] Thus on graphs where pH is plotted *vs.* sodium ion uptake, the first plateau is about 0.5 pH units higher for sample 4.5:48 than for crystalline α-ZrP. Remembering that the experiments were performed at constant sodium ion concentration in the solutions we can conclude that the free-energy change upon exchange is a little lower for the latter exchanger. The difference, however, is small (<1 kcal mol^{-1}). It is evidently of the same sign and moreover of the same size as the difference in the heats of exchange on the two samples. Consequently up to half exchange the entropy changes for the sodium ion exchange on the two exchangers are much the same despite the relatively large difference in crystallinity.

From half to full exchange the pH values (at least in the beginning of the step) are a little lower for sodium ion exchange on sample 4.5:48 than those for crystalline α-ZrP. Thus the Na^+–H^+ selectivity is higher and the free energy less positive for the exchange on sample 4.5:48. The difference is again roughly accounted for by the difference in heats of exchange on the two exchangers. Thus even for the second step the two exchangers virtually give entropy changes of much the same magnitude.

Sample 0.5:48. The ΔH°_X function for this almost amorphous ZrP, Figure 3, is significantly different from those of the two more crystalline ones. In this instance two distinct steps were not observed but rather a smooth curve throughout. In the beginning of the curve, up to $\bar{X}_{Na} = 0.25$, ΔH°_X is virtually a linear function of the load. Then the heat function passes through a broad maximum from $\bar{X}_{Na} = 0.35$ to $\bar{X}_{Na} = 0.55$ and then the reaction exhibits a progressively increasing endothermicity. Since this gel exhibits a comparatively high sodium ion selectivity at low loads it was possible to reach a sodium ion loading of *ca.* 1.2 mequiv g^{-1} ($\bar{X}_{Na} = 0.15$) without addition of base. The data at high loadings are somewhat less accurate because the exchange reactions are slower. Thus the attainment of equilibrium required up to 25 min when $\bar{X}_{Na} > 0.6$. This made the graphical evaluation of the heat changes from the resistance–time diagrams a little more uncertain because of the lengthy extrapolations. Moreover the increase of phosphate release at higher sodium loadings contributed to larger corrections in the calculation of the sodium ion uptake. The differential free energies of exchange were calculated by eq 23 from corrected selectivity coefficients determined in a previous

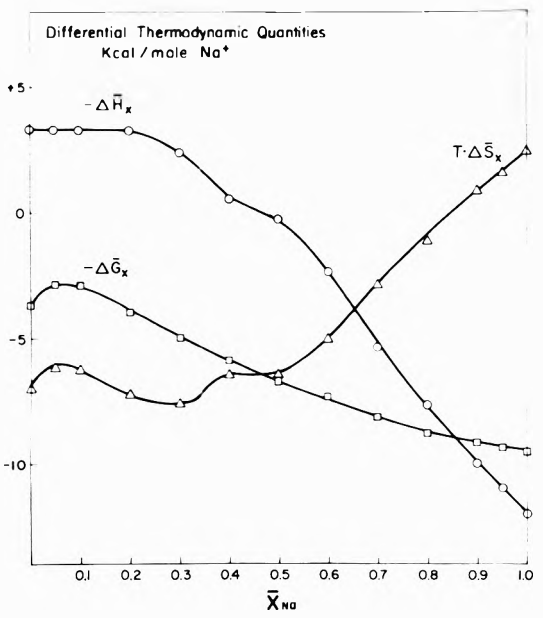

Figure 6. Differential thermodynamic quantities of exchange as a function of sodium ion for exchanger 0.5:48

study of this system.[5] The differential quantities are plotted in Figure 6. It is to be remembered that for this exchange there are 2 mol of Na^+ per mole of exchanger. In the beginning of the exchange both $\Delta\bar{H}_X$ and $T\Delta\bar{S}_X$ exhibit small variations with the extent of exchange. At higher loadings, however, the increasing endothermicity of the reaction is not fully counterbalanced by the progressively more favorable entropy term, causing a gradual decrease in the preference for sodium ions. The standard integral functions are collected in Table I, where it can be seen that both the enthalpy and the entropy terms counteract the exchange reaction.

Discussion

The entropy change for a cation exchange (univalent cation, M^-) reaction on an exchanger in the hydrogen form can be written[24]

$$\Delta S^\circ = \overline{\Delta S_{EX}} + (S^\circ_H - S^\circ_M) \qquad (26)$$

where ΔS°_{EX} represents the entropy differences between the corresponding ionic forms of the exchanger and $(S^\circ_H - S^\circ_M)$ the difference in the entropies of hydration of the exchanging ions. Values of $\Delta\bar{S}_{EX}$ reflect (i) changes in hydration of the exchanger accompanying the reaction and (ii) the differences in lattice distortion of the two forms of the exchanger.

The value of the difference $(S^\circ_H - S^\circ_M)$ refers to the entropy change, $\Delta S^\circ_{con,h}$, of the hypothetical exchange reaction

$$H^+(g) + M^+(aq) \longrightarrow H^+(aq) + M^+(g) \qquad (27)$$

For sodium $\Delta S^\circ_{con,h} = -5.1$ eu.[25]

The entropy changes of the two reaction steps in the sodium ion exchange on crystalline α-ZrP are listed in Table I as well as the calculated $\Delta\bar{S}_{EX}$ values. A rationale for the large differences in entropy for the two exchange steps can be given.

The different phases occurring in the sodium exchange on crystalline α-ZrP have been characterized in previous investigations.[13,26] In the first reaction step the crystals of composition $Zr(HPO_4)_2\cdot H_2O$ are converted to $Zr(NaPO_4)(HPO_4)\cdot 5H_2O$. In the second reaction stage the half-exchanged phase is converted to $Zr(NaPO_4)_2\cdot 3H_2O$. The degrees of freedom possessed by water molecules are lower in the ion exchanger phase than in the solution phase. Thus sorption of water must result in a decrease in entropy while release of water results in an entropy increase. In the sodium exchange on α-ZrP there are an additional 4 mol of water bound to the exchanger during the first reaction step. Consequently this should make a large negative contribution to $\Delta\bar{S}_{EX}$. A noteworthy comparison can be made with the entropy decrease accompanying the "binding" of water on freezing. The entropy of fusion of ice at 25° is 6.07 eu. Thus the freezing of 4 mol of water will rise to an entropy decrease of *ca.* 24.2 eu. This value is surprisingly very close to our value of $-\Delta\bar{S}_{EX} = 25.9$ eu. It is to be remembered, however, that the expansion of the layers from 7.6 to 11.8 Å during the reaction step probably will give a small positive contribution to $\Delta\bar{S}_{EX}$.

In the second step there is a release of 2 mol of water from the exchanger. Consequently it is to be expected that $\Delta\bar{S}_{EX}$ is positive. If it is again assumed that an entropy increase of 6 eu per mole of released water obtains, we should anticipate a contribution to $\Delta\bar{S}_{EX}$ of *ca.* 12 eu from hydration effects. This value is a little more positive than the value found. However, a difference is to be expected since the distance between the layers in the exchanger decreases from 11.8 to 9.8 Å during this reaction step. The final phase has a highly ordered structure judging by analogy with the NH_4^+ exchanged phase.[27] This tightening of the structure should give a small entropy decrease.

An interpretation of the entropy changes accompanying sodium ion exchange on gel 0.5:48 is more complicated as this function shows large variations with the extent of exchange. Furthermore the phase(s) present during exchange are not well characterized but appear(s) to be a single solid solution with large interlayer spacing at low load which decreases with loading.[5] Up to half-exchange $T\Delta\bar{S}_X$ fluctuates about an average value of *ca.* −6.5 kcal mol^{-1} (see Figure 6). This means that $\Delta\bar{S}_X$ is equal to about −22 eu and $\Delta S_{EX} = -17$ eu. This negative entropy change can be partly explained by the fact that upon sodium exchange on gel 0.5:48 the water content in the exchanger increases in the beginning of the exchange.[5] Thus the unexchanged gel has been found to contain 5.0 mol of water per mole exchanger, while the corresponding value is 5.5 at a loading of 0.6 mequiv g^{-1}.

At higher sodium loadings, on the other hand, the water content in the exchanger decreases. It was found that at a loading of 6.0 mequiv g^{-1} there are 5.3 mol of water per formula weight of exchanger. Thus there is a fairly small net decrease (0.2 mol of water per formula weight of exchanger) in going from a loading of 0.6 to 6.0 mequiv/g. Despite this there is a remarkable increase in entropy (see Figure 6) at loadings above 50% of exchange. However, it is probable that a distinction between "free" water and "bound" water within the gel can be made. Such distinctions have been made for organic resins.[28] There is a difference in entropy between these two kinds of water, the entropy of free water being higher than that of bound water. For the amorphous gel 0.5:48 where the water content is high at all loadings, the amount of free water in the exchanger can be of considerable magnitude. As the hydration number for the smaller hydrogen ion is much higher than the hydration number for the sodium ion,[25,28] sodium exchange at approximately constant water contents of the exchanger should be accompanied by an in-

crease in free water and a decrease in hydrated water. This process should consequently give rise to an entropy increase large enough to account for the observed change. However, it is not known how much of the exchangeable hydrogen is present as hydrated ions in the gel, although it has been proposed that the amount is considerable to bring about the swelling observed on wetting the dried gels.[5]

Another factor contributing to the entropy increase is the disordering of the gel structure as evidenced by the high phosphate release observed at higher Na^+ loadings.

In contrast to entropy changes which, as seen above, in many cases can be approximated semiquantitatively by the model set up, enthalpy changes are more difficult to predict because of the large magnitude of bonding energies and heats of hydration. The heat of hydration of H^+ ion is more exothermic than that of the larger Na^+ ion. This is illustrated by the hypothetical exchange reaction of eq 27 for which $\Delta H^\circ = -163.8$ kcal mol^{-1} when $M^+ = Na^+$.

This high value of hydration energy must be counterbalanced by a comparable endothermic change resulting from the bond breaking-bond making or various electrostatic interactions resulting from the ion-exchange reaction. In the case of the α-ZrP crystals each replacable hydrogen atom is closely associated with one oxygen atom (probably through a covalent bond), whereas the sodium ions probably are distributed or shared among several anionic sites.[27] This corresponds to an anionic field strength which would be weak for Na^+ and strong for hydrogen.[29] Thus a large endothermic effect is to be expected. Assuming this effect is nearly the same in both halves of the ion-exchange reaction, the difference in enthalpies for the two reactions can be accounted for as being mainly a hydration effect. In the first step a five hydrate is formed so that the sodium ions within the crystal lattice must be fully hydrated. In the second step the five hydrate is converted to a three hydrate or 1.5 waters per sodium ion are available for hydration. This means that ΔH° for the first step should be more exothermic than that for the second in agreement with observation. However, other factors such as expanding or shrinking of the layers also might give rise to heat effects and should be considered.

It has been shown previously[5] that, in general, the less crystalline the sample of zirconium phosphate the greater is its relative preference for sodium ion at low loads. However, this preference decreases with loading and eventually is reversed. In the case of gel 0.5:48 K_c, the corrected rational selectivity coefficient, varies from approximately 10^{-2} at low loads to 10^{-6} near full load. This large decrease is now seen to result from a comparable increase in the endothermicity of the exchange reaction with sodium ion uptake. Increased sodium ion uptake in 0.5:48 is accompanied by a steady decrease in the interlayer spacing. Thus at higher levels of exchange the sodium ions are forced closer to each other setting up increasingly larger electrostatic repulsions.

In the hydrogen form of α-ZrP crystals the layers form a network of zeolite-like cavities.[30] There is one such cavity per zirconium atom. Thus, at half-exchange each cavity contains one sodium ion. Further exchange requires that a second ion enter the cavities. The sodium–sodium distance at half-exchange is about 5.3 Å whereas in the fully exchanged form this distance is of the order of 3.8 Å (judging from the structure of the NH_4^+ exchanged form[27]). The large change in differential heat of exchange which occurs at half-exchange may well be the result of increased electrostatic repulsions coupled with the lesser hydration.

It has been proposed that the size of the cavities in gel and semicrystalline samples of zirconium phosphate is not uniform as in the crystals, but varies over a range of values.[3] Thus the exchange sites are not energetically equivalent. The incoming ions would thus occupy the most favorable sites initially, *i.e.*, probably the largest cavities because these would require little or no dehydration of the ions to occur. As exchange proceeds the sites become progressively less favorable because of the greater dehydration and larger electrostatic repulsions resulting from two sodium ions occupying successively less space. This could account for the rather large increase in $\Delta \bar{H}_X$ observed for the exchange reaction on 0.5:48.

References and Notes

(1) (a) This work is part of a cooperative research program jointly sponsored by the National Science Foundation and the Swedish Natural Science Research Council. The Swedish portion is under the direction of Professor Sten Ahrland, Lund University, Lund, Sweden. The present work was supported by NSF Grant No. GP-8108. (b) Post-doctoral Fulbright Fellow, Lund University, Lund, Sweden.
(2) V. Veseley and V. Pekarek, *Talanta*, 19, 219 (1972).
(3) A. Clearfield, G. H. Nancollas, and R. H. Blessing, "Ion Exchange and Solvent Extraction," Vol. 5, J. A. Marinsky and Y. Marcus, Ed., Marcel Dekker, New York, N. Y., 1973, pp 1–120.
(4) A. Clearfield and J. A. Stynes, *J. Inorg. Nucl. Chem.*, **26**, 117 (1964).
(5) A. Clearfield, A. Oskarsson, and C. Oskarsson, *Ion Exch. Membranes*, 1, 91 (1972).
(6) J. Albertsson, *Acta Chem. Scand.*, **20**, 1689 (1966).
(7) S. Ahrland and J. Albertsson, *Acta Chem. Scand.*, **18**, 1861 (1964).
(8) C. B. Amphlett, P. Eaton, L. A. McDonald, and A. J. Miller, *J. Inorg. Nucl. Chem.*, **26**, 297 (1964).
(9) J. P. Harkin, G. H. Nancollas, and R. Paterson, *J. Inorg. Nucl. Chem.*, **26**, 306 (1964).
(10) G. H. Nancollas and B. V. K. S. R. A. Tilak, *J. Inorg. Nucl. Chem.*, **31**, 3643 (1969).
(11) E. M. Larsen and D. R. Vissers, *J. Phys. Chem.*, **64**, 1730 (1960).
(12) A. Clearfield and A. S. Medina, *J. Phys. Chem.*, **75**, 3750 (1971).
(13) A. Clearfield, W. L. Duax, A. S. Medina, G. D. Smith, and J. R. Thomas, *J. Phys. Chem.*, **73**, 3424 (1969).
(14) S. Sunner and I. Wadso, *Sci. Tools*, **13**, 1 (1966).
(15) I. Wadso, *Sci. Tools*, **13**, 33 (1966).
(16) R. J. Irwing and I. Wadso, *Acta. Chem. Scand.*, **18**, 195 (1964).
(17) J. O. Hill, G. Ojelund, and I. Wadso, *J. Chem. Thermodyn.*, **1**, 11 (1969).
(18) J. Berrum, G. Schwarzenbach, and L. G. Sillen, "Stability Constants," The Chemical Society, London, Burlington House, 1964.
(19) T. F. Young, Y. C. Wu, and A. A. Krawetz, *Discuss. Faraday Soc.*, **34**, 37 (1957).
(20) H. S. Harned and B. B. Owen, "Physical Chemistry of Electrolyte Solutions," Reinhold, New York, N. Y., 1957, p 707.
(21) I. Grenthe, H. Ots, and O. Ginstrup, *Acta Chem. Scand.*, **24**, 1067 (1970).
(22) J. D. Hale, R. M. Izatt, and J. J. Christensen, *J. Phys. Chem.*, **67**, 2605 (1963).
(23) K. S. Pitzer, *J. Amer. Chem. Soc.*, **59**, 2365 (1937).
(24) H. S. Sherry, "Ion Exchange," Vol. II, Marcel Dekker, New York, N. Y., 1968.
(25) D. R. Rosseinsky, *Chem. Rev.*, **65**, 467 (1965).
(26) A. Clearfield and A. S. Medina, *J. Inorg. Nucl. Chem.*, **32**, 2775 (1970).
(27) A. Clearfield and J. M. Troup, *J. Phys. Chem.*, **77**, 243 (1973).
(28) F. Helfferich, "Ion Exchange," McGraw-Hill, New York, N. Y., 1962, pp 104 and 106.
(29) G. Eisenman, "Glass Electrodes for Hydrogen and Other Cations," Marcel Dekker, New York, N. Y., 1967, pp 70–75.
(30) A. Clearfield and G. D. Smith, *Inorg. Chem.*, **8**, 431 (1969).

Pulse Radiolytic Polarography. Competitive Oxidation and Reduction of Hydroxycyclohexadienyl Radicals at the Mercury Drop Electrode in Aqueous Solutions

K. M. Bansal and A. Henglein*

Hahn-Meitner-Institut fur Kernforschung Berlin GmbH, Bereich Strahlenchemie, 1 Berlin 39 *(Received April 9, 1973; Revised Manuscript Received June 28, 1973)*

Publication costs assisted by the Hahn-Meitner-Institut fur Kernforschung

Hydroxycyclohexadienyl radicals are produced in the pulse irradiation of aqueous N_2O-saturated solutions of aromatic compounds by a 20-nsec pulse of high-energy electrons in the vicinity of a hanging mercury drop electrode. The polarographic current is recorded as a function of time and at constant potential. Simultaneously, the changes in the optical absorption of the radicals with time in the bulk of solution are measured. Short-time polarograms of radicals are obtained by plotting the current at about 20 μsec after the pulse *vs.* the electrode potential. Many hydroxycyclohexadienyl radicals show a steep polarographic wave with an anodic part immediately followed by a cathodic part. These waves are interpreted in terms of competitive oxidation and reduction of radicals. In addition, the problem of disproportionation of hydroxycyclohexadienyl radicals *via* electron transfer is discussed. Both electrode processes can occur with large rate constants in a certain potential range. Shifts of the waves to more negative potentials in the case of phenol and cresol are explained by the existence of mesomeric structures of α-alcohol radicals in the dihydroxycyclohexadienyl radicals formed. In strongly alkaline solutions, O^- reacts with toluene and benzylalcohol to form the benzyl radical and the benzyl alcohol radical anion, respectively. The polarograms of these radicals have well separated anodic and cathodic waves. The current *vs.* time curve of some radicals show a change in the sign of the current signal at potentials close to the foot of the polarographic wave. This effect is attributed to temporary changes in the relative concentrations of adsorbed and mobile radicals in the vicinity of the mercury drop electrode.

I. Introduction

The oxidation and reduction of short-lived free radicals at a mercury drop electrode has already been described.[1-3] Radicals are produced in homogeneous distribution near the drop by irradiation of an aqueous solution with a 20-nsec pulse of high-energy electrons and their polarographic current is then measured as a function of time in the micro- to millisecond range. Simultaneously, the optical absorption as a function of time is measured. The "short time polarogram" of a radical is constructed by plotting the current at 20 μsec after the pulse *vs.* the potential of the electrode.

These polarograms are characteristic for the various types of radicals. Most of the waves are totally irreversible since the products of oxidation or reduction of many radicals (such as carbonium or carbanions) rapidly undergo reactions with the aqueous solvent before their back reactions at the electrode can occur. At a given potential, a radical may be oxidized as well as reduced (as in reactions 1a and 1b, where P = product). Radicals are often more

$$\mathrm{R\cdot} \xrightarrow{k_a} \mathrm{R^+} \xrightarrow{\mathrm{H_2O}} \mathrm{P + OH^+} \quad (1a)$$

$$\mathrm{R\cdot} \xrightarrow{k_c} \mathrm{R^-} \xrightarrow{\mathrm{H_2O}} \mathrm{RH + OH^-} \quad (1b)$$

apt to undergo oxidation and reduction with comparable rates in a certain potential range than stable organic molecules which have hitherto mainly been investigated by conventional polarography. The current observed will, therefore, be the result of the superposition of the cathodic and anodic currents i_c and i_a which are determined by the respective rate constants k_c and k_a. If $k_c > k_a$, a net cathodic current will be observed; if $k_c < k_a$, an anodic current will be recorded.

In certain cases, the anodic wave is well separated from the cathodic wave; *i.e.*, there exists an intermediate potential range where both k_a and k_c are too small to produce any measurable current. In other cases, the two waves are very close together. It is the purpose of this paper to discuss the competition between oxidation and reduction according to eq 1a and 1b and to interpret the polarograms of a number of radicals that have a system of delocalized electrons from this point of view. It is important to note here that k_a and k_c or i_a and i_c have a different meaning in this work than usually used in electrochemistry. In general, anodic and cathodic currents and their respective rate constants are attributed to the back and forward reactions of the two substances of a redox couple at the electrode. In the present paper, these terms are used to characterize two competing irreversible electrode reactions of one single species.

II. Theoretical Considerations

1. Construction of Irreversible Polarographic Waves. The number of moles of a radical being consumed per unit time and per unit area of the electrode is

$$-\frac{dN}{dt} = (k_c + k_a)c_{(0,t)} \quad (2)$$

where $c_{(0,t)}$ is the concentration of the radical at the distance $x = 0$ from the electrode. The rate constants k_c and k_a characterize the heterogeneous electrode process and are expressed in centimeters per second. The radical is supplied to the electrode by diffusion. The consumption of the radical by chemical reactions can be neglected, if the time of observation is essentially shorter than its first half-life time. A boundary condition is obtained by equat-

ing the rate given by eq 2 to the flux of the radical according to Fick's first law

$$(k_c + k_a)c_{(0,t)} = D\left(\frac{\partial c_{(x,t)}}{\partial x}\right)_{x=0} \quad (3)$$

where D is the diffusion coefficient of R.

One initial condition is $c_{(x,0)} = c^0$ where c^0 is the bulk concentration of the radical immediately after the pulse. Moreover, $c_{(x,t)}$ approaches c^0 for $x \to \infty$. The solution to the problem (where either k_c or k_a is zero) has in principle already been given by Delahay and Strassner[4] and by Evans and Hush.[5] One obtains

$$-\frac{dN}{dt} = \frac{D^{1/2}c^0}{t^{1/2}}\lambda \exp \lambda^2 \operatorname{erfc} \lambda \quad (4)$$

where the dimensionless parameter λ is

$$\lambda = (k_c + k_a)\frac{t^{1/2}}{D^{1/2}} = \lambda_c + \lambda_a \quad (5)$$

t being the time of observation after the pulse and

$$\lambda_c = k_c\frac{t^{1/2}}{D^{1/2}};\ \lambda_a = k_a\frac{t^{1/2}}{D^{1/2}}$$

The cathodic component of the current is

$$i_c = \left|\frac{dN}{dt}\right| nFA\frac{k_c}{k_c + k_a} \quad (6)$$

where A is the surface area of the electrode, $F = 9.65 \times 10^4$ C mol^{-1}, and n is the number of electrons transferred in an elementary electrode process. The anodic component of the current is

$$i_a = -\left|\frac{dN}{dt}\right| nFA\frac{k_a}{k_c + k_a} \quad (7)$$

The observed current $i = i_c + i_a$ is obtained from eq 4, 6, and 7, as

$$i = i_d F(\lambda)\frac{k_c - k_a}{k_c + k_a} = i_d F(\lambda)\frac{\lambda_c - \lambda_a}{\lambda_c + \lambda_a} \quad (8)$$

where $F(\lambda) = \pi^{1/2}\lambda \exp \lambda^2 \operatorname{erfc} \lambda$. $i_d = (nFAD^{1/2}c^0)/(\pi^{1/2} \cdot t^{1/2})$ represents a total discharge current (including oxidation plus reduction) under diffusion controlled conditions, *i.e.*, at values of $F(\lambda)$ close to unity. The function $F(\lambda)$ is shown in the upper left part of Figure 1; it has, for example, been tabulated by Nürnberg.[6] The rate constants k_c and k_a may be expressed as functions of the potential

$$k_c = k_c' e^{-\alpha_c(nF/RT)\epsilon} \quad (9)$$

$$k_a = k_a' e^{\alpha_a(nF/RT)\epsilon} \quad (10)$$

where k_c' and k_a' are preexponential factors and α_c and α_a are transfer coefficients.

Figure 1 shows the construction of the wave for an irreversible cathodic process ($\lambda = \lambda_c$; $\lambda_a = 0$). λ is plotted logarithmically *vs.* the negative potential $-\epsilon$ (full straight line). For a given value of the potential, λ can be read and the corresponding value of $F(\lambda) = i/i_d$ can be formed. i in units of i_d is plotted on a linear scale *vs.* the potential (dashed line). The logarithmic scale for λ was chosen to make $\lambda = 0.03$ coincide with $F(0.03) = 0.06$ on the current scale and also $\lambda = 3.0$ coincide with $F(3.0) = 0.95$. As can be seen, the polarographic wave deviates little from the log λ *vs.* $-\epsilon$ plot over the significant range from $i/i_d = 0.06$ to 0.95 in this kind of presentation.

Figure 2 shows three polarograms for the cases in which the radical can be reduced as well as oxidized. The dashed straight lines are plots of λ_c and λ_a *vs.* the negative potential using the logarithmic scales on the left-hand side. In case A, λ_c and λ_a are quite different at all potentials. λ_c can therefore be neglected in the range where λ_a is large and vice versa. The two waves corresponding to reduction and oxidation can be drawn as described by Figure 1. The observed current as function of the potential shows an anodic wave at less negative potentials, an intermediate range where the current is practically zero since both λ_a and λ_c are too small, and a cathodic wave at more negative potentials. The plateaus of the waves are reached when $F(\lambda_a)$ or $F(\lambda_c)$ are close to unity which is practically the case for $\lambda > 4$.

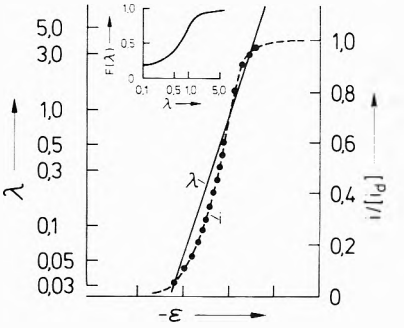

Figure 1. The parameter λ (solid line) and the cathodic current i (dotted line) as functions of the negative potential for a totally irreversible cathodic wave. Upper left: the function $F(\lambda)$ *vs.* λ.

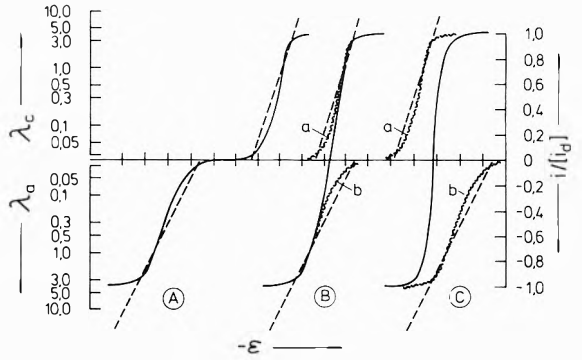

Figure 2. Irreversible polarographic waves in the case of competitive oxidation and reduction (solid lines). Dashed lines: λ_c and λ_a as function of negative potential. Curled lines a and b: theoretical waves for reduction and oxidation if λ_a or λ_c, respectively, is zero. Case A: no overlap of curves a and b; case B: little overlap; case C: strong overlap.

In case B of Figure 2, λ_a and λ_c are comparable over a certain potential range. The curves a and b give the cathodic and anodic waves which would be observed if λ_a or λ_c, respectively, were negligible. These two theoretical waves overlap in a certain potential range. To obtain the true wave, i has to be calculated at a given value of the potential using eq 8. The curve obtained this way (solid line) shows an anodic wave immediately followed by a cathodic wave, the steepness of the curve being larger than that of the single theoretical waves a and b. If such a wave is observed, α_a and α_c cannot be derived because of this complicated superposition of partial cathodic and anodic currents. In case B, the overlap is rather weak; *i.e.*, $\lambda = \lambda_a + \lambda_c$ has rather small values (<3.0) in the range where the observed polarographic curve has its steep increase. Case C in Figure 2 represents a much stronger overlap of the theoretical curves a and b; λ now has large values along the whole polarographic curve; *i.e.*, $F(\lambda)$ in eq 8 is practically equal to unity at all potentials. The resulting polarographic curve again shows an anodic and

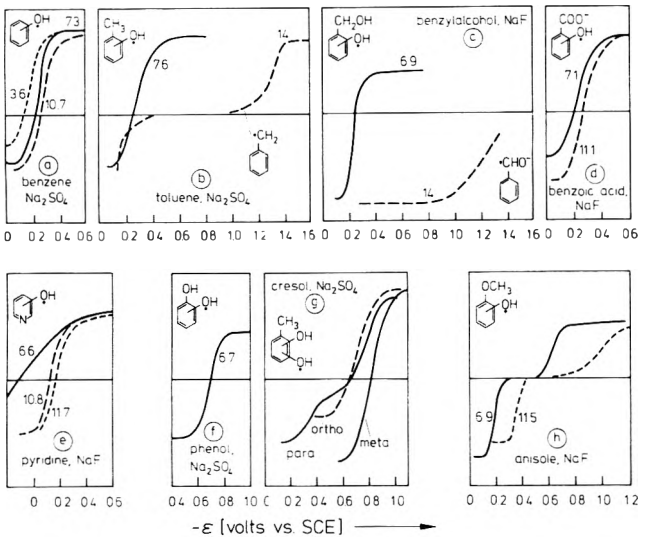

Figure 3. Polarograms 20 μsec after the pulse of various radicals. Signals below the horizontal line correspond to oxidation, signals above the line to reduction. The compounds from which the radicals were formed by OH attack are also given together with the supporting electrolyte. The numbers at the curves give the pH.

immediately following this a cathodic part and the steepness of the curve is even larger than in case B.

2. Adsorption Effects. It was pointed out earlier that the current *vs.* time curves of radicals may show severe distortions if they are measured at the foot of polarographic waves, *i.e.*, at potentials where the rate constant is low.[7,8] These distortions were attributed to the adsorption of radicals at the mercury electrode. If the transfer reaction is very slow, the whole electrode process may be described to occur in two more or less separated steps

$$R \rightleftharpoons R_a \xrightarrow{\pm e} P$$

At first, the adsorption equilibrium at the electrode is established by diffusion of mobile radicals R to the electrode surface and the adsorbed radicals R_a are subsequently reduced or oxidized to give products P. The current *vs.* time curve rises after the pulse and slowly goes to zero after having passed through a maximum value under these conditions. The maximum is shifted to longer times with decreasing rate constant of the transfer reaction.[8]

Effects of this kind may be expected in case A of Figure 2 at the feet of the two separated waves. Similarly, they may occur in case B at potentials close to the potential where the polarographic curve passes through zero current. However, adsorption effects should not be observable in case C, since the sum of the rates of oxidation and reduction is always so high here that the lifetime of an adsorbed radical is shorter than the response time of our apparatus.

It has as yet been tacitly assumed that the ratio of the rate constants k_a and k_c has a fixed value at a given potential independent of time. This ratio could, however, depend on time, if radicals already adsorbed at the electrode are easier oxidized or reduced than mobile radicals in the vicinity of the electrode and if the relative concentrations of adsorbed and mobile radicals experience temporary changes. Such changes may occur through the establishment of the adsorption equilibrium of a radical. Let us, for example, regard case B in Figure 2 and discuss the current *vs.* time curve at a potential slightly less negative than the potential at which the polarographic curve passes through zero current. Immediately after the pulse when the surface concentration of adsorbed radicals is practically zero, a small negative current signal due to the ratio k_a/k_c being slightly larger than 1 will be observed. We may now assume that the radical in its adsorption state has a ratio k_a/k_c slightly lower than unity. Since the surface concentration of the radical increases, the preferential reduction of the adsorbed radical will become more significant at longer times. The initially weak negative current signal will therefore rapidly decrease and switch to a small positive signal which at longer times will decay toward zero. This switch from a negative to a positive current signal at the foot of a polarographic wave is not expected in case A of Figure 2, since the waves are too much separated and also not in case C of Figure 2 since no significant accumulation of radicals on the surface can occur here as pointed out above. We finally conclude that a switch from an initially positive current signal to a negative signal would occur if the ratio k_a/k_c is slightly lower than unity for the mobile radical and slightly above unity for the adsorbed radical at a potential little more negative than the potential at which the polarographic curve passes through zero current.

III. Results and Discussion

1. Production of Radicals. The details of the method of pulse radiolytic polarography have already been described.[1-3] In the present investigation, N_2O saturated solutions were used in which the hydrated electron from the radiolysis of water is converted into the OH radical

$$N_2O + e_{aq}^- \xrightarrow{H_2O} N_2 + OH^- + OH$$

The OH radicals attack the dissolved aromatic compound (10^{-3} to 10^{-2} *M*) within less than 1 μsec to yield the organic radical to be investigated. The initial radical concentration was around 10^{-6} *M*. No significant changes in pH by either irradiation or subsequent electrochemical reactions could therefore be expected. OH generally is believed to add to the aromatic ring to form a hydroxycyclohexadienyl radical.[9] In strongly alkaline solutions, OH is present in its base form O^- ($pK = 11.9$).[10] O^- has less tendency to add to the aromatic ring but preferentially abstracts a hydrogen atom from a side group. NaF or Na_2SO_4 were used as supporting electrolytes at concentrations of 0.70 and 0.35 *M*, respectively.

2. OH Addition Products of Benzene, Toluene, Benzyl Alcohol and Benzoic Acid. The polarogram of the product of the OH addition to benzene has already been described[1,2] and is shown again in Figure 3a. It has the typical form resulting from the overlap of oxidation and reduction as described by Figure 2B and C. In the earlier investigation with lower time resolution, no pH dependence of the wave could be observed.[2] However, the slight shift toward more negative potentials with increasing pH could be detected now. The limiting current value for the reduction wave is higher than that of the oxidation wave. This effect is mainly due to changes in the differential capacity of the double layer with potential which will be dealt with in a later publication.

The OH addition products of a number of substituted benzenes have polarograms which resemble that of the hydroxycyclohexadienyl radical itself as can be recognized from Figure 3b-d. The curves are slightly shifted on the potential scale and depend also a little on the pH of the solutions. Only in the cases of toluene and benzyl alcohol are the polarograms completely different in strongly

alkaline solutions, since they consist here of two separated waves corresponding to case A in Figure 2. In both cases, the radicals that are formed in strongly alkaline solutions are different from those produced in neutral or acid solutions. Reaction of O^- with toluene yields mainly the benzyl radical $C_6H_5CH_2\cdot$ and attack on benzyl alcohol yields mainly the benzyl alcohol radical $C_6H_5\dot{C}HOH$ or its anion $C_6H_5\dot{C}HO^-$.[11]

A comparison of these polarograms with those of aliphatic β-hydroxy radicals[2] in neutral solution shows that the reduction of hydroxycyclohexadienyl radicals already occurs at lower negative potentials. While the cathodic waves of aliphatic β-alcohol radicals are strongly shifted toward less negative potentials with increasing H^+ concentration, the effect of protons is not very pronounced in the case of hydroxycyclohexadienyl radicals. One could suppose that this effect is due to the fact that the unpaired electron in the hydroxycyclohexadienyl radicals is part of a system of delocalized π electrons. However, this fact cannot be the reason since the benzyl radical shows a completely different behavior (Figure 3b). Its polarogram is quite similar to that of an aliphatic carbon radical.

The addition products of OH to aromatic compounds thus show an unexpected behavior which may be related to another unusual property of hydroxycyclohexadienyl radicals which has recently been described by Schulte-Frohlinde and his coworkers.[12,13] They proposed that the OH radical does not add to the aromatic ring at a specific position, but rather forms a complex. Complexes are intermediates in the reactions of halide atoms with organic compounds.[14] The specificity of position of OH in the end product is determined in the final oxidation of the OH addition product. Nakken, *et al.*, have expressed similar views.[15] As has recently been pointed out by Simic and Hoffman, neither pulse- nor steady-state radiolysis studies have yet clarified that suggestion.[16] Regardless of the question of the structure of hydroxycyclohexadienyl radicals, we postulate the elimination of OH^- in the cathodic process. This elimination should strongly be favored by the restoration of the aromatic system.

The disproportionation of radicals is generally formulated as an H atom transfer process. It could, however, occur *via* the transfer of an electron in certain cases. One might suppose that disproportionation *via* electron transfer requires high rate constants of both oxidation and reduction of a radical at a certain potential, *i.e.*, a polarogram as in Figure 2C. Disproportionation of the hydroxycyclohexadienyl radical *via* electron transfer according to

$$\cdot C_6H_6OH + \cdot C_6H_6OH \longrightarrow C_6H_6OH^+ + C_6H_6OH^-$$
$$\downarrow \qquad\qquad \downarrow$$
$$C_6H_5OH + H^+ \quad C_6H_6 + OH^-$$

would yield equal amounts of phenol and benzene. On the other hand, phenol plus hydroxycyclohexadiene would be formed in the disproportionation *via* H-atom transfer. The yields of the various products formed in the irradiation of N_2O saturated aqueous benzene solution have not yet been determined with sufficient accuracy to allow one to draw a definite conclusion about the mechanism of disproportionation. Our polarographic findings may perhaps act as a stimulus for work in this direction.

3. OH Addition Products of Phenol, Cresol, Pyridine, and Anisole. The polarograms of these addition products are shown in Figure 3e-h. The OH addition to phenol and to the cresols is rapidly followed by the loss of water to form phenoxy radicals in the presence of H^+ or OH^- ions.[17] Experiments were therefore carried out only with neutral solutions, in which the OH addition products are known to be long-lived with respect to the loss of water. The polarographic behavior of phenoxy radicals will be described in a subsequent paper. All the polarograms of Figure 3e-h show significant deviations from those of Figure 3a-d described above. These deviations may now be discussed with respect to the nature of the substituents.

The polarogram of the OH-phenol addition product in Figure 3f again contains an anodic wave immediately followed by a cathodic wave. The curve is, however, shifted by about 0.4 V toward more negative potentials with respect to the curve for benzene which indicates that the OH addition product to phenol has a stronger tendency to be oxidized. We explain this tendency by the existence of mesomeric structures of the radical in which the phenolic $\geqslant$C-OH group has some α-alcohol radical character.

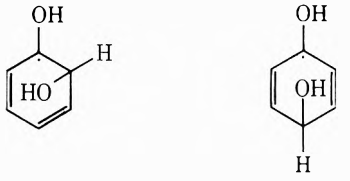

α-alcohol radicals are known to have anodic waves extending to rather high negative potentials.[1,2,7]

The polarographic waves of the various OH-cresol addition products (Figure 3g) are also shifted to more negative potentials. This effect is most pronounced for *m*-cresol. The curves for *p*- and o-cresol are less steep than that for the meta isomer. A slight bend toward the horizontal direction at the foot of the anodic part of the curve can even be observed in the case of *p*-cresol. These effects indicate that the product of OH addition to the meta isomer is most readily oxidized. We explain this fact again by the existence of mesomeric α-alcohol radical structures in either the OH addition complex or in the mixture of OH-addition isomers. One can easily recognize that whereas in the case of *m*-cresol three mesomeric structures of this kind are possible only two such structures can be written for *p*- and o-cresol. The use of mesomeric structures for our understanding of the polarograms may be regarded as being in contradiction to the postulate of an OH-aromatic complex[12,15] (see part III. 2).

The product of the attack of OH on pyridine shows a polarographic curve which is similar to that of the OH-benzene product if measured in alkaline solutions. Reduction is, however, strongly favored in neutral solution and even possible at 0 V *vs.* sce as can be recognized from Figure 3e. Čerček and Ebert[18] have shown that OH adds to pyridine, probably mainly to a carbon atom. They also discussed an addition to the nitrogen atom. The fast reduction at the mercury electrode may be explained either by the existence of the $\geqslant$N-OH addition products to the N atom or by the existence of a mesomeric structure >N· of a nitrogen radical in the OH addition product to a C atom.

The OH addition products of anisole have two separated polarographic waves of oxidation and reduction (Figure 3h) corresponding to case A in Figure 2. The anodic wave lies in the potential range where the hydroxycyclohexadienyl radical (Figure 3a) is oxidized, while the cathodic wave is shifted towards more negative potentials. The structure >Ċ-O-CH_3 of an ether radical exists in the various mesomeric forms of the OH addition products of

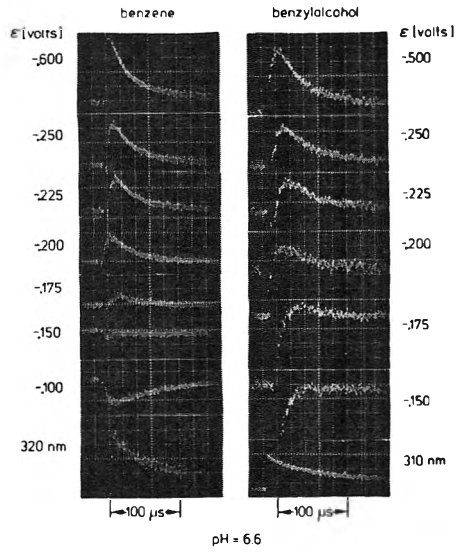

Figure 4. Polarographic current *vs.* time curves at different potentials ϵ for the OH addition products to benzene and to benzyl alcohol at pH 6.6. Lower oscillograms: optical absorption as a function of time. Supporting electrolyte: Na_2SO_4.

anisole; since radicals of this type are less rapidly reduced than carbon radicals,[2] the observed effect may be explained by the existence of such a structure. However, at present, we cannot exclude possible complications arising from the oxidation-reduction behavior of the radical that may be formed by the reaction of ·OH radicals with the methyl group in the side.

4. Current vs. Time Curves. Figure 4 shows current *vs.* time curves at various potentials for the products of OH attack on benzene and on benzyl alcohol at pH 6.6. On the left-hand side of each oscillogram, the zero current line before triggering of the pulse can be recognized. About 15 μsec after the pulse, the current signal can be read. The current signal decays afterward because of the formation of a diffusion layer before the electrode surface by electrochemical consumption of the radical and by the disappearance of radicals by mutual reaction. The change in radical concentration in the bulk of solution after the pulse can be recognized from the oscillograms at the lower ends of the two rows in Figure 4 where the optical absorption is recorded as a function of time. Cathodic currents produce positive signals; anodic currents produce negative signals.

In the case of benzene, either reduction (at more negative potentials) or oxidation (at more positive potentials) can be observed without any effects that indicate adsorption of radicals at the mercury electrode. This result is expected for case C in Figure 2. It is concluded that both rate constants k_a and k_c are rather large over the whole potential range of the polarographic wave. In the case of benzyl alcohol, however, a switch from an initially negative signal to a positive signal which finally decays can be seen at potentials between about −225 to −175 mV, *i.e.*, close to the potential where the polarographic wave passes through zero current. As mentioned in section II.2, such a switch may be observed in case B of Figure 2 if the ratio k_a/k_c is different for adsorbed and mobile radicals. Such a switch from oxidation to reduction has been observed in the polarographic current-time curves of a large number of radicals in which the anodic and cathodic waves lie close together. The reverse effect, *i.e.*, the switch from an initial positive to a final negative signal has, however, not yet been found. It seems therefore that a radical is in general a little easier reduced in the adsorbed state (or close to the electrode) than in the free state (or farther away from the electrode). Finally, it seems that the effect of changing the sign of the signal occurs more distinctly in solutions containing NaF as supporting electrolyte than in the case of Na_2SO_4.

It may finally be argued that the protons which are initially formed in the oxidation of the radical can subsequently facilitate the reduction and thus cause the switch in the current signal. In this case, the signal should oscillate around the zero line which was not observed. Furthermore, the switch in the signal should disappear in the case of buffered solution. Experiments with benzyl alcohol solutions containing 10^{-2} *M* phosphate buffer at pH 6.8 led to the same results as with the unbuffered solutions used in the experiments of Figure 4.

References and Notes

(1) J. Lilie, G. Beck, and A. Henglein, *Ber. Bunsenges. Phys. Chem.*, **75**, 458 (1971).
(2) M. Gratzel, A. Henglein, J. Lilie, and M. Scheffler, *Ber. Bunsenges. Phys. Chem.*, **76**, 67 (1972).
(3) M. Gratzel and A. Henglein, *Ber. Bunsenges. Phys. Chem.*, **77**, 2 (1973).
(4) P. Delahay and J. E. Strassner, *J. Amer. Chem. Soc.*, **73**, 5219 (1951); P. Delahay, "New Instrumental Methods in Electrochemistry," Interscience, New York, N. Y., 1954, p 76.
(5) M. G. Evans and N. S. Hush, *J. Chim. Phys.*, **49**, C 159 (1952).
(6) Nurnberg, "Studien mit modernen polarographischen Techniken . . . ," Report Jül-475-CA, Kernforschungsanlage Jülich 1967, pp 66, 392.
(7) M. Gratzel, K. M. Bansal, and A. Henglein, *Ber. Bunsenges. Phys. Chem.*, **77**, 11 (1973).
(8) A. Henglein and M. Gratzel, *Ber. Bunsenges. Phys. Chem.*, **77**, 17 (1973).
(9) P. Neta and L. M. Dorfman, *Advan. Chem. Ser.*, **No. 81**, 222 (1968).
(10) J. Rabani and M. S. Matheson, *J. Amer. Chem. Soc.*, **86**, 3175 (1964).
(11) P. Neta, M. Z. Hoffman, and M. Simic, *J. Phys. Chem.*, **76**, 847 (1972).
(12) O. Volkert and D. Schulte-Frohlinde, *Tetrahedron Lett.*, **No. 17**, 2151 (1968).
(13) K. Eiben, D. Schulte-Frohlinde, C. Suarez, and H. Zorn, *Int. J. Radiat. Phys. Chem.*, **3**, 40 (1971).
(14) R. E. Bühler, *Helv. Chim. Acta*, **51**, 1558 (1968).
(15) K. F. Nakken, T. Brustad, and A. K. Hansen, *Advan. Chem. Ser.*, **No. 81**, 251 (1968).
(16) M. Simic and M. Z. Hoffman, *J. Phys. Chem.*, **76**, 1398 (1972).
(17) G. E. Adams, E. J. Land, and B. D. Michael, *Nature (London)*, **211**, 293 (1966); G. E. Adams and B. D. Michael, *Trans. Faraday Soc.*, **63**, 1171 (1967).
(18) B. Čerček and M. Ebert, *Trans. Faraday Soc.*, **63**, 687 (1967).

Experimental Determination and Scaled Particle Theory Calculation of the Activity Coefficients of Benzene and Cyclohexane in Aqueous Sodium Chloride Solutions[1]

Yuh-Loo Tien Chang, Martha Y. Schrier, and Eugene E. Schrier*

Department of Chemistry, State University of New York at Binghamton, Binghamton, New York 13901 *(Received June 11, 1973)*

Publication costs assisted by the U.S. Public Health Service

The ratio of the solubility of the nonelectrolyte in sodium chloride solution (ws) to its solubility in water (w) has been measured over a wide range of sodium chloride molalities for the nonelectrolytes, cyclohexane and benzene. The technique of gas–liquid chromatography was utilized in the analysis. The activity coefficient ratios (γ^{ws}/γ^{w}) obtained for each nonelectrolyte from the solubility ratios were correlated with salt molality using an equation of the form, $\log(\gamma^{ws}/\gamma^{w}) = Am_s + Bm_s^{3/2}$. The value of A obtained for benzene compared favorably with that from previous work. The scaled particle theory has been employed to calculate the limiting interaction parameter, A, for both benzene and cyclohexane using recently derived values of the Lennard-Jones parameters and molecular diameters for these molecules. The agreement between experimental and calculated values was poor. Use of Lennard-Jones well depths calculated from the Mavroyannis–Stephen equation gave values of the limiting interaction parameter in excellent agreement with experiment.

Introduction

Masterton and Lee[2] have shown that the scaled particle theory as extended by Shoor and Gubbins[3] can be used to calculate interaction parameters for salt–nonelectrolyte interactions in aqueous solutions. Calculations were performed on a variety of nonpolar substances including the rare gases and various simple hydrocarbons for which experimental data were available in the literature. Notable in this otherwise successful application of the theory were the large discrepancies between the observed and calculated limiting interaction parameters for benzene with various electrolytes. It was concluded that either the theory is defective or aromatic molecules provide some anomalous feature in aqueous solution.

Cyclohexane is similar to benzene with respect to molar volume and polarizability but exhibits differences in conformational properties and does not have π electrons. It thus provides an interesting compound with which to further test this discrepancy.

Experimental Section

Materials. Cyclohexane (Matheson Coleman and Bell) was purified by the method of Morgan and Lowry.[4] A small residual impurity amounting to about 2.5% of the material was resolved sufficiently from the cyclohexane peak in the glc analysis so that it could be disregarded. Benzene and sodium chloride were ACS reagent grade and were used without further purification. The sodium chloride was dried overnight at 140° before use.

Solubility Determinations. Saturated solutions of the nonelectrolytes in water or the appropriate sodium chloride solution were prepared by equilibrating the phases in 250-ml Pyrex aspirator bottles. The outlet near the bottom of these bottles was sealed with a silicone rubber septum. An aspirator bottle containing the sample of interest was immersed in a constant temperature water bath controlled at 25.00 ± 0.05°. A submersible magnetic stirrer was used to stir the sample solution until the aqueous phase was saturated with nonelectrolyte. The stirring speed was kept as slow as possible to prevent formation of cyclohexane droplets. A time test indicated that saturation was attained after 24 hr of equilibration.

Analysis of the Samples. A Beckman Model GC-4 gas chromatograph equipped with flame ionization detector was used for the analysis of the samples. In order to facilitate the analysis of nonelectrolyte in aqueous salt solution, the copper sample column was divided into three sections: (1) a section of empty column which trapped the sodium chloride after the remainder of the sample had vaporized, (2) a section containing gelatin and firebrick which selectively removed water from the sample,[5] and (3) a section for partition which was packed with 25% (w/w) SE-30 gum rubber on 80/100 Mesh Chromosorb G, AW-DMCS.

Samples of the aqueous solution saturated with nonelectrolyte were obtained by removing the aspirator bottle from the water bath and inserting the needle of a gastight Hamilton 10-μl syringe through the rubber septum into the aqueous phase. This sampling procedure was done at a point in the room where the ambient temperature was 25°. Five samples of water saturated with nonelectrolyte were withdrawn from the appropriate aspirator bottle and injected sequentially into the gas chromatograph. Next, five samples of NaCl solution saturated with nonelectrolyte were injected onto the column. Finally, another five samples of the nonelectrolyte saturated water were injected. This procedure allowed for compensation of any drift of the instrument during the time of analysis.

The area under each peak was integrated using a disk chart integrator and average peak areas were calculated for each group of five injections. The average standard deviation of the mean for a series of five nonelectrolyte peaks was 2.5%.

Results

In the development of the experimental method, it was assumed that the ratio of the peak heights for a nonelectrolyte in water (w) and in salt solution (ws) was equal to

TABLE I: Coefficients for Representation of Log γ^{ws}/γ^{w} by Eq 2

Nonelectrolyte	Coefficient		% standard deviation of fit
	A, kg/mol	B, $(kg/mol)^{3/2}$	
Benzene	0.1999 ± 0.0096	−0.0143 ± 0.0074	2.2
Cyclohexane	0.2713 ± 0.0064	−0.0160 ± 0.0044	5.4

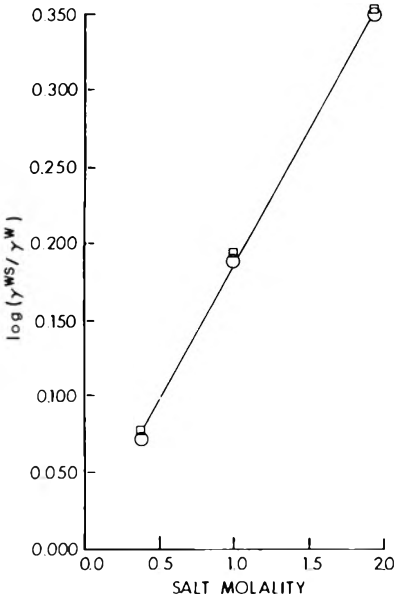

Figure 1. The logarithms of the activity coefficient ratios for benzene plotted as a function of NaCl molality, m_s, at 25°: O, this work; □, data from ref 5. The line shown was calculated from eq 2 using the coefficients given in Table I.

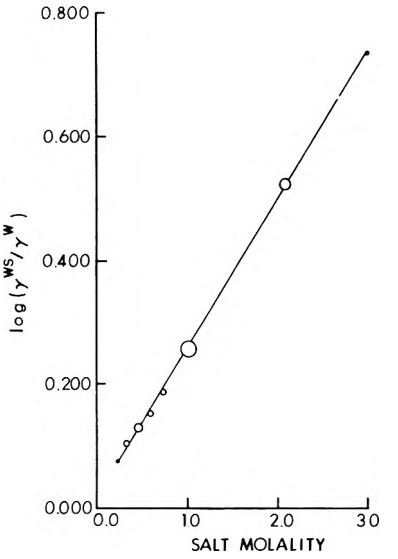

Figure 2. The logarithms of the activity coefficient rates for cyclohexane plotted as a function of NaCl molality, m, at 25°. The size of the points indicates the range of the experimental values at a given salt molality. The line shown was calculated from eq 2 using the coefficients given in Table I.

the ratio of the solubilities of the nonelectrolyte in the same solution. The ratio of the activity coefficients of the nonelectrolyte could then be determined by the relationship

$$m^{w}/m^{ws} = \gamma^{ws}/\gamma^{w} \quad (1)$$

where m^{w} and m^{ws} are the molalities of nonelectrolyte in the respective saturated aqueous solutions and the symbol γ denotes activity coefficients on the molality scale.

The measurements made on benzene–sodium chloride–water were carried out with a view toward testing the experimental procedure since good data obtained using a different analytical procedure were available in the literature.[6] The experimental results are shown[7] in Figure 1 along with the results of McDevit and Long recalculated so as to express their salt concentrations in terms of molality. The agreement between the two sets of data is very good with the maximum deviation between the results being 4.5% at 1.94 m NaCl.

The present data were also fit to an equation of the form[8] using a least-squares routine (eq 2). The line shown

$$\log (\gamma^{ws}/\gamma^{w}) = Am_s + Bm_s^{3/2} \quad (2)$$

in Figure 1 has been calculated in conformance to this equation. The parameters A and B, their standard deviations, and the per cent standard deviation of the fit are given in Table I.

Figure 2 shows similar results for the cyclohexane–sodium chloride–water system. These data were also fit to eq 2 with the line shown in Figure 2 the result of that fitting process. The parameter A and B and the associated uncertainties are also given in Table I.

TABLE II: Comparison of Calculated and Experimental Values of the Limiting Interaction Parameter, A, for Benzene and Cyclohexane in Sodium Chloride Solutions

Nonelectrolyte	σ (nonelectrolyte) × 10^8 cm	ϵ/k	A_{calcd}	A_{exptl}
Benzene	5.26[a]	531[a]	0.102	0.200
	5.26[a]	214[b]	0.205	0.200
Cyclohexane	5.63[a]	573[a]	0.101	0.271
	5.63[a]	183[b]	0.245	0.271

[a] Reference 13. [b] Calculated from eq 3; see text.

Discussion

Theoretical calculation of the limiting interaction parameter, A in eq 2, is readily accomplished using the extended scaled particle formulation.[2,3] We have used eq 11, 19, and 32 in the paper of Masterton and Lee[2] for these calculations. The polarizabilities for Na^+, Cl^-, and benzene are those employed by Masterton and Lee. The polarizability for cyclohexane was calculated from the bond refractions for the C–H and C–C bonds given in the compilation of Price.[9] The diameters for sodium ion and chloride ion were those derived by Waddington[10] in accordance with the recent findings of Masterton, Bolacofsky, and Lee[11] regarding the best set of ionic diameters to be used in calculations involving the scaled particle theory. The hard sphere diameter for water is taken[2] to be 2.75 × 10^{-8} cm. The depth of the potential well, ϵ/k, for each of the ions was given by the Mavroyannis–Stephen equation[2,12]

$$\frac{\epsilon_i}{k} = 2.28 \times 10^{-8} \frac{\alpha_i^{3/2} z_i^{1/2}}{\sigma_i^6} \quad (3)$$

where α_i is the polarizability of the ion, Z_i is the total number of electrons in the ion, and σ_i is its diameter. The value of the apparent molal volume of sodium chloride at infinite dilution, ϕ_v^0, is taken as 16.32 ml/mol.

The choice of the molecular parameters, σ and ϵ/k for benzene and cyclohexane, is particularly important in the situation under consideration. Wilhelm and Battino[13] (WB) recently calculated the Lennard-Jones parameters for a number of different solvents from gas solubility data using the scaled particle theory to calculate the work of cavity formation. Their values of σ, the hard-sphere diameter, and ϵ/k for benzene and cyclohexane are in good agreement with the same parameters calculated previously from liquid-state properties. The agreement is not as good with parameters calculated from transport properties of the gas-phase molecules. The values of σ tend to be smaller in the WB calculation and the values of ϵ/k are larger than those derived from gas-phase properties of these molecules. In any case, it seemed to us that the parameters derived from interactions in the liquid phase would be better suited for use in further calculations involving species in solution. We have, therefore, adopted the WB values. In addition to these values of σ and ϵ/k, an alternative value of ϵ/k was made available by using the WB value of σ for each nonelectrolyte in conjunction with eq 3 as suggested previously.[2]

The results of the calculation are given in Table II. Equation 9 of the paper by Masterton, *et al.*,[11] has been used to bring the calculated values of the limiting interaction parameter into the molality scale. The experimental limiting interaction parameters are not in agreement with those calculated on the basis of the WB values of σ and ϵ/k. Indeed, no set of Lennard-Jones parameters obtained from the literature gave calculated results in agreement with experiment for both nonelectrolytes. On the other hand, the limiting interaction parameters calculated using ϵ/k derived from eq 3 are in excellent agreement with the experimental values. It is noteworthy that the values of ϵ/k derived from eq 3 for the nonelectrolytes are very much smaller than those obtained from the literature.

Clearly, the anomaly in the scaled particle theory representation of ion–nonelectrolyte interactions in aqueous solution is not restricted to aromatic nonelectrolytes as had been suggested previously.[11] This problem most likely arises from one of two causes. First, the assumption of a spherical symmetry in the theoretical treatment may break down for these disk-shaped molecules.[14] Indeed, the assumption of a random distribution of water and ions around even a spherical nonelectrolyte could stand refinement. Second, the effective ion–nonelectrolyte interaction potential may be smaller than that given by the geometric mean of ϵ/k values for the ion and the nonelectrolyte because of the considerable disparity in size between the two particles. More work, both experimental and theoretical, is required to distinguish the precise cause of this interesting discrepancy. In addition, the utility of the Mavroyannis–Stephen equation in the prediction of molecular properties in condensed phases is worthy of further investigation.

If we take into account the increase of the apparent molal volume of the salt, ϕ_v, with increasing salt concentration, it is also possible to estimate a value for the B coefficient of eq 2 from the theoretical treatment.[15] The calculation can be carried out by using values of ϕ_v calculated from the equation,[16] $\phi_v = 16.62 + 1.868c^{1/2} + 0.02c_s$, at various salt concentrations in the equations of Masterton and Lee.[2] After bringing the resulting data onto the molal scale,[11] calculated values of $\log(\gamma^{ws}/\gamma^{w})/m_s$ were plotted as a function of the square root of the salt molality. The slope of this plot is equal to B. The calculated values of B, -0.025 (kg/mol)$^{3/2}$ for cyclohexane and -0.021 (kg/mol)$^{3/2}$ for benzene, compare favorably with the experimental values given in Table I of -0.016 ± 0.004 (kg/mol)$^{3/2}$ for cyclohexane and -0.014 ± 0.007 (kg/mol)$^{3/2}$ for benzene. Since ϕ_v comes into the scaled particle equations in several places, the ability of the theory to account for a coefficient such as B which is important only at finite salt molalities is pleasing.

References and Notes

(1) This work was supported in part by Public Health Service Grant No. GM11762 from the Institute of General Medical Sciences.
(2) W. L. Masterton and T. P. Lee, *J. Phys. Chem.*, **74**, 1776 (1970).
(3) S. K. Shoor and K. E. Gubbins, *J. Phys. Chem.*, **73**, 498 (1969).
(4) S. O. Morgan and H. H. Lowry, *J. Phys. Chem.*, **34**, 2385 (1930).
(5) H. A. Syzmanski and T. Amabile, *J. Chromatogr. Sci.*, **7**, 575 (1969).
(6) W. McDevit and F. A. Long, *J. Amer. Chem. Soc.*, **74**, 1773 (1952).
(7) Complete tables of experimental data are given in the M.S. Thesis of Y. L. Tien, State University of New York, Binghamton, 1971.
(8) M. Y. Spink and E. E. Schrier, *J. Chem. Thermodyn.*, **2**, 821 (1970).
(9) A. H. Price in "Dielectric Properties and Behavior," N. E. Hill, Ed., Van Nostrand-Reinhold, London, 1969, p 238.
(10) T. C. Waddington, *Trans Faraday Soc.*, **62**, 1482 (1966).
(11) W. L. Masterdon, D. Bolacofsky, and T. P. Lee, *J. Phys. Chem.*, **75**, 2809 (1971).
(12) C. Mavroyannis and M. J. Stephen, *Mol. Phys.*, **5**, 629 (1962).
(13) E. Wilhelm and R. Battino, *J. Chem. Phys.*, **55**, 4012 (1971).
(14) M. A. Cotter and F. H. Stillinger, *J. Chem. Phys.*, **57**, 3356 (1972).
(15) We are grateful to a referee for pointing out this possibility.
(16) F. J. Millero in "Water and Aqueous Solutions," R. A. Horne, Ed., Wiley-Interscience, New York, N. Y., 1972, p 519.

Heteroconjugation of Inorganic Anions in Nonaqueous Solvents. II. Perchlorate Complexes of Some Organic Hydroxy Compounds

Lajos Barcza[1] and Michael T. Pope*

Department of Chemistry, Georgetown University, Washington, D. C. 20007 *(Received June 8, 1973)*

Publication costs assisted by the Air Force Office of Scientific Research

Heteroconjugates of 1,2-dihydroxybenzene (pyrocatechol), phenol, 1,2-dihydroxyethane (ethylene glycol), and ethanol with perchlorate anion in nitrobenzene solution have been investigated by nmr spectroscopy. The computed formation constants (at 37°) of the 1:1 complexes are pyrocatechol, 20.6; phenol, 4.40; ethylene glycol, 3.04; and ethanol, 0.36 M^{-1}. Self-association (dimerization) constants for glycol and ethanol under these conditions were found to be 0.80 and 0.11 M^{-1}, respectively. It is proposed that the relatively high differences in stability between complexes of mono- and dihydroxy derivatives are due to chelate type hydrogen bonding in the latter complexes. Differences between the stabilities of the complexes of aromatic and aliphatic derivatives have not been previously observed with halide complexes.

Introduction

We have recently measured the formation constants of heteroconjugates of pyrocatechol with some inorganic anions in nitromethane solution, and suggested the probability of chelate hydrogen bond formation.[2] In connection with our interests in the interactions of organic molecules with heteropoly and isopoly oxocomplexes, we report here the formation constants of complexes of perchlorate anion with some mono- and dihydroxy compounds. These data show the importance of chelation in the stabilization of such complexes.

Experimental Section

Nitrobenzene proved to be a more effective and general solvent than the nitromethane used previously;[2] the Baker Analyzed reagent was dried over Molecular Sieve Type 5A and filtered before use. Absolute ethanol (<0.2% water), ethylene glycol (<0.1% water), and phenol (<0.5% water) were commercial products and were used without further purification. Pyrocatechol and tetra-*n*-butylammonium perchlorate (J. T. Baker) were dried in a vacuum desiccator over silica gel before use. The nmr measurements were made as described previously.[2] Formation constants were evaluated using a Hewlett-Packard programmable calculator.

Results

The chemical shift of the phenolic protons of pure pyrocatechol in nitrobenzene was found to be independent of concentration within the range 30–250 mM. The chemical shift of the phenolic proton in pure phenol solutions increased by some hundredths of a part per million if the concentrations were over 0.1 M. Assuming that only the first step of polymerization, dimerization, takes place

$$2HB \rightleftharpoons (HB)_2$$

the computed dimerization constant

$$K_D = [H_2B_2]/[HB]^2 \quad (1)$$

has a value of 0.1 ± 0.06 M^{-1}. Since this formation constant is much smaller than that of the perchlorate–phenol heteroconjugate, it was neglected, and the stability constants for pyrocatechol- and phenol-perchlorate complexes could be computed from eq 2–5 of the previous paper[2] (or from simplified versions of eq 4–7 of this paper).

On the other hand, dimerization (as the first step of polymerization in relatively dilute solutions) of ethylene glycol and ethanol are almost as important as the formation of their perchlorate complexes, even in nitrobenzene.

The dimerization of ethylene glycol was studied in 6–130 mM, and that of ethanol in 50–300 mM solutions. The equilibrium constants were computed from the following equations

$$C^*(H_nB) = [H_nB] + 2K_D[H_nB]^2 \quad (2)$$

$$(\delta(M) - \delta(H_nB))C^*(H_nB) = 2(\delta(H_{2n}B_2) - \delta(H_nB))K_D[H_nB]^2 \quad (3)$$

where n is the number of hydroxy groups (ethanol: $n = 1$; glycol: $n = 2$); $C^*(H_nB)$ is the analytical concentration in solutions containing no acceptor ion; $\delta(M)$ is the measured chemical shift; $\delta(H_nB)$ and $\delta(H_{2n}B_2)$ are the (constant) chemical shifts of monomeric and dimeric species.

Values of $C^*(H_nB)$ and $\delta(M)$ for several solutions were used to determine K_D (and incidentally $\delta(H_nB)$, $\delta(H_{2n}B_2)$, and [HB]) from eq 2 and 3 by a routine iterative procedure. The following values (in nitrobenzene, at 37 ± 1°) were found: ethylene glycol, $K_D = 0.80 \pm 0.11$ M^{-1}; ethanol, $K_D = 0.11 \pm 0.02$ M^{-1}.

The formation of the perchlorate complexes was studied using the above concentration ranges for the H donors. Molar ratios [anion]/[donor] were varied from 0.2 to 2.5.

The heteroconjugation constant

$$K_C = [AH_nB^-]/[A^-][H_nB] \quad (4)$$

was computed from the analytical concentrations of the H donor ($C(H_nB)$) and perchlorate ($C(A^-)$), and the measured relative chemical shifts ($\Delta(M)$)

$$C(H_nB) = [H_nB] + K_C[H_nB][A^-] + 2K_D[H_nB]^2 \quad (5)$$

$$C(A^-) = [A^-] + K_C[H_nB][A^-] \quad (6)$$

$$\Delta(M)C(H_nB) = \Delta(AH_nB^-)K_C[H_nB][A^-] + 2\Delta(H_{2n}B_2)K_D[H_nB]^2 \quad (7)$$

TABLE I: Formation Constants of Heteroconjugates of Perchlorate Anion with Some Organic Hydroxy Derivatives in Nitrobenzene at 37°

Compound	K_C, M^{-1}
Pyrocatechol (1,2-dihydroxybenzene)	20.6 ± 1.2
Phenol (1-hydroxybenzene)	4.40 ± 0.32
Glycol (1,2-dihydroxyethane)	3.04 ± 0.56
Ethanol (1-hydroxyethane)	0.36 ± 0.08

where

$$\Delta(M) = \delta(M) - \delta(H_nB) \quad (8)$$

$$\Delta(AH_nB^-) = \delta(AH_nB^-) - \delta(H_nB) \quad (9)$$

$$\Delta(H_{2n}B_2) = \delta(H_{2n}B_2) - \delta(H_nB) \quad (10)$$

The values of K_D, $\delta(H_nB)$, and $\delta(H_{2n}B_2)$ were known from the preliminary measurements (eq 1-3), so these equations could be solved by a rather simple iterative procedure. The final results are presented in Table I.

The formation of 1:2 complexes of perchlorate with phenol or ethanol is considered to be very small for the following reasons. The increase in relative chemical shift caused by 1:2 complex formation is

$$\Delta = 2\{\delta(AH_2B_2^-) - \delta(HB)\}\beta_{12}[A^-][HB]^2/C(HB) \quad (11)$$

where $\beta_{12} = [AH_2B_2^-]/[A^-][HB]^2$. If the reasonable assumptions are made that $\beta_{12} \geq 2K_C$ and that $\delta(AH_2B_2^-) = \delta(AHB^-)$, the magnitude of Δ (eq 11) is large enough to be detected by our measurements. Since there was no anomalous chemical shift, *i.e.*, over and above that required by eq 7, we can safely conclude that the pyrocatechol-perchlorate complex is much more stable than $(PhOH)_2ClO_4^-$; and that ethylene glycol-perchlorate is more stable than $(EtOH)_2ClO_4^-$.

Discussion

In the previous paper,[2] based on our data and those of Green, *et al.*,[3] the pyrocatechol complexes were presumed to be chelate type, twin hydrogen bonded species. The rather high differences between the stabilities of mono- and dihydroxy complexes (phenol-pyrocatechol, ethanol-glycol), shown by the present work, point to the same conclusion.

The results show another phenomenon: the stabilities of the perchlorate complexes seem to be markedly influenced by the aromatic or aliphatic character of the H-donor molecules. The stability constants of pyrocatechol and phenol complexes are about ten times higher than those of glycol and ethanol, respectively. This behavior contrasts with that reported for complexes of halide ions. The formation constants of complexes of bromide ion with alcohols and 4-methylphenol[3] are of similar magnitudes; indeed the bromide-methanol heteroconjugate ($K = 70 \pm 18\ M^{-1}$) is about twice as stable as that of 4-methylphenol ($K = 32 \pm 8\ M^{-1}$).

There are very few data concerning heteroconjugates of oxyanions in nonaqueous solution so that at this point we cannot say whether the aromatic-aliphatic differences noted here are significant or not. Similar differences have been observed in aqueous solution, although the complexes formed are probably not the simple hydrogen bonded adducts under consideration here. Thus Roy, *et al.*,[4] found the stability constant of the 1:1 boric acid-pyrocatechol complex to be 7800 M^{-1} and that of the ethylene glycol complex to be 1.85 M^{-1}.[5] Values for the corresponding complexes of arsenite are 110 and 0.07 M^{-1}, respectively.[4]

Acknowledgment. The support of this research, by AFOSR, through Grant No. AF 70-1833, is gratefully acknowledged.

References and Notes

(1) Present address, Institute of Inorganic and Analytical Chemistry, L. Eotvös University, Budapest, Hungary.
(2) L. Barcza and M. T. Pope, *J. Phys. Chem.*, **77**, 1795 (1973).
(3) R. D. Green, J. S. Martin, W. B. McG. Cassie, and J. B. Hyne, *Can. J. Chem.*, **47**, 1639 (1969).
(4) G. L. Roy, A. L. Laferrier, and J. O. Edwards, *J. Inorg. Nucl. Chem.*, **4**, 106 (1957).
(5) These figures have since been corrected for the acidic characters of pyrocatechol and glycol. The new stability constants are 4950 and 2.15 M^{-1}, respectively. (J. M. Connor and V. C. Bulgrin, *J. Inorg. Nucl. Chem.*, **29**, 1953 (1967).)

Effects of Solutes on the Strength of Hydrophobic Interaction and Its Temperature Dependence

A. Ben-Naim*[1] and M. Yaacobi

Department of Inorganic and Analytical Chemistry, The Hebrew University of Jerusalem, Jerusalem, Israel
(Received July 12, 1973)

The effect of various solutes on the strength of hydrophobic interaction in aqueous solutions has been determined by a method devised previously for this purpose. The solubilities of methane and ethane in aqueous solutions of electrolytes and nonelectrolytes were measured in the range of temperatures between 5 and 25°. These data have been used to compute the standard free energy, entropy, and enthalpy of solution of methane and ethane in these solutions. It is found that most added solutes increase the strength of hydrophobic interaction. An opposite effect has been noted by some nonelectrolytes which are presumed to enhance the structure of the solvent.

I. Introduction

It is well known that natural biopolymers in solutions undergo conformational changes as a result of the addition of various solutes to the system. The present state of our knowledge of these phenomena has been recently summarized by Tanford.[2] From the theoretical point of view little is known on the precise mechanism by which an added solute induces a conformational change in a biopolymer. Kauzmann[3] has advocated the study of this complex problem by disentangling it into separate factors. For instance, one may study the effect of adding solute on the strength of hydrogen bond, charge-charge interaction, or hydrophobic interaction (HI), in "model systems," where the situation is simpler in order of magnitude as compared with the one in the original systems.

This paper is concerned with the effect of various solutes on the strength of hydrophobic interaction. The study is being carried out in a simple "model system" devised recently for this purpose.[4,5] Similar studies of the effect of solutes on the conformation of biopolymers have been carried out by many authors.[6-9] However, because of the great complexity of these systems, it is very difficult to draw any quantitative conclusions regarding the effects on the separate factors.

For the convenience of the reader we present here a brief description of the method employed in this study.[4,5,10]

Consider the process of bringing two simple solutes, such as methane molecules, from fixed positions at infinite separation, to the final positions $\mathbf{R}_1$ and $\mathbf{R}_2$. The process being carried out at constant temperature T, pressure P, and number of solvent molecules (the solvent may be either a pure component or a mixture of various components).

The Gibbs free energy associated with this process may be written as

$$\Delta G(\mathbf{R}_1,\mathbf{R}_2) = U(\mathbf{R}_1,\mathbf{R}_2) + \delta G^{\mathrm{HI}}(\mathbf{R}_1,\mathbf{R}_2) \qquad (1.1)$$

where $U(\mathbf{R}_1,\mathbf{R}_2)$ is the *direct* interaction energy between the two solutes at the configuration $\mathbf{R}_1,\mathbf{R}_2$, which is presumed to be independent of the nature of the solvent. The indirect part of the work, $\delta G^{\mathrm{HI}}(\mathbf{R}_1,\mathbf{R}_2)$ is referred to as the HI between the two solutes at the specified configuration.

Using arguments based on classical statistical mechanics the HI may be expressed as an average over all the configurations of the solvent molecules, in the appropriate ensemble,[10] namely

$$\delta G^{\mathrm{HI}}(\mathbf{R}_1,\mathbf{R}_2) = -kT \ln \langle \exp[-U(\mathbf{X}_1 \cdots \mathbf{X}_N/\mathbf{R}_1,\mathbf{R}_2)/kT] \rangle - 2\Delta\mu_{\mathrm{Me}}^{\circ} \qquad (1.2)$$

where k is the Boltzmann constant, $U(\mathbf{X}_1 \ldots \mathbf{X}_N/\mathbf{R}_1,\mathbf{R}_2)$ is the total interaction energy between the solvent molecules at configuration $\mathbf{X}_1 \ldots \mathbf{X}_n$ ($\mathbf{X}_i$ being the vector specifying the location and the orientation of the ith solvent molecule), and the two solutes at $\mathbf{R}_1,\mathbf{R}_2$. $\Delta\mu_{\mathrm{Me}}^{\circ}$ is the standard free energy of solution of methane. In (1.2) the average is taken over all the configurations of the solvent molecules, using the T,P,N basic distribution function.

In order to relate $\delta G^{\mathrm{HI}}(\mathbf{R}_1,\mathbf{R}_2)$ to experimental quantities, we note that the average in (1.2) does not involve the direct solute-solute pair potential, hence it is permissible to substitute any $\mathbf{R}_1$ and $\mathbf{R}_2$ even when the distance $R = |\mathbf{R}_2 - \mathbf{R}_1|$ is smaller than the effective diameter of the solute σ. This feature of the average has been exploited[4,5] to make a particular choice of $R = 1.533$ Å, which is the C-C distance in ethane, and thereby obtain the approximate relation

$$\delta G^{\mathrm{HI}}(R = 1.533\text{Å}) \cong \Delta\mu_{\mathrm{Et}}^{\circ} - 2\Delta\mu_{\mathrm{Me}}^{\circ} \qquad (1.3)$$

TABLE I: Representative Values of the Ostwald Absorption Coefficients, $\gamma \times 10^3$, for Methane and Ethane in Water and in Aqueous Solutions at 15°

	Solvent			
	H_2O	NaCl 1 *M*	LiCl 1 *M*	Urea 7 *M*
	Methane			
This work	40.5	28.00	31.06	28.50
Other works	37.9[a]	32.10[a]	32.80[a]	27.00[b]
	40.6[b]			
	40.57[c]			
	Ethane			
This work	59.12	37.95	42.78	44.20
Other works	49.60[a]	40.80[a]	41.90[a]	45.10[b]
	59.00[b]			
	58.54[c]			

[a] Reference 13. [b] Reference 14. [c] Reference 12.

TABLE II: Polynomial Coefficients in (3.2) and the Standard Deviation for Each Set of Measurements of Methane in Aqueous Solutions

Solution	c	b	a	Standard deviation
Urea 1 M	−0.10534	77.00	−11,562.0	3.813
Urea 2 M	−0.14153	96.928	−14,255.0	2.838
Urea 4 M	−0.09407	−41.018	6,004.4	4.415
Urea 7 M	−0.02528	−2.980	855.0	2.565
Sucrose 0.5 M	−0.09063	68.957	−10,386.5	2.605
1-Propanol (mol fraction 0.03)	−0.03677	36.091	−5,537.5	1.426
Dimethyl sulfoxide (x = 0.03)	−0.06316	52.042	−7,904.5	1.617
1,4-Dioxane (x = 0.03)	−0.03996	37.008	−5,531.6	3.372
NaCl 0.25 M	−0.06846	56.405	−8,677.1	3.040
NaCl 0.50 M	−0.07855	61.966	−9,392.2	5.008
NaCl 1 M	−0.07209	57.885	−8,645.6	3.345
NaCl 2 M	−0.08605	64.964	−9,327.1	2.734
NaBr 1 M	−0.07352	58.231	−8,631.7	4.197
NaI 1 M	−0.14190	97.387	−14,243.5	5.132
LiCl 1 M	−0.05380	47.609	−7,264.1	3.625
KCl 1 M	−0.01219	23.037	−3,595.6	3.596
CsCl 1 M	−0.21072	138.831	−20,487.3	2.045
NH_4Cl 1 M	−0.01195	9.329	−1,721.5	2.196

TABLE III: Polynomial Coefficients in (3.2) and the Standard Deviation for Each Set of Measurements of Ethane in Aqueous Solutions

Solution	c	b	a	Standard deviation
Urea 1 M	−0.03621	41.403	−7,273.4	2.516
Urea 2 M	−0.08917	70.985	−11,371.2	2.805
Urea 4 M	−0.02140	30.054	−5,153.0	4.094
Urea 7 M	−0.16662	112.90	−16,909.2	5.577
Sucrose 0.5 M	−0.07542	64.765	−10,670.4	3.470
1-Propanol (mole fraction 0.03)	−0.12906	93.490	−14,662.0	0.853
Dimethyl sulfoxide (x = 0.03)	−0.09180	72.532	−11,689.2	1.852
1,4-Dioxane (x = 0.03)	−0.11940	86.676	−13,529.1	3.149
NaCl 0.25 M	−0.04395	46.822	−8,164.1	2.958
NaCl 0.50 M	−0.14339	105.52	−16,759.7	4.330
NaCl 1 M	−0.16366	115.82	−17,910.6	4.297
NaCl 2 M	−0.13182	96.230	−14,678.7	1.401
NaBr 1 M	−0.11675	88.641	−13,998	2.378
NaI 1 M	−0.05728	53.458	−8,825.0	3.585
LiCl 1 M	−0.09657	77.186	−12,418	4.327
KCl 1 M	−0.07538	64.337	−10,431.2	2.996
CsCl 1 M	−0.19810	135.77	−20,843	2.307
NH_4Cl 1 M	−0.04356	4.078	−677.2	3.456

with $\Delta\mu_{Et}^{\circ}$ the standard free energy of solution of ethane. In (1.3) we have on the right-hand side two experimentally measurable quantities. Thus by measuring the standard free energy of solution of methane and ethane, an estimate may be made of the strength of the HI and its temperature dependence in various solvents.

Thus the process of bringing two methane molecules from infinite separation to a short distance R serves here as a probe for estimating the strength of HI. Furthermore, to the best of our knowledge this is the only method which has so far been used to detect changes in the strength of HI due to the addition of various solutes.

II. Experimental Section

The solubilities of methane and ethane in various aqueous solutions were determined according to the method developed by Ben-Naim and Baer,[11] with some modifications as suggested by Wen and Hung.[12] We have carried out a series of measurements in aqueous solutions of both electrolytes and nonelectrolytes. In most cases, we have measured the solubility of methane and ethane in an aqueous solution at a fixed concentration. For solutions of NaCl and urea we have also determined the dependence on the concentration of these solutes as well.

Methane and ethane were purchased from Matheson (purity: methane 99.97%, ethane 99.9%). Water was doubly distilled after being run through an ion exchanger.

All solutes, electrolytes, and nonelectrolytes were of AR grade except for dimethyl sulfoxide and 1-propanol which were CP.

The Ostwald absorption coefficients for methane and ethane were calculated directly from the volume of the gas dissolved in a fixed volume of the solvent. A sample of comparisons of our results with the corresponding ones from the literature is presented in Table I.

The discrepancies between our results and those of Morrison and Billet[13] are quite large. On the other hand, more satisfactory arrangement exists between our results

TABLE IV: Values of the Ostwald Absorption Coefficient γ_s for Methane in Various Aqueous Solutions

Solution	$\gamma_s \times 10^3$				
	10°	15°	20°	25°	30°
H_2O	44.80	40.51	37.00	34.20	31.92
Urea 1 *M*	41.17	37.57	34.71	32.44	30.65
Urea 2 *M*	37.82	34.80	32.49	30.78	29.55
Urea 4 *M*	32.28	30.66	28.94	27.15	25.32
Urea 7 *M*	26.76	25.79	24.82	23.87	22.94
Sucrose 0.5 *M*	35.92	32.76	30.20	28.13	26.46
1-Propanol (mole fraction 0.03)	45.94	42.48	39.51	36.96	34.75
Dimethyl sulfoxide (x = 0.03)	43.29	39.77	36.84	34.40	32.36
1,4-Dioxane (x = 0.03)	45.16	42.11	39.49	37.24	35.30
NaCl 0.25 *M*	40.47	36.79	33.75	31.23	29.14
NaCl 0.50 *M*	37.00	33.74	31.08	28.90	27.11
NaCl 1 *M*	30.48	28.00	25.94	24.24	22.85
NaCl 2 *M*	21.23	19.77	18.60	17.65	16.91
NaBr 1 *M*	30.62	28.23	26.26	24.65	23.32
NaI 1 *M*	31.02	28.57	26.71	25.33	24.35
LiCl 1 *M*	33.94	31.06	28.64	26.61	24.83
KCl 1 *M*	31.29	28.88	26.76	24.88	23.21
CsCl 1 *M*	32.50	29.36	27.10	25.53	24.53
NH_4Cl 1 *M*	35.56	32.73	30.17	27.86	25.77

TABLE V: Values of the Ostwald Absorption Coefficient γ_s for Ethane in Various Aqueous Solutions

Solution	$\gamma_s \times 10^3$				
	10°	15°	20°	25°	30°
H_2O	69.05	59.12	51.39	45.33	40.54
Urea 1 *M*	64.01	56.03	49.42	43.91	39.28
Urea 2 *M*	60.42	53.25	47.50	42.85	39.08
Urea 4 *M*	54.20	48.79	44.17	40.18	36.74
Urea 7 *M*	48.97	44.21	40.63	37.98	36.07
Sucrose 0.5 *M*	56.09	48.80	42.93	38.18	34.30
1-Propanol (mole fraction 0.03)	74.37	65.46	58.54	53.11	48.86
Dimethyl sulfoxide (x = 0.03)	70.95	62.33	55.44	49.89	45.39
1,4-Dioxane (x = 0.03)	77.29	68.77	62.07	56.78	52.62
NaCl 0.25 *M*	61.51	53.41	46.78	41.31	36.76
NaCl 0.50 *M*	55.79	47.72	41.56	36.80	33.11
NaCl 1 *M*	43.67	37.95	33.60	30.29	27.77
NaCl 2 *M*	28.62	25.36	22.82	20.83	19.29
NaBr 1 *M*	45.40	39.55	34.97	31.35	28.48
NaI 1 *M*	47.13	41.47	36.83	33.00	29.81
LiCl 1 *M*	49.20	42.78	37.68	33.61	30.33
KCl 1 *M*	45.22	39.63	35.11	31.44	28.43
CsCl, 1 *M*	47.36	41.00	36.27	32.77	30.20
NH_4Cl 1 *M*	52.36	45.96	40.36	35.48	31.20

and those of Wetlaufer, *et al.*,[14] and of Wen and Hung.[12] It should be noted however that the direction of the change of the solubility of the gas upon the addition of the solute is the same in all the works cited above.

III. Thermodynamics of Solution

The standard free energy of solution of a solute s is related to the Ostwald absorption coefficient by[10]

$$\Delta\mu_s^\circ = -kT \ln \gamma_s \qquad (3.1)$$

TABLE VI: Values of the Standard Free Energy, Entropy, and Enthalpy of Solution[a] for Methane in Aqueous Electrolyte Solutions[b]

Solution	t, °C	$\Delta\mu_s^\circ$	ΔS_s°	ΔH_s°
H_2O	10	1747.0	−18	−3400
	25	2000.0	−15	−2600
NaCl 0.25 *M*	10	1805.1	−18	−4600
	25	2054.2	−16	−4300
NaCl 0.50 *M*	10	1855.7	−17	−5300
	25	2100.2	−15	−4000
NaCl 1 *M*	10	1964.7	−17	−4800
	25	2204.4	−15	−3400
NaCl 2 *M*	10	2168.2	−16	−4100
	25	2392.3	−14	−3000
NaBr 1 *M*	10	1962.1	−17	−2700
	25	2194.5	−14	−2100
NaI 1 *M*	10	1954.8	−17	−2900
	25	2178.3	−13	−1600
LiCl 1 *M*	10	1904.1	−17	−3000
	25	2149.3	−16	−2500
KCl 1 *M*	10	1949.8	−16	−2600
	25	2189.0	−16	−2500
CsCl 1 *M*	10	1928.5	−20	−3600
	25	2173.6	−13	−1800
NH_4Cl 1 *M*	10	1877.8	−16	−2700
	25	2121.9	−16	−2800

[a] Computed by the relations in section III. [b] The units for $\Delta\mu_s^\circ$ and ΔH_s° are cal/mole and for ΔS_s° are cal/(mole degree).

TABLE VII: Values of the Standard Free Energy, Entropy, and Enthalpy of Solution[a] for Ethane in Aqueous Electrolyte Solutions[b]

Solution	t, °C	$\Delta\mu_s^\circ$	ΔS_s°	ΔH_s°
H_2O	10	1504.0	−24	−5200
	25	1833.0	−20	−4200
NaCl 0.25 *M*	10	1569.5	−22	−4600
	25	1888.5	−21	−4300
NaCl 0.50 *M*	10	1624.4	−24	−5300
	25	1957.1	−20	−4000
NaCl 1 *M*	10	1762.2	−23	−4800
	25	2072.5	−18	−3400
NaCl 2 *M*	10	2000.0	−22	−4100
	25	2294.2	−18	−3000
NaBr 1 *M*	10	1740.4	−23	−4600
	25	2052.0	−19	−3600
NaI 1 *M*	10	1719.3	−21	−4200
	25	2021.7	−19	−3700
LiCl 1 *M*	10	1695.1	−23	−4700
	25	2010.8	−20	−3800
KCl 1 *M*	10	1742.6	−22	−4400
	25	2050.4	−19	−3700
CsCl 1 *M*	10	1716.6	−24	−5000
	25	2025.8	−18	−3200
NH_4Cl 1 *M*	10	1660.1	−21	−4200
	25	1978.7	−22	−4500

[a] Computed by the relations in section III. [b] Units as in Table VI.

About eight values of γ_s were measured for each solution in the range of temperatures between 5 and 25°. The temperature dependence of $\Delta\mu_s^\circ$ was fitted to a second-degree polynomial of the form

$$\Delta\mu_s^\circ = a + bT + cT^2 \qquad (3.2)$$

where T is the absolute temperature, and the coefficients a, b, and c were determined by the method of least squares; these as well as the standard deviations are reported in Tables II and III.

The smoothed values of γ_s (obtained from (3.1), after finding the polynomial coefficients) are given in Tables IV and V.

TABLE VIII: Values of the Standard Free Energy, Entropy, and Enthalpy of Solution[a] for Methane in Various Solutions of Nonelectrolytes[b]

Solution	t, °C	$\Delta\mu_s°$	$\Delta S_s°$	$\Delta H_s°$
H_2O	10	1747.0	−18	−3400
	25	2000.0	−15	−2600
Urea 1 *M*	10	1795.3	−17	−3100
	25	2031.8	−14	−2200
Urea 2 *M*	10	1843.1	−17	−2900
	25	2063.0	−13	−1700
Urea 4 *M*	10	1932.4	−12	−1500
	25	2137.4	−15	−2400
Urea 7 *M*	10	2037.8	−11	−1200
	25	2213.5	−12	−1400
Sucrose 0.5 *M*	10	1872.2	−18	−3100
	25	2116.3	−15	−2300
1-Propanol	10	1733.8	−15	−2600
(mole fraction 0.03)	25	1954.5	−14	−2300
Dimethyl sulfoxide	10	1767.2	−16	−2800
(x = 0.03)	25	1997.0	−14	−2300
1,4-Dioxane	10	1743.4	−14	−2300
(x = 0.03)	25	1950.0	−13	−2000

[a] Computed by the relations in section III. [b] Units as in Table VI.

TABLE IX: Values of the Standard Free Energy, Entropy, and Enthalpy of Solution[a] for Ethane in Various Solutions of Nonelectrolytes[b]

Solution	t, °C	$\Delta\mu_s°$	$\Delta S_s°$	$\Delta H_s°$
H_2O	10	1504.0	−24	−5200
	25	1833.0	−20	−4200
Urea 1 *M*	10	1547.0	−21	−4400
	25	1852.4	−20	−4000
Urea 2 *M*	10	1579.5	−20	−4200
	25	1866.8	−18	−3400
Urea 4 *M*	10	1640.7	−18	−3400
	25	1905.0	−17	−3300
Urea 7 *M*	10	1697.7	−19	−3600
	25	1938.3	−14	−2100
Sucrose 0.5 *M*	10	1621.4	−22	−4600
	25	1935.2	−20	−4000
1-Propanol	10	1462.6	−20	−4300
(mole fraction = 0.03)	25	1739.6	−17	−3200
Dimethyl sulfoxide	10	1489.1	−21	−4300
(x = 0.03)	25	1776.7	−18	−3500
1,4-Dioxane	10	1440.9	−19	−4000
(x = 0.03)	25	1700.0	−15	−2900

[a] Computed by the relations in section III. [b] Units as in Table VI.

The standard entropy and enthalpy of solution were computed from the relations

$$\Delta S_s° = -[\partial\Delta\mu_s°/\partial T] \quad (3.3)$$

$$\Delta H_s° = \Delta\mu_s° + T\Delta S_s° \quad (3.4)$$

Note that all these quantities refer to the process of transferring a solute s from a fixed position in a gas to a fixed position in the liquid, the process being carried out at constant temperature and pressure (for more details see ref 10).

The standard free energies, entropies, and enthalpies of methane and ethane in these solutions at 10 and 25° are reported in Tables VI, VII, VIII, and IX.

IV. Hydrophobic Interaction and Its Temperature Dependence

By hydrophobic interaction (HI) in this section, we refer to the quantity $\delta G^{HI}(R)$, for R = 1.533 Å computed by the approximate relation 1.3 In the previous section we have computed all the necessary thermodynamic quantities required for estimating the HI. Furthermore, the entropy and the enthalpy change associated with the process of HI are computed by the approximate relations

$$\delta S^{HI} = \Delta S_{Et}° - 2\Delta S_{Me}° \quad (4.1)$$

$$\delta H^{HI} = \Delta H_{Et}° - 2\Delta H_{Me}° \quad (4.2)$$

The values of δG^{HI}, δS^{HI}, and δH^{HI} are presented in Tables X and XI. In Figure 1 we present the dependence of the HI on the concentration of the solute (NaCl in the range 0–2 *M*, and urea in the range 0–7 *M*).

Perhaps the most interesting finding is that all solutes used in this work caused a strengthening effect on the HI. Furthermore this effect seems to be linear with the concentration of the solute at least in so far as we are con-

TABLE X: Hydrophobic Interaction and the Corresponding Entropy and Enthalpy Values for the Reaction 2(Methane) → Ethane in Various Aqueous Solutions of Electrolytes[a]

Solution	t, °C	δG^{HI}	δS^{HI} (15°)	δH^{HI} (15°)
H_2O	10	−1990.0	11	1500
	25	−2168.0		
NaCl 0.25 *M*	10	−2050.7	13	1500
	25	−2220.7		
NaCl 0.50 *M*	10	−2087.0	11	900
	25	−2243.3		
NaCl 1 *M*	10	−2167.2	10	1100
	25	−2336.3		
NaCl 2 *M*	10	−2336.4	10	700
	25	−2490.4		
NaBr 1 *M*	10	−2183.8	11	700
	25	−2337.0		
NaI 1 *M*	10	−2190.3	12	900
	25	−2335.0		
LiCl 1 *M*	10	−2113.1	12	1200
	25	−2287.8		
KCl 1 *M*	10	−2157.0	12	1000
	25	−2327.6		
CsCl 1 *M*	10	−2140.4	12	1600
	25	−2321.4		
NH_4Cl 1 *M*	10	−2095.5	11	1100
	25	−2265.1		

[a] Units as in Table VI.

TABLE XI: Hydrophobic Interaction and the Corresponding Entropy and Enthalpy Values for the Reaction 2(Methane) → Ethane in Various Aqueous Solutions of Nonelectrolytes[a]

Solution	t, °C	δG^{HI}	δS^{HI} (15°)	δH^{HI} (15°)
H_2O	10	−1990.0	11	1500
	25	−2168.0		
Urea 1 *M*	10	−2043.6	11	1300
	25	−2211.2		
Urea 2 *M*	10	−2106.7	10	1000
	25	−2259.2		
Urea 4 *M*	10	−2224.1	8	200
	25	−2370.0		
Urea 7 *M*	10	−2377.0	7	−700
	25	−2488.7		
Sucrose 0.5 *M*	10	−2123.0	13	1400
	25	−2297.4		
1-Propanol	10	−2005.0	11	1100
(mole fraction 0.03)	25	−2169.4		
Dimethyl sulfoxide	10	−2045.3	12	1300
(x = 0.03)	25	−2217.3		
1,4-Dioxane	10	−2046.0	10	800
(x = 0.03)	25	−2200.0		

[a] Units as in Table VI.

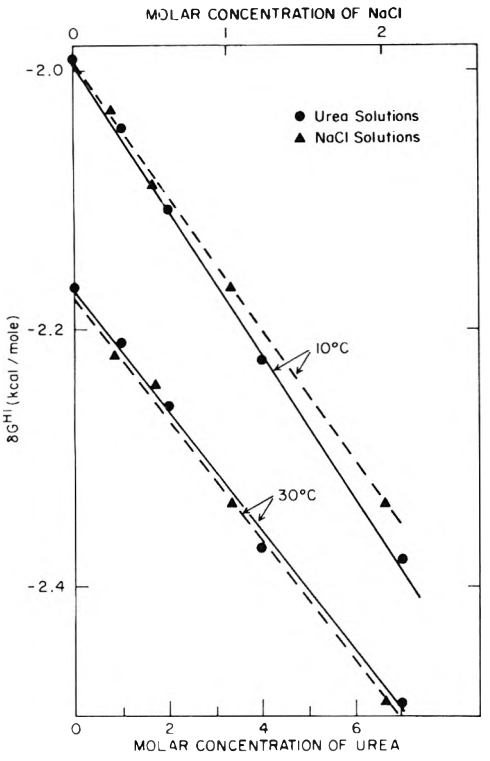

Figure 1. Dependence of the strength of hydrophobic interaction (δG^{HI} in kcal/mole) on the concentration of NaCl and urea. Note that upper scale corresponds to the concentration of NaCl.

cerned with the two examples shown in Figure 1. The implication of the above conclusion to more complex systems such as biopolymers is quite clear. If the HI was the dominating factor which determines the stabilization of the native conformation of a biopolymer, then it is expected that added solutes would all show a stabilization effect. The fact that some solutes do enhance denaturation must therefore be attributed to the weakening of other forces, such as hydrogen bonds or ion-ion interaction which successfully compete with the strengthening effect on the HI. It is worthwhile noting that very small amounts of ethanol were found to weaken the HI.[16]

In a previous paper,[16] we have discussed the origin of the large and positive entropy and enthalpy of HI in terms of the structural changes in the solvent (this topic is treated in more precise terms in ref 10). From Tables X and XI it is clear that increasing the concentration of either NaCl or urea, while increasing the strength of the HI, have a decreasing effect on the entropy and the enthalpy associated with the process. This finding lends further support to the conclusion reached previously[10,15,16] that increasing the structure of the solvent leads to a decrease of the strength of the HI. At the same time less structural changes in the solvent are involved in the process of HI which is reflected in the decreasing values of the entropy and the enthalpy of this process.

Another point which is worth discussion is the comparison of $\Delta\mu_s^\circ$ with δG^{HI} as a measure of the strength of HI. Consider, for instance, the process of transfering a single methane molecule from a fixed position in water to a fixed position in an aqueous solution (at T,P constant). The free energy change for this process is

$$\Delta\mu_{tr}^\circ = \Delta\mu_{Me}^\circ(\text{solution}) - \Delta\mu_{Me}^\circ(\text{water}) \quad (4.3)$$

Kauzmann[3] has advocated the use of $\Delta\mu_{tr}^\circ$ as a measure of the tendency of methane molecules to avoid the aqueous environment. In fact a negative value of $\Delta\mu_{tr}^\circ$ should indicate that the solution is a more favorable environment for methane compared with pure water.

A different measure of the tendency of the two methane molecules to adhere to each other is δG^{HI}. A comparison of δG^{HI} in two solvents indicates to what extent the two methanes tend to avoid the solvent environment in each case.

A glance at Tables X and XI and a comparison with the thermodynamic quantities of section III shows that in most cases the two indices lead to consistent conclusions, but there exist exceptions which warrant some care in drawing such a conclusion. We present here two examples.

(1) Let W stand for water and S for 1 M solution of NaCl. Then we have (at 10°)

$$\Delta\mu_{tr}^\circ = \Delta\mu_{Me}^\circ(S) - \Delta\mu_{Me}^\circ(W) = 1965 - 1747 = 218 \text{ cal/mol} \quad (4.4)$$

$$\delta G^{HI}(S) = -2167.2 \text{ cal/mol} \quad \delta G^{HI}(W) = -1990 \text{ cal/mol} \quad (4.5)$$

Equation 4.4 indicates that the water environment is more favorable for methane than the solution ("salting out"). Equation 4.5 shows that the tendency to avoid the solvent environment is stronger in S compared with W. Hence the two conclusions are consistent with each other. A contrary example is the following.

(2) Let W stand for water and S for a solution of 1-propanol (mole fraction of propanol 0.03) all at 10°, then

$$\Delta\mu_{tr}^\circ = \Delta\mu_{Me}^\circ(S) - \Delta\mu_{Me}^\circ(W) = 1733.8 - 1747 = -13.2 \text{ cal/mol} \quad (4.6)$$

$$\delta G^{HI}(S) = -2005 \text{ cal/mol} \quad \delta G^{HI}(W) = -1990 \text{ cal/mol} \quad (4.7)$$

Here the propanol solution is more favorable for methane, as indicated by the negative standard free energy of transfer. On the other hand, the tendency to avoid the solvent is *stronger* in S than in W (as in the previous example). The absolute values of $\Delta\mu_{tr}^\circ$ and of $\Delta(\delta G^{HI})$ are admittedly very small. Nevertheless we feel that an important conclusion may be drawn from these observations. Namely, that free energies of transfer and hydrophobic interaction (as measured by δG^{HI}), in general, need not be compatible with each other. Other examples where the discrepancy between the two quantities are more pronounced were reported elsewhere.[10,16]

Although variations in the strength of HI in different solutions of electrolytes are small, we believe that they are significant. For example, in 1 M solutions of NaCl, KCl, and CsCl (at 10°) the strength of HI decreases, *i.e.*, −2.167, −2.157, and −2.140 kcal/mol, respectively. On the other hand, increasing the size of the anion for a fixed cation shows an opposite effect. Namely, for 1 M solutions of NaCl, NaBr, and NaI (at 10°) the corresponding values are −2.167, −2.184, and −2.19 kcal/mol.

The variations in both the entropies and the enthalpies associated with the HI process in the different solutions are estimated to be well within the experimental error in these quantities.

We believe that in spite of the approximate nature of our "model" for measuring HI, the various trends found in

this work are correct and manifest the corresponding trends that one would have measured in real processes, *i.e.*, when the final configuration of the particles is more realistic than the one employed in the model.

Acknowledgment. This work has been partially supported by the Israel commission for basic research for which the authors are very grateful.

References and Notes

(1) Present address, National Institutes of Health, NIAMDD, LMB, Bethesda, Md. 20014.
(2) (a) C. Tanford, *Advan. Protein Chem.*, **23**, 121 (1968); (b) **24**, 1 (1970).
(3) W. Kauzmann, *Advan. Protein Chem.*, **14**, 1 (1959).
(4) A. Ben-Naim, *J. Chem. Phys.*, **54**, 1387, 3696 (1971).
(5) A. Ben-Naim, *J. Chem. Phys.*, **57**, 5257, 5266 (1972).
(6) J. F. Brandts and L. Hunt, *J. Amer. Chem. Soc.*, **89**, 4826 (1967).
(7) Z. Priel and A. Silberberg, *J. Polym. Sci., Part A-2*, **8**, 689, 705, 713 (1970).
(8) I. M. Klotz, *Fed. Proc., Fed. Amer. Soc. Exp. Biol., Part III*, **24**, S-24 (1965).
(9) S. Y. Gerlsma, *J. Biol. Chem.*, **243**, 957 (1968).
(10) A. Ben-Naim, "An Introduction to a Molecular Theory of Water and Aqueous Solutions," Plenum Press, New York, N. Y., in press.
(11) A. Ben-Naim and S. Baer, *Trans. Faraday Soc.*, **59**, 2735 (1963).
(12) Wen-Yang Wen and J. H. Hung, *J. Phys. Chem.*, **74**, 170 (1970).
(13) T. J. Morrison and F. Billet, *J. Chem. Soc.*, 3819 (1952).
(14) D. B. Wetlaufer, S. K. Malik, L. Stoller, and R. L. Coffin, *J. Amer. Chem. Soc.*, **86**, 508 (1964).
(15) A. Ben-Naim, J. Wilf, and M. Yaacobi, *J. Phys. Chem.*, **77**, 95 (1973).
(16) M. Yaacobi and A. Ben-Naim, *J. Solution Chem.*, **2**, 425 (1973).

Solvophobic Interaction

M. Yaacobi and A. Ben-Naim*[1]

Department of Inorganic and Analytical Chemistry, The Hebrew University of Jerusalem, Jerusalem, Israel
(Received July 12, 1973)

The solubilities of methane and ethane were measured in the following solvents: water, methanol, ethanol, 1-propanol, 1-butanol, 1-pentanol, 1-hexanol, 1,4-dioxane, and cyclohexane. The standard free energies, entropies, and enthalpies of solution of methane and ethane in these solvents were computed. From these data the strength of the "solvophobic interaction" is estimated in these solvents. It is found that the strength of solvophobic interaction is distinctly larger in water as compared with the other nonaqueous solvents. The entropy and enthalpy associated with the process of bringing two solutes from infinite separation to a short distance is also amonalous in water as compared with other solvents.

I. Introduction

The term "hydrophobic interaction" (HI) has been used in previous articles[2] to describe the indirect part of the work required to bring two solutes from infinite separation to a final configuration $\mathbf{R}_1,\mathbf{R}_2$ (the process being carried out within the solvent at constant temperature T and pressure P).

$$\Delta G(\mathbf{R}_1,\mathbf{R}_2) = U(\mathbf{R}_1,\mathbf{R}_2) + \delta G^{\mathrm{HI}}(\mathbf{R}_1,\mathbf{R}_2) \qquad (1.1)$$

One of the central questions in the study of the role of water in biological systems is to what extent the properties of water are unique as compared with other nonaqueous solvents.

The purpose of this article is to compare the strength of the HI in water with the corresponding quantity, which may be referred to as "solvophobic interaction" (SI), in other solvents. The latter term has been suggested earlier[2a] for the quantity $\delta G^{\mathrm{HI}}(\mathbf{R}_1,\mathbf{R}_2)$ defined in (1.1) for any solvent (we shall use the superscript HI for water and the superscript SI for the same quantity in a nonaqueous system).

The approximate measure of the SI developed in previous articles[2] is given by

$$\delta G^{\mathrm{SI}}(R = 1.533\ \text{Å}) = \Delta\mu_{\mathrm{Et}}^{\circ} - 2\Delta\mu_{\mathrm{Me}}^{\circ} \qquad (1.2)$$

where $\Delta\mu_{\alpha}^{\circ}$ is the standard free energy of solution of the solute α in the appropriate solvent (Et represents ethane and Me methane).

A different estimate of the SI using the quantity $\delta G^{\mathrm{SI}}(R = 0)$ has been suggested earlier[2a] and was studied in some details by Wilhelm and Battino[3] (for a review of this topic see ref 4). In this paper we use the quantity δG^{SI} defined in (1.2) as a probe for the strength of SI. This has an obvious advantage over $\delta G^{\mathrm{SI}}(R = 0)$. The reason is that δG^{SI} is based on the measurements of experimental quantities $\Delta\mu_{\mathrm{Et}}^{\circ}$ and $\Delta\mu_{\mathrm{Me}}^{\circ}$, whereas the estimation of $\delta G^{\mathrm{SI}}(R = 0)$ is based on the scaled particle theory, the application of which to a complex liquid such as water is doubtful.[4]

In order to compute the values of δG^{SI} in water and in some nonaqueous solvent we have measured the solubilities of methane and ethane in a series of solvents. These data furnish the required information necessary for estimating the solvophobic interaction through (1.2).

Although we have used only a limited number of solvents, one can safely conclude that water is indeed an outstanding liquid as far as we are concerned with both the values and the temperature dependence of δG^{SI}.

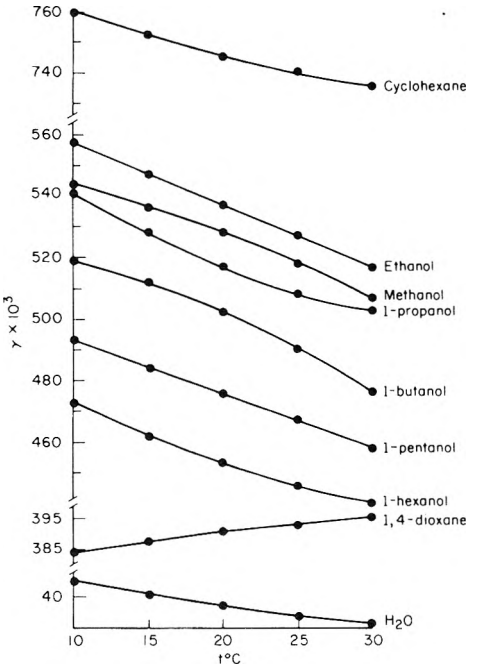

Figure 1. Ostwald absorption coefficients as a function of temperature for methane in various solvents.

TABLE I: Polynomial Coefficients in (2.2) and the Standard Deviation for Each Set of Measurements

Solvent	a	b	c	Standard deviation
		Methane		
Methanol	0.03729	−18.546	2,604.5	1.137
Ethanol	0.01024	−2.636	255.3	0.912
1-Propanol	−0.04361	29.028	−4,378.1	1.977
1-Butanol	0.05623	−29.065	4,090.4	1.760
1-Pentanol	0.01150	−3.230	390.8	2.233
1-Hexanol	−0.02895	20.591	−3,087.6	1.753
1,4-Dioxane	0.00988	−4.781	1,099.8	3.997
Cyclohexane	−0.01791	12.053	−1,822.9	1.678
		Ethane		
Methanol	−0.03440	25.237	−4,979.8	1.135
Ethanol	−0.04241	30.439	−5,901.0	1.800
1-Propanol	0.00607	2.606	−1,928.0	1.182
1-Butanol	−0.07884	51.627	−9,001.0	1.585
1-Pentanol	−0.01155	12.817	−3,395.6	3.505
1-Hexanol	−0.02364	19.124	−4,183.0	3.824
1,4-Dioxane	0.20190	−115.36	15,942.3	3.056
Cyclohexane	0.05878	−29.932	2,712.0	2.970

II. Experimental Section

The solubilities of methane and ethane were determined as described in the preceeding article.[2] The solvents 1-propanol, 1-hexanol, and cyclohexane were CP whereas all other solvents were of analytical grade.

The Ostwald absorption coefficients γ for methane and ethane in water, methanol, ethanol, 1-propanol, 1-butanol, 1-pentanol, 1-hexanol, 1,4-dioxane, and cyclohexane were calculated directly from the volume of gas dissolved in a given volume of the solvent.

A comparison of the values of γ of methane and ethane in alcoholic solutions measured in this work with those of Boyer and Bircher[5] shows that our results are about 0–6% lower than theirs. It is difficult, however, to trace the source of the discrepancies between the two sets of results.

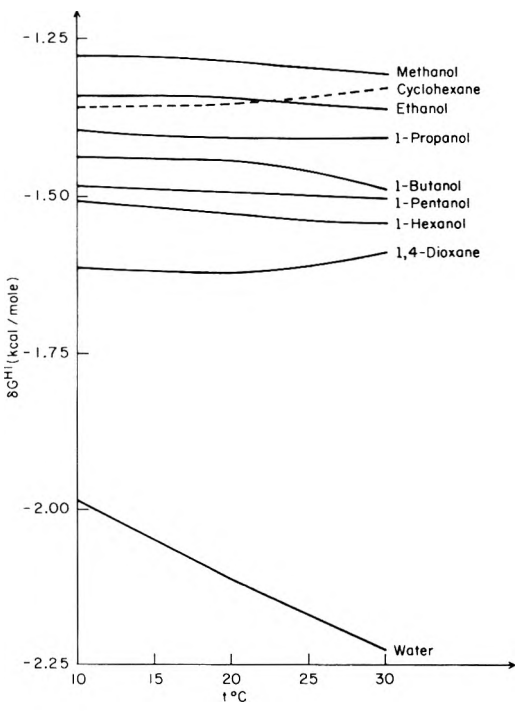

Figure 2. The temperature dependence of the solvophobic interaction δG^{SI} in kcal/mole computed from (3.4) for water and nonaqueous solvents.

TABLE II: Values of the Ostwald Absorption Coefficient γ_s for Methane and Ethane in Various Solvents

Solvent	$\gamma_s \times 10^3$ 10°	15°	20°	25°	30°
			Methane		
Water	44.8	40.5	37.0	34.2	31.9
Methanol	543.7	536.4	527.8	518.0	507.0
Ethanol	556.7	546.8	537.0	527.2	517.5
1-Propanol	541.7	528.2	517.4	509.0	502.9
1-Butanol	519.4	511.5	501.6	489.8	476.5
1-Pentanol	492.5	484.3	476.0	467.6	459.2
1-Hexanol	472.7	462.2	453.5	446.3	440.4
1,4-Dioxane	384.1	387.6	390.7	393.3	395.6
Cyclohexane	760.3	752.0	745.0	739.5	735.3
			Ethane		
Water	69.1	59.1	51.4	45.3	40.5
Methanol	2864	2678	2518	2379	2258
Ethanol	3361	3117	2909	2731	2578
1-Propanol	3492	3241	3014	2808	2621
1-Butanol	3491	3225	3008	2830	2686
1-Pentanol	3403	3155	2935	2740	2566
1-Hexanol	3252	3034	2842	2674	2526
1,4-Dioxane	2590	2548	2465	2347	2201
Cyclohexane	6470	6067	5673	5291	4921

The standard free energy of solution of a solute s is computed by the relation

$$\Delta\mu_s^\circ = RT \ln \gamma_s \tag{2.1}$$

and the temperature dependence of $\Delta\mu_s^\circ$ was fitted to a second-degree polynomial of the form

$$\Delta\mu_s^\circ = a + bT + cT^2 \tag{2.2}$$

where T is the absolute temperature. The coefficients a, b, and c (obtained by the method of least squares) as well as the standard deviation for each set of measurements are reported in Table I.

TABLE III: Values of the Standard Energy, Entropy, and Enthalpy of Solution for Methane in Several Solvents[a]

Solvent	t, °C	$\Delta\mu_s°$	$\Delta S_s°$	$\Delta H_s°$
Water	10	1747	−18	−3400
	25	2000	−15	−2600
Methanol	10	343.0	−3	−400
	25	390.0	−4	−700
Ethanol	10	329.7	−3	−600
	25	379.4	−3	−700
1-Propanol	10	345.0	−4	−900
	25	400.2	−3	−500
1-Butanol	10	368.7	−3	−400
	25	423.0	−4	−900
1-Pentanol	10	398.6	−3	−500
	25	450.5	−4	−600
1-Hexanol	10	421.7	−4	−800
	25	478.2	−3	−500
1,4-Dioxane	10	538.5	−1	300
	25	553.0	−1	200
Cyclohexane	10	154.2	−2	−400
	25	179.0	−1	−200

[a] The units for $\Delta\mu_s°$ and $\Delta H_s°$ are cal/mole and for $\Delta S_s°$ are cal/mole degree.

TABLE IV: Values of the Standard Free Energy, Entropy and Enthalpy of Solution for Ethane in Several Solvents[c]

Solvent	t, °C	$\Delta\mu_s$[c]	$\Delta S_s°$	$\Delta H_s°$
Water	10	1504	−24	−5200
	25	1833	−20	−4200
Methanol	10	−592.2	−6	−2200
	25	−513.6	−5	−1900
Ethanol	10	−682.2	−6	−2500
	25	−595.4	−5	−2100
1-Propanol	10	−703.8	−6	−2400
	25	−611.8	−6	−2500
1-Butanol	10	−703.6	−7	−2700
	25	−616.6	−5	−2000
1-Pentanol	10	−689.2	−6	−2500
	25	−597.4	−6	−2400
1-Hexanol	10	−663.7	−6	−2300
	25	−583.0	−5	−2100
1,4-Dioxane	10	−535.6	1	−200
	25	−505.6	−5	−2000
Cyclohexane	10	−1050.8	−3	−2000
	25	−987.3	−5	−2500

[a] Units as in Table III.

The smoothed values of the Ostwald coefficients for methane and ethane in the various solvents are reported in Table II. Note that the solubility of methane (as measured by γ) in 1,4-dioxane increases with temperature. In all others the solubility decreases with temperature. This behavior is depicted in Figure 1.

III. Solvophobic Interaction (SI)

In order to compute the SI and its temperature dependence we need the standard free energy, entropy, and enthalpy of solution of methane and of ethane in the various solvents. These are computed from the relations

$$\Delta\mu_s° = -RT \ln \gamma_s \quad (3.1)$$

$$\Delta S_s° = -[\partial\Delta\mu_s°/\partial T] \quad (3.2)$$

$$\Delta H_s° = \Delta\mu_s° + T\Delta S_s° \quad (3.3)$$

Note that these quantities refer to the process of transferring a solute s from a fixed position in the gas to a fixed position in the liquid. The process being carried out at constant temperature and pressure (for more details see ref 4). The computed values of $\Delta\mu_s°$, $\Delta S_s°$, and $\Delta H_s°$ are reported in Tables III and IV.

TABLE V: Solvophobic Interaction and the Corresponding Entropy and Enthalpy Values for the Reaction 2(Methane) → Ethane in Several Solvents[a]

Solvent	t, °C	δG^{SI}	δS^{SI} (10°)	δH^{SI} (10°)
Water	10	−1990	11	+1500
	25	−2168		
Methanol	10	−1278.2	0	−1400
	25	−1293.6		
Ethanol	10	−1341.6	0	−1300
	25	−1354.2		
1-Propanol	10	−1393.8	2	−600
	25	−1412.2		
1-Butanol	10	−1441.0	−1	−1900
	25	−1462.6		
1-Pentanol	10	−1486.4	0	−1500
	25	−1498.4		
1-Hexanol	10	−1507.1	2	−700
	25	−1539.4		
1,4-Dioxane	10	−1612.6	3	−800
	25	−1611.6		
Cyclohexane	10	−1359.2	1	−1200
	25	−1345.3		

[a] Units as in Table III.

Note that the entropy of solution of methane and ethane in water is between −20 and −24 eu whereas in organic solvents the corresponding values range between −1 and −6 eu. The outstanding low and negative enthalpy of solution of these gases in water is also clear from Tables III and IV.

The strength of the SI and the corresponding entropy and enthalpy associated with the process of bringing two methane molecules to a short distance are computed by the approximate relations

$$\delta G^{SI} = \Delta\mu_{Et}° - 2\Delta S_{Me}° \quad (3.4)$$

$$\delta S^{SI} = \Delta S_{Et}° - 2\Delta S_{Me}° \quad (3.5)$$

$$\delta H^{SI} = \Delta H_{Et}° - 2\Delta H_{Me}° \quad (3.6)$$

Values of δG^{SI}, δS^{SI}, and δH^{SI} are reported in Table V and the temperature dependence of δG^{SI} is exhibited in Figure 2.

From Figure 2 it is clear that both the values of δG^{SI} and its temperature dependence in water are markedly different from the corresponding behavior in nonaqueous solvents.

The significance of the strong HI in water to biological systems has long been recognized.[6-8] Various processes such as conformational changes of biopolymers, adsorption of a substrate on an enzyme, etc. are all affected by the strength of the HI. We should like to conclude this article by pointing out that the temperature dependence of HI is also of important biological significance.[9] Consider, for example, the helix coil transition in proteins or any process of denaturation of a biopolymer. One expects that as the temperature increases, the system would tend to break its structure. The fact that the HI strengthened with the increase of temperature may be considered as a counteraction to the tendency of randomization, and aids to maintain the stable conformation of the polymer.

Acknowledgment. This work has been supported in part by the Israel Commission for Basic Research, for which the authors are very grateful.

References and Notes

(1) Present address, National Institutes of Health, NIAMDD, LMB, Bethesda, Md. 20014.
(2) (a) Ben-Naim, *J. Chem. Phys.*, **54**, 1387, 3696 (1971); (b) A. Ben-Naim and M. Yaacobi, *J. Phys. Chem.*, **78**, 170 (1974).
(3) E. Wilhelm and R. Battino, *J. Chem. Phys.*, **56**, 563 (1972).
(4) A. Ben-Naim, "An Introduction to a Molecular Theory of Water and Aqueous Solutions," Plenum Press, New York, N. Y., in press.
(5) F. L. Boyer and L. J. Bircher, *J. Phys. Chem.*, **64**, 1330 (1960).
(6) W. Kauzmann, *Advan. Protein Chem.*, **14**, 1 (1959).
(7) G. Nemethy and H. L. Scheraga, *J. Phys. Chem.*, **66**, 1773 (1962).
(8) C. Tanford, *Advan. Protein Chem.*, **23**, 121 (1968).
(9) H. L. Scheraga, G. Nemethy, and I. Z. Steinberg, *J. Biol. Chem.*, **237**, 2506 (1962).

Thermodynamic Studies of Binary Charge Unsymmetrical Fused Salt Systems. Cerium(III) Chloride–Alkali Chloride Mixtures

G. N. Papatheodorou* and O. J. Kleppa

The James Franck Institute and The Department of Chemistry, The University of Chicago, Chicago, Illinois 60637

(Received June 11, 1973)

Publication costs assisted by the National Science Foundation

The molar enthalpies of mixing (ΔH^M) in the liquid alkali chloride–cerium chloride mixtures have been measured at 845°. All the interaction parameters ($\lambda^M = \Delta H^M/X_1X_2$) are negative, increasing sharply from about −1 kcal/mol in LiCl–$CeCl_3$ to about −25 kcal/mol in CsCl–$CeCl_3$. The systems also have significant energetic asymmetries with more negative values of λ^M in the alkali chloride-rich than in the cerium chloride-rich regions. The results are discussed with respect to the following points: (1) comparison with the Davis conformal solution theory for the enthalpies of mixing of charge unsymmetrical fused salt mixtures; (2) "complexing" in the mixture.

Introduction

While thermochemical and thermodynamic information is now available for a significant number of binary charge unsymmetrical fused salt mixtures of the type $AX–BX_2$,[1] much less is known about the corresponding $AX–BX_3$ systems. The present paper represents the first detailed thermochemical study of a system of this type, and covers the liquid systems ACl–$CeCl_3$, where A = Li, Na, K, Rb, or Cs.

The thermodynamic properties of these mixtures previously were studied by equilibrium emf[2-4] and phase diagram[5] methods. The emf[2] data were interpreted to indicate the formation of various complex entities such as $CeCl_4^-$ and $CeCl_6^{3-}$. Strong evidence was presented for $CeCl_4^-$, while the evidence for $CeCl_6^{3-}$ was much less conclusive.

In the present communication we report the enthalpies of mixing (ΔH^M) of cerium(III) chloride with the alkali chlorides. The purpose of this work is to obtain information on the systematics of the thermodynamic behavior of unsymmetrical solution systems and to examine the possibilities of "complex" formation in these mixtures. The new data are compared with the enthalpy measurements on the $LaCl_3$–ACl[6] systems and are discussed in terms of the conformal solution theory of Davis.[7] Finally by combining the calorimetric and emf data we have obtained the partial excess entropies of mixing of $CeCl_3$ in liquid $CeCl_3$–NaCl and $CeCl_3$–KCl mixtures.

Experimental Section

The measurements of the integral enthalpies of mixing were of the "crucible-double breakoff" type, where both liquid salts were contained in fused silica containers.[1,8] The calorimetric apparatus used, its calibration, and the required corrections have been described elsewhere.[1,8] All experiments were carried out at 845°.

The cerium(III) chloride was purchased from Alfa Inorganics Inc. The salt was first dried under vacuum by slowly increasing the temperature to 200°. At that temperature a gaseous mixture of CCl_4–N_2 was passed over the salt and the temperature was raised slowly (~50°/hr) to 500°. Finally, the salt was melted under a N_2 atmosphere. The sources and methods of purification of the alkali halides were the same as before.[1] The purity of the salts was checked by passing an aqueous solution through a cation-exchange column and titrating the resulting acidic solution. The premelted salt assayed 98.8 mol % $CeCl_3$.

Results and Discussion

All experimental results obtained in the course of the present investigation are recorded in Table I.[9] Graphs of the enthalpy interaction parameter, $\lambda^M = \Delta H^M/X_1X_2$, *vs.* mole fraction, $X_2 = X_{CeCl_3}$, are given in Figure 1. For each system listed in Table I the values of λ^M were fitted, by the method of least squares, to fifth-order polynomials of X_2. The coefficients of the least-squares expressions

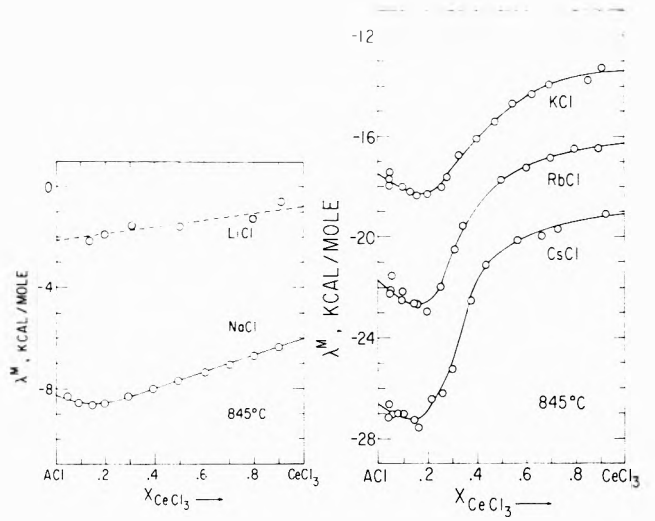

Figure 1. Enthalpy interaction parameters in liquid mixtures of cerium(III) chloride with alkali chlorides. The solid lines represent the "best curves."

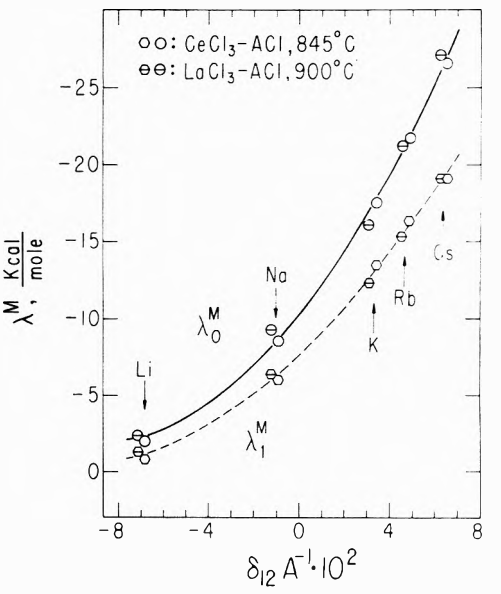

Figure 2. Dependence of the interaction parameter on the size parameter: (——) interaction parameter at $X_{LCl3} = 0$, (λ_0^M); (-----) interaction parameter at $X_{LCl3} = 1$, (λ_1^M).

and the standard deviations of the experimental points from the fitted curves are given in Table II.

All the systems investigated have negative interaction parameters which increase sharply from about −1 kcal/mol for LiCl–$CeCl_3$ to about −25 kcal/mol for CsCl–$CeCl_3$. This trend is entirely consistent with the behavior of the previously studied $AX–BX_2$ mixtures.[1] Note also that all the considered systems show more negative values of the interaction parameter in the alkali chloride-rich than in the cerium chloride-rich region. For the mixtures involving CsCl, RbCl, and KCl a broad minimum is found in λ^M near $X_2 \approx 0.2$, while λ^M increases sharply to less negative values at somewhat higher mole fractions of cerium chloride. A similar variation of λ^M with composition also is found in the corresponding ACl–$LaCl_3$ mixtures.[6] In both cases it is attributed to the formation of LCl_6^{3-} complexes in the alkali chloride-rich mixtures. The existence of complex configurations in such mixtures is indicated by recent Raman structural studies of lanthanum chloride dissolved in liquid potassium chloride.[10] Due to the similarity of the ionic radii and polarizabilities of the La^{3+} and Ce^{3+} ions, it is expected that the electrostatic (coulombic) and polarization forces associated with the formation of the $CeCl_6^{3-}$ and $LaCl_6^{3-}$ configurations should be of comparable magnitude. In view of Figure 1, and in analogy with our earlier work on ACl–BCl_2 mixtures, such configurations presumably are formed and stabilize the solutions of $CeCl_3$ in CsCl, RbCl, and KCl. However, for the mixtures containing NaCl and LiCl our thermochemical data cannot be interpreted to either exclude or confirm the presence of complex configurations. Finally, we find no evidence in the present enthalpy data for the existence of other complex entities such as, *e.g.*, $CeCl_4^-$. This question is discussed in greater detail in ref 6.

We shall now discuss the interaction parameters of the cerium chloride–alkali chloride mixtures in terms of the conformal solution theory of Davis.[7] This theory predicts that at a fixed temperature, pressure, and composition the relative values of the interaction parameter, λ^M, in a sequence of $AX–LX_n$ systems (A = Li–Cs), should to a second-order approximation be a function of the size parameter $\delta_{12} = (d_1 - d_2)/d_1d_2$. ($d_1$ and d_2 are the characteristic interionic distances in the two salts which are mixed.) Thus

$$\lambda^M = a(T,P,X) + b(T,P,X)\delta_{12} + c(T,P,X)\delta_{12}^2 \quad (1)$$

Here a, b, and c are complicated integral functions of T, P, and X; their numerical values will depend on the physical properties of the particular LX_n salt which is taken as the "reference" salt.

In Figure 2 we test the dependence of the interaction parameter on the size parameter, for the $CeCl_3$–ACl mixtures by plotting λ_0^M ($X_2 = 0$) and λ_1^M ($X_2 = 1$) against δ_{12}. In the same figure we have included the corresponding values of the interaction parameter for the $LaCl_3$–ACl systems. The figure shows that the theoretically predicted form of eq 1 can be fitted to the data within experimental error. Furthermore, it appears that for both sequences of LCl_3–ACl (L = La and Ce) mixtures, the coefficients a, b, and c are approximately the same. Least-squares treatment of the data shown to eq 1 yields

$$\lambda_0^M = -10.3 - 188\delta_{12} - 1050\delta_{12}^2 \quad (2a)$$

$$\lambda_1^M = -7.7 - 139\delta_{12} - 668\delta_{12}^2 \quad (2b)$$

Thus the variation of the interaction parameter with δ_{12} is

TABLE II: Least-Squares Coefficients for the Binary Liquid Alkali Chloride–Cesium Chloride Mixtures[a]

$\lambda^M = A + BX_2 + CX_2^2 + DX_2^3 + EX_2^4$ kcal/mol

System	$-A$	$-B$	C	$-D$	E	Std deviation
Cs–Ce	26.16	28.67	178.61	258.12	115.5	0.38
Rb–Ce	21.20	27.33	145.20	198.54	35.6	0.36
K–Ce	17.16	18.46	89.41	112.06	44.9	0.20
Na–Ce	8.15	6.88	29.4	34.9	14.6	0.06
Li–Ce	2.2	−1.55				0.14

[a] In deriving these coefficients, apart from all the experimental points we have made use of the limiting values of the interaction parameter (λ_0, λ_1) obtained from the best curves in Figures 1 and 2. This treatment makes the algebraic representation of the data valid for the complete range of composition.

TABLE III: Characteristic Properties of Some L^{3+} Ions and LCl Salts[a]

	Interionic distance, d, Å	Polarizability of L^{3+}, α, Å^3	Ionization potentials[b] of L^{3+}, kcal I_2	I_3	Electronegativity[b] of L^{3+}, χ	Reduced melting temp, $\tau_m = (dkTm/e^2) \times 10^2$	Reduced vapor[c] pressure at $T = 1.3T_m$, $\pi'' \times 10^{-1}$	Reduced[c] volume at $T = T_m$, $\theta'' \times 10^{-19}$
$LaCl_3$	2.87	1.03	255	442	1.08	218	1.98	2.4
$CeCl_3$	2.84	(1.05)[d]	250	454	1.08	207	1.52	1.4
$PrCl_3$	2.82	(1.07)[d]	243	535	1.07	205	1.14	
$NdCl_3$	2.80	(1.09)[d]	247		1.07	192	0.81	

[a] Interionic distances, melting points, densities, and vapor pressures taken from G. J. Janz, "Molten Salt Handbook," Academic Press, New York, N. Y., 1967; D. Brown, "Halides of the Lanthanides and Actinides," Wiley-Interscience, New York, N. Y., 1968. [b] From D. A. Jonson, "Thermodynamic Aspects of Inorganic Chemistry," Cambridge University Press, New York, N. Y., 1968. [c] Reduced quantities as defined by K. D. Luks and H. T. Davis (ref 11). [d] Estimated quantities.

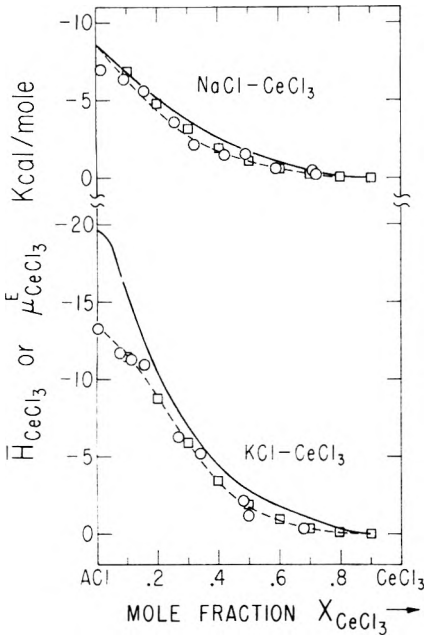

Figure 3. Partial enthalpies and chemical potential in liquid $CeCl_3$-NaCl and $CeCl_3$-KCl systems: (——) partial enthalpies of $CeCl_3$ calculated by the method of intercepts; (- - - - -) excess chemical potentials; O data from ref 2 at 850°; □, data from ref 4 at 825°.

approximately the same both for the $CeCl_3$-ACl sequence with $CeCl_3$ as the reference salt, and for the $LaCl_3$-ACl binaries where $LaCl_3$ is the reference salt. Of course, this is not very surprising since the physical and chemical properties of the reference salts $CeCl_3$ and $LaCl_3$ are very similar. This point is documented further in Table III, which presents some of the characteristic properties of $CeCl_3$ and $LaCl_3$ along with similar data for $PrCl_3$ and $NdCl_3$. Table III shows that for these four salts both the quantities (d, α, l) which determine the magnitude of the dispersion interactions, and the "reduced" parameters defined by Luks and Davis[11] (τ_m, θ'', π'') do not vary a great deal from one salt to the other. This in turn implies that the integrals a, b, and c in eq 1 will be roughly the same for corresponding sequences of mixtures ACl-LCl_3. We accordingly would expect that eq 2a and 2b would be capable of describing all four families of mixtures to a reasonable approximation, and also that the dependence of λ^M on mole fraction would be quite similar in the other systems to that of the ACl-$CeCl_3$ binaries (Figure 1).

Before we close this discussion we want to compare[12] our new enthalpy data for NaCl-$CeCl_3$ and KCl-$CeCl_3$ with the corresponding emf data.[2,4] This comparison is presented in Figure 3 which gives the excess chemical potentials, $\mu^E_{CeCl_3}$, taken from ref 2 and 4, along with the partial enthalpies derived from our own integral enthalpies by the method of intercepts. It is apparent from this figure that there is very good agreement between the chemical potentials obtained by the two independent emf studies.

In view of the experimental error in the emf results, and the inherent uncertainties associated with the derivation of partial enthalpies from integral data, it is not surprising that the calculated values of $\bar{S}^E_{CeCl_3}$ will be associated with significant error.[13] Even so, Figure 3 indicates that for all compositions in NaCl-$CeCl_3$, and for X_{CeCl_3} larger than about 0.2 in KCl-$CeCl_3$, $\mu^E_{CeCl_3}$ and $\bar{H}_{CeCl_3}$ are very similar in magnitude. Since the numerical values of μ^E are somewhat smaller than $\bar{H}$, the excess entropies are negative, but quite small. It appears that in these mixtures the partial entropies of $CeCl_3$ are fairly well described by the Temkin model,[14] which assumes complete randomization of the two different cations on the cation "sites" in the fused salt mixture.

However, for $X_{CeCl_3} < 0.2$ in the KCl-$CeCl_3$ system, the values of $\mu^E_{CeCl_3}$ are less negative than $\bar{H}_{CeCl_3}$ by several kcal/mole. As a consequence, the excess entropies have very significant negative values. This may be the result of local order associated with extensive complex formation, and is consistent with the presence of complex configurations such as $CeCl_6^{3-}$ in the strongly interacting ACl-$CeCl_3$ mixtures.

Acknowledgments. We record our thanks to J. J. Egan for informing us about his research cited here. This work has been supported by the National Science Foundation. It also has benefited from the general support of materials research at The University of Chicago provided by the NSF-MRL Program.

Supplementary Material Available. Table I will appear following these pages in the microfilm edition of this volume of the journal. Photocopies of the supplementary material from this paper only or microfiche (105 × 148 mm, 24× reduction, negatives) containing all of the supplementary material for the papers in this issue may be obtained from the Journals Department, American Chemical Society, 1155 16th St., N.W., Washington, D. C. 20036. Remit check or money order for $3.00 for photocopy or $2.00 for microfiche, referring to code number JPC-74-178.

References and Notes

(1) G. N. Papatheodorou and O. J. Kleppa, *J. Inorg. Nucl. Chem.*, **33**, 1249 (1971), and references therein.

(2) S. Senderoff, G. E. Mellors, and R. I. Bretz, *N. Y. Acad. Sci.*, **79**, 878 (1960).
(3) D. E. Neil, *Diss. Abstr.*, **20**, 2591 (1960).
(4) J. J. Egan and J. Bracker, *J. Chem. Thermodyn.*, in press.
(5) Sun In'-Chzhn and I. S. Morozov, *Zh. Neorg. Khim.*, **3**, 1914 (1958).
(6) G. N. Papatheodorou and T. Østvold, *J. Phys. Chem.*, **78**, 181 (1974).
(7) H. T. Davis, *J. Phys. Chem.*, **76**, 1629 (1972), and references therein.
(8) G. N. Papatheodorou and O. J. Kleppa, *Z. Anorg. Allg. Chem.*, in press.
(9) See paragraph at end of paper regarding supplementary material.
(10) V. Maroni, E. J. Hathaway, and G. N. Papatheodorou, to be submitted for publication.
(11) K. D. Luks and H. T. Davis, *Ind. Eng. Chem., Fundam.*, **6**, 194 (1967).
(12) Following the suggestion of G. J. Janz and C. M. Dijkhuis (*Nat. Stand. Ref. Data Ser., Nat. Bur. Stand.*, **No. 28**, 12 (1969)), we have not used the data of ref 3 for this comparison.
(13) We have estimated that at $X_2 \sim 0.5$, the uncertainties in $\Delta\bar{H}_{CeCl_3}$ and $\mu(CeCl_2)$ are of the order of ±300 and ±300 cal/mol. Thus the uncertainty in $T\Delta\bar{S}^E(CeCl_3)$ may be as large as ±500 cal/mol.
(14) M. Temkin, *Acta Physicochim. USSR*, **20**, 411 (1945).

Thermodynamic Studies of Binary Charge Unsymmetrical Fused Salt Systems. Calorimetric and Electromotive Force Measurements of Liquid Lanthanum(III) Chloride–Alkali Chloride Mixtures

G. N. Papatheodorou*

The James Franck Institute, The University of Chicago, Chicago, Illinois 60637

and Terje Østvold

Institute of Physical Chemistry, NTH, The University of Trondheim, Trondheim, Norway (Received July 16, 1973)

Publication costs assisted by the National Science Foundation

The thermodynamic quantities of mixing in the liquid $LaCl_3$–ACl (A = Li, Na, K, Rb, or Cs) mixtures have been measured. The integral enthalpies of mixing (ΔH^M) for all the above binaries and the partial enthalpies of mixing in the $LaCl_3$–KCl system have been determined calorimetrically. The partial Gibbs energies of mixing (A ≠ Cs) have been determined by emf measurements. Two graphite–chlorine (C(s)|Cl_2(g)) electrodes were used in a galvanic cell of the type: C(s), Cl_2(g)|ACl(l)|alkali glass|$LaCl_3$(l)–ACl(l)|Cl_2(g), C(s). The data are discussed with respect to the following points: (1) comparison with conformal solution theory for the enthalpies of mixing of charge unsymmetrical fused salt mixtures, and (2) "complexing" in the mixture. The thermodynamic data indicate tendencies for "complex" formation in the mixtures of $LaCl_3$ with CsCl, RbCl, and KCl, while for the mixtures with NaCl and LiCl the Temkin model is applicable.

Introduction

A knowledge of the thermodynamic properties of fused salt mixtures has been found to be a powerful tool aiding the understanding of the interionic interactions and structure of the melts. The contributions and importance of the coulombic energy, polarization energy, and van der Waals dispersion energy to the excess thermodynamic functions of mixing were born out semiqualitatively by the studies of the common anion symmetrical binary systems. The results on symmetrical alkali halide systems (AX–A′X; A,A′ = Li, Na, K, Rb, or Cs; X = F, Cl, Br, or I)[1-3] and on divalent charge unsymmetrical systems of the alkaline earth halides (BX_2–AX, B = Ca, Sr, or Ba)[4] are in general accord with the behavior anticipated from conformal solution theory.[5-9]

A somewhat different position is found in the studies of charge unsymmetrical systems of the type MX_2–AX where M^{2+} = Mg^{2+}[4,10] or a transition metal cation (M^{2+} = Mn^{2+}, Fe^{2+}, Co^{2+}, Ni^{2+}, Zn^{2+}, or Cd^{2+})[11-14] and X is mainly chloride. For these systems the measured thermodynamic quantities (integral enthalpy-partial free energy) increase to quite large negative values as the size of the alkali metal cation is increased in the sequence Li < Na < K < Rb < Cs. For mixtures with K, Rb, and Cs, the enthalpy interaction parameter, $\lambda^M = \Delta H^M/X_i(1 - X_i)$($\Delta H^M$ = integral enthalpy, X_i = mole fraction of component i) varies strongly with composition and shows a distinct minimum near $X_{MX_2} \approx 1/3$. Near this composition the partial entropies of mixing of the alkali halides show inflection points. The conformal solution theory[5-9] and the quasichemical theory[15] have not been developed to the point when they can justify the existence of a sharp minimum in the enthalpy interaction parameter. However, semiquantitative descriptions for the MX_2–AX mixtures were possible with the aid of structural information obtained from electronic absorption[16,17] and Raman[18,19] spectroscopy. The structural studies show that in mixtures rich in alkali halide the divalent cation forms MX_4^{2-} configurations (or "complexes") where the M^{2+} cation is in an approximately tetrahedral chloride field having only A^+ cations as second nearest neighbors. The "complexing" in these mixtures is reflected in the ther-

modynamic quantities by the appearance of a minimum in the enthalpy interaction parameter[11-14,20] and inflection points in the partial entropy of the alkali halide.[20-22]

Most of the physicochemical studies of unsymmetrical binary mixtures of the type LX_3-AX have been aimed toward LX_3 salts which are strong halide acceptors and which tend to form molecular type liquids of the L_2X_6 type (*e.g.*, most of the group IIIb metal halides).[23] These halides in their mixtures with the alkali halides were found to form appreciable quantities of tetrahedral LX_4^- ions. Other studies[24,25] have been concerned with the more "ionic" type LX_3-AX liquids (*e.g.*, AlF_3, lanthanide metal halides) and have argued the formation of octahedral LX_6^{3-} "complex" ions in the mixture.

So far there have been relatively few studies of the thermodynamic properties of the LX_3-AX binaries. With the exception of phase diagrams studies,[26] and studies of the $CeCl_3$-ACl binaries,[27,28] the thermodynamic properties of mixing are unknown. The present paper reports the results of a calorimetric and an emf investigation of the binary liquid mixtures of lanthanum(III) chloride with the alkali chlorides. The directly and indirectly measured thermodynamic functions of mixing (integral and/or partial enthalpy, Gibbs energy, and entropy) are discussed in terms of (1) the conformal solution theory for charged unsymmetrical binaries and (2) possible ordering (or complexing) in the mixture.

Experimental Section

Chemicals. The sources and methods of purification of the alkali halides were the same as before.[4,11] The lanthanum(III) chloride was prepared by dissolving, in concentrated HCl, lanthanum oxide purchased from A. D. Mackay Inc. Slow evaporation of the solution gave the hydrated $LaCl_3$, which was first dried under vacuum at temperatures up to 200° and then treated with gaseous CCl_4 and N_2. Finally the salt was melted and treated with gaseous HCl and N_2. The purity of the salt was checked by passing an aqueous solution through a cation-exchange column and titrating the resulting acidic solution. The premelted salt assayed 99.9% $LaCl_3$. Lanthanum(III) chloride purchased from Schuchardt, Germany, was used for the emf measurements. The salt was first dried under vacuum up to 200° and then heated with HCl to 450°. The premelted salt assayed 99.8 mol % $LaCl_3$ as determined by the above-mentioned method.

Calorimetric Experiments. The measurements of the integral enthalpies of mixing were of the "crucible-break off" type where both liquid salts are contained in fused silica containers.[11-14] The calorimetric apparatus used, its calibration, and the required corrections have been described elsewhere.[11-14] The measurements of the partial enthalpies in the KCl-$LaCl_3$ system were carried out by dissolving small amounts of KCl or $LaCl_3$ ($\sim$0.001 mol of solute) in KCl-$LaCl_3$ mixtures ($\sim$0.2 mol of solvent) of different compositions. In order to eliminate any possible volatilization of the solute liquid (large surface to mass ratio), for these measurements we have used the previously described[14] "double break-off" technique.

Emf Experiments. The measurements of the chemical potentials of the alkali chloride of mixing in the $LaCl_3$-MCl mixtures were performed with galvanic cells of the type C(s), Cl_2(g)|ACl(l)|A^+ glass |ACl-$LaCl_3$(l)|Cl_2(g), C(s), where C(s) and Cl_2(g) are graphite-chlorine electrodes and the A^+ glass membrane is alkali ion conducting only. The experimental technique and cell design are described elsewhere.[20]

The emf (E) of the cell is related to the chemical potential ($\Delta\mu_{ACl}$) of the ACl salt in this mixture through the equation

$$\Delta\mu_{ACl} = -FE \qquad (1)$$

where F is the Faraday constant.

Results and Discussion

In Table I[29] we present the results of the liquid-liquid enthalpy of mixing experiments. In Figure 1 the interaction parameter, λ^M, is plotted *vs.* mole fraction of $LaCl_3$. The line drawn in the figure represents the "best" curves. With the exception of the LiCl-$LaCl_3$ system the deviation of the actual experimental points from these curves represent an error of $\pm$2% or less of the interaction parameter. For the LiCl-$LaCl_3$ system an error of $\pm$5% is estimated. The values of the interaction parameters were least-squares fitted to fifth-order polynomials of X_2 ($X_2 = X_{LaCl_3}$). The coefficients of the least squares and the standard deviation of the experimental points from the fitted curve are given in Table II.

In Table III[29] and Figure 2 we present the results of the partial enthalpy measurements in the $LaCl_3$-KCl system. The measured partial enthalpies are compared in Figure 2 with the partial enthalpies obtained from the integral enthalpy data by using the graphical method of intercepts. Finally in Table IV[29] we present the result of the emf measurements. In Figures 2 and 3 the chemical potentials of the alkali chlorides on mixing are plotted *vs.* mole fraction of $LaCl_3$ together with the partial enthalpies obtained by using the graphical method of intercepts and the experimental $\Delta\bar{H}_{KCl}$ in the $LaCl_3$-KCl system.

Integral Enthalpies. Figure 1 shows that the magnitude of λ^M increases to quite large negative values with increasing size of the alkali metal cation. All the systems studied have more negative values of λ^M in the alkali chloride-rich than in the lanthanum chloride-rich region. The composition dependence of λ^M for the NaCl-$LaCl_3$ and especially for the LiCl-$LaCl_3$ systems is rather simple. For the systems involving KCl, RbCl, and CsCl, the composition dependence of λ^M is somewhat more complicated. Two prominent features can be distinguished: (a) in the range $1 > X_2 > 0.25$ the values of λ^M change sharply with composition, and (b) for $X_2 < 0.25$ the relative changes of λ^M are small and a broad minimum appears to exist. The experimental uncertainty, however, does not permit an exact determination of the position of this minimum.

According to the Davis, *et al.*,[6-9] conformal solution theory the interaction parameter for charge unsymmetrical binary systems LX_z-AX, which consist of purely ionic components, is a function of the size parameter $\delta_{12} = d_1 - d_2/d_1d_2$ (d_i = interionic distance of the ith salt). In a family of related systems LX_z-AX with a common component LX_z (taken as the reference salt) and at fixed T, P, and composition (X) the first- and second-order approximation to the enthalpy of mixing is

$$\lambda^M = a(T,P,X) + b(T,P,X)\delta_{12} + c(T,P,X)\delta_{12}^2 \qquad (2)$$

where a, b, and c are complicated integral functions of T, P, and X. When polarization and dispersion[8,9] interactions are included in the pair potential of the component salts the a, b, and c coefficients are modified to include

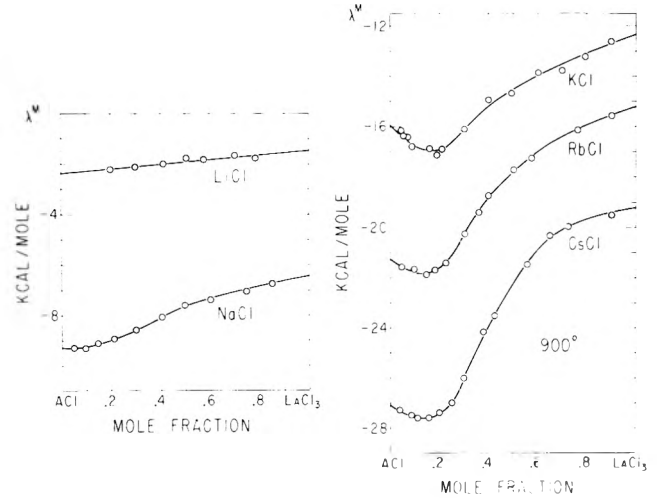

Figure 1. Enthalpy interaction parameters in liquid mixtures of lanthanum(III) chloride with alkali chlorides.

TABLE II: Least-Squares Coefficients for the Binary Liquid Alkali Chloride–Lanthanum Chloride Mixtures[a]

$$\lambda^M = A + BX_2 + CX_2^2 + DX_2^3 + EX_2^4 \text{ kcal/mol}$$

System	$-A$	$-B$	C	$-D$	E	Std deviation
$CsCl–LaCl_3$	26.76	21.81	124.18	156.62	61.76	0.224
$RbCl–LaCl_3$	21.23	14.07	86.68	115.45	48.93	0.198
$KCl–LaCl_3$	15.71	18.57	85.33	111.40	48.16	0.204
$NaCl–LaCl_3$	9.29	1.96	23.41	33.65	15.09	0.045
$LiCl–LaCl_3$	2.38	−0.93	0.07			0.070

[a] In deriving these coefficients, apart from all experimental points, we have made use of the limiting values of the interaction parameter (λ_0, λ_1) obtained from the "best" curves in Figure 1. This treatment makes the algebraic representation of the data valid in the complete range of composition.

additional integral terms which arise from these interactions.

The majority of the thus far investigated divalent binary systems ($z = 2$) indicate that the experimental interaction parameter is roughly a linear function of δ_{12}(*i.e.*, $c \approx 0$). However, significant deviations from linearity occur for LiCl[11-14] and for the limiting interaction parameters at $X_2 = 1$ (*i.e.*, λ_1^M) in the case of transition metal chloride–alkali chloride binaries.[12]

In Figure 4 we give a plot of the enthalpy interaction parameter *vs.* δ_{12} for the family of $LaCl_3$–ACl binary mixtures. The values of λ^M at $X_2 = 0$ (λ_0^M), $X_2 = 0.5$($\lambda_{1/2}^M$), and $X_2 = 1$(λ_1^M) are given for each binary. It appears that for these systems ($z = 3$) λ^M varies quadratically with δ_{12} and thus the theoretically predicted second-order terms in eq 2 are not negligible ($c \neq 0$). All three coefficients a, b, and c increase with increasing mole fraction (*i.e.*, $a_{x=0} < a_{x=1/2}$, etc.).

As mentioned in the Introduction the concentration dependence and the possible existence of a minimum in the interaction parameter cannot be explicitly deduced from conformal solution theory. However, using a simple model, previously introduced[11] for the study of the divalent charge unsymmetrical systems, we can give a semiquantitative explanation of the concentration dependence of λ^M as follows. Let us first assume that the enthalpy of mixing in the $LaCl_3$–ACl systems can be separated into two parts

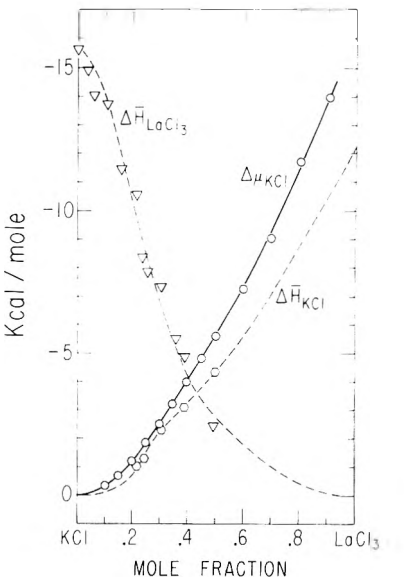

Figure 2. Partial enthalpies and chemical potential in the liquid $LaCl_3$–KCl system: ○, experimentally determined partial enthalpy of KCl; ▽, experimentally determined partial enthalpy of $LaCl_3$; ○, experimentally determined chemical potential of KCl; (---) partial enthalpy of KCl obtained by the method of intercepts.

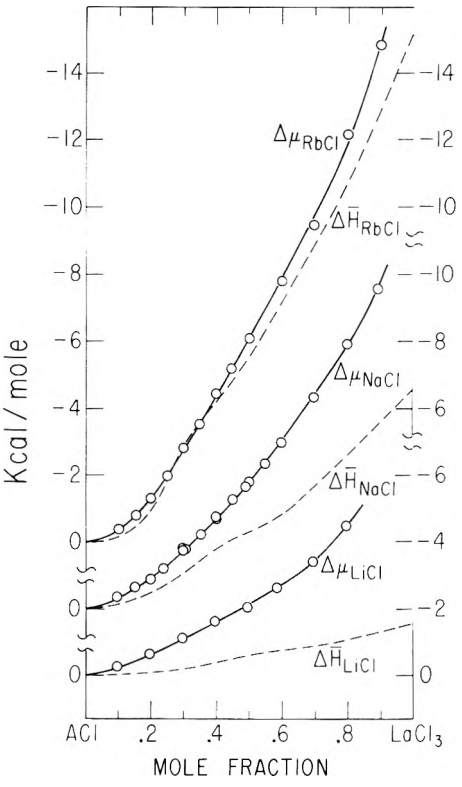

Figure 3. Partial enthalpy and chemical potential of RbCl, NaCl, and LiCl (see Figure 2 caption for details).

$$\Delta H^M = \Delta H^C + \Delta H^K \quad (3)$$

The first term (ΔH^C) in this equation is attributed to the changes of the coulombic and dispersion interactions during the formation of the mixture. The second term represents the enthalpy associated with ordering effects (or complexing) in the mixture. This last term was introduced in view of the recent Raman studies on KCl–$LaCl_3$ liquid mixtures.[20] These studies indicate the presence of

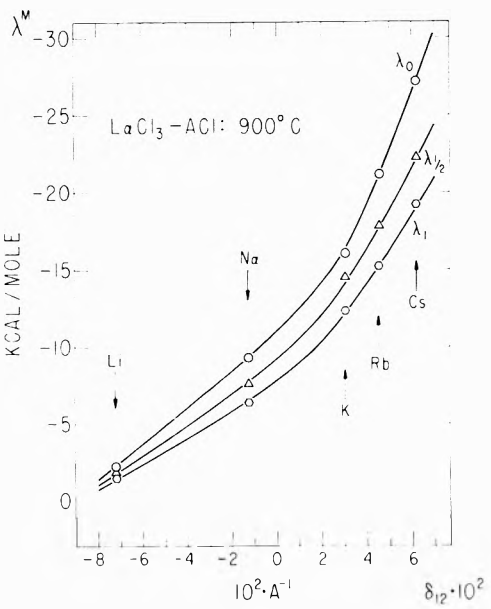

Figure 4. Dependence of the interaction parameter on the size parameter $\delta_{12} = d_2 - d_1/d_1d_2$.

TABLE V: The *A*, *B*, and *C* Coefficients in kcal/mol

$$\lambda^M = A + BX_2 - \begin{cases} K/1 - X_2 & X_2 \leq 1/4 \\ K/3X_2 & X_2 \geq 1/4 \end{cases}$$

System	$-A$	B	$-K$
$CsCl-LaCl_3$	24.2	7	3.4
$RbCl-LaCl_3$	20.1	6	2
$KCl-LaCl_3$	14.4	2.6	2
$NaCl-LaCl_3$	9.1	3	0.3
$LiCl-LaCl_3$[a]	2.3	1	

[a] Assuming $K_{Li} = 0$.

at least one highly symmetrical complex species whose maximum concentration appears to occur near 25 mol % $LaCl_3$. Assuming that these complexes are characterized by a La^{3+} cation having six Cl^- anions in the first coordination sphere and only A^+ cations in the second shell, we can write the equation

$$X_2LaCl_3 + (1 - X_2)ACl \longrightarrow X_2[(LaCl_6^{3-})3A^+] + (1 - 4X)\text{"}ACl\text{"}$$

$$\Delta H^K = X_2K \quad X_2 \leq 1/4 \tag{4}$$

and

$$X_2LaCl_3 + (1 - X_2)ACl \longrightarrow \left(\frac{1 - X_2}{3}\right)[(LaCl_6^{3-})3A^+] + \left(\frac{4X_2 - 1}{3}\right)\text{"}LaCl_3\text{"}$$

$$\Delta H^K = \left(\frac{1 - X_2}{3}\right)K \quad X_2 \geq 1/4 \tag{5}$$

where $-K$ is the enthalpy of formation of 1 mol of $(LaCl_6^{3-})3A^+$. The values of K depend on the ionic potential of the alkali metal cation and are expected[11,12] to increase in sequences Li < Na < K < Rb < Cs. Equations 4 and 5 imply that the thermodynamic stability of the "complex" is not affected by composition changes and that the complexing is complete (no dissociation). The results of previous studies of charge symmetrical and charge unsymmetrical binaries in which little or no evidence of "complex" formation is indicated (*e.g.*, the alkaline earth–alkali halides[4] or MX_2–LiX and MX_2–NaX binaries[10-14]) suggest that the λ^C ($\lambda^C = \Delta H^M/X_2(1 - X_2)$) to a first approximation varies linearly with X_2

$$\lambda^C = A + BX_2 \tag{6}$$

Thus, from eq 4-6 we have

$$\lambda^M = \lambda^C + \lambda^K = \begin{cases} A + BX_2 - K/(1 - X_2) & X_2 \leq 1/4 \\ A + BX_2 - K/3X_2 & X_2 \geq 1/4 \end{cases} \tag{7}$$

In Figure 5 we give plots of λ^K, $\lambda^C = \Delta H^C/X_2(1 - X_2)$ and λ^M(calcd) for the above model. The values of the coefficients A, B, and K were calculated by fitting eq 7 to the experimental data for the $LaCl_3$–CsCl binary. A set of experimental values of λ^M(obsd) at three different compositions (*e.g.*, $X_{2i} = 0.1$, $X_{2i} = 0.25$, $X_{2i} = 0.9$) were used in eq 7 and the coefficients A_i, B_i and K_i were calculated by solving a system of three simultaneous equations. This step was repeated for 10 different sets of λ^M(obsd) and the average values of A, B, and K were calculated and used in Figure 5. The model curve λ^M(calcd) shown in the figure is somewhat comparable with the experimentally determined λ^M(obsd) for the CsCl–$LaCl_3$ system. Similar calculations of A, B, and K for the binaries involving RbCl, KCl, and NaCl show (Table V) that λ^M(calcd) for these systems are (within experimental error) in agreement with λ^M(obsd). Thus it appears that it is possible, at least in principle, to account for the gross features of the shape of λ^M, for the complex forming $LaCl_3$–ACl systems, in terms of the sum $\lambda^C + \lambda^K$.[30] Furthermore, the model shows that even complete short-range ordering at $X_2 = 1/4$ (*i.e.*, when $LaCl_6^{3-}$ does not dissociate and λ^K possesses a cusp at $X_2 = 1/4$) does not necessarily imply a sharp minimum in the overall interaction parameter. When the energetic asymmetry of λ^C (*i.e.*, the B coefficient) is comparable in magnitude with the K values the existence of a minimum in λ^M may not be recognized.

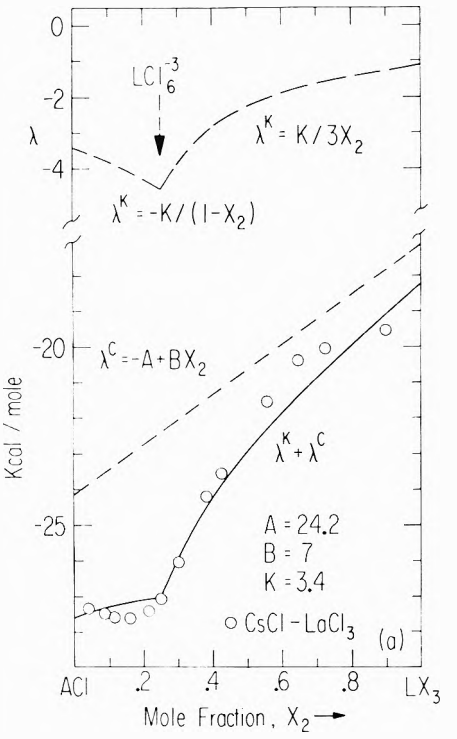

Figure 5. Interaction parameters in system forming LX_6^{3-} configurations (——) and experimental values for the CsCl–$LaCl_3$ binaries (O).

Finally before we close this part of the discussion, we should like to stress that the vanishing K values for the NaCl (and LiCl) containing binaries do not exclude the presence of $LaCl_6^{3-}$ configuration in the mixture. Such entities may be thermodynamically stabilized by an entropy rather than an enthalpy contribution to the Gibbs energy.

Partial Quantities. In Figures 2 and 3 we compare the experimentally determined chemical potentials with the measured and calculated partial enthalpies. For the binaries containing LiCl and NaCl the differences between $\Delta\mu_{ACl}$ and $\Delta\bar{H}_{ACl}$ are discrete and increase with increasing X_2, while for the binaries mixtures of KCl and RbCl the differences seems to show a minimum value around $X_2 \simeq 0.25$. Even if the errors in the $\Delta\bar{H}_{ACl}$ values obtained are relative great (±200 cal/mol for $0.15 < X_{LaCl3} < 0.4$) we have estimated the partial entropies of mixing and compare them with the predicted from the Temkin[32] model partial entropies, $\Delta\bar{S}_{ACl} = R \ln (1 - X_2)$. The comparison shows that in the strongly interacting $LaCl_3$–KCl and $LaCl_3$–RbCl systems and for $X_2 > 0.25$ the experimental partial entropies are less positive than the entropies expected for a random cation mixture. This is consistent with entropy observations in the binary MCl_2–ACl (M = Mn, Co, Mg; and A = K, Rb, Cs) mixtures. In these systems the partial entropy *vs.* X_{MCl_2} curves showed inflection points at $X_{MCl_2} = 0.33$.[20-22]

Finally for the mixtures containing LiCl and NaCl the partial entropies are within experimental error, in agreement with the Temkin model. Thus, as in the case of the MX_2–LiX (M = Mn, Co, Mg)[10,20,21] mixtures, the $LaCl_3$–LiCl and NaCl–$LaCl_3$ systems do not deviate significantly from random cation mixtures. This is not very surprising, since the ionic potential Z/R^{Z+} of the La^{3+} cation is comparable in magnitude with that of Mg^{2+}, Co^{2+}, and Mn^{2+}.

Acknowledgments. This work has been supported by the National Science Foundation (Grant No. NSF-GP-30847X). It also has benefited by the general support of materials science at the University of Chicago provided by the NSF-MRL Program.

Supplementary Material Available. Tables I, III, and IV will appear following these pages in the microfilm edition of this volume of the journal. Photocopies of the supplementary material from this paper only or microfiche (105 × 148 mm, 24× reduction, negatives) containing all of the supplementary material for the papers in this issue may be obtained from the Journals Department, American Chemical Society, 1155 16th St., N.W., Washington, D. C. 20036. Remit check or money order for $3.00 for photocopy or $2.00 for microfiche, referring to code number JPC-74-181.

References and Notes

(1) L. S. Hersh and O. J. Kleppa, *J. Chem. Phys.*, **42**, 1309 (1965).
(2) M. E. Melnichak and C. J. Kleppa, *J. Chem. Phys.*, **52**, 1790 (1970).
(3) M. E. Melnichak and C. J. Kleppa, *J. Chem. Phys.*, **57**, 5231 (1972).
(4) T. Østvold, *J. Phys. Chem.*, **76**, 1616 (1972).
(5) H. Reiss, J. L. Katz, and O. J. Kleppa, *J. Chem. Phys.*, **36**, 144 (1962).
(6) H. T. Davis and S. A. Rice, *J. Chem. Phys.*, **41**, 14 (1964).
(7) H. T. Davis, *J. Chem. Phys.*, **41**, 2761 (1964).
(8) K. D. Luks and H. T. Davis, *Ind. Eng. Chem., Fundam.*, **6**, 194 (1967).
(9) H. T. Davis, *J. Phys. Chem.*, **76**, 1629 (1972).
(10) O. J. Kleppa and F. G. McCarty, *J. Phys. Chem.*, **70**, 1249 (1966).
(11) G. N. Papatheodorou and O. J. Kleppa, *J. Inorg. Nucl. Chem.*, **30**, 889 (1970).
(12) G. N. Papatheodorou and O. J. Kleppa, *J. Inorg. Nucl. Chem.*, **33**, 1249 (1971).
(13) G. N. Papatheodorou and O. J. Kleppa, *Inorg. Chem.*, **10**, 872 (1972).
(14) G. N. Papatheodorou and O. J. Kleppa, *Z. Anorg. Allg. Chem.*, in press.
(15) M. Blander in "Molten Salts Characterization and Analysis," G. Mamantov, Ed., Marcel, New York, N. Y., 1969.
(16) G. P. Smith, C. R. Boston, and J. Brynestad, *J. Chem. Phys.*, **45**, 829 (1967).
(17) W. E. Smith, J. Brynestad, and G. P. Smith, *J. Chem. Phys.*, **52**, 3890 (1970).
(18) V. Maroni, *J. Chem. Phys.*, **55**, 4789 (1971).
(19) J. H. R. Clarke, P. J. Hartley, and Y. Kuroda, *J. Phys. Chem.*, **76**, 1831 (1972).
(20) T. Østvold, *High Temp. Sci.*, **4**, 51 (1972).
(21) T. Østvold, *Acta Chem. Scand.*, **26**, 2788 (1972).
(22) Y. Dutt and T. Østvold, *Acta Chem. Scand.*, **26**, 2743 (1972).
(23) C. R. Boston in "Advances in Molten Salt Chemistry," J. Braustein, G. Mamantov, and G. P. Smith, Ed., Plenum Press, New York, N. Y., 1971.
(24) A. Schneider, *et al.*, "Chemie der Seltenen Erden in Geschmolzenen Alkalihalogeniden I to XII," XII; G. Vogel and A. Schneider, *Inorg. Nucl. Chem. Lett.*, **8**, 513 (1972), and references therein.
(25) G. J. Janz and C. G. M. Dijkhuis, *Nat. Stand. Ref. Data Ser., Nat. Bur. Stand.*, **No. 28**, 12 (1969).
(26) E. M. Levin, C. R. Robbins, and H. F. McMurdre, "Phase Diagrams for Ceramists," American Ceramic Society, 1969.
(27) S. Senderoff, G. E. Mellors, and R. I. Bretz, *N. Y. Acad. Sci.*, **79**, 878 (1960).
(28) G. N. Papatheodorou and O. J. Kleppa, *J. Phys. Chem.*, **78**, 178 (1974).
(29) See paragraph at end of paper regarding supplementary material.
(30) If we apply the same model to $LaCl_4^{-1}$ species we find that the calculated interaction parameter, λ^M(calcd), shows a minimum near 50 mol % $LaCl_3$ and that no satisfactory correlation with λ^M(obsd) can be made. Complexes of the $LaCl_n^{n-3}$ ($n \geq 7$) type are in agreement with the thermodynamic model but, as suggested by the Raman work,[31] are not highly symmetrical and thus can be ruled out. Binuclear lanthanum species $La_2Cl_9^{3-}$ (*i.e.*, two $LaCl_6^{3-}$ octahedral sharing phases) are also satisfying the model. However, these complexes are expected (as in the case of $Zn_2Cl_7^{3-}$ [14]) to have high dissociation constants to monomeric $LaCl_6^{3-}$ species.
(31) V. Maroni, E. J. Hathaway, and G. N. Papatheodorou, to be submitted for publication.
(32) M. Temkin, *Acta Physicochim. USSR*, 20, 411 (1945).

The Solubility of Mercury in Polar Gases

Harvey S. Rosenberg* and Webster B. Kay

Battelle's Columbus Laboratories and The Ohio State University, Columbus, Ohio 43201 *(Received June 20, 1973)*

Publication costs assisted by Battelle's Columbus Laboratories

The concentration of mercury in the gas phase when liquid mercury is in equilibrium with methanol or acetone was measured at pressures up to 30 atm from 220 to 300° using a radioisotope tracer technique. These concentrations were up to 21.6% greater than the concentrations in pure mercury vapor at the same temperature. The data were used to determine the mixed second virial coefficients for mercury and the polar organic molecules. The experimental values for these coefficients were compared with theoretical values calculated from intermolecular potential functions. The solubility of mercury in methanol or acetone can cause an error of about 1 part in 500 in the pressure of gas isotherms measured in the presence of mercury at about 30 atm if the measured pressure is corrected by subtraction of the normal vapor pressure of mercury at the same temperature.

Introduction

The phenomenon of solubility of solids and liquids in compressed gases is of great practical interest and is important wherever compressed gases or vapors are used. Of particular interest is the effect of mercury solubility on the accuracy of measurements of the volumetric behavior of compressed gases in those experiments in which mercury is used as the confining liquid.

Previous work on the solubility of mercury in compressed gases is very limited. The expression for the solubility has been derived by Ewald, Jepson, and Rowlinson[1] using the equilibrium condition that the chemical potential of the liquid mercury must equal the chemical potential of the mercury in the gas phase

$$\ln\left(\frac{c_2}{c_2^0}\right) = \frac{v_2^l - 2B_{12}}{v} + \frac{v_2^l B_{11} - (3/2)C_{112}}{v^2} + \cdots \quad (1)$$

The ratio c_2/c_2^0 is a representation of the solubility and is the ratio of the concentration of mercury atoms in the presence of the added gas to the concentration of mercury atoms in pure saturated mercury vapor. B_{12} and C_{112} are the second and third virial coefficients for the interaction of one and two molecules of the added gas with one atom of mercury. B_{11} is the second virial coefficient of the added gas, v_2^l is the molar volume of liquid mercury, and v is the molar volume of the gas mixture. It is assumed in the derivation of eq 1 that (1) none of the added gas dissolves in the liquid mercury, (2) liquid mercury is incompressible, (3) the molar volume of saturated mercury vapor is much larger than the molar volume of the compressed gas mixture, and (4) the mole fraction of mercury in the mixture is very small.

Experimental determinations have been made of the solubility of mercury in compressed argon by Stubley and Rowlinson,[2] and in compressed propane and *n*-butane by Jepson, Richardson, and Rowlinson[3] at pressures up to 30 atm from 184 to 305°. The concentrations of mercury in the compressed gases were up to 35% greater than the concentrations in pure mercury vapor at the same temperature, thus confirming previous calculations by Jepson and Rowlinson[4] that this increase in the mercury concentration must affect adversely the accuracy of gas isotherms measured in the presence of mercury. No data could be found in the literature on the solubility of mercury in the gases of polar compounds.

The present study was undertaken to obtain more data on the accuracy of gas isotherms measured in the presence of mercury. The solubility of mercury was determined in compressed methanol and acetone gas, both of which are polar compounds.

Apparatus

The apparatus used in this work is a modification of that for the radioactive tracer technique developed by others[3] to measure the concentration of mercury atoms in sealed glass tubes. The method avoids the obvious difficulties of trying to sample and analyze a compressed gas mixture in which one of the components is present in very small amounts. The concentration of mercury near the bottom of a vertical glass tube was determined first for a tube containing only mercury vapor and then for an identical tube containing the compressed gas saturated with mercury at the same temperature. Since the count rate is directly proportional to the number of mercury atoms, the ratio of the two observed count rates is a direct measurement of the solubility of the mercury vapor in the added gas. Each tube contained a small excess of liquid mercury in a cup at the top to ensure saturation at all temperatures. Figure 1 is a diagram of the apparatus.

The glass sample tube was made of Pyrex precision-bore tubing with an internal diameter of 5.00 mm, an external diameter of about 9 mm, and a length of about 40 cm. It contained about 27 mg of radioactive mercury, and a closely fitting Mu metal (a highly magnetic iron–nickel alloy) stirrer, 30 mm long, sealed in a 4 mm o.d. glass tube. The stirrer could be moved over the whole length of the tube up to the mercury cup by two C-shaped, 6-oz permanent magnets placed with opposing poles about 2.25 in. apart on the outside of a vapor bath. The magnets were moved up and down continuously by axial bearings and a chain-drive mechanism powered by a simple 25-rpm gear motor. During actual counting, the stirrer was held stationary near the top of the tube by the magnets.

For safety, the glass sample tube was placed in a nonmagnetic stainless steel tube, with a wall thickness of 1/16 in. and an outside diameter of 0.5 in., sealed on the bot-

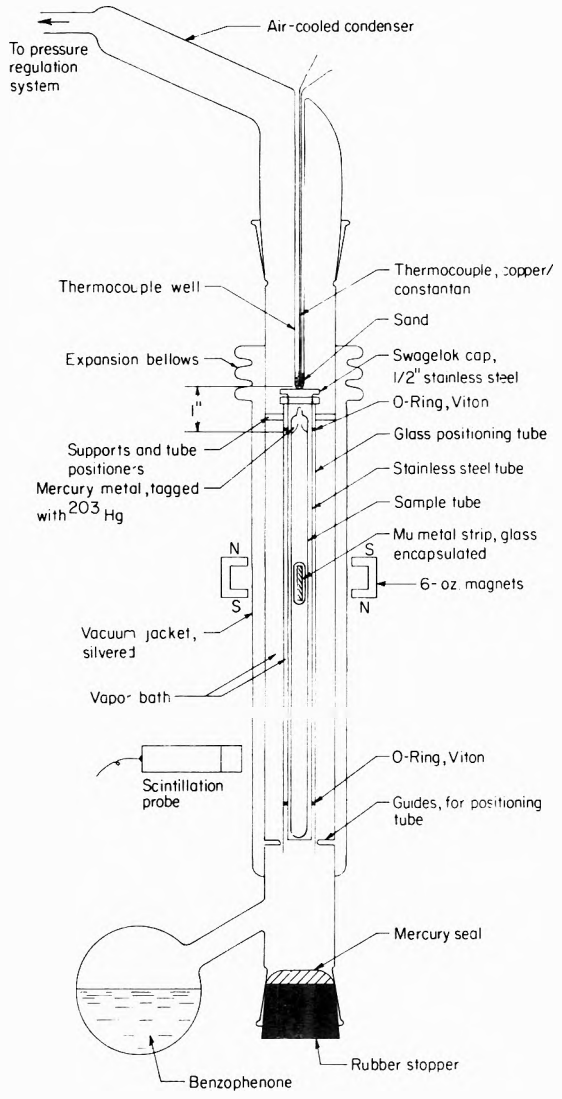

Figure 1. Diagram of apparatus.

tom by a welded plug and on the top by a 0.5-in. stainless steel Swagelok cap. The glass sample tube and the stainless steel case were maintained at constant temperature by total immersion in a benzophenone vapor bath. The vapor bath was surrounded by a vacuum jacket and contained a glass tube to position the sample tube for counting. The bath temperature was adjusted and maintained at the desired value in the range 220–300° by close regulation of the pressure in the closed system. The temperature was measured accurately with a calibrated copper-constantan thermocouple junction located about 1 in. away from the mercury droplet in the sample tube. The mercury droplet was located in a cup near the top of the sample tube so as to prevent spurious condensations of mercury during start-up and operation of the vapor bath.

The concentration of the mercury was measured, in arbitrary units, by a NaI scintillation probe which was completely surrounded by 4-in. lead-brick shielding (not shown in Figure 1). The counting face of the probe was shielded by 2 in. of lead but had a 1-in. square collimator so that it received almost all its radiation from the mercury in the gas phase and very little from the liquid mercury at top of the tube. The probe was maintained at a constant 28° by a stream of water flowing through a copper coil wrapped around the probe.

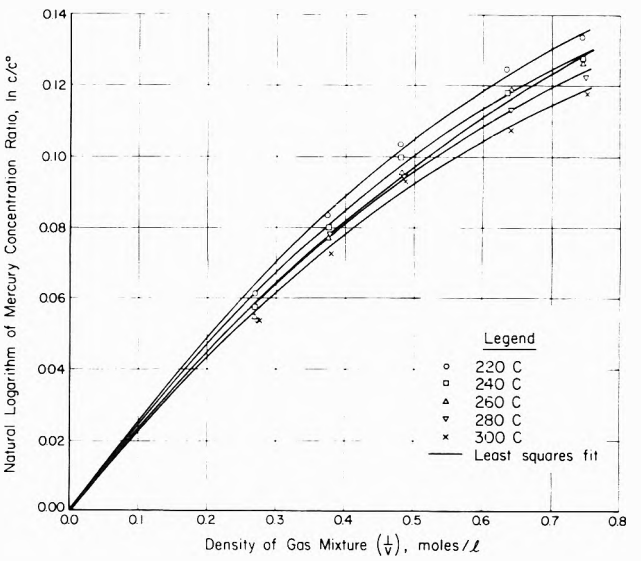

Figure 2. The concentration of mercury in saturated gaseous mixtures with methanol.

The glass sample tubes were loaded upside down, first by pipetting 2×10^{-3} ml of liquid mercury, tagged with ^{203}Hg($t_{1/2}$ = 46.59 days) at an initial specific activity of 7.5 mCi/g, and ensuring that the droplet fell through the cup hole and into the tip at the bottom of the tube. Next the stirrer was added and the sample tube was attached to a vacuum manifold so that the polar vapor could be added by distillation *in vacuo* from ultra-high-purity methanol or acetone. The volume of vapor was measured at low pressure (3–10 cm) and 28.0° in a calibrated and thermostatted reservoir, and the mass was determined from the equation of state up to the second virial coefficient. Values of B_{11} for methanol and acetone at 28.0° were obtained from the literature.[5] The filled sample tube was sealed off under vacuum with a gas-oxygen torch and turned right side up.

A filled tube was inserted in the stainless steel case and placed in the vapor bath which was then brought up to the desired temperature. The sample was stirred continuously while the count rate was measured on a recording rate meter. After the count rate leveled off, which usually required 2 days, counts were taken on a scaler at intervals of about 4 hr until the agreement between successive count rates was less than the statistical error of 0.3% for an accumulated count of 100,000. The background was never more than 10% of the count rate. Tubes containing only the mercury vapor were counted twice, once during the methanol series and once during the acetone series. Each series consisted of five tubes loaded with mercury and organic compound at different densities, and one tube loaded with mercury alone. The mercury concentration was measured at five temperatures for each tube. At the conclusion of the experiments, the tips of the sample tubes were broken open to remove the mercury and organic compound, and to fill the tubes with distilled water. The volumes of the tubes were determined from the weight and density of water contained in them.

Results

The solubilities were tabulated as the ratio c_2/c_2^0.[6] The pressures listed in this tabulation were determined from the equation of state up to the second virial coefficient using literature values for B_{11}.[7,8] The ratio c_2/c_2^0 in-

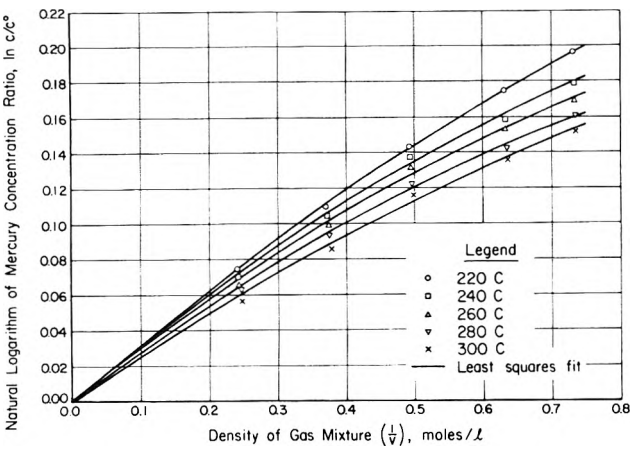

Figure 3. The concentration of mercury in saturated gaseous mixtures with acetone.

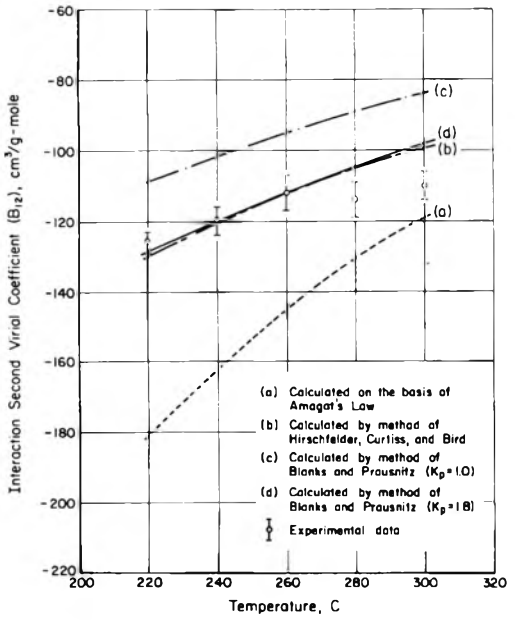

Figure 4. Second virial ccefficients of interaction for mercury–methanol system.

creases with increasing gas density at constant temperature and decreases with increasing temperature at constant density. Figures 2 and 3 show ln (c_2/c_2^0) as a function of the density of the gas. According to eq 1, the mixed second virial coefficient B_{12} may be calculated from the initial slopes of the curves in these figures.

The solubility data were subjected to a regression analysis which indicated that a second-order polynomial gave the most statistically significant fit to the data. Therefore, the experiments were not sufficiently accurate for a reliable measurement of the third virial coefficient C_{112}. However, there is no doubt that C_{112} must be positive as would be expected from the discussion of Rowlinson, Sumner, and Sutton.[9] Values of B_{12} were calculated from the first coefficient of the second-order polynomials and are listed in Table I as functions of temperature. The values of B_{12} are precise to within 5% and estimated to be accurate to within 10%.

Discussion

The experimental values of B_{12} may be compared with those calculated by various methods. The force constants

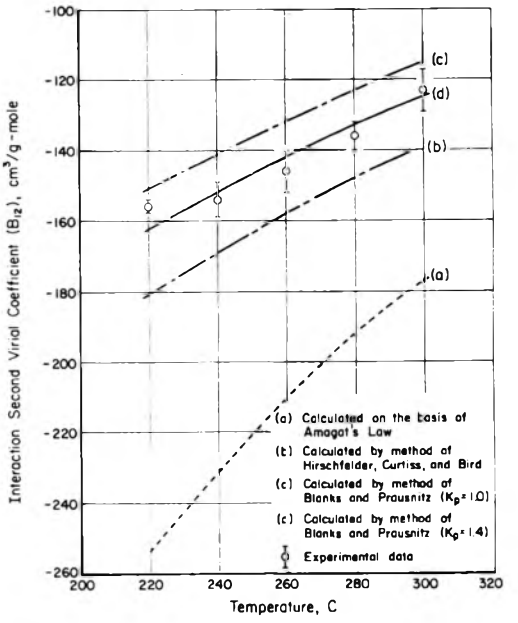

Figure 5. Second virial coefficients of interaction for mercury–acetone system.

TABLE I: Second Virial Coefficients of Interaction for Mercury–Methanol and Mercury–Acetone Systems

	B_{12}, cm³/mol	
Temp, °C	Mercury–methanol	Mercury–acetone
220.0	−126	−156
240.0	−120	−154
260.0	−112	−146
280.0	−114	−136
300.0	−110	−123

describing the potential of interaction between a nonpolar atom or molecule (subscript n) and a polar molecule (subscript p) may be obtained from the following empirical combining laws given by Hirschfelder, Curtiss, and Bird[10]

$$\sigma_{np} = \tfrac{1}{2}(\sigma_n + \sigma_p)(1 + \xi)^{-1/6} \quad (2)$$

$$\epsilon_{np} = \epsilon_n\epsilon_p(1 + \xi)^2 \quad (3)$$

$$\xi = \frac{\alpha_n\mu_p^2}{4\sigma_n^3\sigma_p^3(\epsilon_n\epsilon_p)^{1/2}} \quad (4)$$

α_n is the polarizability of the nonpolar molecule and μ_p is the dipole moment of the polar molecule. The effective total energy of interaction between a nonpolar and a polar molecule has the same form as that between two nonpolar molecules so that B_{12} may be estimated from the tabulations of the Lennard-Jones potential. Values of B_{12} calculated from these interaction force constants (refer to Table II) are shown as curve b in Figures 4 and 5. The agreement between experimental and calculated values is very good for the mercury–methanol system, but poor for the mercury–acetone system. Also shown as curve a in these figures are values of B_{12} calculated for ideal binary mixtures by the method of Prausnitz and Gunn,[11] using literature values for B_{11} and B_{22};[7,8,12] not surprisingly, there is a complete lack of agreement with the experimental data.

A method has been presented by Blanks and Prausnitz[13] for estimating B_{12} for nonpolar–polar binary mixtures which corrects for the displacement of the dipole

TABLE II: Molecular Force Constants[a]

Item (potential function)	Mercury (Lennard-Jones)	Methanol (Stockmayer)	Acetone (Stockmayer)	Ethane (Lennard-Jones)	Propane (Lennard-Jones)
ϵ/k, °K	610	634	479	243	242
σ, A°	2.85	2.40	3.68		
α_n, A°	5.39				
μ_p, D		1.66	2.74		
v_c, cm³/mol		118	211		

[a] References 7, 8, 10, and 12.

from the center of the polar molecule and which emphasizes many of the nonpolar characteristics of the polar material. The interaction force constants are still obtained from eq 2, 3, and 4, but σ_p, ϵ_p, and ξ are replaced by σ_p', ϵ_p', and ξ'. σ_p' is defined as

$$\sigma_p' = 0.84 v_c^{1/3} \tag{5}$$

where v_c is the critical molar volume of the polar molecule. Since polar forces do not seriously affect the molar volume at the critical point, eq 5 is an approximate method for estimating the collision diameter due to nonpolar forces only. ϵ_p' is defined as the Lennard-Jones energy parameter of the hydrocarbon homomorph of the polar molecule. The homomorph of a polar molecule is a nonpolar molecule having very nearly the same size and shape, *i.e.*, ethane and propane are the hydrocarbon homomorphs of methanol and acetone, respectively. ξ' is defined as

$$\xi' = K_p \xi \tag{6}$$

where K_p is an empirical, temperature-independent correction factor which reflects the displacement of the polar dipole from the center of the molecule. K_p is equal to unity when the dipole is at the molecular center and larger than unity for all other cases, but is independent of the properties of the nonpolar molecule.

Values of B_{12} estimated from the modified interaction force constants (refer to Table II) with K_p equal to unity are shown as curve c in Figures 4 and 5. In both cases, calculated absolute values of B_{12} are considerably less than experimental absolute values, possibly because the dipole is not located at the center of the polar molecule. A trial-and-error calculational procedure was used to determine which value of K_p for methanol and acetone gave the best fit to the experimental data. The results yielded a value of 1.8 for methanol and 1.4 for acetone and the appropriate calculated values for B_{12} are shown as curve d in Figures 4 and 5. However, in view of the very limited data available, not much confidence can as yet be placed on the reliability of values for K_p.

The effect of mercury on the observed gas pressure may be calculated by comparing the virial expansions for the pressure, p_1, of n_1 moles of gas in a volume, V, in the absence of mercury with the pressure, p, of n_1 moles of gas and n_2 moles of mercury in the same volume, V, at the same temperature, T. The result can be mathematically approximated as[4]

$$\frac{\Delta p}{p} = -x_2\left(1 + \frac{2B_{12} - B_{11}}{v_1} + \cdots\right) \tag{7}$$

Values of x_2, the mole fraction of mercury in the gas mixture, may be calculated from eq 1 since, for small values of n_2, x_2/x_2^0 is about equal to c_2/c_2^0. Equation 7 was used to calculate $\Delta p/p$ for methanol and acetone in the presence of mercury at 260° up to a gas density of 1 M. These corrections were compared with the usual procedure of subtracting the normal vapor pressure of mercury from the observed pressure and it was found that at about 30 atm, an error of up to 0.2% can be introduced into the pressure measurement. At higher pressures, the error would be expected to increase. However, estimates of this error at higher pressures are difficult to make because of the lack of accurate data for third virial coefficients.

Supplementary Material Available. A tabulation of mercury solubility in compressed methanol and acetone as a function of gas density and temperature will appear following these pages in the microfilm edition of this volume of the journal. Photocopies of the supplementary material from this paper only or microfiche (105 × 148 mm, 24× reduction, negatives) containing all of the supplementary material for the papers in this issue may be obtained from the Journals Department, American Chemical Society, 1155 16th St., N.W., Washington, D. C. 20036. Remit check or money order for $3.00 for photocopy or $2.00 for microfiche, referring to code number JPC-74-186.

References and Notes

(1) A. H. Ewald, W. B. Jepson, and J. S. Rowlinson, *Discuss. Faraday Soc.*, **15**, 238 (1953).
(2) D. Stubley and J. S. Rowlinson, *Trans. Faraday Soc.*, **57**, 1275 (1961).
(3) W. B. Jepson, M. J. Richardson, and J. S. Rowlinson, *Trans. Faraday Soc.*, **53**, 1586 (1957).
(4) W. B. Jepson and J. S. Rowlinson, *J. Chem. Phys.*, **23**, 1599 (1955).
(5) J. D. Lambert, G. A. H. Roberts, J. S. Rowlinson, and V. J. Wilkinson, *Proc. Royal Soc. Ser. A*, **196**, 113 (1949).
(6) See paragraph at end of paper regarding supplementary material.
(7) J. S. Rowlinson, *Trans. Faraday Soc.*, **45**, 974 (1949).
(8) I. Brown and F. Smith, *Aust. J. Chem.*, **13**, 30 (1960).
(9) J. S. Rowlinson, F. H. Sumner, and J. R. Sutton, *Trans. Faraday Soc.*, **50**, 1 (1954).
(10) J. O. Hirschfelder, C. F. Curtiss, and R. B. Bird, "Molecular Theory of Gases and Liquids," Wiley, New York, N. Y., 1954, p 223.
(11) J. M. Prausnitz and R. D. Gunn, *AIChE J.*, **4**, 430 (1958).
(12) J. B. Douglas A. F. Ball, and D. C. Giddings, *J. Res. Nat. Bur. Stand.*, **46**, 334 (1951).
(13) R. F. Blanks and J. M. Prausnitz, *AIChE J.*, **8**, 430 (1962).

Luminescence Decay of Hydrophobic Molecules Solubilized in Aqueous Micellar Systems. A Kinetic Model

P. P. Infelta,[1a] M. Grätzel, and J. K. Thomas*

Department of Chemistry and the Radiation Laboratory,[1b] University of Notre Dame, Notre Dame, Indiana 46556
(Received June 28, 1973)

Publication costs assisted by the U. S. Atomic Energy Commission

A phenomenological model describing the kinetics of quenching reactions in micelles is presented. Its validity is tested by laser photolysis experiments with aqueous solutions containing micellized sodium lauryl sulfate (NaLS) solubilized pyrene as a fluorescent probe and methylene iodide or nitromethane as quenchers. The constants of the distribution equilibrium of these quenchers between NaLS micelles and water were determined as $K(CH_3NO_2) = 1.64 \times 10^2\ M^{-1}$ and $K(CH_2I_2) = 2.5 \times 10^3\ M^{-1}$ (296°K) using the pulse radiolysis method. From the kinetic evaluation we obtain for the specific rates of association and dissociation of methylene iodide and NaLS micelles $n = 2.5 \times 10^{10}\ M^{-1}\ sec^{-1}$ and $k' = 9.5 \times 10^6\ sec^{-1}$ (296°K). Triplet lifetime measurements with solutions containing micellized cetyltrimethylammonium bromide (CTAB), anthracene, and Cu^{2+} ions show that the rate constant for the exit of anthracene from the CTAB micelle into the aqueous phase is as low as $2 \times 10^2\ sec^{-1}$ (296°K).

Introduction

Studies of reaction kinetics in micelles are presently a topic of increasing interest in biochemical research, arising from the similarity of these systems with other multimolecular aggregates like biomembranes and from the analogy of micellar and enzymatic catalysis.[2] These investigations are facililitated by new information on the static and dynamic properties of micellized surfactants obtained from the application of novel techniques in this field. Thus an aqueous sodium lauryl sulfate (NaLS) or cetyltrimethylammonium bromide (CTAB) micelle is now well defined with respect to its size, aggregation number, density, surface potential[3] and microviscosity.[4,5] For many solubilized "guest" molecules the dynamic sites of incorporation in the micelles are known,[6] whereas their exit rate into the aqueous phase has only been estimated or measured in a few cases.[7-9] No clear picture exists yet from the rate of micelle dissociation since spin resonance and temperature jump techniques have yielded inconsistent results, the latter technique predicting much slower rates than the former.[10]

Recently laser and nanosecond flash photolysis techniques have been successfully applied to micellar systems using solubilized fluorescent probes and suitable quenchers. Information has been obtained on the diffusion rate of the probe inside the micellar core,[5] the specific adsorption of counter ions in the Stern layer,[5,11,12] and factors which determine the permeability of micelles.[5] The photochemically active probe such as pyrene which is dissolved almost exclusively in the micelle is excited by a laser pulse. The behavior of the excited state may then be observed, in particular its reaction with a quencher which may be primarily dissolved in the water.

Changes in the micelle permeability become manifest in changes in the rate constant of the quenching reaction or ease of entry of the quencher to the probe. During the discussion of these results the postulated simple correlation between the observed quenching rate and the entry rate of the quencher into the micelle may be questioned. The opinion is frequently expressed that the dynamics of the quenching process reflect only the stationary amount of quencher inside the micelle since the quencher is in a dynamic equilibrium between the aqueous and micellar phase, which is not disturbed by the excitation of the probe. To elucidate this problem we present now a simple kinetic treatment of quenching reactions in micellar solutions. The resultant equations are scrutinized using two quenchers with different affinity to the micellar phase. In addition, experiments were designed to determine the micelle–guest dissociation rate for polycyclic aromatic hydrocarbons such as anthracene.

Experimental Section

Materials. Sodium dodecylsulfate (Matheson Coleman and Bell, USP grade) and hexadecyltrimethylammonium bromide (Fluka purum) were recrystallized from methanol. Pyrene (Kodak) was passed through silica gel in cyclohexane solution and then recovered. Nitromethane and diiodomethane were purchased from Eastman Organic Chemicals and used without further purification. Copper sulfate was Baker's reagent grade. Laboratory distilled water was redistilled from potassium permanganate.

Sample Preparations. Pyrene and anthracene were solubilized in freshly prepared aqueous NaLS (0.1 *M*) and CTAB (0.05 *M*) solutions by stirring the mixtures at 70°. The concentration of solubilizate was finally checked by optical density measurements. All samples were deoxygenated by bubbling with nitrogen for 30 min.

Dynamic Solubilization Site of Pyrene. Evidence for the dynamic solubilization site of pyrene in NaLS micelles was obtained from nmr experiments. Shifts of the αCH_2, CH_2, and CH_3 hydrogen resonance lines to higher fields are observed on the addition of pyrene to solutions of NaLS in D_2O. The largest change was found in the position of the CH_2 peaks suggesting that pyrene dissolves predominantly in the core of these micelles.

Apparatus. Laser photolysis experiments were carried out with a ruby laser Korad KlQP with outputs of 2 J and 250 mJ in the 695.2- and 347.1-nm lines, respectively. The uv pulse had a duration of 20 nsec. Pulse radiolysis experiments were carried out using 10-nsec pulses of 2-MeV

electrons from a Van de Graaff accelerator. The principles and experimental setup of these techniques have been described elsewhere.[13,14]

Theory

Fluorescence Quenching inside the Micelle, Migration of Quenchers between the Aqueous and Micellar Phase. The reaction under investigation occurs in an aqueous solution containing the fluorescent probe P solubilized exclusively inside the micelles as one reactant. The other reactant, the quencher A, is in a dynamic equilibrium between the aqueous and micellar phase M

$$A + M \underset{k'}{\overset{n}{\rightleftharpoons}} AM \tag{1}$$

where n denotes the second-order rate constant for the entry of the quencher into the micelle and k' is the exit rate constant. The ratio n/k' is identical with the distribution constant of the quencher between the micelles and water.

$$K = n/k' = [AM]/[M][A]_W \tag{2}$$

We intend to evaluate the intensity of the fluorescence emission, which is proportional to the concentration of excited probes P^*, as a function of time. Since the excited states can disappear *via* a radiative and nonradiative channel, we write

$$-dP^*(t) = F(t)\,dt + Q(t)\,dt \tag{3}$$

$F(t)$ denotes the rate of the fluorescence decay if no quencher is added to the solution and $Q(t)$ is the rate of quenching of P^* by A. It is obvious that $F(t)$ can be written as

$$F(t) = k_1 P^*(t) \tag{4}$$

where k_1 is the rate constant for the fluorescence decay in a quencher free micellar solution.

The term $Q(t)\,dt$ is the number of moles of P^* that disappear during t and $t + dt$ as a result of the quenching action of A. We will write the number of moles of A that enter the micelles between t_1 and $t_1 + dt_1$ as

$$n[A]_W[M]\,dt_1 \tag{5}$$

where $[A]_W$ stands for the concentration of A in the aqueous phase and [M] is the concentration of micelles. The number of moles of P^* per mole of micelles is given by

$$P^*(t)/[M] \tag{6}$$

We will assume that the probability for a molecule A, which entered a micelle at time t_1, to be in the micelle at time t is given by

$$\exp[-k'(t - t_1)] \tag{7}$$

Finally the probability that the quenching by a molecule of A, entered at time t_1, will occur between t and $t + dt$ is given by

$$k_q \exp[-k_q(t - t_1)]\,dt \qquad \text{if } t_1 > 0 \tag{8}$$

$$k_q \exp[-k_q t]\,dt \qquad \text{if } t_1 < 0 \tag{9}$$

$t = 0$ corresponds to the time of excitation of the probe and k_q is the rate constant for the quenching event inside the micelle expressed in units of sec^{-1}. Although k_q represents the rate of the reaction between two particles (the excited probe and the quencher) it should be noted as different from the normal second-order rate constant involving diffusion of two reactants in a solvent in that Fick's law cannot be applied to two or three molecules in a micelle. Combination of eq 5 to 8 allows us to evaluate $Q(t)\,dt$

$$Q(t)\,dt = \frac{P^*(t)}{[M]}\int_{-\infty}^{0} \exp[-k'(t - t_1)]k_q \times \exp[-k_q t]n\,[A]_W[M]\,dt_1\,dt + \frac{P^*(t)}{[M]}\int_{0}^{t} \exp[-k'(t - t_1)]k_q \times \exp[-k_q(t - t_1)]n\,[A]_W[M]\,dt_1\,dt \tag{10}$$

where the integration is performed over t_1. After evaluation

$$Q(t)\,dt = \frac{k_q n[A]_W P^*(t)}{k' + k_q}\left[\frac{k_q \exp[-(k' + k_q)t]}{k'} + 1\right] dt \tag{11}$$

Taking into account that at $t = 0$, $P^*(t) = P_0$

$$P^*(t) = P_0 \exp\left[-\left(k_1 + \frac{k_q n[A]_W}{k' + k_q}\right)t - \frac{K k_q^2[A]_W}{(k' + k_q)^2}(1 - \exp[-(k' + k_q)t])\right] \tag{12}$$

The first term in the exponential of eq 12 describes the quenching kinetics if the value of the parameter B (*cf.* eq 15) is low. In this case pseudo-first-order behavior is expected. The rate constant for the quenching reaction is represented by the complex expression

$$C = k_q n/(k' + k_q) \tag{13}$$

and is therefore proportional to the entry rate of the quencher into the micelle.

For large values of B the influence of the second term in the exponent of eq 12 will lead to complex decay kinetics at the beginning of the reaction. However at longer times where $\exp[-(k' + k_q)t \ll 1$ we again expect first-order kinetics. Under these conditions a log P^* *vs.* t plot should yield a straight line, whose slope as well as the intercept with the ordinate axis (log P_0) obtained from extrapolation to zero time is expected to be proportional to the quencher concentration

$$\log P_0' - \log P_0 = K k_q^2[A]_W/(k' + k_q)^2 = -B[A]_W \tag{14}$$

where

$$B = K k_q^2/(k' + k_q)^2 \tag{15}$$

Relations between the experimental parameters K, B, and C and the kinetic parameters k', n, and k_q can be written as follows

$$k' = C/\sqrt{KB} \tag{16}$$

$$n = C\sqrt{K/B} \tag{17}$$

$$k_q = C/(K - \sqrt{KB}) \tag{18}$$

Hence k_q, n, and k' can be evaluated using this kinetic analysis provided K, the constant for the distribution equilibrium of the quencher between the micellar and aqueous phase, is known.

Migration of Triplets from the Micellar into the Aqueous Phase. It has been assumed throughout that the fluorescent probe does not leave the micelle during the reaction time of a few hundred nanoseconds. Evidence to justify this assumption is presented in this paper. For the elucidation of these experiments we develop now a kinetic

equation describing the quenching of long-lived excited probe molecules, *e.g.*, triplets, solubilized in a micellar solution. The model makes allowance for the probe to leave the micelle; however, the location of the triplet quencher is restricted to the aqueous phase. The triplets inside the micelles disappear according to

$$-\mathrm{d}P^*(\mathrm{M})/\mathrm{d}t = (k_1 + k')P^*(\mathrm{M}) - n[\mathrm{M}]P^*(\mathrm{H_2O}) \quad (19)$$

while in the aqueous phase the triplets disappear according to

$$-\mathrm{d}P^*(\mathrm{H_2O})/\mathrm{d}t = -k'P^*(\mathrm{M}) + (k_q[\mathrm{A}] + k_1 + n[\mathrm{M}])P^*(\mathrm{H_2O}) \quad (20)$$

In the above equations, $P^*(\mathrm{M})$ and $P^*(\mathrm{H_2O})$ are the concentration of triplet present in the micellar or aqueous phase. k_1 is the rate constant for the phosphorescence decay if no quencher is added to the solution, k' is the exit rate of the triplet from the micelles, k_q is the second-order rate constant for the triplet quenching in water. [A] and [M] are the concentrations of quenchers and micelles, respectively, and finally n is a second-order rate constant describing the reentry of a triplet molecule from the aqueous phase into a micelle.

Taking into account that at time $t = 0$

$$P^*(\mathrm{M}) = P_0 \text{ and } P^*(\mathrm{H_2O}) = 0 \quad (21)$$

The total amount of triplet present obtained from eq 19 and 20 with the boundary conditions (21) is given by

$$P^* = \frac{P_0}{A}\left\{\left(C - \frac{B-A}{2}\right)\exp\left[\frac{B-A}{2}t\right] - \left(C - \frac{B+A}{2}\right)\exp\left[\frac{B+A}{2}t\right]\right\}$$

where

$$A = \{k_q[\mathrm{A}] + n[\mathrm{M}] + 2k_1 + k')^2 - 4[(k_1 + k')(k_q[\mathrm{A}] + k_1 + n[\mathrm{M}]) - n[\mathrm{M}]k']\}^{1/2}$$

$$B = -(k_q[\mathrm{A}] + n[\mathrm{M}] + 2k_1 + k')$$

$$C = -(k_q[\mathrm{A}] + k_1 + n[\mathrm{M}] + k')$$

At low micelle concentration and high quenching efficiency in the aqueous phase the reentry of triplets into a micelle is completely negligible and under this assumption, we obtain

$$P^* = P_0^* \exp[-(k_1 + k')t] \times \left[1 + \frac{k'}{k_q[\mathrm{A}] - k'}(1 - \exp[-(k_q[\mathrm{A}] - k')t])\right] \quad (22)$$

At higher quencher concentration we have $k_q[\mathrm{A}] \gg k'$ and the second term in the bracket is much smaller than 1. The observed half lifetime of the triplet is then given by

$$\tau = \ln 2/(k_1 + k') \quad (23)$$

Results

Fluorescence Decay Kinetics. To examine the validity of the kinetic equations derived above, laser photolysis experiments were carried out with aqueous solutions of micellized NaLS using pyrene as a fluorescent probe. Methylene iodide and nitromethane were chosen as quenchers because their distribution constants can be determined with the help of the pulse radiolysis method.

Determination of Distribution Constants. Upon irradiation of an aqueous solution with a short pulse of high-energy radiation hydrated electrons are formed whose reactions with added scavengers can be followed by fast kinetic spectroscopy. The rate constant for the reaction of e_{aq}^- with nitromethane is known to be $2.9 \times 10^{10}\ M^{-1}\ \mathrm{sec}^{-1}$ [15] and we determined a value of $3.4 \times 10^{10}\ M^{-1}\ \mathrm{sec}^{-1}$ for the scavenging rate constant of methylene iodide. In an aqueous micellar solution of NaLS only those scavenger molecules will react with the hydrated electron which are present in the aqueous phase since the solubilized part is screened by the negative surface charge of the NaLS micelles.[8] Hence the amount of methylene iodide or nitromethane dissolved in the aqueous phase can be calculated from the relation

$$[\mathrm{A}]_\mathrm{W} = \frac{\ln 2}{k_s}\left(\frac{1}{\tau} - \frac{1}{\tau_0}\right) \quad (24)$$

where k_s is the bimolecular rate constant for the reaction of e_{aq}^- with the scavenger and $1/\tau$ or $1/\tau_0$ are the half lifetimes of the hydrated electron in the presence or absence of scavengers, respectively. From $[\mathrm{A}]_\mathrm{W}$ and the total scavenger concentration the distribution constant K can be obtained (eq 2). To calculate the concentration of NaLS micelles from the amount of dissolved surfactant we used an aggregation number of 62 and a critical micelle concentration of $8.2 \times 10^{-3}\ M$.[16] From a series of experiments with different soap concentrations we obtain[17] $K(\mathrm{CH_2I_2}) = 2.5 \times 10^3\ M^{-1}$ and $K(\mathrm{CH_3NO_2}) = 1.64 \times 10^2\ M^{-1}$. With a knowledge of the distribution of methylene iodide and nitromethane between the micellar and aqueous phase we now proceed to examine the kinetics of the fluorescence of solubilized pyrene in the presence of these quenchers. First we will describe experiments with methylene iodide.

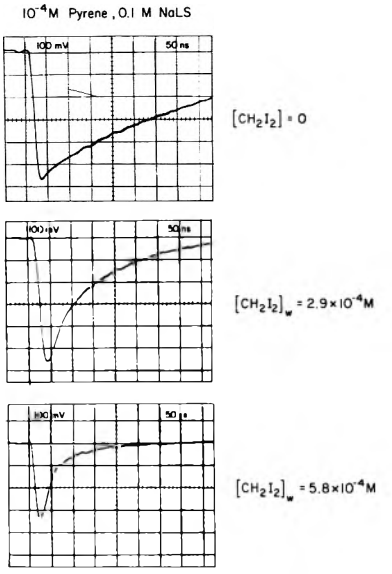

Figure 1. 347.1-nm laser photolysis of aqueous solutions of pyrene (10^{-4} *M*) labeled NaLS (0.1 *M*), oscilloscope traces of pyrene singlet fluorescence decay monitored at 400 nm, added quencher: methylene iodide.

Typical oscilloscope traces of the fluorescence decay monitored at $\lambda = 400$ nm are shown in Figure 1. In the absence of quenchers a smooth exponential decay is observed. Addition of methylene iodide causes a fast spike to appear in the initial part of the curves and at higher concentrations a reduction of the signal height immediately after the laser pulse. Figure 2 shows semilogarithmic plots

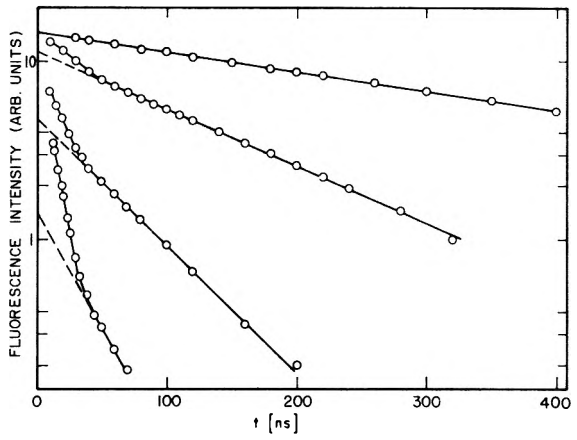

Figure 2. Semilogarithmic plots of pyrene fluorescence decay curves: [pyrene] = 10^{-4} *M*, [NaLS] = 0.1 *M*, $[CH_2I_2]_W$ = 0, 2.9 × 10^{-4} *M*, 5.8 × 10^{-4} *M*, 1.16 × 10^{-3} *M* (from the top).

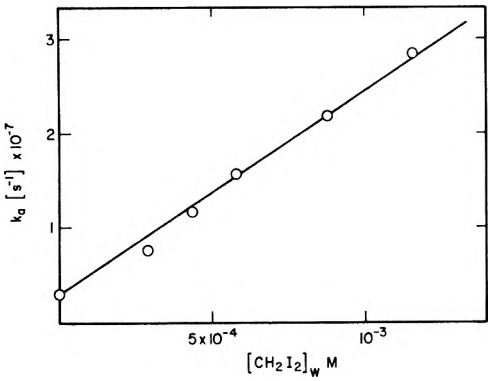

Figure 3. The effect of aqueous methylene iodide concentration on the first-order decay rate of the pyrene singlet fluorescence. [pyrene] = 10^{-4} *M*, [NaLS] = 0.1 *M*.

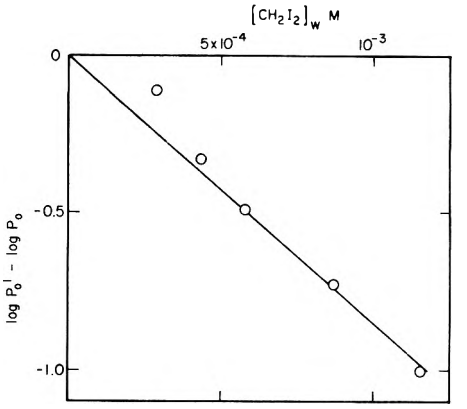

Figure 4. The effect of aqueous methylene iodide concentration on the extrapolated intercept log I_0'.

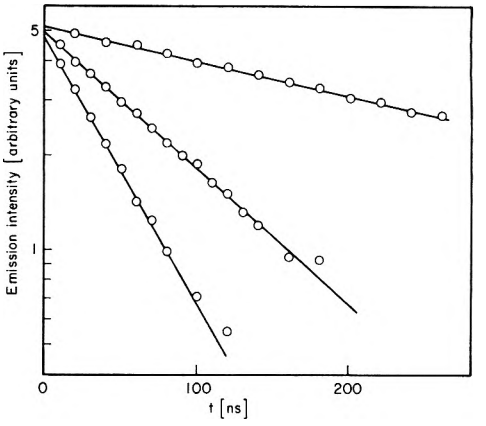

Figure 5. Fluorescence decay data in aqueous solutions of pyrene labeled NaLS and added nitromethane: [pyrene] = 10^{-4} *M*, [NaLS] = 0.1 *M*, $[CH_3NO_2]_W$ = 0, 2.7 × 10^{-3}, 5 × 10^{-3} *M* (from the top).

of the fluorescence intensity *vs.* time at various quencher concentrations. The curves obtained with solutions containing CH_2I_2 evidently consist of two parts. A very steep decay at the beginning of the reaction is followed by a less steep linear part after longer times which obeys first-order kinetics. These straight lines represent the tails of fluorescent decay curves such as Figure 1b and 1c and an apparent rate constant for the quenching reaction can be obtained from their slope

$$k_\phi = k_1 + C[CH_2I_2]_W \qquad (25)$$

k_ϕ values from Figure 2 and other curves which we have omitted for clarity of representation are plotted *vs.* the methylene iodide concentration in the aqueous phase in Figure 3 and we evaluate C = 2.1 × 10^{10} M^{-1} sec^{-1}. To determine the parameter B defined in eq 15 the straight lines in Figure 2 were extrapolated back to the ordinate axis to yield the intercepts log I_0' and log I_0, the intercept for the upper decay curve where no quencher was present in the solution. In order to account for the finite length of the laser pulse the zero of the time axis was set 10 nsec after the beginning of the pulse. The difference log I_0' − log I_0 is identical with the difference log P_0' − log P_0 since the intensity of the fluorescence emission is always proportional to the number of excited molecules. Log P_0' − log P_0 is plotted *vs.* the concentration of methylene iodide in Figure 4. To fit eq 14 a straight line was drawn through the experimental points and the origin of the coordinate system. From the slope we obtain B = 1970 M^{-1}. Inserting the values of B, C, and K in eq 16–18 we can calculate the rate constants of the entry, exit, and quenching reaction of methylene iodide: n = 2.5 × 10^{10} M^{-1} sec^{-1}, k' = 9.5 × 10^6 sec^{-1}, and k_q = 7.5 × 10^7 sec^{-1}. An analogous investigation was carried out with micellized NaLS solutions containing solubilized pyrene as a fluorescent probe and nitromethane as a quencher. In contrast to the results obtained with methylene iodide we find for this quencher simple pseudo-first-order kinetics within the concentration range studied. This is illustrated by Figure 5 where the logarithm of the fluorescence intensity is plotted *vs.* the time for several quencher concentrations. The straight lines meet at the ordinate axis nearly at the same log I_0 that is obtained from the fluorescence decay curve of the nitromethane free solution. Hence the parameter B must be relatively small for this system. The quenching rate constant C = 2.7 × 10^9 M^{-1} sec^{-1} was obtained from a plot analogous to Figure 3.

Exit Rate of Anthracene from Aqueous CTAB Micelles. In an effort to determine the exit time of polycyclic aromatic hydrocarbons from the interior of the micelles into the aqueous bulk phase we have used triplet excited anthracene as a probe. The advantage of this probe is a long lifetime (radiative rate constant of the phosphorescence k = 30 sec^{-1}) and a strong and clearly distinguishable optical absorption (ϵ = 6.47 × 10^4 M^{-1} sec^{-1} at 425 nm). To facilitate the kinetic evaluation and to comply with the boundary conditions of the kinetic model derived above,

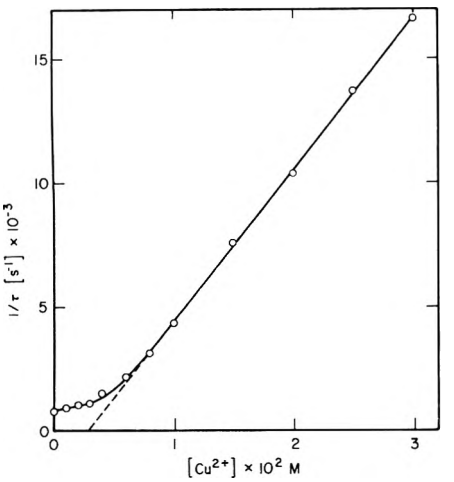

Figure 6. The effect of cupric ions on triplet half-lifetimes of anthracene (10^{-4} *M*) solubilized in 5 × 10^{-2} *M* CTAB.

we used Cu^{2+} ions as triplet quenchers, as the access of these ions to the micellar interior is restricted by the positive surface charge of the CTAB micelles. Both the rate constant for triplet–triplet annihilation and the quenching reaction by Cu^{2+} are known, their respective values being 2 × 10^{10} and 10^{8} M^{-1} sec^{-1}. Solutions of 10^{-4} *M* anthracene solubilized in 5 × 10^{-2} *M* CTAB were used throughout the experiments. We find that the half lifetime of triplet excited anthracene in such a solution is between 1.5 and 2 msec decreasing slightly with increasing intensity of the laser beam. Probably impurities at a concentration level below 10^{-6} *M* are responsible for this behavior. Addition of 5 × 10^{-4} *M* Cu^{2+} decreases the half lifetime to 1.2 msec. The half lifetime observed is hardly affected by further addition of Cu^{2+} as is illustrated by Figure 6 which shows a plot of the reciprocal triplet half lifetime *vs.* the concentration of Cu^{2+} ions. The curve bends sharply at $[Cu^{2+}]$ = 4 × 10^{-3} *M*. Apparently at this bulk concentration the amount of copper ions present in the Stern layer is substantial enough to cause a direct quenching of triplets solubilized inside the micelle. The kinetics of this process are pseudo-first-order with respect to the bulk concentration of Cu^{2+} and a rate constant 4.3 × 10^{5} M^{-1} sec^{-1} is obtained from the slope of the straight line in Figure 6. It should be noted, however, that this line has a positive intercept with the abscissa at $[Cu^{2+}]$ = 2.8 × 10^{-3} *M*. This means that at $[Cu^{2+}] \leq 2.8 \times 10^{-3}$ *M* there is no contribution from this latter type of quenching process to the radiationless deactivation of anthracene triplets and the triplet decay is described by eq 22. In the plateau region the rate of the quenching reaction in the aqueous phase is much higher than the exit rate of anthracene. The half lifetime in the plateau region ($\tau \simeq 1$ msec) is then given by eq 23 from which we evaluate k' = 2 × 10^{2} sec^{-1}.

Discussion

The results presented above illustrate some of the kinetic characteristics of reactions in micellar solutions where the reactants may be found in either the aqueous bulk phase or in the distinct microenvironment of the hydrocarbon interior of the micelle.

To describe the kinetics of reaction of a fluorescent probe solubilized exclusively in the micellar core with a quencher, which can be present in water and micelles, it is necessary to know the distribution of quenchers between the two phases. Fortunately the pulse radiolysis method provides a convenient means of determining the distribution constants for nitromethane and diiodomethane. The value K = 2.5 × 10^{3} M^{-1} obtained for CH_2I_2 reflects the strong affinity of this solute toward NaLS micelles and is comparable to K = 4.58 × 10^{3} M^{-1} reported for di-*tert*-butyl nitroxide.[9] Nitromethane on the other hand dissolves in micelles to a much smaller extent. The value K = 1.64 × 10^{2} M^{-1} implies that in a solution of 0.1 *M* NaLS only 20% of the quencher is associated with the micelles. However, this is still greater than we would expect if a statistical distribution of nitromethane between the two phases existed as in a 0.1 *M* NaLS solution only 2% of the total volume is hydrocarbon phase.[18]

In general the picture of the fluorescence decay curves obtained with these two quenchers substantiates the validity of the kinetic model presented here. This is illustrated in Figures 2–4 where the results for methylene iodide are evaluated according to eq 12, 14, and 25. In particular, Figure 4 shows that the intercepts log P_0' plotted *vs.* the concentration of methylene iodide in water fit a straight line passing through the origin of the coordinate system as predicted by eq 14. An exception is the point representing the lowest value of $[CH_2I_2]_{H_2O}$ which deviates remarkably from that line. Evidently this reflects a decrease of B and therefore a decrease of k_q at lower methylene iodide concentration in the micelle. Such a change of k_q could be caused by a change in the site of incorporation of CH_2I_2. The periphery region of NaLS micelles is apparently preferred by the first few CH_2I_2 molecules, the penetration of the inner core occurring only at higher methylene iodide concentration. Such behavior is common in solubilization processes[19] and we have additional evidence to support this interpretation from other laser photoionization experiments. (Photoelectrons are ejected from pyrene which is solubilized in the interior of NaLS micelles. They can react with suitable scavenger molecules the cross section of this reaction depending on the solubilization site of the scavenger. Molecules residing in the periphery region of the micelles are much more efficient scavengers than those incorporated in the micellar core.)

From the kinetic analysis it is possible to derive rate constants for the entry and exit of methylene iodide, which show that NaLS micelles are very permeable to such a small molecule. The entry rate constant n = 2.5 × 10^{10} M^{-1} sec^{-1} (296°K) is more than 10 times greater than n = 1.48 × 10^{9} M^{-1} sec^{-1} reported for di-*tert*-butyl nitroxide probably because of the bulky size of the latter. Our value is however still below the upper limit for a diffusion controlled rate which for a micelle with r = 16 Å is about 10^{11} M^{-1} sec^{-1}. The exit rate constant k' = 9.5 × 10^{6} sec^{-1} has to be compared with k' = 4.3 × 10^{5} sec^{-1}, 1.2 × 10^{5}, and $\geq 10^{4}$ sec^{-1} reported for di-*tert*-butyl nitroxide,[9] biphenyl,[8] and benzene,[7] respectively. Finally the specific rate of the quenching reaction in the micellar interior k_q = 7.5 × 10^{7} sec^{-1} is the five times larger than k_q = 1.5 × 10^{7} found for the specific rate of pyrene excimer formation in dodecyltrimethylammonium bromide micelles.[20] This is not surprising since the rate constants for these two reactions in cyclohexane differ already by nearly a factor of 3 and steric requirements may slow down the excimer formation in the micelle.

In solutions of pyrene labeled NaLS micelles and nitromethane the quenching reaction obeys simple pseudo-

first-order kinetics as illustrated by Figure 5. It remains to check if this is in accordance with the present model. Inspection of eq 12 shows that pseudo-first-order behavior is expected only if parameter B for nitromethane is much smaller than that for methylene iodide. The value of $B(CH_3NO_2)$ may be estimated by assuming that the ratio of k_q for the quenching reaction of methylene iodide and nitromethane in the micelle is equal to the ratio of the rate constants in cyclohexane.

$$k_q(CH_2I_2)/k_q(CH_3NO_2) = 3$$

Then $k'(CH_3NO_2)$ can be calculated from eq 2 and 5 as

$$k' = \frac{1}{K/C - 1/k_q}$$

and the following value is obtained: $k' \simeq 6 \times 10^7$ sec^{-1}, $n \simeq 10^{10}$ M^{-1} sec^{-1}, $B \simeq 14$ M^{-1}. Although this value of B can only be regarded as a rough estimate it shows that the contribution of the third term in eq 12 is negligible in the concentration range of CH_3NO_2 that was investigated. Under the conditions used, eq 12 predicts pseudo-first-order kinetics in agreement with the observation.

While the micelle–water boundary does not greatly prevent the movement of small molecules from the micellar into the aqueous phase it certainly restricts the exit rate of polycyclic aromatic hydrocarbons. In aqueous solutions of anthracene solubilized in CTAB micelles the half lifetime for its triplet state is 1.6 to 2 msec. If the exit rate constant k' for anthracene was in the order of 10^5–10^7 sec^{-1}, the triplet-triplet annihilation in the aqueous phase would determine the decay kinetics. The rate constant of this reaction ($k = 2 \times 10^{10}$ M^{-1} sec^{-1}) and the initial concentration of anthracene triplets ($c^0 = 5 \times 10^{-6}$ M) yield a first half lifetime of 10 μsec. From the measured half lifetime it is alread possible to infer that $k' < 10^3$ sec^{-1}. The results obtained with solutions containing Cu^{2+} ions as quencher amplify this conclusion. Upon addition of 5×10^{-4} M Cu^{2+} to anthracene labeled CTAB micelles, the triplet lifetime decreases from 1.6 to 1.2 msec. From this plateau value we calculate $k' = 2 \times 10^2$ sec^{-1}. Since the half lifetime in the plateau region is close to that of solutions without added cupric ions this value may possibly represent only a higher limit of k'.

Conclusions

The kinetic model presented in this paper describes some of the unique features of reactions in micellar solutions. Experimental results obtained from quenching experiments are in good agreement with the predictions of the kinetic equations and yield values for exit and entry rates of guest molecules. It is shown that the rate constants depend on the size and hydrophobicity of the solubilized entities and differ by many orders of magnitude, very low values being obtained for polycyclic aromatic hydrocarbons.

Acknowledgment. Acknowledgment is made to the donors of The Petroleum Research Fund, administered by the American Chemical Society, for partial support of this research.

Supplementary Material Available. A listing of distribution coefficients will appear following these pages in the microfilm edition of this volume of the journal. Photocopies of the supplementary material from this paper only or microfiche (105 × 148 mm, 24× reduction, negatives) containing all of the supplementary material for the papers in this issue may be obtained from the Journals Department, American Chemical Society, 1155 16th St., N.W., Washington, D. C. 20036. Remit check or money order for $3.00 for photocopy or $2.00 for microfiche, referring to code number JPC-74-190.

References and Notes

(1) (a) Present address, Interuniversity Reactor Institute, Berlageweg 15, Delft, The Netherlands. (b) The Radiation Laboratory of the University of Notre Dame is operated under contract with the U. S. Atomic Energy Commission. This is AEC Document No. COO-38-906.
(2) (a) E. H. Cordes, "Reaction Kinetics in Micelles," Plenum Press, New York, N. Y., 1973, p 127; (b) E. H. Cordes and C. Gitler, *Progr. Bioorg. Chem.*, **2**, 1 (1973).
(3) D. Stigter, *J. Colloid Interface Sci.*, **32**, 286 (1970).
(4) (a) M. Shinitzky, A. C. Dianoux, C. Gitler, and G. Weber, *Biochemistry*, **10**, 2106 (1971); (b) U. Cogan, M. Shinitzky, G. Weber, and T. Nishida, *ibid.*, **12**, 521 (1973); (c) H. J. Pownall and L. C. Smith, *J. Amer. Chem. Soc.*, **95**, 3136 (1973).
(5) M. Grätzel and J. K. Thomas, *J. Amer. Chem. Soc.*, **95**, 6885 (1973).
(6) P. H. Elworthy, A. T. Florence, and C. B. MacFarlane, "Solubilisation by Surface Active Agents," Chapmann and Hall, London, 1968.
(7) T. Nakagawa and K. Tori, *Kolloid-Z. Z. Polym.*, **194**, 143 (1964).
(8) S. C. Wallace and J. K. Thomas, *Radiat. Res.*, **54**, 49 (1973).
(9) N. M. Atherton and S. J. Strack, *J. Chem. Soc., Faraday Trans. 2*, **68**, 374 (1972).
(10) Reference 2, p 2.
(11) R. R. Hautala and N. J. Turro, *Mol. Photochem.*, **4**, 545 (1972).
(12) L. K. Patterson and E. Vieil, *J. Phys. Chem.*, **77**, 1191 (1973).
(13) R. McNeil, J. T. Richards, and J. K. Thomas, *J. Phys. Chem.*, **74**, 2290 (1970).
(14) T. Kajiwara and J. K. Thomas, *J. Phys. Chem.*, **76**, 1700 (1972).
(15) J. Sutton and D. H. Tran Dinh Son, *J. Chim. Phys.*, **64**, 688 (1967).
(16) K. J. Mysels and L. H. Princen, *J. Phys. Chem.*, **63**, 1696 (1959).
(17) See paragraph at end of paper regarding supplementary material.
(18) K. Shinoda and T. Soda, *J. Phys. Chem.*, **67**, 2072 (1963).
(19) J. C. Erikson and G. Gillbert, *Acta Chem. Scand.*, **20**, 2019 (1966).
(20) R. C. Dorrance and T. F. Hunter, *J. Chem. Soc., Faraday Trans. 1*, **68**, 1312 (1972).

Equilibria between Triplet States of Aromatic Hydrocarbons[1a]

A. Kira[1b] and J. K. Thomas*

Department of Chemistry and the Radiation Laboratory, University of Notre Dame, Notre Dame, Indiana 46556
(Received September 5, 1973)

Publication costs assisted by the U. S. Atomic Energy Commission

An equilibrium between triplet states, $D^T + A \rightleftarrows D + A^T$, was directly observed by pulse radiolysis and laser photolysis techniques. It was demonstrated that the free-energy difference calculated from the equilibrium constant is equivalent to the difference in energy between the triplet states. The triplet energy of a solute can be determined by measuring the equilibrium between the triplet state of this solute and another triplet of known energy. Triplet energies thus obtained are (in eV) biphenyl, 2.93, *m*-terphenyl, 2.88, and *p*-terphenyl, 2.66 which are higher than the phosphorescence energies and 1,1′-binaphthyl, 2.53 and 1,2′-binaphthyl, 2.43 which agree with the phosphorescence energies. The triplet energy obtained by this method is considered to correspond to the nonvertical triplet energy.

Introduction

Sandros[2a] has found that in solution triplet energy transfer from a donor triplet to an acceptor proceeds with a diffusion-controlled rate constant and that the reverse reaction occurs with a diffusion-controlled rate constant multiplied by $\exp(-\Delta E_T/RT)$, where ΔE_T is the difference in triplet energy between the donor and acceptor molecules. The relationship between the forward and the back reaction rate constants or the equilibrium constant has been used to estimate the triplet energy of several compounds,[2b,3] and it has also successfully explained the dependence of emission[4,5] and esr signals of excited states in mixed crystals on temperature.[6]

It is possible to observe directly an equilibrium between two excited triplet states

$$D^T - A \rightleftarrows D + A^T \quad (1)$$

where D and A refer to the donor and acceptor, respectively, and the superscript T refers to the triplet state. In particular Kikuchi and coworkers[7] have observed such an equilibrium in the eosin–anthracene system. An equilibrium constant K may be defined by

$$K = [A^T][D][A]^{-1}[D^T]^{-1} \quad (2)$$

and provided a true equilibrium is attained then the free-energy change in the process ΔG is given by

$$-\Delta G = 2.303RT \log K \quad (3)$$

The assumption then may be made that $-\Delta G$ is equivalent to the difference in the energies of the triplet states ΔE_T.

In the present study the equilibrium constant K was measured directly by using the pulse radiolysis and laser photolysis techniques. A prior examination in systems where the triplet energies are known precisely confirmed the assumption that $-\Delta G = \Delta E_T$. The technique was then applied to determine the triplet energies of biphenyl, terphenyls, and binaphthyls. It is suggested[3,8] that these molecules have a twisted configuration in the ground state and a planar configuration in the triplet state. Hence phosphorescence studies do not necessarily give the correct triplet energy. However in the present technique the nonvertical energy of triplet state is measured rather than the vertical energy which is measured by phosphorescence studies.

Experimental Section

The nanosecond pulse radiolysis and laser photolysis systems have already been described.[9] The pulse radiolysis experiments were carried out with 5-nsec pulses of 7-MeV electrons with a dose of 10^{20} eV/l./pulse. The laser photolysis experiments were carried out with 15-nsec pulses of light of wavelength of 347.1 nm with 0.1 J in the pulse. All samples were degassed by bubbling with N_2 gas for a prolonged period, and all experiments were carried out at a temperature of 26 ± 1°.

Benzene was obtained from Fisher Chemicals as 99 mol % reagent grade. Naphthalene and chrysene were recrystallized from ethanol; phenanthracene and *m*-terphenyl were zone refined by the J. Hinton Co.; pyrene was purified by column chromatography. All other chemicals were reagent grade and were used without further purification.

Results

Benzene was used as a solvent in all the systems studied as it has been established that in radiolysis excited states with a yield of G(singlet) = 1.62 and G(triplet) = 3.8 molecules/100 eV are produced[10] while the yield of ions is much lower with G(ions) ≃ 0.3 molecules/100 eV.[10b,c] Hence the overall picture is the production of excited states in the radiolysis of benzene with a subsequent transfer of both singlet and triplet energy to the solutes. Intersystem crossing will rapidly produce exclusively triplet states of the solutes for observation

$$\underset{(B)}{\text{benzene}} \xrightarrow{h\nu} B^S + B^T \xrightarrow[(S)]{\text{solute}} S^S + S^T \searrow S^T$$

Naphthalene–Chrysene. The transitory triplet spectra of naphthalene and chrysene are observed in the pulse radiolysis of these solutes in benzene. Typical spectral data are shown in Figure 1, where the 425-nm absorption maximum of the naphthalene triplet which is observed at the end of the pulse is subsequently partially replaced at 400 nsec by the 580-nm band of the chrysene triplet. The much higher concentration of naphthalene first accepts the energy from the benzene, followed by the formation of

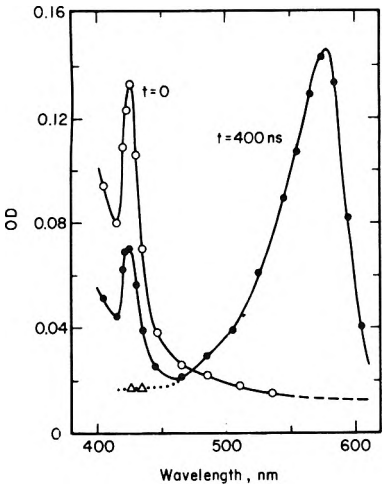

Figure 1. Time dependence of the transient spectrum in a 236 m*M* naphthalene–0.54 m*M* chrysene solution in benzene. Triangle marks indicate the absorption of chrysene triplet alone.

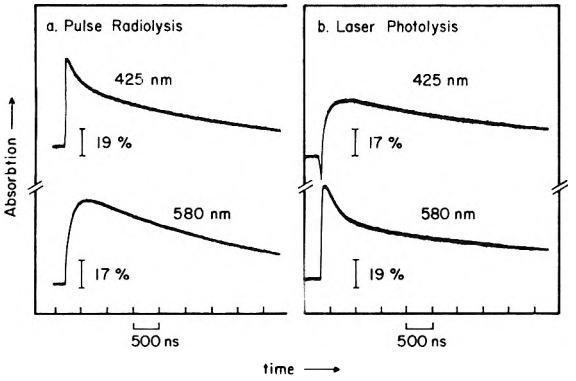

Figure 2. The growth and decay of triplet states of naphthalene (425 nm) and chrysene (580 nm) in the pulse radiolysis (a) and in the laser photolysis (b).

an equilibrium between the triplet states of the two solutes. In Figure 2a, the 425-nm absorption decay is accompanied by the concomitant growth of the 580-nm absorption up to a certain point, after which both triplet states show identical decay. In Figure 3 the ratio of both absorptions is plotted *vs.* time for different chrysene concentrations. Initially the ratio decreases but a plateau is attained after 1 msec, indicating the identical decay of both triplets and the establishment of an equilibrium. The equilibrium constant is then calculated from the ratio obtained at the plateau.

Other examples of transient spectra in some systems under equilibrium conditions are shown in Figure 4.

In the pulse radiolysis experiments triplet energy is transferred from naphthalene to chrysene, due primarily to the choice of experimental conditions. However, for a true equilibrium it should be possible to transfer the energy from chrysene to naphthalene. This is conveniently carried out in the above system by selectively exciting the chrysene which has a 0-0′ band at 27,700 cm^{-1} with the 347.1-nm line (28,800 cm^{-1}) from a doubled ruby laser. Naphthalene does not absorb at this frequency and the chrysene is selectively excited to the singlet state, which subsequently produces the triplet state by intersystem crossing, and finally the equilibrium between the solute triplets is set up. It is also possible to study the chrysene 1,1′-binaphthyl by the laser technique. The data for the

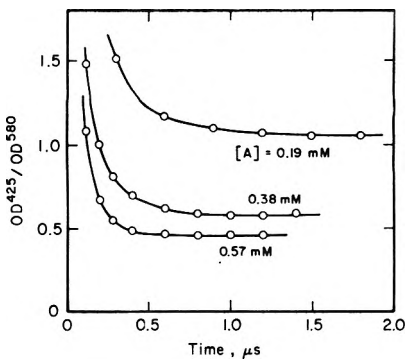

Figure 3. The change in the ratio of the triplet absorptions of naphthalene (425 nm) and chrysene (580 nm): naphthalene concentration, 204 m*M*. Chrysene concentrations are given in the figure.

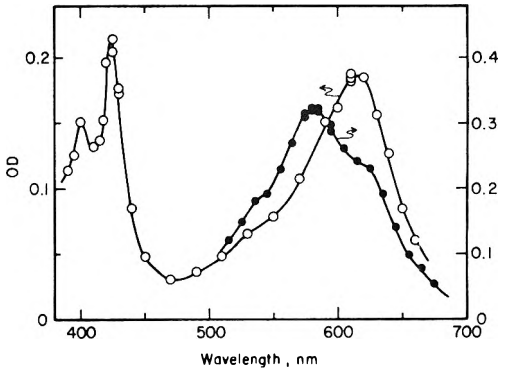

Figure 4. Transient spectra under the equilibrium: O, 208 m*M* naphthalene–2.3 m*M* 1,1′-binaphthyl at 200 nsec and ●, 16.5 m*M* 1,1′-binaphthyl–1.3 m*M* chrysene at 600 nsec.

naphthalene–chrysene system is shown in Figure 2b where in contrast to the pulse radiolysis data the chrysene triplet is first formed and the naphthalene triplet is subsequently formed. A small portion of naphthalene triplet is formed initially due to a two photon excitation of the naphthalene.

Evaluation of the Equilibrium Constant. To evaluate the equilibrium constant, eq 2 is modified as follows. Optical densities at wavelengths d and a where the triplet state of the donor and acceptor, respectively, absorb predominantly are given by

$$OD^d = l(\epsilon_A{}^d[A^T] + \epsilon_D{}^d[D^T]) \quad (4)$$

$$OD^a = l(\epsilon_A{}^a[A^T] + \epsilon_D{}^a[D^T]) \quad (5)$$

where subscripts D and A indicate triplet states of the donor and acceptor, respectively. These lead to

$$OD^a - mOD^d = \epsilon_A{}^a(1 - mn)[A^T] \quad (6)$$

$$OD^d - nOD^a = \epsilon_D{}^d(1 - mn)[D^T] \quad (7)$$

with $m = \epsilon_D{}^a/\epsilon_D{}^d$ and $n = \epsilon_A{}^d/\epsilon_A{}^a$.

Substitution of eq 2 with eq 6 and 7 produces the relationship

$$(OD^a - mOD^d)(OD^d - nOD^a)^{-1} = K\epsilon_A{}^a(\epsilon_D{}^d)^{-1}[A][D]^{-1} \quad (8)$$

Values of m and n were determined from the spectra of the triplet states of the donor and acceptor. The plots of eq 8 shown in Figures 5 and 6 establish the validity of the treatment. The analysis is successful even in a 1,1′-binaphthyl–chrysene system where the absorption spectra of both triplet states overlap as shown in Figure 4.

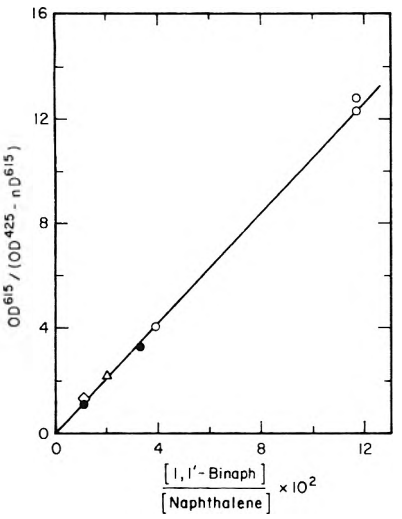

Figure 5. A plot based on eq 8 for a naphthalene–1,1′-binaphthyl system, where $m \simeq 0$. Concentrations of naphthalene are: O, 23.4 m*M*; △, 55.0 m*M*; ●, 82.5 m*M*; ◊, 204 m*M*.

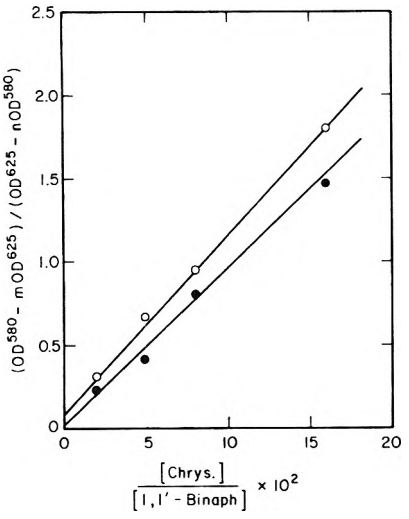

Figure 6. A plot for a 1,1′-binaphthyl–chrysene system. The same samples were measured by means of the pulse radiolysis (O) and laser photolysis (●) methods.

TABLE I: Energy Difference in eV between Triplet States in Various Systems

Donor	Acceptor	$-\Delta G$	ΔE(phos)	ΔE_T
Naphthalene	Chrysene	0.172	0.16	
Naphthalene	1,1′-Binaphthyl	0.124	0.11	
1,1′-Binaphthyl	Chrysene	0.050	0.05	
Phenanthrene	*p*-Terphenyl	0.032	0.14	0.03
p-Terphenyl	Chrysene	0.172	0.07	0.18
p-Terphenyl	1,1′-Binaphthyl	0.134	0.02	0.13
Benzophenone	Biphenyl	0.081	0.16	0.08
Benzophenone	*m*-Terphenyl	0.132	0.22	0.13
Chrysene	2,2′-Binaphthyl	0.052	0.06	
Pyrene	1,2′-Benzanthracene	0.036	0.03	

The extinction coefficient ratio, $\epsilon_A{}^a/\epsilon_D{}^d$, is needed in order to evaluate the equilibrium constants. The extinction coefficients of some of the triplet absorptions studied have been measured by Bensasson and Land.[11] For other compounds not listed in their paper, the extinction coefficient was determined in a similar fashion by transferring

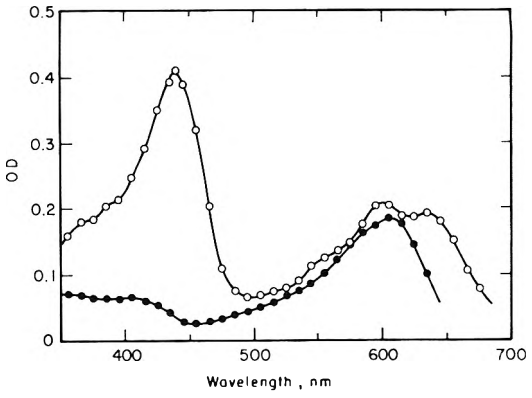

Figure 7. T–T absorption spectra of 1,1′- (●) and 2,2′-binaphthyl (O) taken at 300 nsec in benzene solution. Short-lived species observed immediately after the pulse have vanished at 300 nsec.

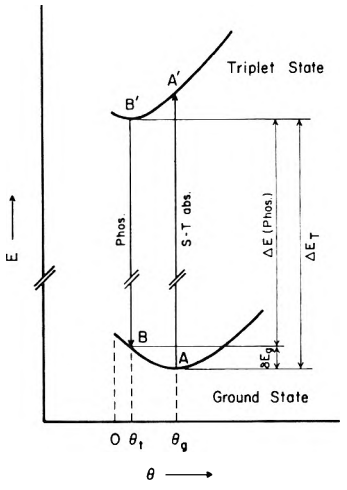

Figure 8. Schematic diagram of ground and triplet states of polyphenyls.

triplet energy from the benzophenone triplet to the acceptor. The extinction coefficient of the benzophenone triplet is 7630 M^{-1} cm^{-1} at 532.5 nm[11] which enables an accurate calculation of the triplet concentration to be carried out from the triplet optical density. As the transfer of triplet energy is quantitative, the concentration of the acceptor triplets is established and the extinction coefficient is then calculated from the optical density in the usual fashion. The extinction coefficients at wavelengths of interest in the present measurements which were not necessarily the absorption maxima are listed in Table II. The spectra of the triplet state of binaphthyls which have not been previously reported are shown in Figure 7.

The energy differences, $-\Delta G$, calculated by eq 3 are summarized in Table I. The total experimental error in the equilibrium constants is less than a factor of 1.5, *viz.* the values are within 67 and 150%. This deviation corresponds to ±0.01 eV in $-\Delta G$.

Discussion

The differences in the triplet energy of various donor–acceptor pairs based on phosphorescence measurements[8,12] are given in Table I and compared with the present $-\Delta G$ measurements. The phosphorescence spectra are affected by both solvent and phase, and the error in the 0–0 energies is believed to be greater than ±0.01 eV.[8] Therefore, the agreement between $-\Delta G$ and ΔE(phos) in Table

TABLE II: Various Parameters for Triplet States

Molecule	$\epsilon_T \times 10^4$ (at λ, nm),[a] M^{-1} cm^{-1}	E(phos), eV	E_T, eV
Benzophenone	0.76 (535)	3.01[b]	
Biphenyl	1.8 (395)	2.85	2.93
m-Terphenyl	1.3 (395)	2.79	2.88
Phenanthrene	1.6 (490)	2.69[b]	
Naphthalene	1.3 (425)	2.64[b]	
p-Terphenyl	9.0 (460)	2.55	2.66
1,1′-Binaphthyl	1.2 (615)	2.53	2.53
Chrysene	1.8 (480)	2.48	
2,2′-Binaphthyl	2.4 (450)	2.42	2.43
Pyrene	2.1 (425)	2.08[c]	
1,2-Benzanthracene	2.1 (495)	2.05[c]	

[a] Extinction coefficient of the T–T absorption. [b] Energy chosen as the standard. [c] A pyrene–1,2-benzanthracene pair was measured only to assure validity of the method.

I may be judged satisfactory if both are within a deviation of ±0.02 eV.

Good agreement between $-\Delta G$ and ΔE(phos) is obtained in the systems, naphthalene–chrysene and pyrene–1,2-benzanthracene, where the phosphorescence energies refer to the correct triplet energy for each component. The agreement also holds in donor–acceptor pairs containing binaphthyls apart from *p*-terphenyl–binaphthyl. The first three systems given in Table I demonstrate the close agreement of the $-\Delta G$ and ΔE(phos) values. Furthermore, for naphthalene–chrysene $-\Delta G = 0.172$ eV, and for naphthalene–1,1′binaphthyl $-\Delta G = 0.124$, from which one can calculate $-\Delta G = 0.048$ for the 1,1′-binaphthyl–chrysene system, which agrees with the measured value of 0.050.

In systems containing biphenyl or terphenyls, the measured $-\Delta G$ does not agree with ΔE(phos). However, in the *p*-terphenyl system good agreement between the calculated ΔE_T and the measured $-\Delta G$ may be obtained if a value of 2.66 eV is used for the *p*-terphenyl triplet instead of 2.55 eV measured in phosphorescence. It is also noted that the energy is not transferred from the triplet naphthalene to *p*-terphenyl which indicates that the triplet energy of *p*-terphenyl is higher than that of naphthalene, *i.e.*, 2.64 eV. Similarly, a triplet energy that is higher than the phosphorescence energy is indicated for biphenyl and *m*-terphenyl by the present data. Revised triplet energies may be calculated from the present data and are listed as E_T in Table II. Benzophenone, naphthalene, and phenanthrene in which the 0-0 band of the phosphorescence agrees with that of the S–T absorption[8,13] were chosen as standards of triplet energy.

Biphenyls and terphenyls take on a twisted conformation in the ground state both in the gas phase and in solution, but become planar in the singlet excited state.[14,15] A similar planar or less twisted conformation is suggested for the triplet state by the fact that the S–T absorption of these molecules appears at shorter wavelengths than the shortest wavelength of phosphorescence. A schematic drawing of the situation is given in Figure 8. In the ground state the molecule is stabilized by rotation around a C–C bond between the phenyl groups by θ_g. The molecule absorbs the energy for the transition A′ ← A and emits the phosphorescence corresponding to B′ → B. The actual triplet energy is given by the difference between B′ and A which is not obtained spectroscopically. The only attempt to determine such nonvertical triplet energies has been made by Wagner, who obtained a triplet energy of 68.5 kcal (2.97 eV)[3b] for biphenyl, from the quenching of the phosphorescence of benzophenone and other compounds by biphenyl and other aromatic solutes. The energy obtained in the present study is considered to be related to the net energy (B′ − A) of the triplet state. Actually, the revised energy for these molecules in Table II lies between the highest phosphorescence band and the lowest S–T absorption band, as expected from the above scheme. The fact that the same triplet energy is obtained for *p*-terphenyl in both measurements where *p*-terphenyl is used as either donor or acceptor suggests that the equilibrium method gives the energy difference B′ − A.

The stabilization energy of the ground state of biphenyl has been reported to be 0.08 eV at $\theta_g = 42°$.[16] The stabilization energy, δE_g, gained by a twisting from θ_t where the molecule phosphoresces to θ_g is evaluated to be 0.08 eV from a relation, $\theta E_g = \Delta E_T - \Delta E$(phos). The agreement of these two values indicates that the triplet state of biphenyl is planar, because if it were not planar, δE_g would be smaller than 0.08 eV. The stabilization energy in the ground state has not been established for other polyphenyls.

The net triplet energy of binaphthyls is in agreement with the literature phosphorescence data. This is not surprising as in 1,1′-binaphthyl the hydrogen atoms attached to the 2 and 8′ positions prevent the molecule from taking a planar conformation. However in 2,2′-binaphthyl such steric hindrance does not exist but the agreement of $-\Delta G$ and ΔE(phos) is good. However, Marchetti and Kearns[8] have found that the relationship between the phosphorescence and S–T absorption spectra of 1-phenyl- and 2-phenylnaphthalenes is similar to that of naphthalene derivatives rather than that of polyphenyls. This observation and the present results suggest that the molecular conformations of naphthalene derivatives are mainly governed by factors other than that of steric hindrance.

References and Notes

(1) (a) The Radiation Laboratory of the University of Notre Dame is operated under contract with the U. S. Atomic Energy Commission. This is AEC Document No. C00-38-915. (b) On leave from the Institute of Physical and Chemical Research, Japan.
(2) (a) K. Sandros, *Acta Chem. Scand.*, **18**, 2355 (1964); (b) C. A. Parker and T. A. Joyce, *Photochem. Photobiol.*, **6**, 395 (1967).
(3) (a) P. J. Wagner, *J. Amer. Chem. Soc.*, **89**, 2820 (1967); (b) *Mol. Photochem.*, 1, 71 (1969).
(4) S. P. McGlynn, T. N. Misra, and E. F. McCoy, *Int. Lumin. Symp., Munich, 1965*, 98 (1966).
(5) H. Port and H. C. Wolf, Beirut Symposium, 1967, p 383. Cambridge University Press, London, 1967.
(6) (a) N. Hirota and C. A. Hutchinson, Jr., *J. Chem. Phys.*, **42**, 2869 (1965); (b) N. Hirota, *ibid.*, **43**, 3354 (1965).
(7) K. Kikuchi, H. Kokubun, and M. Koizumi, *Bull. Chem. Soc. Jap.*, **43**, 2732 (1970).
(8) A. P. Marchetti and D. R. Kearns, *J. Amer. Chem. Soc.*, **89**, 768 (1967).
(9) T. Kajiwara and J. K. Thomas, *J. Phys. Chem.*, **76**, 1700 (1972).
(10) (a) R. Cooper and J. K. Thomas, *J. Chem. Phys.*, **48**, 5097 (1968); (b) J. H. Baxendale and M. Fitz, *J. Chem. Soc., Faraday Trans. 1*, **68**, 218 (1972); (c) T. Gangwer and J. K. Thomas, *Radiat. Res.*, **54**, 192 (1973).
(11) R. Bensasson and E. J. Land, *Trans. Faraday Soc.*, **67**, 1904 (1971).
(12) (a) J. B. Birks, "Photophysics," Wiley-Interscience, London, 1970, pp 256–263; (b) K. A. Zachariasse, Thesis, Vrije Universiteit, Amsterdam, The Netherlands.
(13) D. R. Kearns and W. A. Case, *J. Amer. Chem. Soc.*, **88**, 5057 (1966).
(14) H. Suzuki, "Electronic Absorption Spectra and Geometry of Organic Molecules," Academic Press, New York, N. Y., 1967, pp 261–290.
(15) A latest paper on this subject is: A. Tajiri, S. Takai, and M. Hatano, *Bull. Chem. Soc. Jap.*, **46**, 1067 (1973).
(16) E. Katon and E. R. Lippincott, *Spectrochim. Acta*, **19**, 627 (1959).

COMMUNICATIONS TO THE EDITOR

Electron Paramagnetic Resonance of Adsorbed Nitroxide

Publication costs assisted by the Petroleum Research Fund

Sir: We have performed epr studies of di-*tert*-butyl nitroxide (DTBN) adsorbed on silica-alumina. As is also true for O_2^- and NO,[1] the parameters of the DTBN spin Hamiltonian (SH)

$$H = \beta \mathbf{S}\cdot\mathbf{g}\cdot\mathbf{H} + A_N S_Z I_Z + B_N(S_X I_X + S_Y I_Y)$$

are sensitive to the nature and strength of surface interactions. In the powder spectra of DTBN on surfaces or in frozen solutions the parallel component of the anisotropic ^{14}N hyperfine splitting (hfs), A_N, gives well-resolved splittings (Figure 1A). Complexing a nitroxide with an electron pair acceptor (A) stabilizes the resonance structure with the unpaired spin on nitrogen, I, shifting spin density

$$\underset{\text{I}}{(t\text{-Bu})_2\overset{+}{\text{N}}\text{—}\overline{\underset{\cdot\cdot}{\text{O}}}\text{:A}} \longleftrightarrow \underset{\text{II}}{(t\text{-Bu})_2\overset{\cdot}{\text{N}}\text{—}\overset{\cdot\cdot}{\text{O}}\text{:A}}$$

toward N and resulting in an increase in A_N. This change in A_N increases with the strength of the interaction, and thus A_N may be used as a measure of electron pair acceptor strength. When the nitroxide is complexed with a strong Lewis acid, additional information may be available from the observation of hfs by the coordinating nucleus of the acid.[2] An advantage to the utilization of DTBN as a surface probe, as opposed to O_2^- or NO, is that it also forms complexes with molecular Lewis acids in free solution;[2] thus for the first time we use a radical to compare the properties of a surface site with those of a well-defined solution species.

Silica-alumina (13% alumina) is first calcined in oxygen at 500° to remove impurities, rehydrated by exposure to water vapor at room temperatures, and then activated *in vacuo* to a selected temperature (125–500°). Exposure to DTBN vapor followed by equilibration at a fixed temperature between 50 and 125° can produce two distinct types of epr spectra, I (Figure 1A) and II (Figure 1B). The adsorbed nitroxides which give these signals are chemically unaltered, for they can be completely removed intact from the surface by exposure to a stronger base such as pyridine. Following such treatment, a spectrum of DTBN in pyridine is observed. In addition, quantitative epr shows that depending upon conditions of activation, some fraction of the applied DTBN is decomposed into diamagnetic products.

In the type I spectrum (Figure 1A), A_N is increased over that in an inert solvent, indicative of perturbation of the nitroxide by interaction with the surface. The value of A_N is within the range found for DTBN in hydrogen-bonding media.[2] Since at the activation temperatures employed, adsorbed water has been removed, we associate this spectrum with nitroxide hydrogen bonded to surface hydroxyls.[3] A similar spectrum is seen for DTBN on pure silica.[4] In particular, from Table I we see that the value of A_N on silica-alumina and in phenol are similar, demonstrating that the interactive strength of the hydroxyls in both systems is similar. As with DTBN in phenol, no splittings are resolved for the hydrogen-bonded proton.

The type II spectrum shows A_N to be further increased, and also exhibits a well resolved six-line hyperfine pattern arising from interaction with a single aluminum nucleus ($I = 5/2$), indicating that the nitroxide is complexed to a coordinatively unsaturated surface aluminum atom.[3a,b] Figure 1 and Table I show the great similarity between the spectrum for DTBN coordinated to surface aluminum and that for the radical complexed with $AlCl_3$ in solution.[5] In contrast, the SH parameters for DTBN complexed with, for example, aluminum alkyls, are quite different from those of Table I.[5] Thus, the electron pair acceptor strength of the surface aluminum is similar to that of $AlCl_3$, greater than that of AlR_3, and considerably greater than that of the surface hydroxyls or phenol.

The type of site observed could be controlled by variation in temperature of activation and/or surface coverage.[4] Type II spectra become increasingly important at the higher activation temperatures (200° and above). For a given temperature type II spectra tend to dominate at low surface coverage, presumably, because the more strongly interacting (larger A_N) surface aluminum ion sites "fill up" first. However, computer simulations suggest a finite amount (~10%) of type I spectrum as a background even in Figure 1B.[4] At all activation temperatures the contribution from nitroxides hydrogen bonded to surface hydroxyls (type I) increases with increasing surface coverage until the type II spectrum is a small or even unobservable fraction of the signal. Finally, when the amount of DTBN approaches monolayer quantities, the type I spectrum begins to exhibit spin–spin interactions between nitroxides.

With a low temperature of activation ($T_A \approx 125°$) a surface aluminum should be left with a bound water, which would then act as a strong proton donor.[3a,b] By analogy to the behavior of the H_2O:$AlCl_3$ complex such a

TABLE I: Hfs (Gauss) for DTBN on Silica Alumina and in Solution (T = 77°K)

Medium	A_N[b]	A_{Al}[d]	B_{Al}[d]	Ref
Toluene	34.6[c]			This work
Silica–alumina, type I[a]	38.6[c]			This work
Phenol	38.3[c]			2c
Silica–alumina, type II[a]	46.1[d]	16.6	17.1	This work
$AlCl_3$ complex	47.0[d]	14.6	16.2	5

[a] Hfs constants from Figure 1. Values vary somewhat with catalyst treatment (ref 4). [b] B_N (= 6 ± 1 G) is not directly observable; it may be estimated from computer simulation (ref 4). [c] Error limits, ±0.2 G. [d] Error limits, ±0.5 G.

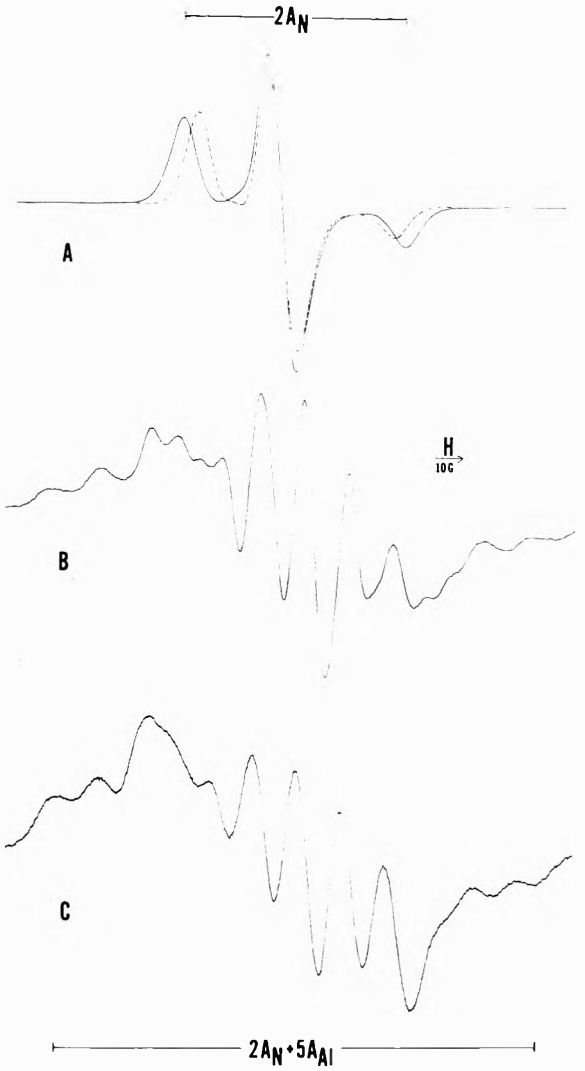

Figure 1. Esr of DTBN at 77°K: (A) type I spectrum on silica–alumina (——) and that of frozen toluene solution (- - -); (B) type II spectrum on silica–alumina; (C) $AlCl_3$ molecular complex (ref 5).

surface species should act as a strong Bronsted acid and be able to protonate a nitroxide.[2b] $DTBNH^+$ has A_N = 47.6[2c] G and no metal splitting, but no such spectrum with that large a splitting was observed either as a predominant or minority species upon addition of nitroxide to catalyst activated at this temperature. However, under these conditions the nitroxide underwent considerable decomposition, far more than was found to occur at higher T_A. A large excess had to be added before the site I spectrum could be observed. Removal of nitroxide by heating and pumping revealed only a weak site II spectrum. Since the protonated nitroxide formed from H_2O:$AlCl_3$ is much less stable than is the $AlCl_3$ complex, it may be inferred that similar behavior occurs on a silica–alumina surface; a Bronsted site is formed by moderate T_A but decomposes the nitroxide whereas coordinately unsaturated surface aluminum itself forms a stable complex with the radical.

We have used DTBN to examine surface sites on silica–alumina and to compare their properties to those of well-defined molecular species. In particular, we have observed a coordinatively unsaturated surface aluminum whose properties as a Lewis acid resemble those of $AlCl_3$ and which is present even with T_A = 125°. More detailed investigations of activation conditions are in progress as well as an extension to other surfaces of catalytic importance, such as silica, alumina, and zeolites.

Acknowledgment. We are deeply indebted to Professor Robert L. Burwell, Jr., for enlightening discussions. This work was supported by DA-ARO-D Grant No. 31-124 and by the donors of the Petroleum Research Fund, administered by the American Chemical Society.

References and Notes

(1) (a) J. H. Lunsford, *J. Catal.*, **14**, 379 (1969); (b) P. H. Kasai and R. J. Bishop, Jr., *J. Amer. Chem. Soc.*, **94**, 5560 (1972); (c) K. M. Wang and J. H. Lunsford, *J. Phys. Chem.*, **74**, 1512 (1970); (d) J. H. Lunsford, *Advan. Catal.*, **22**, 265 (1972); (e) B. M. Hoffman and N. J. Nelson, *J. Chem. Phys.*, **50**, 2598 (1969).
(2) (a) T. B. Eames and B. M. Hoffman, *J. Amer. Chem. Soc.*, **93**, 3141 (1971); (b) B. M. Hoffman and T. B. Eames, *Ibid.*, **91**, 2169 (1969); (c) A. H. Cohen and B. M. Hoffman, *ibid.*, **95**, 2061 (1973).
(3) (a) J. J. Fripiat, A. Leonard, and J. B. Uytterhoeven, *J. Phys. Chem.*, **69**, 3274 (1965); (b) M. R. Basila and T. R. Kantner, *ibid.*, **71**, 467 (1967); (c) E. P. Parry, *J. Catal.*, **2**, 371 (1963); (d) J. B. Peri, *J. Phys. Chem.*, **70**, 2937 (1966).
(4) G. Lozos and B. M. Hoffman, to be submitted for publication.
(5) A. H. Cohen, T. B. Eames, and B. M. Hoffman, to be submitted for publication.
(6) Alfred P. Sloan Fellow.

Department of Chemistry
Northwestern University
Evanston, Illinois 60201

George P. Lozos
Brian M. Hoffman*[6]

Received September 12, 1973

Solvent Effects on the Fluorescence Lifetime of 2-Aminopyridine

Sir: The absence of luminescence from electronically excited states in pyridine has remained a problem of continuing interest. In previous reports from this laboratory we demonstrated significant solvent effects on the fluorescence of aminopyridines.[1,2] It was also shown that the lowest excited singlet states of these molecules were more basic than the ground state, which is usually observed in heterocyclic molecules. Aromatic amines exhibit increased acidity upon excitation to S_1*.[3] We have selected 2-aminopyridine (2-AMP) as a model compound, which approximates the excited state behavior of pyridine, but exhibits fluorescence so that environmental changes could be followed. Our choice was prompted by the gas-phase spectral analysis by Hollas, *et al.*,[4] that the 2980-Å system in 2-AMP is essentially a pyridine π,π^* transition perturbed by the amino group. Lamotte and Loustauneau,[5] on the other hand, reported that the first excited electronic state in 2-aminopyridine shows n,π^* character. With the aim of trying to better understand radiationless processes in pyridine we have measured the fluorescence lifetimes of 2-AMP in different solvents, in order to establish, if possible, (1) the constancy of the triplet yield, (2) the constancy of the natural radiative lifetime of the lowest excited singlet, and (3) whether or not radiationless processes occur from the singlet, triplet, or in both manifolds.

The fluorescence lifetime for vacuum degassed solutions were measured using the time correlated single photon counting technique and are tabulated in Table I, for five different solvents, in the order of increasing dielectric con-

TABLE I: Fluorescence Lifetime of 2-Aminopyridine in Different Solvents (25°, Degassed)

Solvent	ϕ_F[a]	τ_F, nsec[b]	$k_F \times 10^{-6}$, sec^{-1}[c]	$k_{ds} \times 10^{-7}$, sec^{-1}[d]	$k_{isc} \times 10^{-6}$, sec^{-1}	ϕ_T[e]
Cyclohexane (2.0)[f]	0.04	24.2 ± 2.5	1.7	40	(<1)[g]	(0.03)
Ethyl ether (4.3)	0.10	10.8 ± 0.4	9.7	83	(43)	(0.47)
Ethanol (26)	0.18	5.1 ± 0.3	36	161	(121)	(0.61)
Acetonitrile (38)	0.25	5.0 ± 0.3	50	150	(110)	(0.55)
Water (80)	0.53	10.7 ± 0.2	50	44	(4)	(0.04)

[a] Fluorescence yields normalized to value of $\phi_F = 0.64$ for degassed 2-AMP in 0.1 N H_2SO_4; R. Rusakowicz and A. C. Testa, *J. Phys. Chem.*, **72**, 2680 (1968). [b] Average of three measurements. [c] $k_F = (1/\tau_F^0) = (\phi_F/\tau_F)$. [d] $k_{ds} = k_{ic} + k_{isc} = [(1/\phi_F) - 1]k_F$. [e] $\phi_T = (k_{isc})/(k_F + k_{ic} + k_{isc})$. [f] Dielectric constant of the solvent. [g] k_{isc} in cyclohexane is estimated assuming $k_{ds} \approx k_{ic} \approx 4.0 \times 10^7$ sec^{-1}. Justification for this assumption lines in the fact that the molecule phosphoresces only in polar glasses.

stant.[6] It is quite evident that the fluorescence lifetime is solvent dependent and is the largest in cyclohexane despite the low fluorescence yield, relative to polar and hydrogen bonding solvents. The long lifetime in this solvent is consistent with our successful attempt to sensitize the fluorescence of biacetyl with 2-AMP in cyclohexane solutions.[7] The natural radiative lifetime, $\tau_F^0 = (1/k_F)$, for 2-AMP is also the longest in cyclohexane, and together with its low fluorescent yield supports our earlier suggestion that in cyclohexane the lowest excited singlet is primarily $^1n,\pi^*$, whereas in polar solvents the lowest singlet state is $^1\pi,\pi^*$.[1] Vibronic coupling between $^1\pi,\pi^*$ and $^1n,\pi^*$ should be largest in the hydrocarbon solvent, where the energy difference between these states is the smallest. It should be noted that there is no apparent correlation between the fluorescence yield and lifetime; however, the rate constant for fluorescence does increase with the dielectric constant of the solvent. There is, in fact, an order of magnitude increase in k_F in all the polar solvents, relative to cyclohexane. The calculated radiative rate constants for pyridine also show an order of magnitude increase in the value for the $^1\pi,\pi^*$ state in comparison to the $^1n,\pi^*$ state.[8] In general the natural radiative lifetime of the lowest excited singlet is insensitive to the nature of the solvent; however, it is seen that this does not occur with 2-AMP.

The calculated rate constants in Table I for deactivation of the lowest excited singlet, k_{ds}, either by intersystem crossing or internal conversion, indicate the slowest relaxation in cyclohexane. The lack of phosphorescence in nonpolar glasses at 77°K[9] suggests that slow deactivation is not *via* intersystem crossing, but rather through internal conversion, *i.e.*, $S_1 \rightsquigarrow S_0$.[10] In contrast to its behavior in cyclohexane, 2-AMP does phosphoresce at 77°K with $\phi_p = 0.07$ in EPA and 0.05 in acetonitrile.[9] There are two routes by which the singlet deactivates, *i.e.*, internal conversion and intersystem crossing, and the effect of solvents on these paths must be considered. With aromatic heterocyclic molecules the movement of singlet and triplet levels can significantly affect intersystem crossing. On the other hand, the internal conversion mode is generally unaffected by solvents. Another possibility is that both k_{ic} and k_{isc} vary with solvents, but since the major effect is on the energy gap between the coupling singlet and triplet states, its effect should be much larger than between the lowest excited singlet and the ground state. Ermolaev[11] has presented evidence to indicate that the rate constant for intersystem crossing in some aromatic heterocyclics is solvent dependent. Accordingly, we consider the rate constant $S_1 \rightsquigarrow S_0$, k_{ic}, to be constant. If we assume that $k_{ds} \approx k_{ic} \approx 4 \times 10^7$ sec^{-1} in cyclohexane, *i.e.*, small triplet yield, then the rate constants for intersystem crossing can be calculated and their values presented in Table I. Of particular interest is that the polar solvents show faster intersystem crossing rates, and exhibit more fluorescence and phosphorescence relative to nonpolar solvents.[9] Recently, we suggested a similar interpretation for the measured triplet-triplet absorption of 4-*N*-dimethylaminopyridine in EPA, which is not observed in 3-methylpentane.[12] From the rate constants in Table I, an estimate of the triplet yield can be made and the values shown (last column of Table I) are in qualitative agreement with the observed phosphorescence behavior of this molecule at 77°K. Thus, it appears that the lack of phosphorescence and the small fluorescence yield ($\phi_F = 0.04$) in cyclohexane is the result of efficient (~93%) internal conversion from the lowest excited singlet state.

The above data provide evidence that the natural radiative lifetime, triplet yield, and the intersystem crossing rate constant of 2-AMP are solvent dependent. Although this conclusion has implications for other heterocyclic molecules, extrapolation of these results to pyridine suggest that its small triplet yield (reported to be 0.03 ± 0.02)[8,13] is not affected sufficiently by solvents to overcome an efficient radiationless decay $S_1 \rightsquigarrow S_0$. This interpretation would also account for the lack of triplet-triplet absorption in pyridine.

References and Notes

(1) A. Weisstuch and A. C. Testa, *J. Phys. Chem.*, **72**, 1982 (1968).
(2) A. C. Testa, A. Weisstuch, and J. Hennessy in "Molecular Luminescence," E. C. Lim, Ed., W. A. Benjamin, New York, N. Y., 1969, p 863.
(3) E. L. Wehry in "Fluorescence: Theory, Instrumentation and Practice," G. G. Guilbault, Ed., Marcel Dekker, New York, N. Y., 1967, p 37.
(4) J. M. Hollas, G.H. Kirby, and R. A. Wright, *Mol. Phys.*, **18**, 327 (1970).
(5) M. Lamotte and P. Loustauneau, *J. Chim. Phys.*, **65**, 1486 (1968).
(6) A description of our photon counting apparatus will be given elsewhere.
(7) J. Hennessy and A. C. Testa, *J. Chem. Phys.*, **49**, 956 (1968).
(8) J. Lemaire, *J. Phys. Chem.*, **71**, 612 (1967).
(9) S. Hotchandani and A. C. Testa, *J. Chem. Phys.*, **59**, 596 (1973).
(10) A referee has suggested that 2-AMP may undergo association in cyclohexane, relative to polar solvents, and thus account for its lack of phosphorescence. This possibility can be rejected on the basis of the dilute solutions ($<10^{-4}M$) used in the present study. There is no unusual behavior in the lowest uv absorption band and the extinction coefficients of 2-AMP relative to polar solvents. Furthermore, our results on the sensitized fluorescence of biacetyl with 2-AMP in cyclohexane give normal Stern-Volmer plots over a tenfold change in the concentration of 2-AMP, indicating that association does not occur.
(11) V. L. Ermolaev and I. P. Kotylar, *Opt. Spectrosc.*, **9**, 183 (1960).
(12) A. C. Testa, *J. Chem. Phys.*, **57**, 3019 (1972).
(13) R. B. Cundall, A. S. Davies, and K. Dunnicliff in "The Triplet State," A. B. Zahlan, Ed., Cambridge University Press, New York, N. Y., 1967, p 183.

Department of Chemistry **S. Babiak**
St. John's University **A. C. Testa***
Jamaica, New York 11439

Received September 10, 1973

The leading American journal devoted to general organic chemistry:

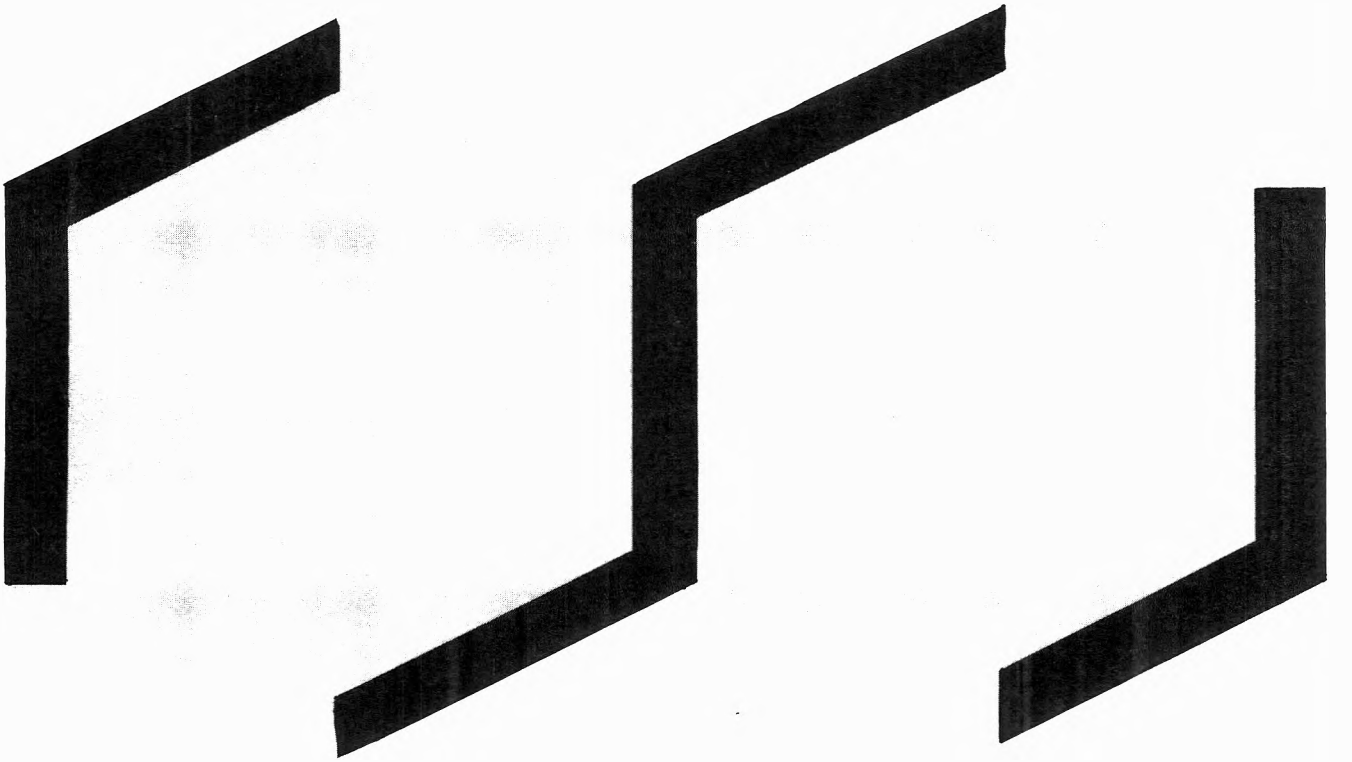

The Journal of Organic Chemistry

The career wise way to keep up with current thinking in the field. You get the *total picture* presented through forty some papers per biweekly issue. Areas of emphasis include:

- Organic reactions
- Natural products
- Studies of mechanism
- Theoretical organic chemistry
- Various aspects of spectroscopy related to organic chemistry

You get all of this, in the 1100 articles and NOTES (brief, concise accounts of studies of smaller scope) and over 4000 pages a year from your big informative issues of THE JOURNAL.

You owe it to your career to find out for yourself why The Journal of Organic Chemistry is the leader in its field.

Send your order today.

. . . *another ACS service*

The Journal of Organic Chemistry
American Chemical Society **1974**
1155 Sixteenth Street, N.W.
Washington, D.C. 20036

Yes, I would like to receive THE JOURNAL OF ORGANIC CHEMISTRY at the one-year rate checked below:

	U.S.	*Canada***	*Latin America***	*Other Nations***
ACS Member One-Year Rate*	☐ $20.00	☐ $25.00	☐ $25.00	☐ $26.00
Nonmember	☐ $60.00	☐ $65.00	☐ $65.00	☐ $66.00

Bill me ☐ Bill company ☐ Payment enclosed ☐

Air freight rates available on request.

Name _____

Street _____ Home ☐ Business ☐

City _____ State _____ Zip _____

*NOTE: Subscriptions at ACS member rates are for personal use only. **Payment must be made in U.S. currency, by international money order, UNESCO coupons, U.S. bank draft, or order through your book dealer.

You don't have to search the archives for data . . .

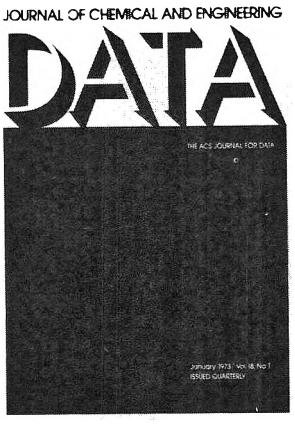

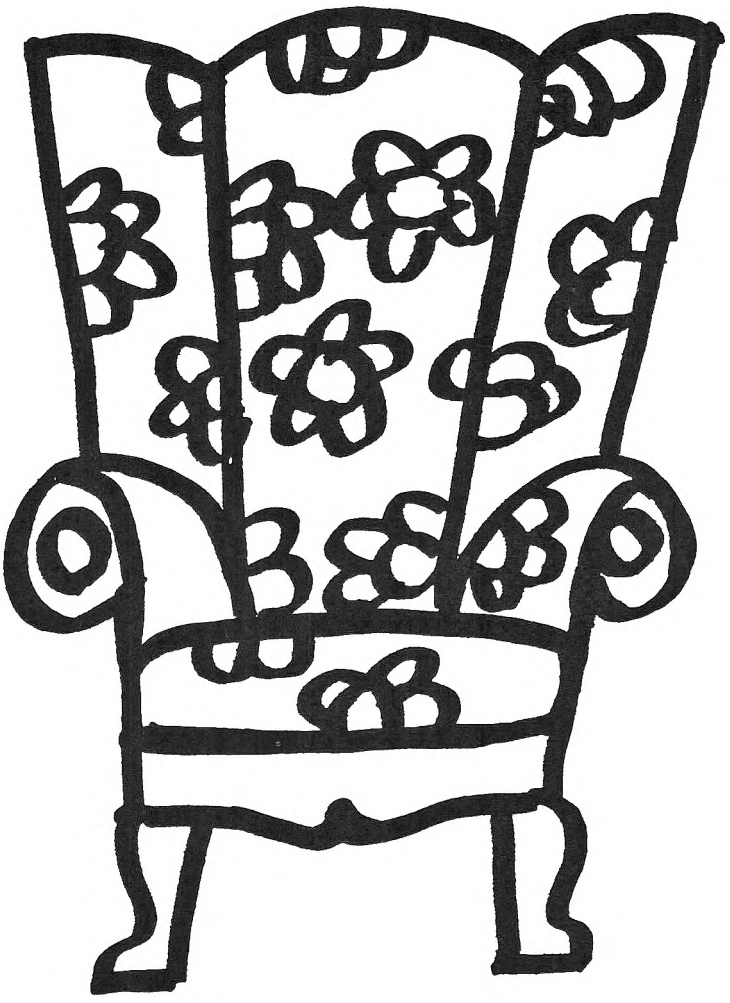

. . . because THE JOURNAL OF CHEMICAL AND ENGINEERING DATA will bring precise, reliable, useful technical information right to your fingertips quarterly! With a year's subscription, you'll receive a total of over 500 pages of valuable science and engineering data that are especially relevant now in light of today's new instrumentation. The information in JCED includes:

- experimental data relating to pure compounds or mixtures covering a range of states;
- manuscripts based on published experimental information which make tangible contributions through their presentation or which set forth a sound method of prediction of properties as a function of state;
- experimental data which aid in identifying or utilizing new organic or inorganic compounds; and
- papers relating primarily to newly developed or novel synthesis of organic compounds and their properties.

Start to benefit now from this "arm-chair" source of pertinent technical data—with your own personal subscription to JCED . . . just complete and return the form below . . . get your data without the dust.

. . . *another ACS service*

Journal of Chemical & Engineering Data

Journal of Chemical & Engineering Data
American Chemical Society
1155 Sixteenth Street, N.W.
Washington, D.C. 20036

1974

Yes, I would like to receive the JOURNAL OF CHEMICAL & ENGINEERING DATA at the one-year rate checked below:

	U.S.	*Canada***	*Latin America***	*Other Nations***
ACS Member One-Year Rate*	☐ $15.00	☐ $18.00	☐ $18.00	☐ $18.50
Nonmember	☐ $45.00	☐ $48.00	☐ $48.00	☐ $48.50

Bill me ☐ Bill company ☐ Payment enclosed ☐
Air freight rates available on request.

Name _____

Street _____ Home ☐ Business ☐

City _____ State _____ Zip _____

*NOTE: Subscriptions at ACS member rates are for personal use only. **Payment must be made in U.S. currency, by international money order, UNESCO coupons, U.S. bank draft, or order through your book dealer.

15 W.A. 251